

Institute for Circuit Theory and Signal Processing
Technische Universität München

Energy Efficient Design and Operation of Wireless Communication Systems

Qing Bai

Vollständiger Abdruck der von der Fakultät für Elektrotechnik und Informationstechnik der Technischen Universität München zur Erlangung des akademischen Grades eines
Doktor-Ingenieurs
genehmigten Dissertation.

Vorsitzender: Prof. Dr. Gerhard Kramer

Prüfer der Dissertation:

1. Prof. Dr. Dr. h.c. Josef A. Nossek
2. Prof. Dr. Deniz Gündüz

Die Dissertation wurde am 26.04.2016 bei der Technischen Universität München eingereicht und durch die Fakultät für Elektrotechnik und Informationstechnik am 01.07.2016 angenommen.

Abstract

Driven by the demand on cost-effectiveness as well as environmental concerns, novel system design and technological advances for improving the energy efficiency of wireless communication systems have been given prominent importance and become one of the central tasks for the next generation of wireless technologies. In this doctoral thesis, we focus on the efficient utilization of energy in two different communication scenarios. First, we consider the throughput maximization of a wireless transceiver on a finite time interval with a given energy budget. Second, we assume the transceiver to be powered by ambient energy harnessed by an energy harvester. This renders the energy available for communications a time-varying function or a stochastic process, thus adding dynamics and randomness to the control optimization of the system. With circuit and processing power of the transceiver taken into account, the trade-off between spectral and energy efficiency and the trade-off between energy consumption and latency are both embodied by the formulated throughput maximization problems.

In the first scenario where the short-term throughput of an energy-constrained system is to be maximized, we formulate the problem within the framework of optimal control theory and derive the optimal solutions to a number of different cases. If a transmitter with continuously adaptable transmit power is under control, the achievable rate and the power consumption of the system can be given as functions of the transmit power. We discover that the throughput-maximizing transmission strategy can be determined based on the property of the achievable rate as a function of the power consumption, the fact of which can be interpreted on the power-rate graph from a geometric viewpoint. For the receive side, we take the resolution employed in A/D conversion as the control variable and find the optimal receive strategies using similar methods as applied to the transmit side. The joint optimization of a transmitter-receiver pair with individual energy budgets is also investigated.

In the second scenario where energy harvesting transceivers are considered, we distinguish mainly between two cases: first, the transceivers have non-causal energy arrival information on the operation interval over which the throughput is to be maximized; second, the random energy arrivals are modeled as a stationary Poisson process, and the transceivers have only causal as well as statistical knowledge about the arrival profile. We maximize in this case the average throughput on the long-term. While the first case can be solved by convex optimization or a sequential construction procedure of the optimal state trajectory on a time-energy graph, the second requires modeling of the system as a Markov decision process to which the policy-iteration algorithm is applied.

Contents

Abstract	1
1. Introduction	5
1.1 Motivation	5
1.2 Overview and Contributions	6
1.3 Notations and Acronyms	9
1.3.1 List of notations	10
1.3.2 List of acronyms	11
2. On Energy Efficient Wireless Communications	13
2.1 Energy Efficiency and its Optimization	14
2.1.1 Shannon limit	14
2.1.2 Constrained optimizations	16
2.2 Power Consumption of Communication Systems	16
2.3 Trade-off between Spectral Efficiency and Energy Efficiency	18
2.3.1 Adaptation of the ADC resolution	19
2.3.2 Optimization of training-based systems	23
2.4 Trade-off between Energy Efficiency and Bandwidth	28
2.5 Trade-off between Energy Consumption and Latency	31
3. Energy-constrained Throughput Maximization on a Finite Time Interval	36
3.1 Problem Formulation	37
3.2 The Maximum Principle	39
3.3 Optimal Control of the Transmitter	40
3.3.1 Case I	41
3.3.2 Case II	45
3.3.3 Case III	49
3.3.4 Case IV	53
3.3.5 Case III + IV	60
3.3.6 Case V	61
3.3.7 Case VI	64
3.4 Optimal Control of the Receiver	67
3.4.1 Case I	67
3.4.2 Case II	70

3.5	Optimal Control of a Pair of Transmitter and Receiver	72
3.5.1	Case I	72
3.5.2	Case II	77
3.6	Summary	87
4.	Optimal Control of Energy Harvesting Transceivers	89
4.1	Energy Harvesting Techniques	91
4.1.1	Photovoltaic	92
4.1.2	Piezoelectric, electromagnetic, and electrostatic	92
4.1.3	Thermoelectric	92
4.1.4	Radio frequency	93
4.1.5	Energy storage	93
4.2	Optimal Control with Non-causal Energy Arrival Information	93
4.2.1	Problem formulation	94
4.2.2	Transmit strategies	97
4.2.3	Receive strategies	116
4.2.4	Transmit and receive Strategies	116
4.3	Optimal Control with Causal Energy Arrival Knowledge	119
4.3.1	MDP modeling and the average throughput maximization	119
4.3.2	Single-stage solutions	122
4.3.3	Policy-iteration algorithm	123
4.3.4	Transmission over a block-fading channel	124
4.3.5	Simulation results and analysis	125
4.3.6	Joint control of a pair of energy harvesting transceivers	132
4.4	Summary	137
5.	Conclusions and Outlook	138
5.1	Summary and Conclusions	138
5.2	Future Perspectives	139
	Appendix	141
A1	Properties of the Capacity Lower Bound (2.49)	141
A1.1	The exponential integral and its expansions	141
A1.2	Monotonicity and asymptotic properties	142
A2	Concavity of the Constructed Rate Function \tilde{R}	144
A3	Markov Chain and Markov Decision Process	146
A3.1	Markov chain	146
A3.2	Stochastic matrices	147
A3.3	Markov decision process	148
A4	Policy-Iteration Algorithm for Average Reward Maximization	148
	Bibliography	151

1. Introduction

1.1 Motivation

As witnesses and beneficiaries of the rapid developments of Information and Communication Technologies (ICT), we enjoy nowadays a modern, connected lifestyle that brings more convenience, safety, and entertainment than ever. The supporting infrastructure and equipments all consume power. As the ICT industry advances fast and tremendously, so increases its energy consumption. In various reports and surveys [1–3], the energy consumption of the ICT is estimated to account for 1.5 to 4.5 percent of the total worldwide energy consumption today. The annual growth rate in the past years has been larger than the global energy growth rate, and the same trend is predicted for the future. Taking into consideration the increasing demand on data rate and growing number of devices in the network, both [1] and [3] give an estimate of more than 10 percent annual energy consumption growth rate of communication networks, suggesting that the corresponding total energy consumption would be doubled in around 2020.

Reducing the energy consumption of ICT and improving the energy efficiency of systems and networks as of today are driven both by environmental responsibility and economical interest. The consumption of electricity as quoted above translates to the emission of greenhouse gases as well as a cost that has to be paid by the service providers and also the customers. As we face the demand and take the challenges of the next generation of wireless technologies known as 5G, the importance of improving the energy efficiency is addressed on multiple levels and for the three most promising candidate technologies: ultra-densification, millimeter wave communication (mmWave), and massive multiple-input multiple-output (MIMO) systems [4,5]. The deployment of nested small cells, aiming at improving the spectral efficiency per area, requires low power base stations and efficient resource allocation algorithms to maintain a reasonable cost level for the network. The increased bandwidth enabled by mmWave and the utilization of a large antenna array by massive MIMO may both lead to significant increment in the power consumption. Therefore, smart design methods and operation strategies are necessary in order to achieve a good balance between the quality of service and the cost in terms of power and energy consumption.

On the other hand, cheaper and renewable sources of energy can be sought for and exploited for communication purposes. The process of harnessing energy from the environment and converting them to electrical energy is known as *energy harvesting*. Common sources for energy harvesting include the sun, temperature gradients, human motions and mechanical vibrations, background radiations, *etc.* Wireless transceivers

can be powered by the harvested ambient energy, and these devices find important applications in wireless sensor networks, wearables for healthcare, and even future mobile terminals. Examples of devices and networks with energy harvesting can be found in the survey paper [6] and the references therein. Because of the unstable and intermittent nature of the harvested energy, the design and optimization of energy harvesting transceivers are different from devices with a constant power supply. New resource management principles and control strategies need to be applied to these devices and the networks they constitute so as to make the most efficient use of the available energy [7].

1.2 Overview and Contributions

With energy efficiency of wireless communication systems as the theme, we present in this doctoral thesis our theoretical investigations on energy-constrained and energy harvesting systems which aim at maximizing their short-term or long-term throughput. The main contents and contributions of each chapter are introduced in this section.

Chapter 2: On Energy Efficient Wireless Communications

Starting an exploration in the area of energy efficient wireless communications, we prepare and equip ourselves with some requisite knowledge and comprehension presented in Chapter 2. In Section 2.1, we first give the common defining metric of energy efficiency as the number of information bits that are successfully delivered per consumed Joule of energy, and then discuss its optimization from an information-theoretic point of view. Derivation of the minimum of E_b/N_0 , *i.e.* the minimal energy per bit normalized with the noise power spectral density, is reviewed and triggers the question of how some fundamental results would change if the cost of the communication system in terms of power or energy is modeled in a more realistic way. An introduction to power consumption of communication systems is given in Section 2.2, where we analyze the general trend as well as the power consumption of a wireless transceiver on a component level. The remaining sections of the chapter focus on three fundamental trade-offs in communication systems which involve energy consumption or energy efficiency:

- Trade-off between spectral and energy efficiency: it is well-known that the two metrics are often competing goals in communication systems. At the transmit side, adapting the transmit power allows the system to operate at the desirable point on the spectral-energy efficiency trade-off curve. With circuit power taken into account, the curve can be non-monotonic and exhibits a non-trivial point at which the energy efficiency is maximized. Similarly, the bit resolution employed by the A/D converter at the front end of the receiver can be adapted to address this trade-off at the receive side. To this end, a capacity lower bound of the quantized channel and the power consumption of the ADC are introduced so that the energy efficiency of the receiver can be quantified with respect to the ADC resolution. Moreover, we discuss the impact of quantization on channel estimation using pilot symbols.
- Trade-off between energy efficiency and bandwidth: given a minimum data rate that the communication should support, this trade-off can be identified with varying transmit power or ADC resolution. Besides the pre-log scaling of channel capacity,

the bandwidth also plays an important role in the power consumption of many circuit components.

- Trade-off between energy consumption and latency: when the system is to deliver a certain amount of data, the promptness in the completion of delivery can be traded off for better energy efficiency of the system. We give an example of packet transmission over a block-fading channel where retransmissions are accounted for in the delay of the packets.

Chapter 3: Energy-constrained Throughput Maximization on a Finite Time Interval

For a wireless transceiver or a pair of transceivers communicating over a single link, Chapter 3 addresses the question of how they can be optimally operated on a finite time interval if they have a given, fixed energy budget. The optimization objective is to maximize the total throughput which equals the integral of the instantaneous data rate on the interval. Accordingly, the energy consumption is calculated as the integral of the power dissipation of the system, which should not exceed the available budget. The optimization variable in this case, instead of a scalar or a vector, is the relevant physical parameter as a function of time. To this end, we formulate the problem within the framework of the optimal control theory which allows for the application of theories and methods therein, including the Pontryagin's maximum principle and the value iteration algorithm. Besides the algebraic derivations, we illustrate and interpret the optimal solution of the problem from a geometric viewpoint on the time-energy graph. The three trade-offs presented in Chapter 2 are embodied in the obtained optimal solutions, and the critical role that the energy efficiency maximizing operation mode plays shall be revealed. In addition, the properties of the maximal achievable throughput with respect to the energy budget and the duration of the operation interval are also discussed.

We investigate a number of communication scenarios under different assumptions, and derive the optimal transmit/receive strategy for each scenario:

- Transmitter: in the very basic setting, the continuously adaptable transmit power can be taken as the control variable, and the communication channel is assumed constant on the operation interval. The achievable data rate and the power consumption of the transmitter can be both modeled as functions of the transmit power, which should meet certain criteria such as being non-negative and non-decreasing, starting from zero with zero transmit power, in order to be consistent with physics. By using the optimal control theory, we find that the strict concavity of the achievable rate function and the convexity of the power consumption function ensure that employing constant transmit power leads to the maximal throughput. On the other hand, if the transmitter operates either in sleep mode with no circuit power, or in active mode where a positive circuit power is always associated, the optimal transmission strategy can be non-constant. We indicate that formulating the achievable rate as a concave function of the power consumption is the key to finding the throughput-maximizing transmission strategy. The scenario with a time-varying channel is also studied, for the respective cases that the channel condition is known non-causally or only causally and statistically.

- Receiver: at the receive side, we take the ADC resolution as the control variable, and discuss the cases that it is real-valued or restricted to integer numbers. Mathematically equivalent counterparts can be found from the transmit side.
- Transmitter-receiver pair: jointly optimal control of a pair of transmitter and receiver can be performed, provided that global knowledge of the system parameters is available, and the two transceivers are synchronized and cooperative. In analogy to the previous discussions, we aim to construct a concave achievable rate function in the power consumption; in contrast to them, the construction is now in the three-dimensional space instead of on a two-dimensional plane. We explore two cases as well, the first one with continuous control variables and second with discrete ones.

Chapter 4: Optimal Control of Energy Harvesting Transceivers

In this chapter we consider the optimal control of energy harvesting transceivers, *i.e.* transceivers that are capable of harvesting energy from the environment, and depend solely on these energy for communications. With uncontrolled surroundings, the energy that can be potentially harvested and employed is unstable, intermittent, and random in nature. Different resource management principles are therefore needed for these transceivers as compared to conventional devices powered by batteries or fixed utilities. Mathematically formulated, the harvested energy imposes an upper bound on the cumulative energy consumption of the transceiver over time. Unlike the situation treated in Chapter 3, this upper bound is time-varying, and practically unknown in advance. Furthermore, we assume that the transceiver is equipped with an energy storage that is limited in capacity. When the storage is full, the device can no longer take in energy from the environment even if they are available. The possibility of such a situation gives rise to a trade-off in the way energy is consumed: if the consumption rate is low, better energy efficiency can be achieved (assuming no circuit power) which results in larger throughput, yet the probability of having a full storage increases; in contrast, employing a high consumption rate is less energy efficient but guarantees the storage room for the incoming energy. Nevertheless, the optimal control of energy harvesting transceivers is closely related to the control problem we investigate in Chapter 3, which is referred to as the basic problem to address its static nature as well as its essential importance to the problem here.

We introduce in Section 4.1 common energy harvesting techniques and related issues in energy storage. In Section 4.2, we consider the throughput maximization problem on a finite time interval for an energy harvesting transceiver, where non-causal energy arrival information is available for the offline optimization and performance limit evaluation. The optimal control strategy can be obtained via construction of the optimal state trajectory on the time-energy graph based on the geometric property of the solution to the basic problem. In case that the harvested energy arrives at discrete time instants, convex optimization techniques can also be applied. We propose a heuristic algorithm with low complexity to cope with the case of communicating over a block-fading channel and having frequent energy arrivals. Section 4.3 considers the more practical scenario that the transceiver possesses only causal and statistical knowledge about the energy arrivals. We assume the energy arrival process as compound Poisson, discretize the energy space and time, and model the system as a Markov decision process. To this end, we seek

for a mapping between the system states in terms of the available energy level in the storage, and the actions to be taken in terms of employment of a transmit power or ADC resolution. The policy iteration algorithm is applied to attain the optimal policy with respect to a predefined single-stage strategy. The joint control of a pair of energy harvesting transmitter and receiver is investigated as well.

1.3 Notations and Acronyms

We summarize in this section the notations and acronyms used in the thesis.

1.3.1 List of notations

Notation	Description
\triangleq	defined as equal to
j	imaginary unit
$\text{erf}(\cdot)$	Gauss error function
\mathbb{R}, \mathbb{C}	field of real numbers, field of complex numbers
$\min\{x, y\}$	the minimum of x and y
$\max\{x, y\}$	the maximum of x and y
x^+	equal to x when x is non-negative, otherwise is equal to 0
$\lfloor x \rfloor$	the largest integer that is smaller or equal to x
$ \mathcal{A} $	cardinality of set \mathcal{A}
$\Pr\{X = x\}$	probability that random variable X is equal to the value x
$E[X]$	expectation of X
$H(X)$	entropy of X
$I(X; Y)$	mutual information between X and Y
$X \sim \mathcal{N}(\mu, \sigma^2)$	X is Gaussian distributed with mean μ and variance σ^2
$X \sim \mathcal{U}(a, b)$	X is uniformly distributed on the interval $[a, b]$
$X \sim \mathcal{CN}(\mu, \sigma^2)$	real and imaginary parts of X are i.i.d. Gaussian distributed with mean μ and variance $\sigma^2/2$
$f \equiv g$	function f is equal to function g at every point
g_x	partial derivative of function g with respect to x
\dot{g}	differential of function g with respect to time
$\mathbf{H}(g)$	Hessian matrix of function g
$\mathbf{a} \succeq \mathbf{b}$	every entry of vector \mathbf{a} is larger or equal to the corresponding entry of vector \mathbf{b}
$\mathbf{0}_L, \mathbf{1}_L$	all zero / all-one vector of dimension L
\mathbf{I}_L	identity matrix of dimension $L \times L$
$(\cdot)^T$	transpose of a vector or a matrix
$(\cdot)^*$	complex conjugate of a vector or a matrix
$(\cdot)^H$	Hermitian (conjugate transpose) of a vector or a matrix
$\text{tr}(\mathbf{A})$	trace of matrix \mathbf{A}
$\det(\mathbf{A}), \mathbf{A} $	determinant of matrix \mathbf{A}
$\text{diag}(\mathbf{A})$	diagonal matrix with the same diagonal entries as matrix \mathbf{A}
$\text{diag}\{x_1, \dots, x_L\}$	diagonal matrix with x_1, \dots, x_L as the diagonal entries

1.3.2 List of acronyms

Acronym	Definition
ACK	acknowledgement
ADC	analog-to-digital converter, A/D converter
ARQ	automatic repeat request
AWGN	additive white Gaussian noise
BER	bit error ratio
BP	bilinear program
CMOS	complementary metal-oxide-semiconductor
CoMP	coordinated multi-point
CSI	channel state information
DAC	digital-to-analog converter, D/A converter
DMC	discrete memoryless channel
DP	dynamic programming
DSP	digital signal processor
ENOB	effective number of bits
FFT	fast Fourier transform
FOM	figure of merit
HARQ	hybrid automatic repeat request
I/Q	in-phase/quadrature
ICT	Information and Communication Technologies
IFA	intermediate frequency amplifier
IFFT	inverse fast Fourier transform
i.i.d.	independent and identically distributed
LNA	low noise amplifier
LO	local oscillator
MAC	medium access control layer
MDP	Markov decision process
MIMO	multiple-input multiple output
MMSE	minimum mean squared error
mmWave	millimeter wave communication
MQAM	M -ary quadrature amplitude modulation
MSE	mean squared error
NACK	negative acknowledgement
ODE	ordinary differential equation

Acronym	Definition
PA	power amplifier
PAR	peak-to-average ratio
PEP	packet error probability
PHY	physical layer
PI	policy-iteration
PMP	Pontryagin's maximum principle
QAM	quadrature amplitude modulation
RF	radio frequency
RX	receiver
SIMO	single-input multiple-output
SISO	single-input single-output
SNR	signal-to-noise ratio
SQR	signal-to-quantization-noise ratio
TTI	transmission time interval
TX	transmitter
VI	value-iteration
ZMCCG	zero-mean circularly symmetric complex Gaussian

2. On Energy Efficient Wireless Communications

As the necessity and importance of improving the energy efficiency of wireless communication systems have been realized and emphasized, enormous efforts are made in the past years for better understanding of the problem and the current situation *e.g.* by European research projects TREND [8] and EARTH [9]. Power consumption data of various parts of the communication network, from base stations and mobile terminals to the core network, have been collected and studied. Based on these investigations, performance bottlenecks of the system are identified, and new design methods and operation strategies have been proposed to enhance the energy efficiency. The improving areas are noticed to be ubiquitous [10]: on the component level, development in the CMOS technology enables the implementation and production of more efficient components such as power amplifiers and A/D converters [11, 12]; for given components, design parameters that govern the trade-off between power consumption and other system performance metrics can be optimized [13, 14]. The emerging and promising large-scale systems, due to the reason of cost, often have to live with hardware imperfections such as I/Q imbalance and phase noise. The effects of the non-ideal hardware on the energy efficiency of these systems are investigated *e.g.* in [15]. On the link level, physical layer parameters can be jointly optimized with parameters of higher layers to achieve better energy efficiency of the system. For instance, packet transmission is considered in [16, 17], where [16] proposes an energy efficient retransmission protocol based on the optimization of the packet length, and [17] designs energy efficient resource allocation algorithms which take power allocation, modulation and coding, as well as retransmission protocols jointly into account. The authors of [18] address the rate-energy trade-off under delay and queueing constraints, and [19] extends the investigation to frequency-selective channels and proposes an efficiency-maximizing power control method. Development of energy efficient algorithms and protocols can be done on the network level as well [20, 21]. Moreover, the trade-off between deployment, spectral, and energy efficiency [22] leads to architectural considerations on the network, promoting the concepts of pico- and femtocells, heterogeneous networks, coordinated multi-point (CoMP) transmission, *etc.* A survey of these techniques can be found in [23].

In this chapter and also in the whole dissertation, we focus on the energy efficiency on component and link levels. Network level considerations are beyond the scope of this thesis, but would be of interest for future research. We start in the first section with a formal definition of the term energy efficiency, and then derive the minimum energy per bit for the AWGN channel. The power consumption of a wireless transceiver is analyzed

in Section 2.2. After that, we introduce some fundamental trade-offs in communication systems which involve energy and energy efficiency, namely, the trade-off between spectral and energy efficiency, the trade-off between energy efficiency and bandwidth, and the trade-off between energy consumption and delay. For each case, we first give a generic derivation, and then elaborate with some specific examples that come from our own contributions. The very basic communication scenario is chosen for discussion: the transmitter and/or receiver have single antenna, the channel is frequency-flat, and there is no interference in the system.

2.1 Energy Efficiency and its Optimization

The efficiency of a system, a process, an operation *etc.* can be evaluated by the ratio between the profit and the associated cost that are generated. For a communication system, the energy efficiency can be measured by the number of information bits that are successfully conveyed per consumed Joule of energy over a certain period of time. Or, on a short-term or instantaneous basis, the energy efficiency can be defined equivalently by the ratio between the capacity or the achievable data rate C (in bit/sec) and the total power consumption P (in Watt) of the system as

$$\eta_E = \frac{C}{P}, \quad (2.1)$$

where η_E denotes the energy efficiency in the unit of bit/Joule. As enhancing the gain or the profit, in this case C , and reducing the cost, in this case P , are usually competing goals in a communication system, the maximization of η_E is a non-trivial and instructive optimization problem. Mathematically, it can be given as

$$\max_{u \in \mathcal{U}} \eta_E(u), \quad (2.2)$$

where the optimization variable u can be one or a set of system parameters that are adaptable and affect both the achievable data rate and the power consumption, and \mathcal{U} denotes the set of feasible values of u . The maximization is based on the trade-off between C and P controlled by u , and we refer to the optimum u as the *energy efficient operation mode*. Some of the early works that consider this metric include [24,25], where the former was driven by energy-constrained transmitter used in underwater communications, and the latter treats the case with arbitrary alphabets of the channel input. Many of the recent research contributions on advanced wireless systems and techniques, *e.g.* [26], also aim at the maximization of η_E to explore the best cost-effectiveness of the system.

The inverse of η_E , *i.e.* the energy that is required to convey one bit, is also a commonly used energy efficiency metric which is often denoted with E_b and normalized with the noise power spectral density N_0 in information-theoretic analysis. Equivalent to the maximization of η_E , the minimization of E_b with respect to u can be formulated. We introduce next the well-known Shannon limit of the minimum energy per bit metric.

2.1.1 Shannon limit

The capacity of the AWGN channel with input power p_{tx} is given by Shannon [27] as

$$C = B \log_2 \left(1 + \frac{p_{tx}}{BN_0} \right) \quad \text{in bit/sec}, \quad (2.3)$$

where B stands for the bandwidth of the channel in Hertz, and $\frac{p_{\text{tx}}}{BN_0}$ gives the receive signal-to-noise ratio (SNR). Assuming $P = p_{\text{tx}}$ *i.e.* the power consumption of the system is equal to the transmit power, we write the normalized energy per bit metric as

$$\frac{E_b}{N_0} = \frac{P}{CN_0} = \frac{p_{\text{tx}}}{BN_0 \log_2 \left(1 + \frac{p_{\text{tx}}}{BN_0} \right)}. \quad (2.4)$$

Based on the inequality $\ln(1+x) > \frac{x}{1+x}$ for $x > 0$, we find that (2.4) as a function of p_{tx} increases monotonically since

$$\left(\frac{E_b}{N_0} \right)_{p_{\text{tx}}} = \frac{B}{N_0 C^2 \ln 2} \left(\ln \left(1 + \frac{p_{\text{tx}}}{BN_0} \right) - \frac{p_{\text{tx}}}{BN_0 + p_{\text{tx}}} \right) > 0. \quad (2.5)$$

This is to say, the minimum of the function is achieved with p_{tx} approaching zero. The relation between E_b/N_0 and p_{tx} is illustrated in Fig. 2.1(a). Applying the L'Hôpital's rule yields

$$\lim_{p_{\text{tx}} \rightarrow 0} \frac{E_b}{N_0} = \lim_{p_{\text{tx}} \rightarrow 0} \frac{P_{p_{\text{tx}}}}{N_0 C_{p_{\text{tx}}}} = \lim_{p_{\text{tx}} \rightarrow 0} \frac{(BN_0 + p_{\text{tx}}) \ln 2}{BN_0} = \ln 2. \quad (2.6)$$

Consequently, we have

$$\left(\frac{E_b}{N_0} \right)_{\min} = \ln 2 = 0.6931 = -1.59 \text{ dB}, \quad (2.7)$$

meaning that the minimum energy to transmit one bit is 1.59 dB below the noise level at the receiver. However, the infinitely small transmit power required to achieve this minimum is not a desirable operation mode as it also leads to trivial capacity. To this end, constraints can be added to the energy efficiency optimization problems to guarantee the fulfillment of other performance requirements of the system.

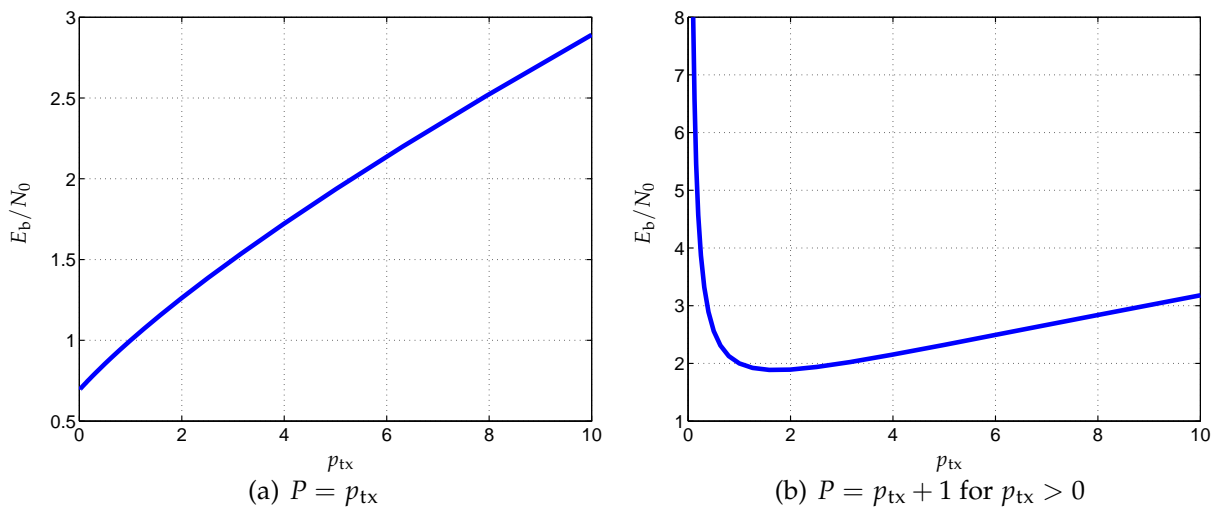


Fig. 2.1: Minimum energy per bit normalized with the noise power spectral density as dependent on the transmit power p_{tx} , $BN_0 = 1$

2.1.2 Constrained optimizations

For most application scenarios, energy efficiency is not the sole performance index that is important to the system. Spectral efficiency, for example, is another important objective since spectrum has been and is still a scarce radio resource, which may not be optimized simultaneously with the energy efficiency. The trade-offs between several common performance metrics including the energy efficiency shall be introduced in the subsequent sections. To take multiple objectives into account, one can employ weighting factors for each objective and optimize the weighted sum of all relevant objectives. Adjustment can be made in the weighting factors to place different values on each objective. On the other hand, when there are hard limits or requirements on certain objectives, constrained optimizations can be formulated such that fulfillment of these limits or requirements is guaranteed while the unspecified objective is optimized. The subject of Chapter 3 is an optimization of this kind: the throughput of the system on a given time interval is to be maximized under a fixed energy budget. The optimal solution can be different from the energy efficient operation mode, yet the two are closely related as we shall find out.

2.2 Power Consumption of Communication Systems

It goes without saying that to improve the energy efficiency, one of the indispensable first steps is to understand which part of the system consumes how much power under which conditions. Studies in this area would then enable the establishment of mathematical models of power consumption, which are the basis of theoretical analysis and optimization of communication systems. The total power consumption of various communication devices and facilities can differ by several orders of magnitude, as shown in Fig. 2.2 where the numbers are based on [28–35]. For wireless sensor nodes alone, the power consumption spans a wide range depending on the specific application scenarios and the data rate requirements. Base stations in heterogeneous networks also exhibit diverse power consumption profiles, not only in the absolute values but also in the power shares of the functional modules [29], which is mainly due to their different coverage areas. For macro base stations and data centers, there is additional power expenditure for cooling the equipment which can be significant. The power consumption of all type of devices also depends heavily on their operation modes, *i.e.* whether the system is actively transmitting or receiving signal, or is in idle or sleep mode where some of the functional modules are shut down resulting in much less power consumption. By adapting to the traffic conditions and appropriately switching between the modes, energy savings can be achieved and better energy efficiency can be realized.

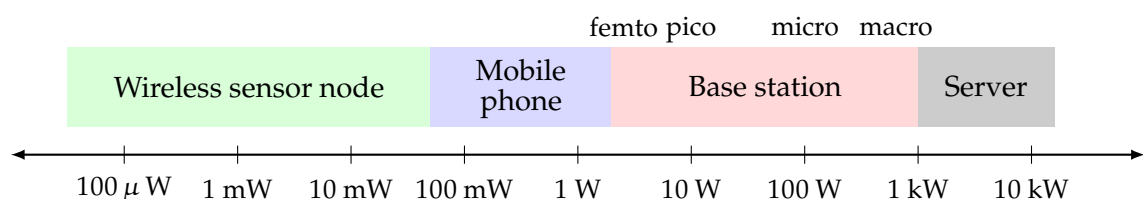
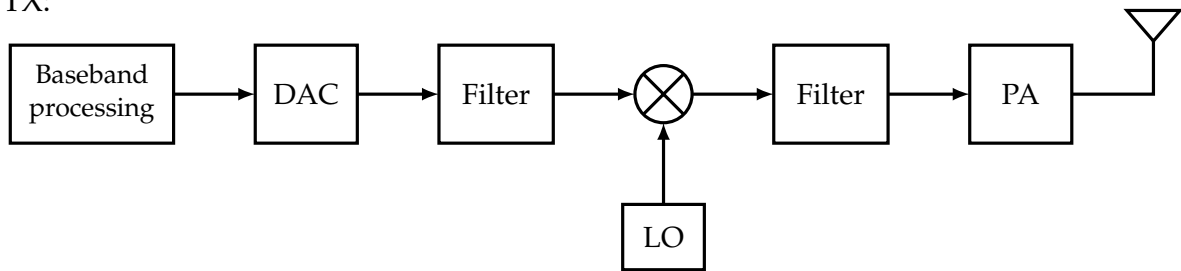


Fig. 2.2: Power consumption of communication devices and facilities

While low-power and energy efficient design has always been stressed in wireless sensor nodes and networks, the trend of green communication calls for similar efforts to be done for mobile terminals, base stations, and also data centers. This means all blocks in Fig. 2.2 shall be shifted leftwards in the future. As mentioned before, we focus in this dissertation on component and link level energy efficient designs, which requires power consumption models on a component-wise basis. Due to the wide deployment of wireless local area networks as well as the ever-shrinking size of cells in a cellular network, wireless communications over short distances have become very common nowadays. As one of the consequences, power consumption incurred by the circuits of the transceivers becomes non-negligible and even dominant in the total power consumption of the system [29,36], and therefore has to be taken into account by the power consumption model.

TX:



RX:

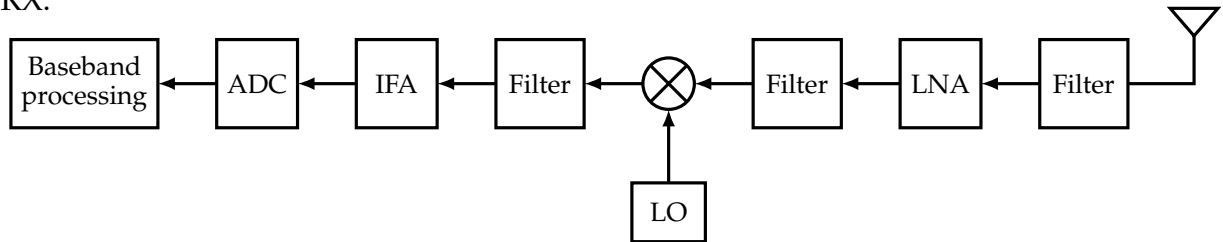


Fig. 2.3: Block diagram of a wireless transceiver

The block diagram of a wireless transceiver is shown in Fig. 2.3. The transmitting signal path includes a digital-to-analog converter (DAC) to convert the baseband signal, a local oscillator (LO) used with a mixer to modulate the signal, and a power amplifier (PA) to drive the transmit antenna. On the receiving path, the filtered receive signal is amplified by the low noise amplifier (LNA), down converted by the LO and an intermediate frequency amplifier (IFA), and then converted to digital format by the analog-to-digital converter (ADC) to enable baseband processing. Multiple transmit and receive filters are employed to confine the signal to the desired frequency bands.

For the transmitting mode, the power consumption of the system is conventionally taken as the radiated power. Limited in efficiency, the power consumption of the power amplifier is usually much larger than the actual radiated power. Other components in the RF front end also consumes power [37], the total amount of which becomes considerably large for a multi-antenna system. For the receiving mode, we address in particular the power consumption of the A/D converter as it is believed to play a critical role in future wireless technologies [38]. Power consumption of other components in the RF front end shall be modeled as a constant. Baseband processing, including digital filtering, channel encoding/decoding, channel estimation, FFT/IFFT for multicarrier systems *etc*, is carried

out by a digital signal processor (DSP). The power consumption of the DSP consists of a dynamic part and a static part [39]. While the two parts both depend on the supply voltage, the dynamic part is proportional to the operating frequency whereas the static part is proportional to the leakage current which is expected to increase as the geometry of the chip shrinks [40]. How much does baseband processing contribute to the total power consumption of the system depends on the complexity of the processing tasks *e.g.* the equalization and decoding algorithms. In [29], the increasing power share of baseband processing in base stations for smaller cells is indicated.

2.3 Trade-off between Spectral Efficiency and Energy Efficiency

Due to the scarcity of RF spectrum, the efficiency in spectral usage has been a major design goal and performance metric of wireless communication systems. Defined as the ratio between channel capacity or achievable data rate and the transmission bandwidth, spectral efficiency of the AWGN channel with input power p_{tx} can be given as

$$\eta_B = \frac{C}{B} = \log_2 \left(1 + \frac{p_{\text{tx}}}{BN_0} \right) \quad \text{in bit/sec/Hz.} \quad (2.8)$$

Note that η_B still depends on the bandwidth through the noise power. Recall that the energy efficiency is expressed as

$$\eta_E = \frac{C}{P} = \frac{B \log_2 \left(1 + \frac{p_{\text{tx}}}{BN_0} \right)}{P} \quad (2.9)$$

where P is a function of p_{tx} . Keeping B constant and varying p_{tx} , we obtain and illustrate the relation between η_B and η_E in Fig. 2.4 for the cases $P = p_{\text{tx}}$ and $P = p_{\text{tx}} + 1$. In the former case, η_E decreases monotonically in η_B , which is to say, the two metrics conflict with each other and the improvement in one leads inevitably to the deterioration of the other. In the latter case where the power consumption of the system consists of the transmit power and an additional constant term which results from the circuit power, the energy efficiency is no longer monotonic in the spectral efficiency but has a maximum which can be determined according to

$$C_{p_{\text{tx}}} P - C P_{p_{\text{tx}}} = 0. \quad (2.10)$$

With $P = p_{\text{tx}} + 1$ and $B = N_0 = 1$, the solution of (2.10) is $p_{\text{tx}}^* = e - 1$ which leads to $\eta_B = \log_2 e = 1.4427$ and $\eta_E = \log_2(e)/e = 0.5307$, as can be seen in the figure. For $p_{\text{tx}} < e - 1$, increasing p_{tx} improves η_E and η_B simultaneously, whereas for $p_{\text{tx}} \geq e - 1$, increased transmit power results in better η_B but lessened η_E .

The analysis above is based on the adaptation of the transmit power in a generic setting and addresses in a straightforward way the importance of taking circuit power into account when energy efficiency is under consideration. The trade-off between spectral and energy efficiency is commonly recognized in communication systems as dictated by various parameters on different protocol layers [41, 42]. We give two more examples in the following.

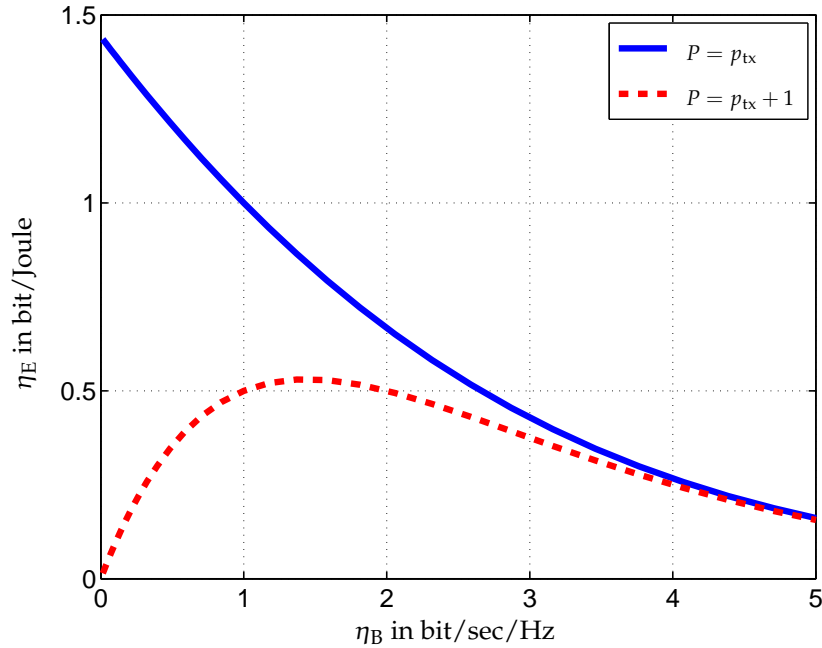


Fig. 2.4: Trade-off between spectral and energy efficiency for the AWGN channel, $B = 1$ Hz, $N_0 = 1$ Watt/Hz

2.3.1 Adaptation of the ADC resolution

In digital communication systems, the received analog signal is sampled and quantized into discrete-time, discrete-valued signals for the subsequent digital processing. This procedure is known as the analog-to-digital conversion. The precision with which the receiver is able to access the received signal has a direct impact on the channel capacity as well as the power dissipation of the receiver. The important role that the A/D converter plays has been realized and drawn a lot of research attention in recent years. It has been reported [43] that the ADC consumes a significant amount of power when operating at high sampling rate and high resolution, hence becoming a bottleneck in system performance. This gives rise to investigations on employing low-precision, in particular 1-bit A/D conversion at the receiver *e.g.* [44,45]. Noticing the trade-off between quantization loss and the power dissipation controlled by the ADC resolution, we take a different perspective and allow the ADC resolution to be adjustable. In the following, we introduce first a capacity lower bound of the quantized channel as dependent on the ADC resolution, and then the relation between the power consumption of the receiver and the ADC resolution. These results are revealed by previous works [43,46,47], and we abstract and review the parts that constitute our model.

2.3.1.1 Capacity lower bound of the quantized SISO channel

With a single receive antenna, the receiver is equipped with two A/D converters to digitize the input analog signal, one for the real part and the other for the imaginary. We let $x \in \mathbb{C}$ be the transmitted symbol with normalized power, and consider only large-scale fading of the wireless communication channel. The channel output $y \in \mathbb{C}$

before quantization is given as

$$y = \sqrt{\alpha}x + n, \quad (2.11)$$

where $\alpha \in \mathbb{R}^+$ denotes the receive signal power, and $n \in \mathbb{C}$ is the i.i.d. zero-mean circularly symmetric complex Gaussian (ZMCCG) noise with variance σ^2 . We assume that both A/D converters act as scalar quantizers and employ b bits to represent each sample of their input signal. In a practical scenario b is an integer with an upper limit, i.e. $b \in \{0, 1, \dots, b_{\max}\}$ where b_{\max} is the maximal number of bits that the ADC could use for a single sample. In the theoretical analysis we often assume real-valued b which, in a continuous-time model, can always be realized via time-sharing of integer-valued resolutions. The quantized output, still given in the form of a complex number, can be written as

$$r = y + q \quad (2.12)$$

where q stands for the quantization error. Intuitively, the higher the bit resolution, the less the quantization error and hence the larger mutual information between channel input and the quantized output. We depict the system diagram in Fig. 2.5.

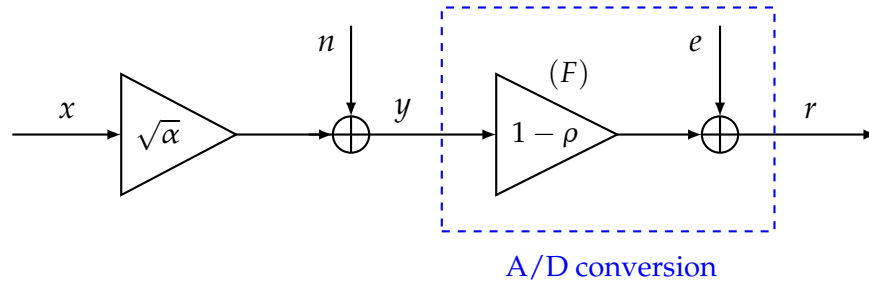


Fig. 2.5: Communication over a quantized SISO channel

The quantization operation is in general nonlinear, and the resulting quantization error is correlated with the input signal. The Bussgang theorem [46, 48] suggests a decomposition of the output of the nonlinear quantizer into a desired signal part and an uncorrelated distortion, which provides us with a convenient analytical approach to formulating the quantization operation. To this end, we write the quantized output r as

$$r = Fy + e, \quad (2.13)$$

where the noise e is uncorrelated with the receive signal y , and the linear operator F is taken as the MMSE estimator of r from y :

$$F = \mathbb{E} [ry^*] \mathbb{E} [|y|^2]^{-1}. \quad (2.14)$$

Consequently, we have

$$r = F(\sqrt{\alpha}x + n) + e = \sqrt{\alpha}Fx + Fn + e \triangleq h'x + n' \quad (2.15)$$

where the effective channel h' , the effective noise n' and its variance are given respectively by

$$h' = \sqrt{\alpha}F, \quad (2.16)$$

$$n' = Fn + e, \quad \mathbb{E} [|n'|^2] = \sigma^2 |F|^2 + \mathbb{E} [|e|^2]. \quad (2.17)$$

Note that the effective noise n' is not necessarily Gaussian. As a result, if we define a new single-input single-output (SISO) channel with the input-output relation $r_G = h'x + n_G$ and assume that $E[|n_G|^2] = E[|n'|^2]$, then the capacity of the new channel provides a lower bound on that of the quantized channel, for Gaussian distributed noise minimizes the mutual information [49]. Based on this observation and assuming that the channel input x is Gaussian distributed, we have

$$I(x; r) \geq \log_2 \left(1 + \frac{|h'|^2}{E[|n'|^2]} \right) = \log_2 \left(1 + \frac{\alpha |F|^2}{\sigma^2 |F|^2 + E[|e|^2]} \right). \quad (2.18)$$

Apparently, the key to computing this lower bound lies in the calculation of F and $E[|e|^2]$, where both terms are expected to be dependent on the bit resolution b .

We let ρ denote the inverse of the signal-to-quantization-noise ratio (SQR), and call it the *distortion factor*. For the quantization of y as given in (2.12), we have

$$\rho = \frac{E[|q|^2]}{E[|y|^2]}. \quad (2.19)$$

When the scalar quantizers are designed to minimize the mean distortion, the condition

$$E[rq^*] = 0 \quad (2.20)$$

is fulfilled due to the orthogonality principle¹. Based on this relation, the following results can be established:

$$E[yq^*] = E[(r - q)q^*] = -E[|q|^2] = -\rho E[|y|^2], \quad (2.21)$$

$$E[ry^*] = E[(y + q)y^*] = (1 - \rho) E[|y|^2], \quad (2.22)$$

$$F = E[ry^*] E[|y|^2]^{-1} = 1 - \rho, \quad (2.23)$$

$$E[|e|^2] = E[|r - Fy|^2] = E[|q + \rho y|^2] = \rho(1 - \rho) E[|y|^2]. \quad (2.24)$$

We see from (2.23) and (2.24), that the quantization operation is modeled as the scaling of the receive signal y by one minus the distortion factor, and the addition of an uncorrelated noise with the variance $\rho(1 - \rho) E[|y|^2]$. Plugging these results into the lower bound on mutual information (2.18), we obtain the capacity lower bound C_L (in bit/sec) as

$$C_L = B \log_2 \left(\frac{\sigma^2 + \alpha}{\sigma^2 + \rho \alpha} \right) = B \log_2 \left(\frac{1 + \gamma}{1 + \rho \gamma} \right), \quad (2.25)$$

where $\gamma = \alpha/\sigma^2$ denotes the receive SNR. With $\rho = 0$ *i.e.* there is no quantization error, the function turns into the Shannon capacity formula for the AWGN channel with receive SNR γ . As a lower bound on the true channel capacity, (2.25) is shown to be tight in the low SNR regime (see [46] and also Fig. 3.24).

Given Gaussian distributed channel input x and uncorrelated Gaussian noise n , the channel output y is also Gaussian distributed. For such a quantization source and

¹Note the important assumption here that the real and imaginary parts of the quantizer input are uncorrelated, which allows us to generalize the results for individual A/D converters to the pair of A/D converters that are associated with the single receive antenna.

Table 2.1: Distortion factor ρ for different ADC resolutions b

b	1	2	3	4
ρ	0.3634	0.1175	0.03454	0.009497
b	5	6	7	8
ρ	0.002499	0.0006642	0.0001660	0.00004151

a distortion-minimizing non-uniform scalar quantizer, the distortion factor attains the values given in Table 2.1 with respect to different bit resolutions [50]. The asymptotic approximation $\rho = \frac{\pi\sqrt{3}}{2} \cdot 2^{-2b}$ is almost accurate for $b > 5$ [51], while for smaller b it tends to be too pessimistic. For the analytical studies we shall use the simple approximation $\rho \approx 2^{-2b}$, which captures the tendency of variation as well as the asymptotic behavior. The resulting capacity lower bound formula is given as

$$C_L = B \log_2 \left(\frac{1 + \gamma}{1 + \gamma \cdot 2^{-2b}} \right). \quad (2.26)$$

2.3.1.2 Power consumption of the receiver

We employ a generic power consumption model for the wireless receiver which mainly addresses the impact of the ADC and other processing units. Power dissipation of the ADC depends heavily on its architecture and design. In the performance evaluation and comparison of different A/D converters, a common figure of merit (FOM) is the energy per conversion step metric which is given as [43, 47]

$$\text{FOM} = \frac{P_{\text{ADC}}}{f_s \cdot 2^{\text{ENOB}}}, \quad (2.27)$$

where P_{ADC} denotes the power dissipation of the ADC, f_s is the sampling frequency, and ENOB stands for the effective number of bits which is dependent on the signal-to-noise-and-distortion ratio. This FOM is defined to address the energy efficiency of A/D converters, and is suited for medium-to-high bit resolutions where thermal noise is not the primary limiting factor. Assuming a pair of ideal ADCs which operate at Nyquist frequency and with low-to-medium bit resolutions, we take FOM as a constant and replace ENOB with b in (2.27) to obtain the following power consumption model:

$$P_{\text{ADC}} = 2 \cdot \text{FOM} \cdot (2B) \cdot (2^b - 1) = a_1(2^b - 1), \quad (2.28)$$

where the scaling of 2 is due to the two ADCs employing the same bit resolution, and the replacement of 2^b with $2^b - 1$ is to ensure zero power dissipation for zero bit resolution. With constant signal bandwidth B , the parameter a_1 is also a constant.

Other sources of power consumption of the receiver include: components in the receive RF chain such as the low-noise amplifier, the mixer, and the receive filters, baseband processing such as channel estimation and decoding, and other control signaling and feedback. The overall contribution of these components and functional tasks are modeled by a positive constant a_0 . Similar to the transmit side, we assume a_0 is

only effective when the receiver is in active mode indicated by a positive bit resolution. In the sleep mode, the receiver does not consume any power. To this end, we give the power consumption function of the receiver as

$$P = \begin{cases} a_1(2^b - 1) + a_0, & b > 0, \\ 0, & b = 0. \end{cases} \quad (2.29)$$

The ratio a_0/a_1 reflects partially how important it is to count the ADC power. In practice, which part of the receiver contributes the most to the total power consumption depends on the choices of the components and the specific design *e.g.* how complex the decoding process is. Note that the model (2.29) is rather generic where only the ADC power is detailed. For other optimization scenarios or purposes of system analysis, measurements from practical systems and more thorough modeling of the individual components could be necessary.

Based on (2.26) and (2.29), the relation between $\eta_B = C_L/B$ and $\eta_E = C_L/P$ is computed and illustrated in Fig. 2.6(a), where b is taken as a real number which increases along the curves from left to right, and B is kept constant. The energy efficiency is maximized at a certain bit resolution b^* which depends on the values of a_0 , a_1 , and γ . In Fig. 2.6(b) we find b^* to be increasing with γ , meaning that higher resolution is in favor when the channel condition is improved. Detailed derivation and analysis of b^* can be found in Section 3.4.1. Note from Fig. 2.6(a) that the energy efficiency drops rapidly after the peak value since further increasing the bit resolution does not lead to much improvement of the achievable rate but results in exponential growth of the power consumption. The indication is therefore, that by sacrificing a small amount in spectral efficiency, significant improvement can be achieved in energy efficiency. Similar to the transmit power, the ADC resolution can be adapted based on the channel and the circuit power conditions, so as to achieve the desirable operation point on the spectral-energy efficiency curve.

2.3.2 Optimization of training-based systems

In wireless communications, having the channel state information (CSI) can greatly improve the performance of communication systems: it enables coherent detection at the receiver and adaptive transmission at the transmitter. An efficient method for the receiver to learn the time-varying channel is through the employment of a training sequence: part of each transmission interval is devoted to sending *pilot symbols* which are known a priori by the receiver and hence enable estimation of the channel coefficients [52]. Depending on its position in the interval, the training sequence can be called as *preamble*, *midamble*, or *postamble*. We consider the preamble case in the sequel, *i.e.* the pilot symbols are sent at the beginning of each transmission interval as shown in Fig. 2.7. How much resources in terms of time and power should be allocated for training has been investigated in a number of works. In [53], the authors consider the training and channel estimation for a multiple-input multiple-output (MIMO) system, and maximize a lower bound on the capacity with respect to the training parameters. In [54], an energy efficiency perspective is taken and training schemes which minimize the energy cost per transmitted information bit are proposed. The basic trade-off in these systems is that

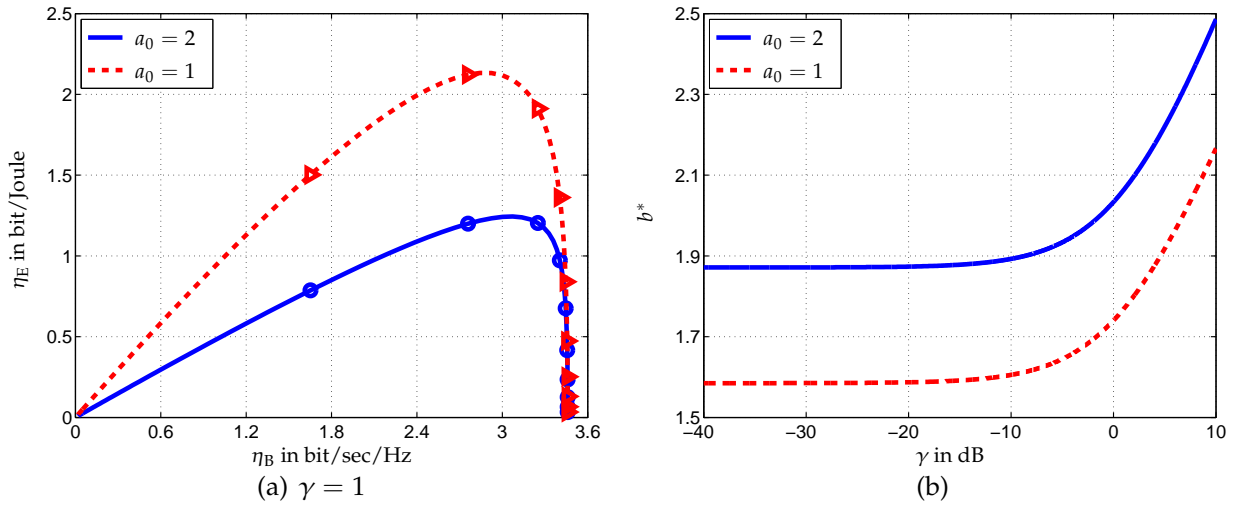


Fig. 2.6: (a) Trade-off between η_B and η_E as governed by the ADC resolution, markers represent points where integer resolutions are employed; (b) Energy efficiency maximizing bit resolution as dependent on the receive SNR, $B = 1$ Hz, $a_1 = 0.1$ Watt

while the resources allocated to the training phase improves the quality of the channel estimation, they are taken away from transmitting the actual information data. Our study here is based on the same consideration but focuses on the effect of quantization of the pilot and data symbols at the receiver, and addresses the trade-off between spectral and energy efficiency governed by the bit resolution as well as the training length in a SISO system. The work can be readily extended to SIMO and MIMO systems and include more design variables [55].

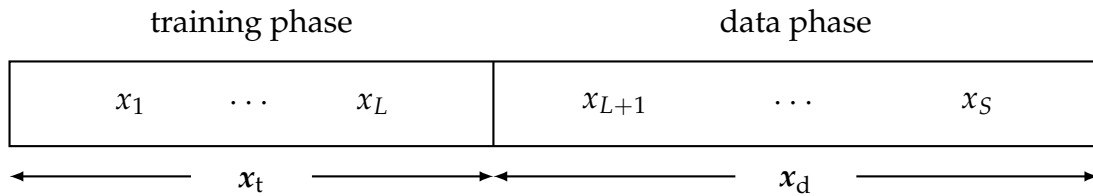


Fig. 2.7: Block structure for a training-based system

The system diagram is still given by Fig. 2.5, and we assume that the channel undergoes block fading with the block length of S symbols. The training phase makes use of the first L symbols in each block for sending pilots, where $1 \leq L < S$ should be satisfied to guarantee the feasibility of channel estimation and data transmission. We let $\mathbf{x}_t = [x_1 \cdots x_L]^T \in \mathbb{C}^L$ be the vector of pilot symbols and $\mathbf{y}_t \in \mathbb{C}^L$ be the vector of received pilots which is given as

$$\mathbf{y}_t = \sqrt{\gamma} h \mathbf{x}_t + \mathbf{n}_t, \quad (2.30)$$

where γ is the average receive SNR, $h \sim \mathcal{CN}(0, 1)$ denotes the channel coefficient, and $\mathbf{n}_t \in \mathbb{C}^L$ is the collection of noise samples during the training phase. The average power of the pilot symbols and the noise are both normalized to have the notations as concise as

possible. The received pilots are sampled, quantized with the bit resolution b , and then used for channel estimation. The quantization operation can be modeled as

$$\mathbf{r}_t = (1 - \rho)\mathbf{y}_t + \mathbf{e}_t, \quad (2.31)$$

where ρ is the distortion factor corresponding to b , and the noise vector \mathbf{e}_t is uncorrelated with \mathbf{y}_t and has the covariance matrix

$$\mathbf{R}_{ee} = \mathbb{E}[\mathbf{e}\mathbf{e}^H] = \rho(1 - \rho) \text{diag}(\mathbf{R}_{yy}). \quad (2.32)$$

Assuming linear minimum mean squared error (LMMSE) estimator $\mathbf{g} \in \mathbb{C}^L$ at the receiver, we compute the channel estimate \hat{h} based on the orthogonality principle as

$$\hat{h} = \mathbf{g}^H \mathbf{r}_t = \mathbf{R}_{hr} \mathbf{R}_{rr}^{-1} \mathbf{r}_t, \quad (2.33)$$

$$\mathbf{R}_{hr} = \mathbb{E}[h \mathbf{r}_t^H] = (1 - \rho)\sqrt{\gamma} \mathbf{x}_t^H, \quad (2.34)$$

$$\mathbf{R}_{rr} = \mathbb{E}[\mathbf{r}_t \mathbf{r}_t^H] = (1 - \rho) \left[(1 - \rho)\gamma \mathbf{x}_t \mathbf{x}_t^H + \rho\gamma \text{diag}(\mathbf{x}_t \mathbf{x}_t^H) + \mathbf{I}_L \right]. \quad (2.35)$$

The variances of \hat{h} and of the estimation error $\tilde{e} = h - \hat{h}$ are calculated respectively as

$$\begin{aligned} \mathbb{E}[|\hat{h}|^2] &= \mathbf{R}_{hr} \mathbf{R}_{rr}^{-1} \mathbf{R}_{hr}^H = (1 - \rho)\gamma \mathbf{x}_t^H \left((1 - \rho)\gamma \mathbf{x}_t \mathbf{x}_t^H + \mathbf{Z} \right)^{-1} \mathbf{x}_t \\ &= \mathbf{x}_t^H \mathbf{Z}^{-1} \mathbf{x}_t \left(\frac{1}{(1 - \rho)\gamma} + \mathbf{x}_t^H \mathbf{Z}^{-1} \mathbf{x}_t \right)^{-1}, \end{aligned} \quad (2.36)$$

$$\mathbb{E}[|\tilde{e}|^2] = \mathbb{E}[|h|^2] - \mathbb{E}[|\hat{h}|^2] = \left(1 + (1 - \rho)\gamma \mathbf{x}_t^H \mathbf{Z}^{-1} \mathbf{x}_t \right)^{-1}, \quad (2.37)$$

where $\mathbf{Z} = \rho\gamma \text{diag}(\mathbf{x}_t \mathbf{x}_t^H) + \mathbf{I}_L$ and the matrix inversion lemma [56] is applied to obtain (2.36). Noting that \mathbf{Z} is a diagonal matrix, we have

$$\mathbf{Z}^{-1} = \text{diag} \left\{ \frac{1}{1 + \rho\gamma|x_i|^2} \right\}_{i=1}^L, \quad \mathbf{x}_t^H \mathbf{Z}^{-1} \mathbf{x}_t = \sum_{i=1}^L \frac{|x_i|^2}{1 + \rho\gamma|x_i|^2}. \quad (2.38)$$

In order to minimize the variance of the estimation error, we need to maximize $\mathbf{x}_t^H \mathbf{Z}^{-1} \mathbf{x}_t$ given fixed ρ and γ . The arithmetic mean of a set of positive numbers a_i , $i = 1, \dots, n$ is known to be no smaller than their harmonic mean, the relation of which can be given as

$$\frac{n}{\sum_{i=1}^n \frac{1}{a_i}} \leq \frac{1}{n} \sum_{i=1}^n a_i, \quad (2.39)$$

where the equality sign holds if and only if all a_i are identical [57]. This result helps us obtain a lower bound on $\mathbb{E}[|\tilde{e}|^2]$ as

$$\begin{aligned} \mathbf{x}_t^H \mathbf{Z}^{-1} \mathbf{x}_t &= \sum_{i=1}^L \frac{|x_i|^2}{1 + \rho\gamma|x_i|^2} = \sum_{i=1}^L \frac{1}{\rho\gamma} \left(1 - \frac{1}{1 + \rho\gamma|x_i|^2} \right) \\ &\leq \frac{L}{\rho\gamma} \left(1 - \frac{L}{L + \rho\gamma \|\mathbf{x}_t\|^2} \right) = \frac{L}{1 + \rho\gamma}, \end{aligned} \quad (2.40)$$

$$\mathbb{E}[|\tilde{e}|^2] \geq \left(1 + \frac{(1 - \rho)\gamma L}{1 + \rho\gamma} \right)^{-1} = \frac{1 + \rho\gamma}{1 + \rho\gamma + (1 - \rho)\gamma L}, \quad (2.41)$$

where the equality sign in (2.41) is achieved when $|x_1| = \dots = |x_L|$, *i.e.* having all pilot symbols of the same norm minimizes the MSE of channel estimation. The corresponding variance of the channel estimate is given as

$$\mathbb{E}[|\hat{h}|^2] = \frac{(1-\rho)\gamma L}{1+\rho\gamma+(1-\rho)\gamma L}. \quad (2.42)$$

The received data symbols before and after quantization, both stacked into column vectors of dimension $S-L$, can be written respectively as

$$\mathbf{y}_d = \sqrt{\gamma}(\hat{h} + \tilde{e}) \mathbf{x}_d + \mathbf{n}_d, \quad (2.43)$$

$$\mathbf{r}_d = \sqrt{\gamma}(1-\rho)\hat{h} \mathbf{x}_d + \sqrt{\gamma}(1-\rho)e \mathbf{x}_d + (1-\rho)\mathbf{n}_d + \mathbf{e}_d, \quad (2.44)$$

where \mathbf{x}_d and \mathbf{n}_d are the transmitted data symbols and the corresponding additive noise samples with $\mathbb{E}[\mathbf{x}_d \mathbf{x}_d^H] = \mathbb{E}[\mathbf{n}_d \mathbf{n}_d^H] = \mathbf{I}_{S-L}$. In the quantized receive data vector \mathbf{r}_d , we consider $\sqrt{\gamma}(1-\rho)\hat{h} \mathbf{x}_d$ as the signal part, and the remaining summation $\mathbf{n}' = \sqrt{\gamma}(1-\rho)\tilde{e} \mathbf{x}_d + (1-\rho)\mathbf{n}_d + \mathbf{e}_d$ as additive Gaussian noise. To this end, the *effective instantaneous SNR* is computed as

$$\Gamma = \frac{\mathbb{E}\left[|\sqrt{\gamma}(1-\rho)\hat{h} x_{d,i}|^2 |\hat{h}|\right]}{\mathbb{E}\left[|\sqrt{\gamma}(1-\rho)\tilde{e} x_{d,i}|^2\right] + \mathbb{E}\left[|(1-\rho)n_{d,i}|^2\right] + \mathbb{E}\left[|e_{d,i}|^2 |\hat{h}|\right]} \quad (2.45)$$

$$\begin{aligned} &= \frac{\gamma(1-\rho)|\hat{h}|^2}{\gamma(1-\rho)\mathbb{E}[|\tilde{e}|^2] + (1-\rho) + \rho(\gamma|\hat{h}|^2 + \gamma\mathbb{E}[|\tilde{e}|^2] + 1)} \\ &= \frac{\gamma(1-\rho)|\hat{h}|^2}{\gamma\mathbb{E}[|\tilde{e}|^2] + 1 + \gamma\rho|\hat{h}|^2}. \end{aligned} \quad (2.46)$$

By using the results of (2.41), (2.42) and replacing \hat{h} with an auxiliary random variable w according to

$$\hat{h} = \sqrt{\mathbb{E}[|\hat{h}|^2]} \cdot w, \quad w \sim \mathcal{CN}(0, 1), \quad (2.47)$$

we further write the effective instantaneous SNR as

$$\Gamma = \frac{L\gamma^2(1-\rho)^2|w|^2}{(1+\gamma)(1+\rho\gamma) + L(1-\rho)\gamma + L\gamma^2\rho(1-\rho)|w|^2}. \quad (2.48)$$

With B denoting the transmission bandwidth, the ergodic channel capacity in bit/sec achieved during the data transmission phase is lower bounded by

$$C_{L,d} = \mathbb{E}\left[B \log_2(1 + \Gamma)\right]. \quad (2.49)$$

A further analysis of $C_{L,d}$ can be found in Appendix A1. The reason that (2.49) is a capacity lower bound is as follows:

- the channel estimation error \tilde{e} is treated as random noise, while it stays constant during each block and changes independently only from block to block;
- the aggregate noise term \mathbf{n}' is taken as Gaussian which is not necessarily true, especially since the additive noise e introduced by quantization is not necessarily Gaussian;

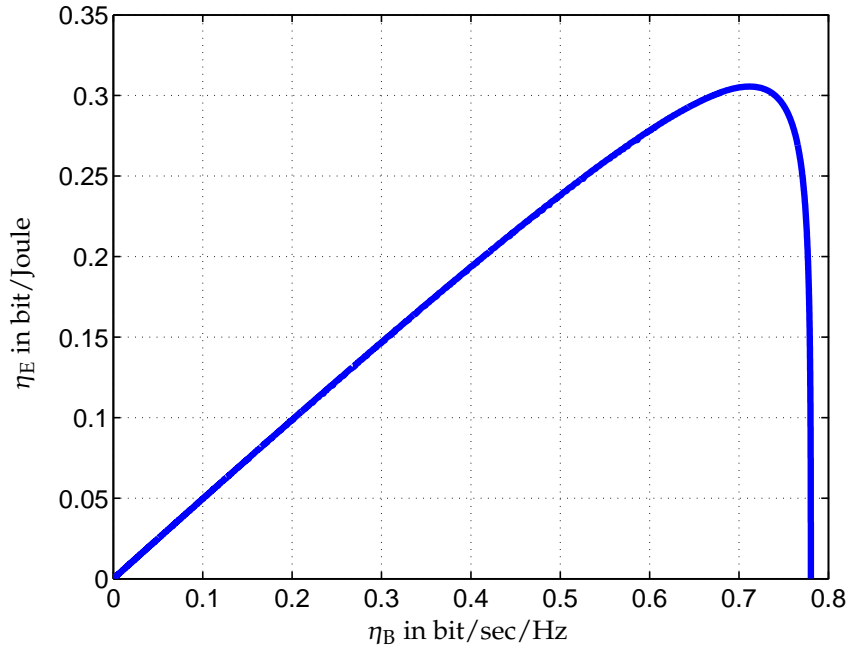


Fig. 2.8: Trade-off between spectral and energy efficiency for the training based system, $B = 1$ Hz, $\gamma = 1$, $a_0 = 2$ Watt, $a_1 = 0.1$ Watt, $S = 1000$

Consequently, what we have considered is the worst case scenario which leads to a lower bound on the channel capacity. Note that in the above derivations, the transmit power and the ADC resolution employed for the training and data phases are assumed the same, which is practically more robust but may not be the optimum design.

We regard the energy consumption of the receiver as the cost of the system, and adapt b and L with fixed average receive SNR. This may address the situation where energy efficiency is not a major concern of the transmitter, or where the transmitter has a strict transmit power constraint. To this end, the spectral and energy efficiency of the system are computed as

$$\eta_B = \frac{(S - L) E[\log_2(1 + \Gamma)]}{S}, \quad \eta_E = \frac{B(S - L) E[\log_2(1 + \Gamma)]}{S(a_1(2^b - 1) + a_0)}. \quad (2.50)$$

Their relation is illustrated in Fig. 2.8 for the SNR $\gamma = 1$. Each pair of ADC resolution and training length corresponds to a point on the η_B - η_E graph, and we show in the figure the boundary of these points in which different resolutions and training lengths are involved. Similar to Fig. 2.6(a), η_E shows a rapid decrease after its peak value is reached. In Fig. 2.9 we show the ADC resolution and the training length that jointly maximize the energy efficiency with respect to the average SNR. In comparison with Fig. 2.6(b), the optimal ADC resolution is not monotonic in γ , but rises up in the very low SNR regime implying the necessity of maintaining the quality of channel estimation in this region. From (2.50), it is clear that for a given b , the training length that maximizes η_E is the one that maximizes η_B as the power consumption is independent of L . In fact, the optimal training length is only slightly larger than the unquantized case for most SNR values [55]. In the very low SNR regime, $L^* \rightarrow S/2$ can be shown which is the same result as obtained by [53] where the imperfection caused by the A/D conversion is not taken into account.

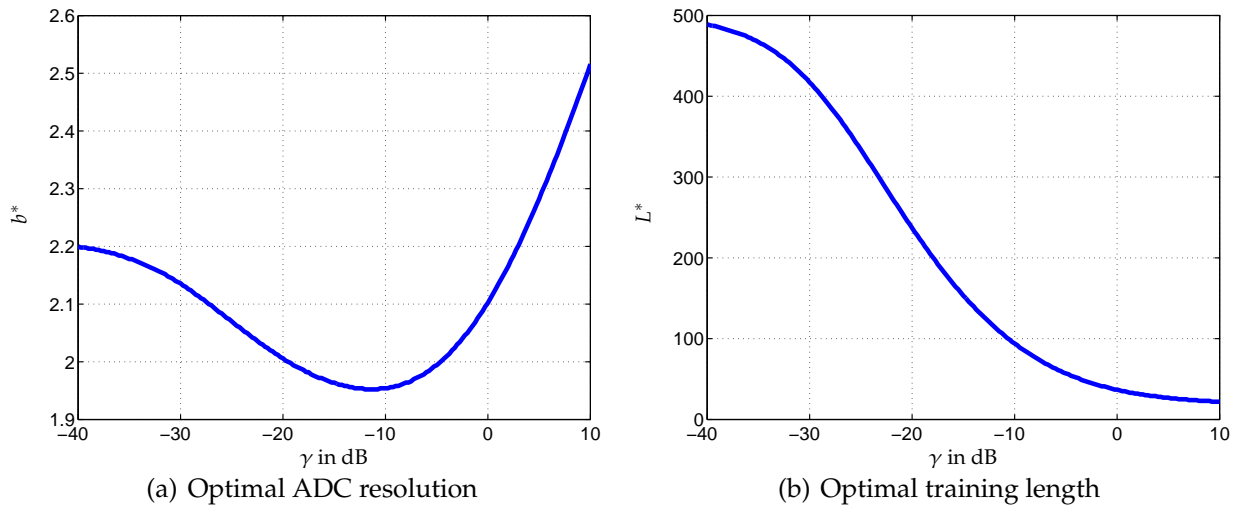


Fig. 2.9: Energy efficiency maximizing ADC resolution and training length as dependent on the average receive SNR, $B = 1$ Hz, $\gamma = 1$, $a_0 = 2$ Watt, $a_1 = 0.1$ Watt, $S = 1000$

2.4 Trade-off between Energy Efficiency and Bandwidth

In the above analysis, the bandwidth B is kept as a constant. From (2.4) we notice that, if B is variable and p_{tx} is kept constant instead, the energy per bit metric is a monotonically decreasing function of B with its minimum achieved when $B \rightarrow +\infty$. On the other hand, if the system has a minimum data rate requirement, the bandwidth that is needed to fulfill it can be determined for any given transmit power, and the corresponding energy efficiency can be computed. For the AWGN channel, trade-off curves between

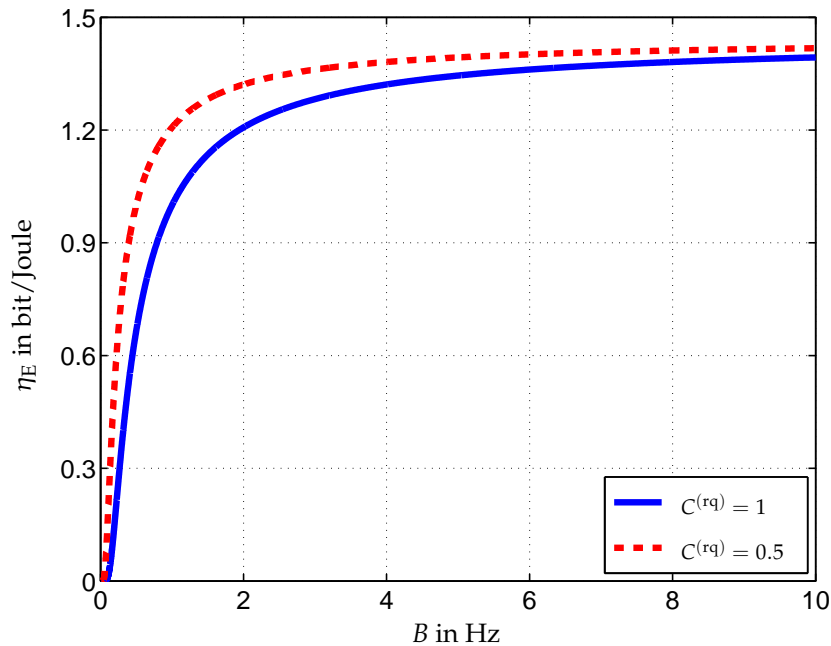
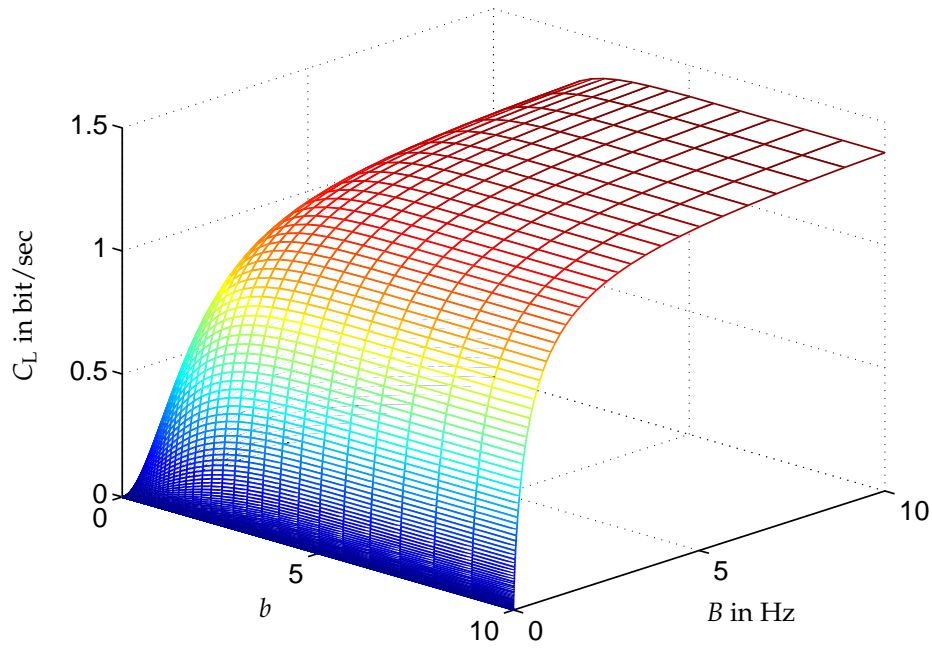
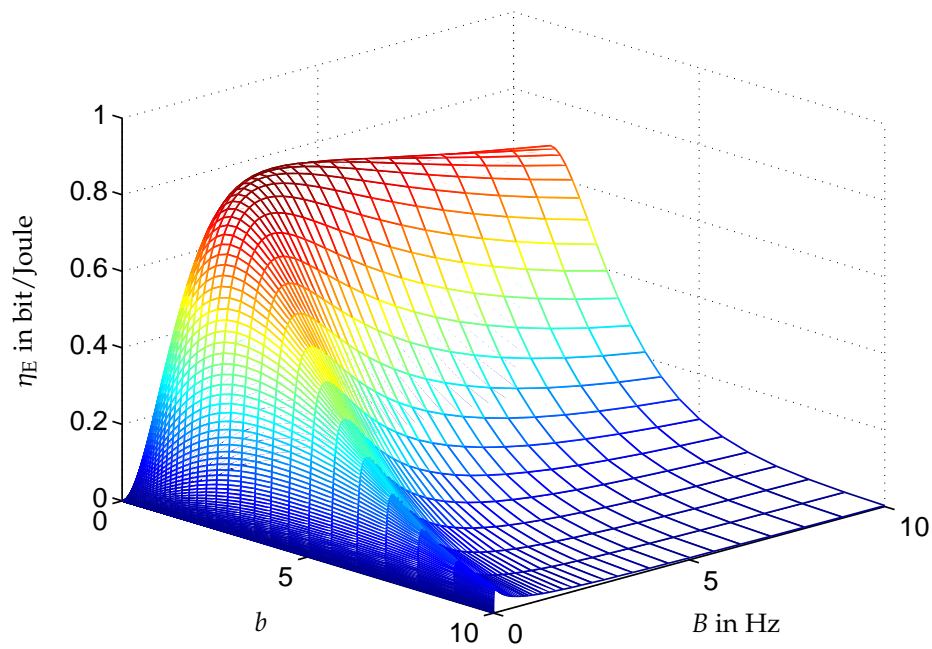


Fig. 2.10: Trade-off between energy efficiency and bandwidth for the AWGN channel, $C^{(\text{rq})}$ is in bit/sec, $P = p_{\text{tx}}$, $N_0 = 1$ Watt/Hz



(a) Capacity lower bound



(b) Energy efficiency

Fig. 2.11: Capacity lower bound and energy efficiency of a receiver as dependent on the ADC resolution b and the bandwidth B , $a_0 = 1$ Watt, $\tilde{a}_1 = 0.05$ Watt/Hz, $\gamma = 1/B$

energy efficiency and the bandwidth are obtained for the power function $P = p_{\text{tx}}$ and illustrated in Fig. 2.10. With decreasing p_{tx} , the energy efficiency is enhanced but the required bandwidth increases as well, leading to a monotonic relation between η_E and B . As $p_{\text{tx}} \rightarrow 0$, we have $B \rightarrow +\infty$ and η_E converge to its maximal of $1/(N_0 \ln 2)$ irrespective of the data rate requirement. This trade-off can be formulated equivalently as the trade-off between transmit power and bandwidth [58,59]. The implication is that the energy efficiency can be improved, or power can be saved, at the expense of using a larger bandwidth which may be infeasible due to regulations or introduce interference into the system.

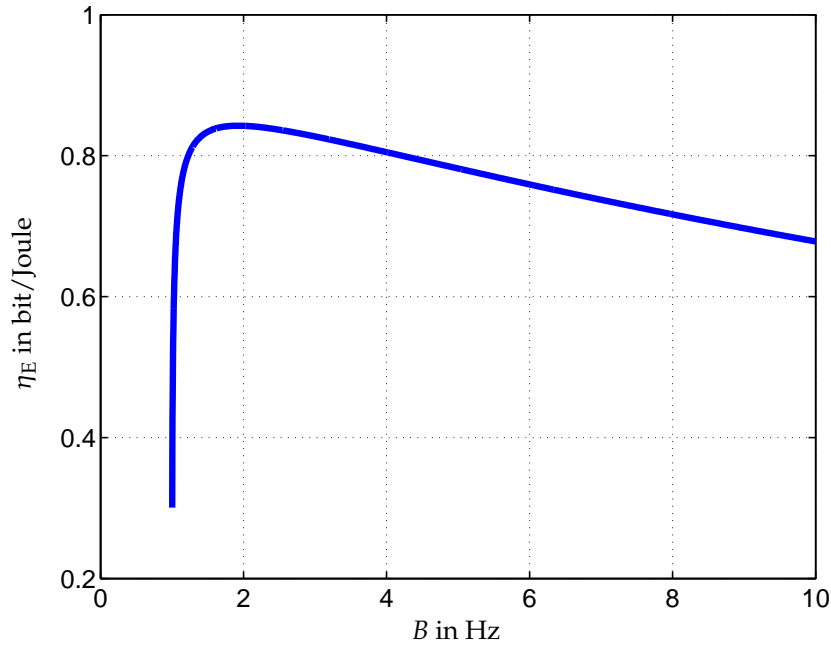


Fig. 2.12: Trade-off between energy efficiency and bandwidth of a receiver, $a_0 = 1$ Watt, $\tilde{a}_1 = 0.05$ Watt/Hz, $\gamma = 1/B$, $R^{(\text{rq})} = 1$ bit/sec

However, the power consumption of the system can be also dependent on the bandwidth. An example at hand would be the power consumption model of the A/D converter as given in (2.28). To this end, by purely adapting B we can obtain a trade-off curve between the spectral and energy efficiency in the same way as we adapt the transmit power or the ADC resolution. On the other hand, for systems with data rate constraints, we can adapt other parameters of the system and find the required bandwidth likewise the resulting energy efficiency, as described above. To elaborate on this, we define $\tilde{a}_1 = 4\text{FOM}$ and consider the rate and power models of the receiver which have been introduced before:

$$C_L = B \log_2 \left(\frac{1 + \gamma}{1 + \gamma \cdot 2^{-2b}} \right), \quad P = \tilde{a}_1 B (2^b - 1) + a_0 \quad \text{for } b > 0, \quad (2.51)$$

and illustrate C_L , η_E as functions of b , B in Fig. 2.11. The capacity lower bound C_L increases monotonically and is concave in both parameters b and B , yet it is not jointly concave in them as a calculation of the determinant of the Hessian matrix reveals. The surface of energy efficiency η_E exhibits rather irregular shape but has a global maximum.

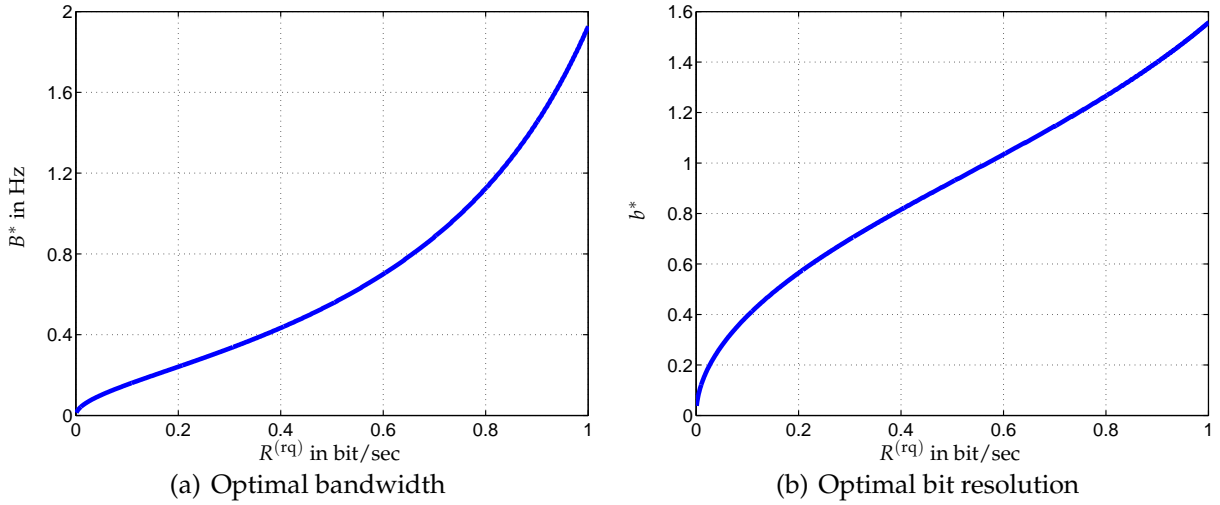


Fig. 2.13: Energy efficiency maximizing bandwidth and ADC resolution as dependent on the data rate requirement, $a_0 = 1$ Watt, $\tilde{a}_1 = 0.05$ Watt/Hz, $\gamma = 1/B$

Assuming a minimum required data rate $R^{(rq)}$ and continuously adaptable ADC resolution b , we compute B and P according to (2.51) for each given b that is large enough to realize $R^{(rq)}$. An exemplary trade-off curve resulting from the procedure is shown in Fig. 2.12. There exists now an optimal bandwidth B^* which maximizes the energy efficiency. For bit resolutions that lead to $B \leq B^*$, bandwidth can be traded off for a rapid increase in energy efficiency. As the bit resolution is further reduced, the required bandwidth increases but the corresponding energy efficiency deteriorates at the same time. The bandwidth and ADC resolution that jointly maximize the energy efficiency are shown in Fig. 2.13 for a range of data rate requirements. As $R^{(rq)}$ increases, the growth of B^* is much faster than b^* due to the linear contribution of bandwidth but exponential contribution of the bit resolution to the power consumption of the system.

2.5 Trade-off between Energy Consumption and Latency

The delay in obtaining the desired information, often called the *latency*, is another important performance metric in communications which is closely related to user experience. For future wireless services where more interactive applications and tactile Internet are prevalent, keeping the latency at an extremely low level can be the most critical design goal. However, reducing the latency in many cases requires more energy consumption of the system, as we introduce in the sequel.

In our derivation of the Shannon limit, we learn that the minimum energy per bit is achieved with p_{tx} approaching zero given fixed bandwidth and $P = p_{tx}$. If a target data volume I is set, using this operation mode leads to the minimum total energy consumption but infinitely long transmission time. We let E (in Joule) be the energy consumption of the transmitter for sending I bits, and let τ (in sec) be the time it takes to

complete the transmission. Assuming constant transmit power over time, we have

$$E = \tau \cdot P(p_{\text{tx}}), \quad \tau = \frac{I}{B \log_2 \left(1 + \frac{p_{\text{tx}}}{BN_0} \right)}. \quad (2.52)$$

If the power consumption function P is convex in p_{tx} , employing constant transmit power is indeed optimal in terms of the overall energy efficiency. We will elaborate on this point in Chapter 3 using the optimal control theory. The relation between E and τ is illustrated in Fig. 2.14 for $I = 100$ bits and normalized B and N_0 . In the case of $P = p_{\text{tx}}$, E decreases monotonically in τ indicating the trade-off between energy consumption and latency for all $p_{\text{tx}} > 0$. In the other case where a constant circuit power term is included, E first decreases and then increases in τ . The valley is reached at $p_{\text{tx}}^* = e - 1$. Further decreasing p_{tx} results in longer transmission time and also larger energy consumption, which is to say, the system should not be operated with $p_{\text{tx}} < p_{\text{tx}}^*$ if possible.

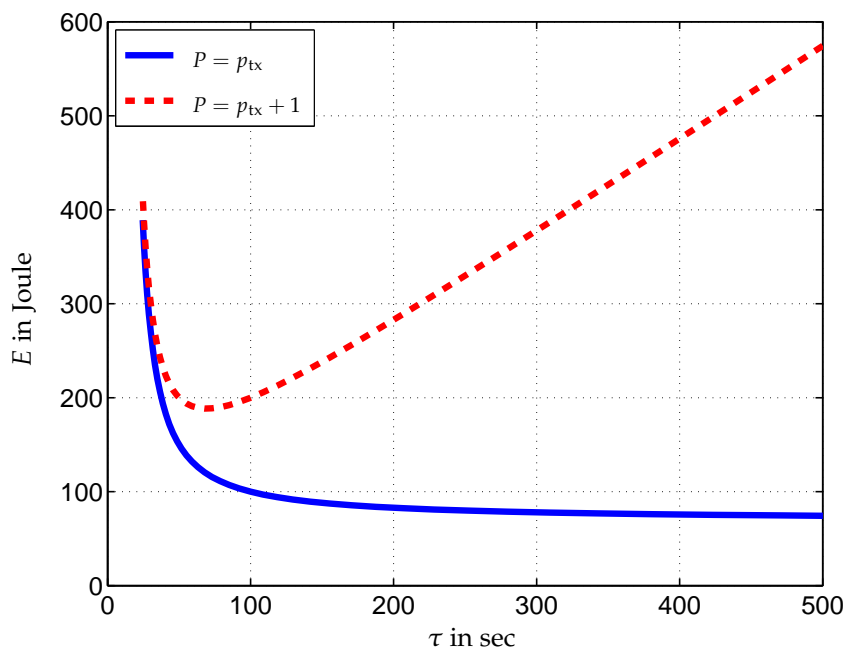


Fig. 2.14: Trade-off between energy consumption and delay for the AWGN channel, $B = 1$ Hz, $N_0 = 1$ Watt/Hz, $I = 100$ bits

When employing the Shannon capacity formula to discuss the system performance, it should be noted that a very long code may be required to actually come close to the channel capacity, which results in a large latency because of decoding. We study in the following, the trade-off between energy consumption and delay with a more realistic model which involves practical modulation and coding schemes [60]. With this model, the latency considered is defined from the perspective of the Medium Access Control (MAC) layer instead of the Physical (PHY) layer.

We consider packet transmission over a block-fading channel. On each *transmission time interval* (TTI), which is the basic signaling unit with a fixed duration smaller than the coherence time of the channel, information bits are coded and encapsulated into packets, and then modulated and sent to the receiver. The receiver attempts

to recover the information via demodulation and decoding, and sends a feedback message to the transmitter. If decoding is successful, the receiver sends a positive acknowledgement (ACK), otherwise it demands packet retransmission by sending a negative acknowledgement (NACK). Upon receiving the retransmission request, the transmitter can either send the same packet again, or send more redundant information *e.g.* parity bits to help the receiver with decoding. The first scheme is called Automatic Repeat reQuest (ARQ), and the second Hybrid ARQ (HARQ) or more precisely, incremental redundancy HARQ. With these error-control methods, reliable data transmission can be realized over an error-prone channel.

We let T_I denote the duration of one TTI, and T_R denote the *round trip delay* which is the time it takes for the transmitter to receive the feedback from the receiver and get ready for the next transmission. The channel condition is assumed to have changed independently over the transmission trials, *i.e.* T_R is larger than the channel coherence time. Let $\pi[m]$ be the packet error probability (PEP) of the m th transmission, $m = 1, 2, \dots$. The probability that it takes exactly m trials to transmit a packet error-free, denoted with $f[m]$, can be calculated as

$$f[1] = 1 - \pi[1], \quad f[m] = (1 - \pi[m]) \prod_{i=1}^{m-1} \pi[i], \quad m = 2, 3, \dots \quad (2.53)$$

The latency τ of a packet is defined as the expected time that is taken until the packet is successfully decoded at the receiver. It can be computed as

$$\tau = \sum_{m=1}^{+\infty} ((m-1)T_R + T_I) f[m]. \quad (2.54)$$

Similarly, letting $E[m]$ be the energy consumption for the m th transmission, we have the expected total energy cost E to convey the packet successfully given as

$$E = \sum_{m=1}^{+\infty} f[m] \left(\sum_{i=1}^m E[i] \right), \quad (2.55)$$

where $E[m] = T_I P(p_{\text{tx}}[m])$ with $p_{\text{tx}}[m]$ denoting the transmit power of the m th transmission and P the power consumption function.

With quadrature amplitude modulated signal and a frequency-flat channel, we apply the *noisy channel coding theorem* [61] to obtain the relation between the PEP and the receive SNR, the modulation order, and the coding rate. Let the modulation alphabet and the coding rate be $\mathcal{M} = \{a_1, \dots, a_M\}$ and R_c respectively. The *cutoff rate* of the channel with receive SNR γ can be expressed as

$$R_0(\gamma, M) = \log_2 M - \log_2 \left[1 + \frac{2}{M} \sum_{i=1}^{M-1} \sum_{j=i+1}^M e^{-\frac{1}{4}|a_j - a_i|^2 \gamma} \right]. \quad (2.56)$$

The noisy channel coding theorem states that there always exists a block code with block length l and binary code rate $R_c \log_2 M \leq R_0(\gamma, M)$ in bit per channel use, such that with maximum likelihood decoding the error probability $\tilde{\pi}$ of a code word satisfies

$$\tilde{\pi} \leq 2^{-l(R_0(\gamma, M) - R_c \log_2 M)}. \quad (2.57)$$

Let N_s be the number of data symbols and I be the number of information bits loaded in one TTI, respectively. With coding rate R_c and modulation order M , we have the relation $N_s \log_2 M = I/R_c = L$ where L denotes the length of the packet. If the packet contains N code words, the PEP can be upper bounded by

$$\pi = 1 - (1 - \tilde{\pi})^N \leq 1 - \left(1 - 2^{-\frac{L}{N}(R_0(\gamma, M) - R_c \log_2 M)}\right)^N. \quad (2.58)$$

We assume that a packet is transmitted with the same power and modulation order for all transmission trials. For the ARQ protocol, the original packet is retransmitted hence the PEP depends only on the channel condition of the corresponding TTI. For the HARQ protocol, new parity bits are sent upon the reception of a NACK, leading to decreasing effective coding rates given as

$$R_c[m] = \frac{1}{m} R_c. \quad (2.59)$$

As a result, the PEP depends also on the number of transmissions that have been taken.

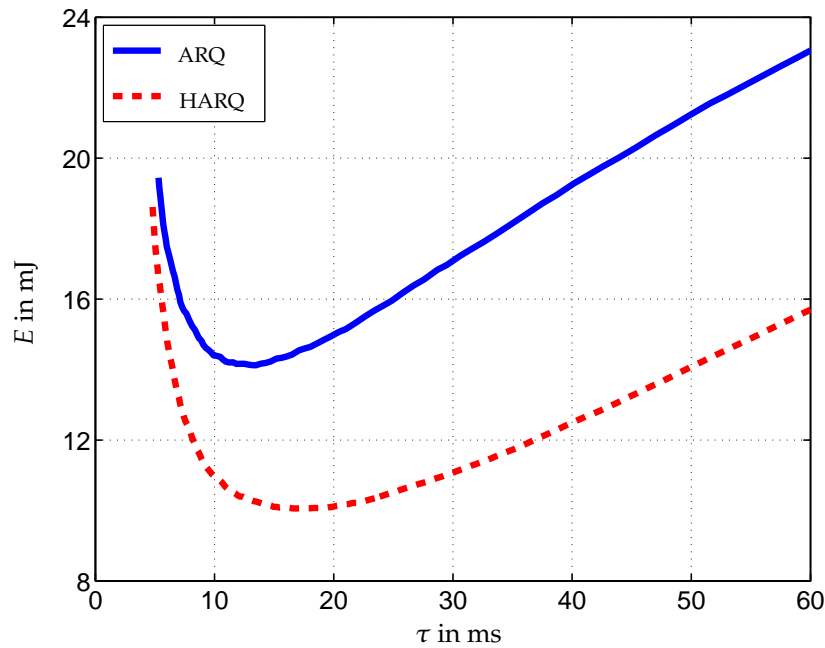


Fig. 2.15: Trade-off between energy consumption and delay for packet transmission over a block fading channel, $T_I = 2$ ms, $T_R = 10$ ms, $M = 4$, $R_c = 0.5$, $N = 1$, $N_s = 1000$, $\alpha/\sigma^2 = 1$, $P = p_{tx} + 1$

We perform Monte-Carlo simulations to evaluate the energy consumption and the latency to convey a packet over a block fading channel with average gain α . The results shown in Fig. 2.15 are produced with the system parameters listed below the figure, and are averaged over 10^4 independent repetitions. The transmit power is varied as we construct the trade-off curves, and to put in an intuitive way, using a higher transmit power helps reduce the PEP and the number of transmissions, whereas using a low transmit power results in less energy consumption for each transmission. From the curves we see that the number of transmissions at the point that the total energy consumption

is minimized is between 2 and 3. The HARQ protocol, by employing previously received information in decoding, requires much less energy for the delivery of one packet.

The system design can be improved and optimized by allowing the transmit power and the modulation and coding scheme to be adaptable based on the instantaneous channel information. For the communication with a feedback channel, it is convenient for the transmitter to learn about the channel condition. Although it might be inaccurate and delayed to some extent, this information can be useful to increase the success rate of each transmission. Since our purpose is to give an exemplary model to illustrate the trade-off between energy consumption and the latency, a simple, straightforward transmission scheme has been used instead of an optimized one.

3. Energy-constrained Throughput Maximization on a Finite Time Interval

In this chapter, we consider the throughput maximization problem on a given finite time interval, where the wireless transceiver is provided with a fixed energy budget and an unlimited amount of data that can be transferred. The optimization addresses the question: *how should the wireless transceiver operate on the given time interval, so that the available energy is utilized to convey the maximal amount of data?* It reflects a scenario in which the transceiver does not have any power supply on a certain time period, but wishes to deliver the most possible information using the readily available energy. A number of circumstances arise when the problem is made more specific: is a transmitter, or a receiver, or a pair of them that is of concern; which are the parameters we can control and how are they related to the performance of the system; how are the parameters that can not be controlled and what do we know about them. In any of the cases, it is crucial to determine the relation between the achievable data rate and the power consumption of the system based on the dependencies of the two quantities on the control variables. This relation helps us identify the so-called energy efficient operation modes of the system, the appropriate time-sharing of which constitutes the optimal solution to the posed problem. We achieve these results by virtue of the *optimal control theory*.

Instead of instantaneous performance metrics, we optimize the *throughput* of the system which is defined as the total amount of data transferred on the given time interval. Mathematically, it is computed as the integral of the instantaneous data rate and is therefore a *functional* of the control variables as functions of time. On the other hand, the state of the transceiver in terms of energy consumption is governed by the instantaneous power consumption as dependent on the control variables, which can be written as a set of differential equations. The given energy budget corresponds then to a constraint on the system state. Our problem, recognized as the maximization of a functional for a system described by a set of differential equations and constrained in its state, is consequently treated within the framework of the optimal control theory. After giving a general problem formulation, we introduce the Pontryagin's maximum principle and discuss its application to each specific scenario to obtain the optimal communication strategy. Notice that in some of the cases, less powerful tools than the maximum principle suffice for the derivation of the optimal solution. We employ nevertheless the maximum principle not only for the consistency, but also for the insight of possible generalization of the obtained results.

Besides the theoretical and practical interest of its own, the optimal solution to the posed problem lays the basis for the optimal control of energy harvesting transceivers. As we shall discuss in the next chapter, the throughput maximization problem of an energy harvesting transceiver can be decomposed into subproblems with fixed energy budgets. While applying the optimal solution to each subproblem does not necessarily yield the global optimum, using a non-optimal solution for any subproblem is bound to be suboptimal. Therefore, being the cornerstone for a more general setting, the fixed energy budget problem we aim to solve to optimality here is also referred to as the *basic problem*. Moreover, since a geometric approach is taken for finding the optimal state trajectory of energy harvesting transceivers, from which the optimal control can be determined, we present and interpret the optimal solutions to the basic problems in various scenarios from a geometric perspective as well.

3.1 Problem Formulation

We formulate the energy-constrained throughput maximization problem in a general form in this section, where we first introduce the elements of the problem using terminology and common notations of the optimal control theory, and then give the mathematical formulation as well as a geometric interpretation of the optimization.

The wireless transceiver shall be regarded as a control system. We let the time interval of interest be $[0, T]$ where $T \in (0, +\infty)$ is a given constant. The adaptation of the control variable, in case there is only one of them, can be described by a *control* $u : [0, T] \rightarrow \mathcal{U}$ which is a function of time with the domain $[0, T]$ and the range $\mathcal{U} \subset \mathbb{R}$. Regulations on u are necessary to guarantee its physical feasibility. In the optimal control theory, u is usually assumed piecewise continuous, meaning that the function is continuous except at a finite number of points where finite discontinuities occur¹. This is a reasonable condition for the system we are studying, since the control parameters of the transceivers can be assumed to vary continuously in time where a sudden jump in their values is also possible, yet to allow for an infinite number of jumps in the control does not make sense. The set of values that the control variable can take, given as \mathcal{U} , is called the *control set* and it can be discrete or connected, finite or infinite. In the following, we present the problem formulation and the maximum principle for the one-dimensional case, as this is what we mostly consider and also gives us a concise notation. The extension to multiple control variables, *i.e.* having a vector-valued control \mathbf{u} , is straightforward.

We define the state of the system at time t as the cumulative energy consumption from the starting point 0 until t , and denote it with $W(t)$. Let $P(u(t))$ be the instantaneous power consumption of the transceiver, which is a non-negative function of the control variable and usually does not depend on time in an explicit manner. Instead of using the integral representation, we employ the ordinary differential equation (ODE)

$$\dot{W} = P(u), \quad W(0) = 0 \quad (3.1)$$

to describe the behavior of the system, which is common practice in formulating optimal control problems. Note that we have followed the convention of suppressing the time

¹A finite discontinuity means that both one-sided limits at the point exist and are finite. An infinite discontinuity, correspondingly, occurs when one of the one-sided limits of the function is infinite.

arguments of W and u . On a time-energy graph, W is represented by a non-decreasing curve starting from the origin, and the slope at any point of the curve is given by the corresponding power consumption of the transceiver. From a more dynamic viewpoint, W can be seen as the *trajectory* of a particle moving from the origin towards an intersection point with the line $t = T$, where the movement of the particle is governed by the control of the system via the power consumption function P . If the function P is invertible, we have one-to-one correspondence between the control u and the trajectory W .

The performance of the system is measured by the *short-term throughput*, or simply *throughput*, which is a functional of the control u defined as

$$I(u) \triangleq \int_0^T R(t, u) dt. \quad (3.2)$$

The function R , also called the *Lagrangian* in this context, stands for the instantaneous achievable rate of the undergoing communication. It depends on the control and possibly explicitly on time, when the channel is time-variant for instance. Following the information-theoretic framework, we usually have the rate function R being concave in the control variable given fixed time argument.

Our goal is to find, among all *admissible* controls, the one that leads to the maximal throughput on the time interval of interest. For a control to be admissible, it needs to fulfill all the constraints of the problem, including those directly on u : $u \in \mathcal{U}, \forall t \in [0, T]$, and also those on the state trajectory W e.g. a specified final state, a pointwise upper or lower bound, *etc.* We consider here that the transceiver has a given energy budget A_0 , which is smaller or equal to the storage capacity of the transceiver, and is available already at $t = 0$. During the time interval of interest, the transceiver has no power supply or other energy input. This is to say, we have a constant pointwise upper bound of value A_0 on the state trajectory W , or equivalently, an inequality constraint on the final state of the system, $W(T) \leq A_0$, to guarantee that the energy expenditure is no more than the energy that is available. To this end, we formulate the energy-constrained throughput maximization as an optimal control problem as

$$\begin{aligned} \max_{u: [0, T] \rightarrow \mathcal{U}} \quad & \int_0^T R(t, u) dt \\ \text{s.t.} \quad & \dot{W} = P(u), \quad W(0) = 0, \\ & W(T) \leq A_0. \end{aligned} \quad (3.3)$$

This problem is referred to as the *basic problem* in the context of finding the optimal control of energy harvesting transceivers. The optimal solution and the corresponding optimal state trajectory, denoted with u^* and W^* respectively, can be obtained by applying the *Pontryagin's maximum principle* (PMP), given certain regulations and assumptions about the rate function R and the power consumption function P , which we shall discuss in detail in the subsequent sections.

The optimal control problem (3.3) is visualized with the time-energy graphs shown in Fig. 3.1. The fixed energy budget A_0 confines a rectangular *admissible region* for the state trajectories with the parallel horizontal lines $E = A_0$ and $E = 0$, where the latter lower bound is naturally fulfilled as W starts at the origin and is non-decreasing in time.

The final state of the transceiver, or the intersection point of W with $t = T$, should not be above the point (T, A_0) . Finding the optimal control can then be understood from a geometric point of view as finding the admissible trajectory, which starts at the origin, increases monotonically, and lies within the admissible region, that leads to the maximal throughput. Moreover, if the functions R and P are both monotonically increasing in the control variable, which is practically almost always the case, the inequality constraint on the final state can be replaced by the equality constraint $W(T) = A_0$. This condition requires the available energy to be exhausted at the termination point, since otherwise one can always increase the value of the control and thus improve the achievable throughput. Taking the new restriction into account, the endpoint of any admissible trajectory is fixed at (T, A_0) on the time-energy graph.

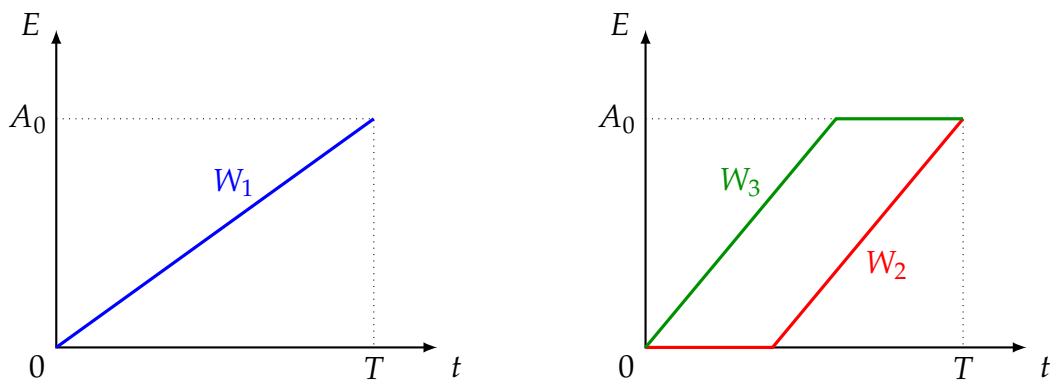


Fig. 3.1: Visualization of the energy-constrained throughput maximization problem and exemplary admissible trajectories

In Fig. 3.1 we illustrate three admissible trajectories, all of which start at the origin, end at (T, A_0) , and are non-decreasing in time. The part of the trajectory that is a straight line segment corresponds to the control variable being constant on that time interval. The trajectory W_1 then represents a completely constant control. In particular, horizontal straight line segments suggest zero power consumption of the transceiver, which can be found in trajectories W_2 and W_3 . For both cases we see that the transceiver is operated actively with a constant control variable for some time period, and turned off for the remaining of the time interval during which no energy is consumed. Moreover, the two trajectories differ only in the location of the horizontal part, but not in its duration. They will be recognized as *equivalent* trajectories later, which form an important class of trajectories for some system setups.

3.2 The Maximum Principle

The *Pontryagin's maximum principle*, proposed by L. Pontryagin *et al.* in the 50s [62] and also known as the *Pontryagin's minimum principle*, is a first-order necessary condition for optimality of optimal control problems. We state the principle here with the notations used in (3.3), except that T represents the endpoint of operation which is not necessarily fixed and known in advance.

The maximum principle gives a set of conditions that the optimal control u^* and the optimal state trajectory W^* should satisfy, under the assumptions that u is piecewise

continuous, and the functions R and P are both continuous in the control variable. The *Hamiltonian* of the problem is introduced as

$$H(t, W, u, \lambda) = -R(t, u) + \lambda \cdot P(u), \quad (3.4)$$

where the auxiliary variable λ is called the *adjoint variable* or the *costate*. At optimality, it satisfies the costate equation

$$\dot{\lambda}^* = -H_W(t, W^*, u^*, \lambda^*). \quad (3.5)$$

Note that a function with one of its variables as the subscript stands for the partial derivative of the function with respect to this variable. The PMP indicates that the Hamiltonian evaluated with W^* and λ^* is minimized by the optimal control u^* , among all admissible controls, at every time instant:

$$H(t, W^*, u^*, \lambda^*) \leq H(t, W^*, u, \lambda^*), \quad \forall t \in [0, T]. \quad (3.6)$$

When the Hamiltonian does not depend explicitly on time and the terminal point T is free, then the condition

$$H(W^*, u^*, \lambda^*) = 0, \quad \forall t \in [0, T] \quad (3.7)$$

should be satisfied. If T is fixed instead, then $H(W^*, u^*, \lambda^*)$ is still constant over time but not necessarily equal to 0. When the final state of the system is specified, an additional *transversality condition* is necessary, which, in the one-dimensional case, states that

$$\lambda^*(T) = 0. \quad (3.8)$$

When the Hamiltonian does depend explicitly on time, one can treat t as another state variable and introduce also a costate for it. In the case that the terminal point T is free, the following condition can be obtained using (3.7) and (3.8):

$$H(T, W^*(T), u^*(T), \lambda^*(T)) = 0. \quad (3.9)$$

The proof as well as more detailed analysis of the PMP can be found in various literatures *e.g.* [62–64].

For the wireless transceiver under consideration, the rate function R and the power consumption function P are both independent of the cumulative energy consumption of the system. As a result, the Hamiltonian as defined by (3.4) does not depend on the system state W explicitly, which suggests that λ^* is a constant according to (3.5). The remaining conditions need to be discussed with additional specifications on R and P , which rely on the features and assumptions of each individual scenario. We investigate in the following sections, the throughput-maximizing operation strategies *i.e.* the optimal solutions to the basic problem of a transmitter, a receiver, and a pair of transmitter and receiver.

3.3 Optimal Control of the Transmitter

In this section we consider a wireless transmitter as the object under control, which exploits the energy budget A_0 to send data to a certain receiver. We discuss a number of different cases which are summarized in Table 3.1.

Table 3.1: Scenarios considered for the transmitter and the optimal control strategies

Case	Features	Rate function R	Power function P
I	Continuous transmit power p_{tx} , constant channel	Strictly concave, monotonically increasing in p_{tx} , $R(0) = 0$	Convex, monotonically increasing in p_{tx} , $P(0) = 0$
	Employ constant transmit power, $p_{tx}^* = P^{-1}(A_0/T)$		
II	Continuous transmit power p_{tx} , constant channel	Same as in Case I	Convex, monotonically increasing for $p_{tx} > 0$, $P(0) = 0$, $P(0^+) = c_0 > 0$
	Employ constant transmit power $p_{tx}^* = P^{-1}(A_0/T)$ if $A_0/T \geq p_0$, otherwise use $p_{tx}^* = p_{tx,0}$ until all energy is exhausted, and then turn into sleep mode, where $p_{tx,0}$ solves $(R \cdot P_{p_{tx}} - R_{p_{tx}} \cdot P)(p_{tx}) = 0$, and $p_0 = P(p_{tx,0})$		
III	Discrete set of modulation orders, constant channel	Discrete (P, R) pairs each corresponding to one available modulation order, for which the Pareto boundary is constructed	
	Employ time-sharing of the bounding modulation orders of A_0/T		
IV	Time-varying, known channel	Same as in Case I or II	Same as in Case I or II
	Employ the water-filling or modified water-filling solution; Convex optimization for block-fading channels		
III + IV	Discrete set of modulation orders, block-fading channel	Log-normal shadowing added to the model of Case III	
	Optimal control obtained by solving a linear program, near-optimal control from proposed heuristic algorithm		
V	Causally known block-fading channel	Same as in Case I or II	Same as in Case I or II
	Online decision making based on dynamic programming		
VI	Stochastic deadline for transmission	Same as in Case I or II	Same as in Case I or II
	Employ monotonically decreasing transmit power until the deadline or the depletion of A_0		

3.3.1 Case I

In a very basic and generic setup, the transmit power, denoted with p_{tx} , is taken as the control variable which assumes continuous values without an upper limit *i.e.*

$\mathcal{U} = [0, +\infty)$. The rate function R is assumed to be time-invariant, strictly concave and monotonically increasing in p_{tx} , and it satisfies $R(0) = 0$. These conditions are met by many common communication systems. An example of such rate functions is given as

$$R(p_{\text{tx}}) = B \log_2 \left(1 + \frac{p_{\text{tx}}}{\sigma^2} \right), \quad (3.10)$$

which is the Shannon formula for the capacity of the AWGN channel in bit/sec, where σ^2 denotes the noise power which has the same unit as p_{tx} , and B denotes the signal bandwidth in Hz.

Circuit power and hardware imperfection are inevitable to digital communication devices. Considerations on these factors are especially important for wireless sensor nodes due to the typically short communication ranges, rendering the transmit power required to achieve a sufficiently good receive SNR not significantly larger than the analog/digital processing power. Consequently, it is necessary and imperative to include the power consumption of the circuitry into account. In the context of the basic generic model, we assume convex and monotonically increasing functions P with $P(0) = 0$. Note that this includes the special case $P(p_{\text{tx}}) = p_{\text{tx}}$, *i.e.* circuit power is neglected and an ideal power amplifier is assumed at the transmitter.

3.3.1.1 Optimal transmission strategy

For the control p_{tx}^* and the costate λ^* to be optimal, it is necessary that

$$H(p_{\text{tx}}, \lambda^*) = -R(p_{\text{tx}}) + \lambda^* \cdot P(p_{\text{tx}}) \quad (3.11)$$

is minimized with p_{tx}^* at every time instant. This implies that the constant costate λ^* is positive, for otherwise $H(p_{\text{tx}}, \lambda^*)$ would be unbounded from below. As $R(\cdot)$ is strictly concave and $P(\cdot)$ is convex, we have $H(\cdot, \lambda^*)$ is strictly convex, suggesting that the minimum of $H(\cdot, \lambda^*)$ is unique *i.e.* p_{tx}^* has to be constant. This is to say, in order to maximize the throughput on $[0, T]$ with a fixed energy budget, the optimal transmission strategy as indicated by the PMP is to *employ constant transmit power*. Since R increases monotonically with p_{tx} , all available energy should be exhausted by the end of the time interval, leading to $p_{\text{tx}}^* = P^{-1}(A_0/T)$, $\forall t \in [0, T]$ where P^{-1} stands for the inverse of function P .

When the functions R and P are differentiable, we can achieve the same result using the first-order condition as required by (3.6):

$$H_{p_{\text{tx}}}(p_{\text{tx}}^*, \lambda^*) = -R_{p_{\text{tx}}}(p_{\text{tx}}^*) + \lambda^* \cdot P_{p_{\text{tx}}}(p_{\text{tx}}^*) = 0, \quad (3.12)$$

which in turn gives

$$\lambda^* = \frac{R_{p_{\text{tx}}}(p_{\text{tx}}^*)}{P_{p_{\text{tx}}}(p_{\text{tx}}^*)}. \quad (3.13)$$

Since R is strictly concave in p_{tx} , the first-order derivative $R_{p_{\text{tx}}}$ decreases monotonically. On the contrary, $P_{p_{\text{tx}}}$ is non-decreasing as P is convex in p_{tx} . As a result, the function $R_{p_{\text{tx}}}/P_{p_{\text{tx}}}$ is monotonically decreasing, hence the optimal control p_{tx}^* has to be constant so that λ^* stays invariant over time. When the first-order derivatives $R_{p_{\text{tx}}}$ and $P_{p_{\text{tx}}}$ are also differentiable, the second-order condition

$$H_{p_{\text{tx}}p_{\text{tx}}}(p_{\text{tx}}^*, \lambda^*) = -R_{p_{\text{tx}}p_{\text{tx}}}(p_{\text{tx}}^*) + \lambda^* \cdot P_{p_{\text{tx}}p_{\text{tx}}}(p_{\text{tx}}^*) > 0 \quad (3.14)$$

suffices to ensure that $H(\cdot, \lambda^*)$ is minimized by the constant control p_{tx}^* .

With the assumption of a concave rate function R and a convex power function P , the convexity of the optimal control problem (3.3) can be easily seen. This guarantees that the local optimal solution we find via the PMP is indeed the global optimum. The corresponding optimal trajectory W^* is exactly the straight line connecting $(0, 0)$ and (T, A_0) on an time-energy graph, as shown on the left side of Fig. 3.1.

In fact, the convexity requirement on P may be too strong for the constant transmit power strategy to be optimal. The PMP requires the function $R_{p_{\text{tx}}}/P_{p_{\text{tx}}}$ to be single-valued, if p_{tx}^* is constant. When both $R_{p_{\text{tx}}}$ and $P_{p_{\text{tx}}}$ are continuous, this translates to $R_{p_{\text{tx}}}/P_{p_{\text{tx}}}$ being monotonic which is equivalent to

$$R_{p_{\text{tx}}p_{\text{tx}}}P_{p_{\text{tx}}} - R_{p_{\text{tx}}}P_{p_{\text{tx}}p_{\text{tx}}} < 0 \quad (3.15)$$

based on (3.13) and (3.14), given that $R_{p_{\text{tx}}}$ and $P_{p_{\text{tx}}}$ are also differentiable. Obviously, P being convex is sufficient but not necessary for (3.15) to hold. One can also come to this point by contemplating that (3.11) is minimized by p_{tx}^* at every time instant, which only requires that the minimum of $H(\cdot, \lambda^*)$ is unique if p_{tx}^* should be constant. For example, $H(\cdot, \lambda^*)$ being strongly unimodal is sufficient, which does not call for the function P to be convex which makes $H(\cdot, \lambda^*)$ convex. However, having non-convex P destroys the convexity of the optimal control problem, which may lead to situations where the PMP is not sufficient for optimality or where the optimal control does not even exist. Taking this into account, we do not discuss further, what are the exact conditions P needs to fulfill such that a constant control is optimal, but settle ourselves with convex functions P for convenience.

The optimal solution can also be understood from a geometric point of view. Intuitively, as we aim at maximizing the throughput with a given energy budget, the operation modes of better energy efficiency should be preferred, *i.e.* those with relatively larger R/P values. To this end, we consider the achievable rate as a function of the power consumption and illustrate it on a power-rate graph. The energy efficiency of any point on the curve corresponds then to the slope of the straight line connecting the point with the origin. We let $f(P) = R(P^{-1})$ denote the rate function as dependent on the power consumption of the transmitter. By using the chain rule, one can obtain that

$$f_P = R_{p_{\text{tx}}} \cdot P_{p_{\text{tx}}}^{-1} = R_{p_{\text{tx}}}/P_{p_{\text{tx}}}, \quad (3.16)$$

which is strictly monotonically decreasing in P since the positive numerator is strictly decreasing whereas the positive denominator is non-decreasing in p_{tx} , and P increases monotonically with p_{tx} . This is to say, the achievable rate R as a function of the power consumption P is strictly concave. Noting that R and P are both equal to zero when no power is radiated, we depict an exemplary R - P curve on the left in Fig. 3.2.

Due to the strict concavity of the curve, the line segment connecting two arbitrary points on the curve lies below the curve. This means, the time-sharing of the two corresponding operation modes, characterized by their (P, R) coordinates, leads to a reduction in the achievable throughput as compared to using the single operation mode with the same average power. Consequently, the optimality of employing a constant control is validated. This consideration shares the same essence as Jensen's inequality, and we will see in the sequel, that the power-rate graph is very helpful in analyzing less

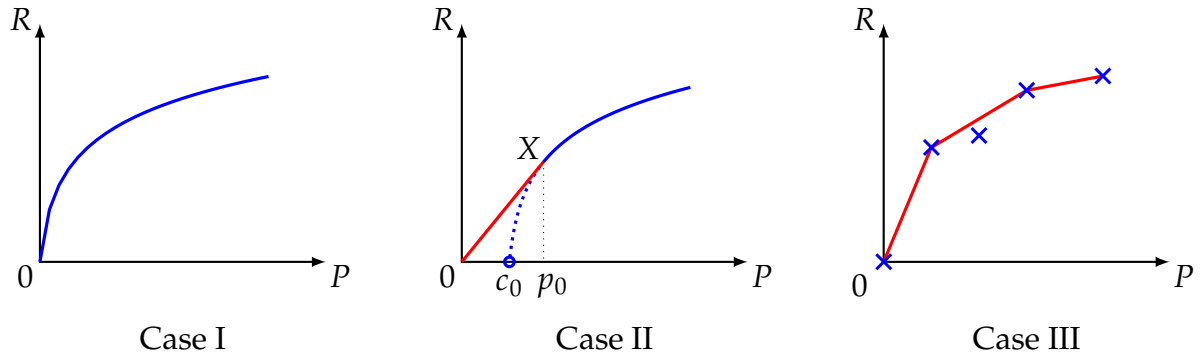


Fig. 3.2: Power-rate graphs and construction of the Pareto boundaries

regular situations. Also notice, by observing equations (3.13) through (3.16), that the strict concavity of R in P is an equivalent condition for the PMP to lead to the constant control conclusion, and is a less demanding one than restricting P to be convex.

3.3.1.2 On the maximum achievable throughput

The maximal throughput achieved by employing p_{tx}^* is given as $I^* = T \cdot f(A_0/T)$. It can be immediately seen that I^* as a function of A_0 shares the properties of the function f for fixed T : it is monotonically increasing and strictly concave. When A_0 is fixed instead, it can be computed for I^* as a function of T that

$$I_T^* = f\left(\frac{A_0}{T}\right) - \frac{A_0}{T} \cdot f_P\left(\frac{A_0}{T}\right) > 0, \quad (3.17)$$

$$I_{TT}^* = \frac{A_0^2}{T^3} \cdot f_{PP}\left(\frac{A_0}{T}\right) < 0, \quad (3.18)$$

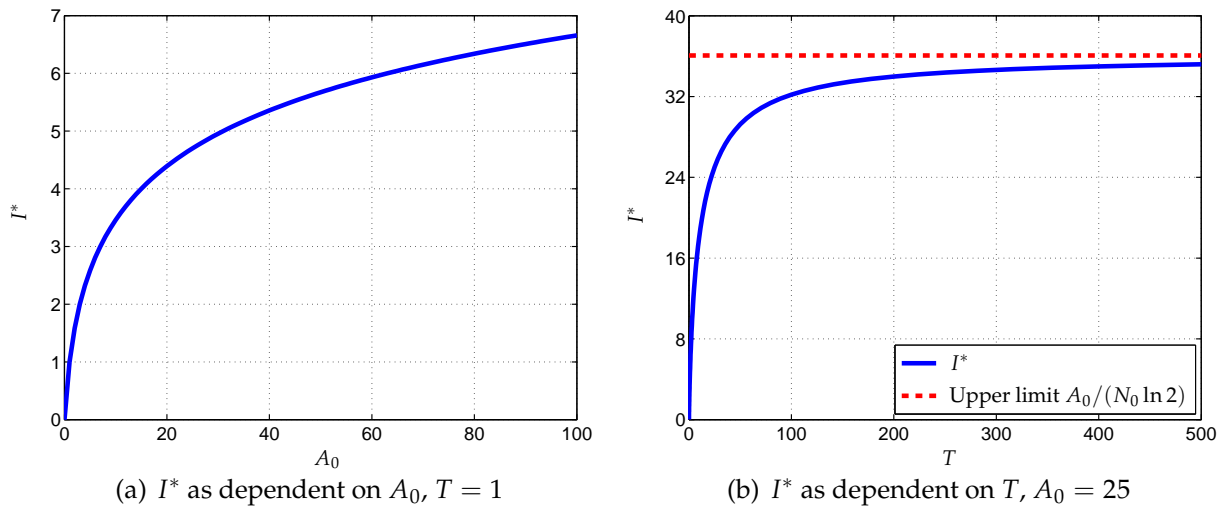


Fig. 3.3: Maximum throughput I^* as functions of A_0 and T , R and P given by (3.20) with $B = 1$, $\sigma = 1$

where (3.17) and (3.18) follow from the first- and second-order concavity conditions [65] of the function f :

$$0 = f(0) < f\left(\frac{A_0}{T}\right) + f_P\left(\frac{A_0}{T}\right)\left(0 - \frac{A_0}{T}\right) = f\left(\frac{A_0}{T}\right) - \frac{A_0}{T} \cdot f_P\left(\frac{A_0}{T}\right), \quad (3.19)$$

$$f_{PP}\left(\frac{A_0}{T}\right) < 0.$$

This is to say, I^* as a function of T is also monotonically increasing and strictly concave. If we take the generic model

$$R = B \log_2 \left(1 + \frac{p_{\text{tx}}}{\sigma^2}\right), \quad P = p_{\text{tx}}, \quad (3.20)$$

then the asymptotic values of $I^* = TB \log_2 \left(1 + \frac{A_0}{T\sigma^2}\right)$ can be calculated by using the L'Hôpital's rule as

$$\lim_{T \rightarrow 0} I^* = \lim_{T \rightarrow 0} \frac{B}{\ln 2} \cdot \frac{A_0 T}{T\sigma^2 + A_0} = 0,$$

$$\lim_{T \rightarrow +\infty} I^* = \lim_{T \rightarrow +\infty} \frac{B}{\ln 2} \cdot \frac{A_0 T}{T\sigma^2 + A_0} = \frac{BA_0}{\sigma^2 \ln 2} = \frac{A_0}{N_0 \ln 2}, \quad (3.21)$$

where N_0 stands for the noise power spectral density. Note that the upper limit of I^* is achieved by the asymptotically minimum energy per bit of $N_0 \ln 2$ which is derived in (2.7), since the system is allowed to operate for infinitely long time in this case. We show some numerical examples in Fig. 3.3 for an illustrative impression that the maximum throughput I^* is monotonically increasing and strictly concave in the energy budget A_0 and the operation time T , respectively. Notice also, that we normalize the fixed parameters and do not always specify the units of variables for the generic model, and focus on the behavior and property of the system mainly from a mathematical perspective.

3.3.2 Case II

When circuit power of the transmitter is taken into account, special attention should be paid to the potential discontinuity brought to the power consumption function P . More specifically, we consider that the transmitter works either in *active mode* or in *sleep mode*. When it is not sending any signal, the transmitter is turned into sleep mode for which we assume there is no power consumption of the circuit, *i.e.* $P(0) = 0$. Otherwise, the transmitter is considered in active mode and its circuit incurs additional power consumption, which means $P > 0$ for $p_{\text{tx}} > 0$. We further assume that switching between the two modes does not require any power or time. This is of course idealistic, and it should be taken care that mode switches in the optimal control is avoided as much as possible. It is necessary to explicitly define these two operation modes since they may lead to a discontinuous point of P at $p_{\text{tx}} = 0$. For instance, there is often a positive constant power consumption term associated with the active mode caused by baseband processing *etc.* Let this constant be denoted with c_0 , and assume that $p_{\text{tx}} = 0$ is the single discontinuous point of P , where $P(0) = 0$ but the right-sided limit $P(0^+) = c_0 > 0$. In addition, for $p_{\text{tx}} > 0$ we assume P is convex and monotonically increasing as before, and the rate function R also fulfills the same conditions as in Case I.

3.3.2.1 Optimal transmission strategy

The PMP takes as prerequisites that the Lagrangian R and the time differential of the system state P are continuous. The discontinuity of P therefore calls for special treatment and the result from Case I needs to be reexamined. Intuitively, turning the transmitter into sleep mode could be beneficial in this case due to the energy that can potentially be saved. Since the channel state is assumed invariable, when is the transmitter sleeping during the time interval $[0, T]$ does not influence the achieved throughput. We therefore assume that the transmitter begins transmission at $t = 0$, and terminates at some time instant t_1 , where $t_1 \leq T$. To this end, an optimal control problem with free endpoint but specified final state can be formulated, for which the function P is continuous. The constant control result we obtain previously is then valid, *i.e.* during the time that the system is in active mode, using constant transmit power is the optimal. The remaining question is to determine t_1 , at which point all available energy is exhausted and the transmission is terminated. For $t_1 < T$, the constant Hamiltonian condition (3.7) applies as

$$H(p_{\text{tx}}^*, \lambda^*) = -R(p_{\text{tx}}^*) + \lambda^* \cdot P(p_{\text{tx}}^*) = 0, \quad (3.22)$$

which, together with the first-order condition (3.13), gives us the relation

$$\lambda^* = \frac{R(p_{\text{tx}}^*)}{P(p_{\text{tx}}^*)} = \frac{R_{p_{\text{tx}}}(p_{\text{tx}}^*)}{P_{p_{\text{tx}}}(p_{\text{tx}}^*)}. \quad (3.23)$$

Consequently, we have that the optimal transmit power is the solution to the equation

$$(R \cdot P_{p_{\text{tx}}} - R_{p_{\text{tx}}} \cdot P)(p_{\text{tx}}) = 0, \quad (3.24)$$

which we denote with $p_{\text{tx},0}$. The corresponding power consumption of the transmitter is given as $p_0 = P(p_{\text{tx},0})$. Note that $p_{\text{tx},0}$ depends only on the inherent properties of the communication system *e.g.* functions R and P . The specific operation parameters A_0 and T determine whether, and for how long, can the transmit power $p_{\text{tx},0}$ be employed.

The optimal transmission strategy for Case II can be stated as follows: *if $A_0/T > p_0$, then the transmit power $P^{-1}(A_0/T)$ should be employed constantly on $[0, T]$; otherwise, the transmit power $p_{\text{tx},0}$ should be used for a time period of length A_0/p_0 , and the transmitter is turned into sleep mode for the rest of the time interval.*

On the time-energy graph, the optimal trajectory in the former case is still the straight line segment connecting $(0,0)$ and (T, A_0) , shown by W_1 in Fig. 3.1. In the latter, the optimal trajectory consists of straight line segments of slope p_0 and horizontal lines, representing the active and the sleep modes of the transmitter, respectively. As we assume mode switches do not cost any power or time, the required sleep period can be realized in infinitely many ways in terms of segmentation and concatenation with the active periods. We call the class of trajectories that begin and end at the same points, in our case that is $(0,0)$ and (T, A_0) , and are comprised exclusively of horizontal lines and straight lines with slope p_0 *equivalent* trajectories. As simple examples, the trajectories W_2 and W_3 in Fig. 3.1 are equivalent, which we denote with $W_2 \sim W_3$. Note that equivalent trajectories all lead to the same throughput.

The result derived above can also be interpreted with geometric illustrations on the power-rate graph. As shown in the middle graph of Fig. 3.2, due to the positive constant

power consumption c_0 associated with the active mode, the achievable rate R as a function of the power consumption P is undefined on the open set $(0, c_0]$ and exhibits an isolated point in its domain at $P = 0$. We make the tangent line from the origin towards the R - P curve and name the tangent point X , with coordinates $(P(p_{\text{tx},X}), R(p_{\text{tx},X}))$. It can be immediately seen, that the time-sharing between the sleep mode and the active mode with transmit power $p_{\text{tx},X}$ outperforms the exclusive use of any power value in the range of $(0, p_{\text{tx},X})$, for the tangent line lies above the part of the R - P curve until the tangent point. The slope of the tangent line satisfies the relation

$$\frac{R(p_{\text{tx},X})}{P(p_{\text{tx},X})} = f_P(p_{\text{tx},X}) = \frac{R_{p_{\text{tx}}}(p_{\text{tx},X})}{P_{p_{\text{tx}}}(p_{\text{tx},X})}, \quad (3.25)$$

which leads to

$$(R_{p_{\text{tx}}} \cdot P - R \cdot P_{p_{\text{tx}}})(p_{\text{tx},X}) = 0. \quad (3.26)$$

Comparing with (3.24), we immediately discover that $p_{\text{tx},X} = p_{\text{tx},0}$. The corresponding total power consumption at the tangent point X is therefore p_0 , as indicated in Fig. 3.2.

Clearly, by making the tangent line OX we have constructed the Pareto boundary of the graph given by R as a function of P . The linear tangent part between $(0,0)$ and $(p_0, R(p_{\text{tx},0}))$ corresponds to the time-sharing region, *i.e.* any transmit power between 0 and $p_{\text{tx},0}$ should be realized by the time-sharing of the two endpoints, whereas the curved part beyond the tangent point, which is strictly concave, corresponds to the constant power region. The slope of the line connecting the origin and any point beyond the tangent point is smaller than that of the tangent line, suggesting that the maximal energy efficiency is achieved at the tangent point. This can also be verified with the algebraic method, via inspection of the maximization of R/P . The stationary point of the optimization is given exactly by (3.24). To this end, we refer to $p_{\text{tx},0}$ as the *energy efficient* transmit power, and claim that using any positive transmit power below $p_{\text{tx},0}$ is bound to be suboptimal.

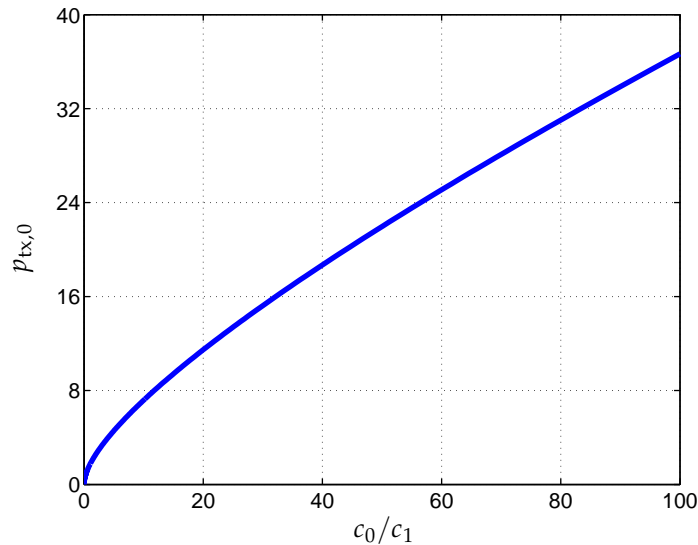


Fig. 3.4: Energy efficient transmit power as the solution to (3.28), $\sigma = 1$

3.3.2.2 On the energy efficient transmit power and the maximum achievable throughput

For the numerical examples, we employ the following rate and power functions:

$$R = B \log_2 \left(1 + \frac{p_{\text{tx}}}{\sigma^2} \right), \quad P = \begin{cases} c_1 \cdot p_{\text{tx}} + c_0, & p_{\text{tx}} > 0, \\ 0, & p_{\text{tx}} = 0, \end{cases} \quad (3.27)$$

i.e. R is given by the Shannon formula and P has a discontinuous affine form with constants $c_1 \geq 1$, $c_0 > 0$. The equation (3.24) that defines the energy efficient transmit power can be written as

$$\frac{p_{\text{tx}} + c_0/c_1}{p_{\text{tx}} + \sigma^2} = \ln \left(1 + \frac{p_{\text{tx}}}{\sigma^2} \right), \quad (3.28)$$

from which $p_{\text{tx},0}$ can be solved using an iterative algorithm. We let $\bar{c} = c_0/c_1$ and define

$$F(p_{\text{tx},0}, \bar{c}) = \ln \left(1 + \frac{p_{\text{tx},0}}{\sigma^2} \right) - \frac{p_{\text{tx},0} + \bar{c}}{p_{\text{tx},0} + \sigma^2} = 0, \quad (3.29)$$

which enables us to study the properties of the energy efficient transmit power as a function of the ratio \bar{c} . It can be computed that

$$\begin{aligned} \frac{dp_{\text{tx},0}}{d\bar{c}} &= -\frac{F_{\bar{c}}}{F_{p_{\text{tx},0}}} = \frac{p_{\text{tx},0} + \sigma^2}{p_{\text{tx},0} + \bar{c}} > 0, \\ \frac{d^2 p_{\text{tx},0}}{d\bar{c}^2} &= \frac{\partial}{\partial p_{\text{tx},0}} \left(\frac{dp_{\text{tx},0}}{d\bar{c}} \right) \frac{dp_{\text{tx},0}}{d\bar{c}} + \frac{\partial}{\partial \bar{c}} \left(\frac{dp_{\text{tx},0}}{d\bar{c}} \right) = -\frac{(p_{\text{tx},0} + \sigma^2)^2}{(p_{\text{tx},0} + \bar{c})^3} < 0, \end{aligned} \quad (3.30)$$

suggesting that $p_{\text{tx},0}$ is monotonically increasing and strictly concave in \bar{c} . We demonstrate the relation between the two quantities in Fig. 3.4. The monotonic behavior of $p_{\text{tx},0}$ is intuitive since the R - P curve is drifted away from the origin and/or pressed more flat along the R -axis with increasing c_0/c_1 , driving the tangent point further to the right on the power-rate graph. As $p_{\text{tx},0} = 0$ for $c_0 = 0$, we see that Case I can actually be regarded as a special instance of Case II, for which the energy efficient transmit power is never employed since the relation $A_0/T > p_0 = 0$ always holds.

The maximum throughput I^* achieved by employing p_{tx}^* is given as

$$I^* = \begin{cases} \frac{A_0}{p_0} B \log_2 \left(1 + \frac{p_{\text{tx},0}}{\sigma^2} \right), & \frac{A_0}{T} \leq p_0, \\ T B \log_2 \left(1 + \frac{P^{-1}(A_0/T)}{\sigma^2} \right), & \text{otherwise.} \end{cases} \quad (3.31)$$

When T is fixed and $A_0 > p_0 T$, time-sharing with the sleep mode is not necessary and the situation is the same as in Case I, *i.e.* I^* is strictly concave in A_0 . When $A_0 \leq p_0 T$ on the other hand, I^* becomes linear in A_0 as indicated by (3.31), since the instantaneous data rate is constant. We illustrate this result in Fig. 3.5(a), where the linear part of I^* is drawn with solid lines and the strictly concave part is drawn with dashed lines. For a fixed energy budget A_0 , on the contrary to Case I, the upper limit of I^* is achieved with finite interval duration which satisfies $T \geq A_0/p_0$, as shown in Fig. 3.5(b). Since A_0 is fully exploited by using the energy efficient transmit power $p_{\text{tx},0}$, reducing T below A_0/p_0 would diminish the achievable throughput.

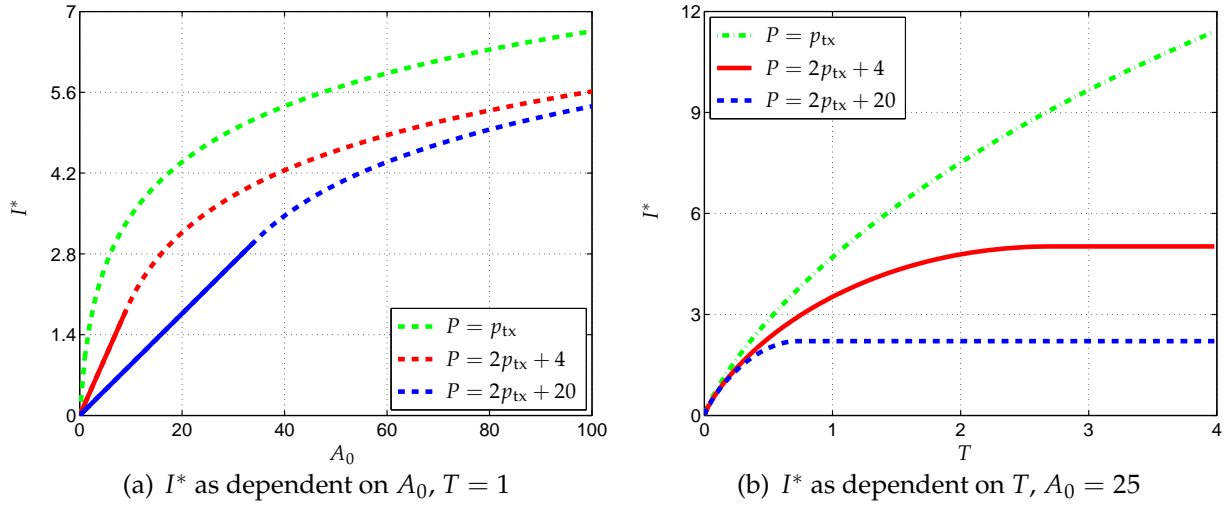


Fig. 3.5: Maximum throughput I^* as functions of A_0 and T , R and P given by (3.27) with $B = 1$, $\sigma = 1$

3.3.3 Case III

In practical communication systems, it is often the case that the transmit power can not be adapted continuously, but has to be chosen from a limited, discrete set. With each allowed transmit power corresponding to a distinct achievable rate, this scenario is characterized by a number of discrete points on the power-rate graph, which are also referred to as the *feasible operation modes*. If time-sharing is allowed, then any point that lies within the convex hull of these discrete points is also achievable. The linear interpolation of the discrete points forms a monotonically increasing rate function in the total power consumption of the transmitter, which, however, can be non-concave.

3.3.3.1 Optimal transmission strategy

To find the optimal transmission strategy, the same approach as used for Case II can be pursued: we construct the Pareto boundary of the given discrete points on the power-rate graph, which satisfies

- Any point on the boundary is achievable;
- There does not exist any achievable point that lies both above and to the left of any point on the boundary.

The resulting rate function as dependent on the power consumption is clearly concave. The Pareto boundary can be constructed as follows: the origin $(0, 0)$ is first selected, and we denote it with (P_o, R_o) . Then, among the points that are to the right of the last selected point, the one with the largest ratio $(R - R_o)/(P - P_o)$ is chosen, and (P_o, R_o) is updated by its coordinates. The process terminates when there is no more point to select, and the eligible discrete points are connected consecutively by straight line segments. The constructed curve, which consists of a series of lines with decreasing slopes, possesses the defining properties of the Pareto boundary as listed above. This can be easily verified by the method of contradiction. In Fig. 3.2, the rightmost graph illustrates the scenario under discussion, with five available operation modes marked by crosses. Four modes

can be found eligible via the proposed procedure, and the Pareto boundary given by the linear interpolation between them is shown with the red curve.

We say that the discrete points on the Pareto boundary represent the *energy efficient operation modes* of the transmitter. Moreover, for a given power consumption, we term the two closest energy efficient points to its left and right as the *bounding operation modes*. Using this concept, we state the optimal transmission strategy as follows: *the two bounding operation modes of the power value A_0/T should be employed in a time-sharing manner such that the same average power is achieved*. If A_0/T is exactly equal to the power consumption of an energy efficient operation mode, then this mode should be used exclusively and no time-sharing is necessary. If, on the other hand, A_0/T is larger than the power consumption of the most power demanding operation mode, then this mode should be used exclusively also, but we will not be able to utilize all the available energy on the given time interval.

3.3.3.2 Optimal control of MQAM transmission

We introduce next, a concrete system model in which the transmitter employs uncoded M -ary quadrature amplitude modulation (MQAM). The modulation format, or equivalently, the constellation size M , is the control parameter here which can be adapted over time within a predefined, limited discrete set. Due to the convenience in implementation and analysis, we discuss only square QAM in the following, meaning that $\log_2 M$ is an even number. The model is based on the one proposed in [36], and modifications are made to include the effect of pulse shaping.

Let the distance between the transmitter and the receiver be denoted with d (in meters), and assume it does not change during $[0, T]$. Considering only path loss for the radio propagation effect, we write the receive SNR as [36,66]

$$\gamma = \frac{p_{\text{rx}}}{N_0 B} = \frac{p_{\text{tx}}}{M_1 G_1 d^\kappa N_0 B}, \quad (3.32)$$

where $\frac{N_0}{2}$ is the double-sided noise power spectrum density, κ is the path loss exponent, and B is the signal bandwidth. The parameter G_1 stands for the power loss at the reference distance of 1 meter which is dependent on the antenna patterns and the wavelength of the transmitted signal. Shadowing, interference, other background noise, and internal hardware loss are compensated with the link margin M_1 . An upper bound on the uncoded bit error probability for the MQAM transmission is given by [67]

$$\begin{aligned} \pi_b &\leq \frac{4}{\log_2 M} \left(1 - \frac{1}{\sqrt{M}}\right) Q\left(\sqrt{\frac{3\gamma}{M-1}}\right) \\ &\leq \frac{2}{\log_2 M} \left(1 - \frac{1}{\sqrt{M}}\right) \exp\left(-\frac{3\gamma}{2(M-1)}\right), \end{aligned} \quad (3.33)$$

$$\text{where } Q(x) = \int_x^\infty \frac{\exp(-u^2/2)}{\sqrt{2\pi}} du \leq \frac{1}{2} \exp\left(-\frac{x^2}{2}\right) \text{ for } x > 0. \quad (3.34)$$

The approximation in (3.33) is due to the improved upper bound of the Q function (3.34) derived by [68], which is one half of the Chernoff bound used in [36]. From (3.33) the minimum receive SNR to achieve a target bit error ratio (BER) can be calculated directly.

Table 3.2: System parameters for the uncoded MQAM transmission

carrier frequency	$f_c = 2.5$ GHz	signal bandwidth	$B = 10$ kHz
path loss exponent	$\kappa = 3.5$	noise power density	$\frac{N_0}{2} = -174$ dBm/Hz
link margin	$M_1 = 10^4$	path loss at 1 meter	$G_1 = 10^3$
drain efficiency of PA	$\eta = 0.35$	constant circuit power	$P_{ct} = 100$ mW
roll-off factor	$\beta = 0.3$	symbol duration	$T_s = \frac{1+\beta}{B} = 0.13$ ms
required BER	$\pi_b^{(rq)} = 10^{-3}$	modulation formats	$M \in \{4, 16, 64, 256\}$

Although even better approximations of the Q function can be found *e.g.* in [69], they are usually more involved in the variable and less convenient to compute.

Let the predefined target BER be denoted with $\pi_b^{(rq)}$. Based on (3.32) and (3.33), the transmit power required to realize the target depends on the constellation size M as well as the static system parameters such as the transmission distance d . The achieved data rate in bit/sec is computed as

$$R = \frac{1 - \pi_b^{(rq)}}{T_s} \cdot \log_2 M, \quad (3.35)$$

where T_s is the symbol duration which relates to the signal bandwidth by $B = (1 + \beta)/T_s$, with β being the roll-off factor of the pulse shaping filter. Note that we assume T_s to be much smaller than T , so that the continuous-time model can still be regarded valid.

We model the total power consumption of the transmitter as

$$P = p_{amp} + p_{ct} = \alpha_{amp} p_{tx} + p_{ct}, \quad (3.36)$$

where p_{ct} is a constant term standing for the sum power dissipation of the DAC, the transmit filters, the frequency synthesizer as well as other processing units, and p_{amp} denotes the power consumption of the power amplifier (PA). Given a Class A linear PA, p_{amp} can be expressed as [37,70]

$$p_{amp} = \alpha_{amp} \cdot p_{tx}, \quad \alpha_{amp} = \frac{\xi}{\eta}, \quad \xi = \xi_{mod} \cdot \xi_{rrc}, \quad (3.37)$$

where η is the drain efficiency of the amplifier, and ξ represents the peak-to-average ratio (PAR) of the input signal. For square MQAM with equally probable symbols, the PAR of the constellation points is given by $\xi_{mod} = 3 \cdot \frac{\sqrt{M}-1}{\sqrt{M+1}}$. Pulse shaping *e.g.* the utilization of a root-raised-cosine filter further changes the PAR. With decreasing roll-off factor β , the impulse response of the filter have higher amplitude in the sidelobes, the frequency response becomes sharper, and the PAR ξ_{rrc} increases [37]. For the roll-off factor $\beta = 0.3$ that we choose, ξ_{rrc} can be taken approximately as 2.8 [71]. The PAR of the input signal to the PA is then given by the product of ξ_{mod} and ξ_{rrc} .

By using (3.35) and (3.36), we obtain the power-rate graphs for different values of d as shown in Fig. 3.6, where the relevant system parameters are summarized in Table 3.2. We have in total 5 possible discrete power levels, determined by the sleep mode and

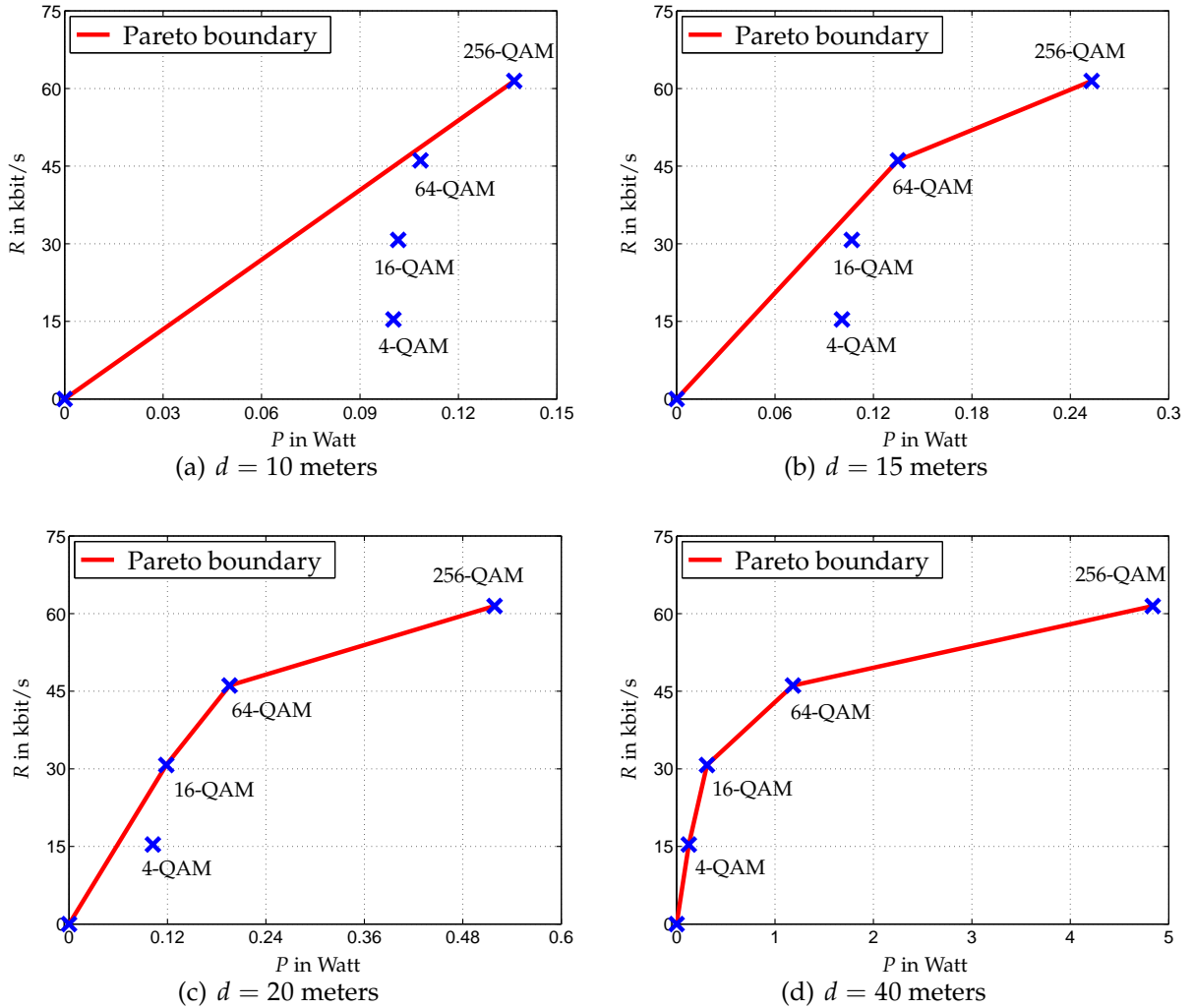


Fig. 3.6: Pareto boundaries of (P, R) pairs for MQAM transmission

the 4 available modulation formats. Depending on the transmission distance, different numbers of these levels can be found energy efficient. With a short distance typically, using higher modulation formats is favorable, since the static circuit power dominates the total power consumption which renders low modulation formats inefficient.

We again take a look at the maximal achievable throughput I^* as dependent on A_0 and T , respectively, the numerical results of which are illustrated in Fig. 3.7. For given energy budget A_0 and interval duration T , one looks for the energy efficient operation modes to realize the average power consumption of A_0/T . If this is feasible, we let the two bounding points be (P_1, R_1) and (P_2, R_2) , which gives

$$\frac{A_0}{T} = \alpha P_1 + (1 - \alpha) P_2 \quad (3.38)$$

with α being the time-share of the first point, $0 \leq \alpha < 1$. Solving for α and plugging the result in, we obtain the maximal throughput as

$$I^* = T(\alpha R_1 + (1 - \alpha) R_2) = \frac{R_1 - R_2}{P_1 - P_2} \cdot A_0 + \frac{R_2 P_1 - R_1 P_2}{P_1 - P_2} \cdot T, \quad P_1 \leq \frac{A_0}{T} < P_2. \quad (3.39)$$

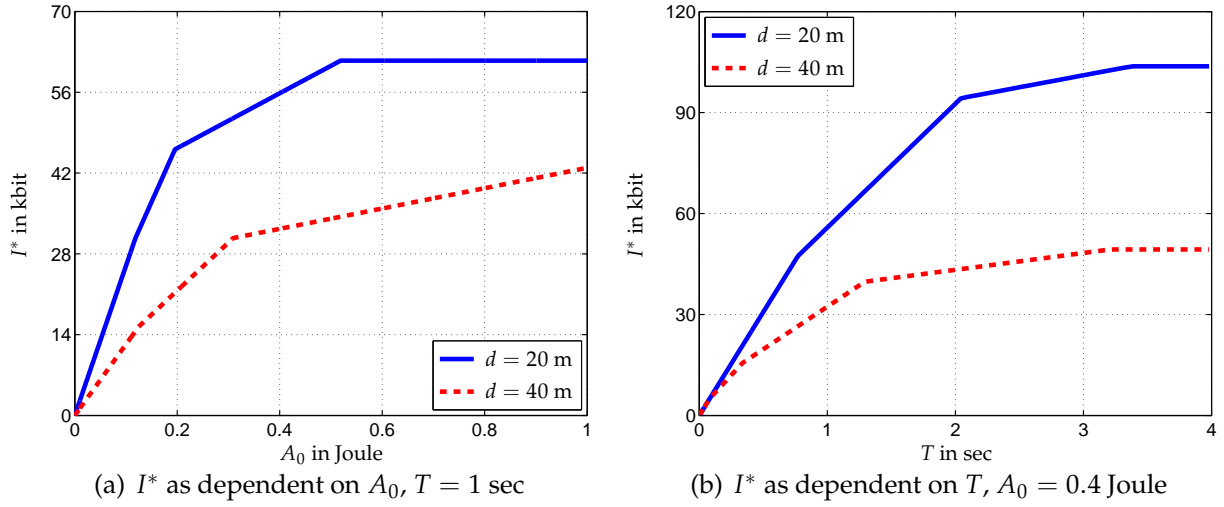


Fig. 3.7: Maximum throughput I^* as functions of A_0 and T for the MQAM model

From (3.39) one can expect the piecewise linear shape of I^* both as functions of A_0 and T . Moreover, it can be shown that the slopes of these linear segments are decreasing. We suppose (P_2, R_2) does not represent the most power demanding operation mode and let the next energy efficient mode be characterized by (P_3, R_3) . Due to the concavity of the Pareto boundary, we have

$$\frac{R_1 - R_2}{P_1 - P_2} > \frac{R_2 - R_3}{P_2 - P_3}, \quad (3.40)$$

$$R_3 = R_2 - (P_2 - P_3) \cdot \frac{R_2 - R_3}{P_2 - P_3} > R_2 + P_3 \cdot \frac{R_2 - R_3}{P_2 - P_3} - P_2 \cdot \frac{R_1 - R_2}{P_1 - P_2}. \quad (3.41)$$

By rearranging the terms in (3.41) we can obtain

$$\frac{R_3 P_2 - R_2 P_3}{P_2 - P_3} > \frac{R_2 P_1 - R_1 P_2}{P_1 - P_2}. \quad (3.42)$$

When T is fixed and A_0 is increased, the average power A_0/T increases and the coefficient of A_0 in (3.39) decreases according to (3.40). The upper limit of I^* is determined by the most power demanding, which also has the maximal rate, operation mode that is available. For the MQAM model, this corresponds to the highest feasible modulation order. On the other hand, when A_0 is fixed and T is increased, the average power decreases and the coefficient of T decreases as well due to (3.42). The upper limit of I^* is achieved by using the most energy efficient operation mode. For the MQAM model, this corresponds to the lowest energy efficient modulation order.

3.3.4 Case IV

We consider in this case that the wireless channel is time-varying on the time interval $[0, T]$, and the transmitter has perfect, non-causal knowledge about the channel state. The transmit power is taken as the control variable again, which is assumed continuous-valued and unbounded from above. The rate function R is now dependent on time via the time-varying channel gain, but is still assumed strictly concave in p_{tx} . The

cases that the power consumption function P is continuous or discontinuous at $p_{\text{tx}} = 0$ shall be discussed respectively.

3.3.4.1 Optimal transmission strategy for the non-constant channel

Let $g(t)$, $t \in [0, T]$ be the channel gain function which is positive and piecewise continuous. Recall that for the constant channel case we assume the rate function R to be strictly concave in the transmit power p_{tx} . As the channel gain usually comes into effect through the product with the transmit power, we write now $R(v) = R(gp_{\text{tx}})$, which has the first- and second-order partial derivatives

$$R_{p_{\text{tx}}}(g, p_{\text{tx}}) = g \cdot R_v(gp_{\text{tx}}) > 0, \quad R_{p_{\text{tx}}p_{\text{tx}}}(g, p_{\text{tx}}) = g^2 \cdot R_{vv}(gp_{\text{tx}}) < 0. \quad (3.43)$$

For such a rate function R and a convex power function P , the Hamiltonian evaluated at the optimal costate *i.e.* $H(t, p_{\text{tx}}, \lambda^*)$ is strictly convex, $\forall t \in [0, T]$. Based on (3.6), the optimal transmit power at any time instant is either the stationary point of $H(t, p_{\text{tx}}, \lambda^*)$ which satisfies the first-order condition

$$-R_{p_{\text{tx}}}(g, p_{\text{tx}}) + \lambda^* \cdot P_{p_{\text{tx}}}(p_{\text{tx}}) = 0, \quad (3.44)$$

or equals 0 if the stationary point at the time is negative. The resulting optimal control p_{tx}^* is obviously non-constant. If the Shannon formula is taken for R and there is no circuit power *i.e.* we have

$$R = B \log_2 \left(1 + \frac{g p_{\text{tx}}}{\sigma^2} \right), \quad P = p_{\text{tx}}, \quad (3.45)$$

then the optimal control follows from (3.44) as

$$p_{\text{tx}}^* = \left(\frac{B}{\lambda^* \ln 2} - \frac{\sigma^2}{g} \right)^+ \triangleq \left(\mu - \frac{\sigma^2}{g} \right)^+, \quad (3.46)$$

where $(x)^+ = \max\{0, x\}$. The constant μ , often referred to as the *marginal gain*, should lead to $W(T) = A_0$ to guarantee that the given energy budget is fully exploited. This is to say, instead of the constant slope condition along the optimal trajectory when the channel is time-invariant, we have now the constant marginal gain condition for the time-varying channel. The result (3.46) is the well-known *water-filling* solution, which can be realized via an iterative search of μ . One could, for instance, start with an arbitrary $\mu > 0$ and compute the corresponding control using (3.46). If the total energy consumption is less than A_0 , then μ is increased by a predefined amount called the step size, otherwise μ is reduced by the same amount. The procedure is ended when the energy consumption of the obtained control is close enough to A_0 . The optimal control given by (3.46) holds for linear power functions as well. For convex functions P in more complex forms, solving (3.44) can be difficult and p_{tx}^* might not have a closed-form expression.

We derive next, the optimal control when P is convex for $p_{\text{tx}} > 0$, but is discontinuous at $p_{\text{tx}} = 0$. Recall from Case II, that the optimal positive transmit power should not be smaller than the so-called *energy efficient transmit power* defined by (3.24). With a time-varying channel, this lower bound changes over time as well. We define

$$G(g, p_{\text{tx},0}) = R_{p_{\text{tx}}}(g, p_{\text{tx},0})P(p_{\text{tx},0}) - R(gp_{\text{tx},0})P_{p_{\text{tx}}}(p_{\text{tx},0}) = 0, \quad (3.47)$$

which gives $p_{\text{tx},0}$ as an implicit function of g . The partial derivatives of G with respect to $p_{\text{tx},0}$ and g can be computed respectively as

$$\begin{aligned} F_g &= g p_{\text{tx},0} R_{vv}(g p_{\text{tx},0}) P(p_{\text{tx},0}) + R_v(g p_{\text{tx},0}) (P(p_{\text{tx},0}) - p_{\text{tx},0} P_{p_{\text{tx}}}(p_{\text{tx},0})) \\ &\leq g p_{\text{tx},0} R_{vv}(g p_{\text{tx},0}) P(p_{\text{tx},0}) < 0, \end{aligned} \quad (3.48)$$

$$F_{p_{\text{tx},0}} = g^2 R_{vv}(g p_{\text{tx},0}) P(p_{\text{tx},0}) - R(g p_{\text{tx},0}) P_{p_{\text{tx}} p_{\text{tx}}}(p_{\text{tx},0}) < 0, \quad (3.49)$$

where the first inequality in (3.48) is due to the convexity of P . Consequently, we have $p_{\text{tx},0}$ decreases monotonically in g since

$$\frac{dp_{\text{tx},0}}{dg} = -\frac{F_g}{F_{p_{\text{tx},0}}} < 0. \quad (3.50)$$

Intuitively, the optimal control should in turn be equal or greater than the energy efficient transmit power on a pointwise basis. To show this, we assume for the moment that the channel power gain g is monotonically decreasing in time. In such a scenario, the optimal control can be expected to also decrease monotonically, which is made clear by observing (3.46). This suggests that there exists a time instant $t_1 \in (0, T]$, such that $p_{\text{tx}}^* > 0$ for $t \in [0, t_1]$, and $p_{\text{tx}}^* = 0$ for $t \in (t_1, T]$. To this end, we obtain a free endpoint, fixed final state problem on $[0, t_1]$ with a continuous state equation, for which the optimal transmit power can be computed by solving (3.44). The transversality condition (3.9) specifies the relation that needs to be fulfilled at the endpoint:

$$H(t_1, p_{\text{tx}}^*(t_1), \lambda^*) = -R(g(t_1) p_{\text{tx}}^*(t_1)) + \lambda^* \cdot P(p_{\text{tx}}^*(t_1)) = 0. \quad (3.51)$$

Plugging in λ^* which can be obtained from (3.44), we have

$$R_{p_{\text{tx}}}(g(t_1), p_{\text{tx}}^*(t_1)) P(p_{\text{tx}}^*(t_1)) - R(g(t_1) p_{\text{tx}}^*(t_1)) P_{p_{\text{tx}}}(p_{\text{tx}}^*(t_1)) = 0, \quad (3.52)$$

which means the optimal transmit power at the endpoint t_1 equals the corresponding energy efficient transmit power. As $p_{\text{tx},0}$ decreases with improving channel, we have $p_{\text{tx}}^* > p_{\text{tx},0}(g(t))$ for all $t \in [0, t_1]$.

When R is given by the Shannon formula and P has the discontinuous affine form

$$R = B \log_2 \left(1 + \frac{g p_{\text{tx}}}{\sigma^2} \right), \quad P = \begin{cases} c_1 \cdot p_{\text{tx}} + c_0, & p_{\text{tx}} > 0, \\ 0, & p_{\text{tx}} = 0, \end{cases} \quad (3.53)$$

where $c_1 \geq 1$, $c_0 > 0$ are given constants, the optimal control can be obtained as

$$p_{\text{tx}}^* = \begin{cases} \mu - \frac{\sigma^2}{g}, & \mu \geq \frac{\sigma^2}{g(t)} + p_{\text{tx},0}(g(t)), \\ 0, & \text{otherwise,} \end{cases} \quad (3.54)$$

where $\mu = \frac{B}{\lambda^* c_1 \ln 2}$ is the constant that ensures all available energy is consumed by time T , which can be found via iterative searching algorithms. Note, however, that (3.54) is only valid for those channel functions that are strictly monotonic or take the same value only at a finite number of points. If there exist time intervals on which the channel is

constant, then (3.54) might not be the optimum. To see this, consider the extreme scenario that g is time-invariant on $[0, T]$. The potentially necessary time-sharing between the sleep mode and using the energy efficient transmit power can not be identified by (3.54), which always gives the same transmit power for the same channel gain. To accommodate for the partially constant channel functions, we modify the optimal control as

$$p_{\text{tx}}^* = \begin{cases} \mu - \frac{\sigma^2}{g}, & \mu > \frac{\sigma^2}{g(t)} + p_{\text{tx},0}(g(t)), \\ 0 \text{ or } p_{\text{tx},0}(g(t)), & \mu = \frac{\sigma^2}{g(t)} + p_{\text{tx},0}(g(t)), \\ 0, & \text{otherwise,} \end{cases} \quad (3.55)$$

where the decision at the exact threshold is dependent on the global energy allocation. For any given positive constant μ , we call the channel gain \bar{g} that satisfies $\mu = \sigma^2/\bar{g} + p_{\text{tx},0}(\bar{g})$ the *critical channel gain*, which acts as a threshold for determining whether the transmitter should be active or not at a certain time instant. At those times that $g(t) > \bar{g}$, the transmitter is active and the constant marginal gain condition needs to be fulfilled. The total energy consumption W during these times can be computed accordingly. If $W > A_0$, then we have set μ too high and a reduction is required; otherwise, we need to determine what to do with the unused energy. If there exists one or more time intervals with exactly the critical channel gain, then the remaining energy could be spent on these intervals with the corresponding energy efficient transmit power $p_{\text{tx},0}(\bar{g})$. If there is still energy left or no such intervals exist, then μ needs to be increased. We can find μ by iteratively going through these steps until a control with the energy consumption approximately equal to A_0 is obtained, which is then the optimum control.

Some simple numerical examples are given for a more direct impression of the results we have derived. In Fig. 3.8, we illustrate the optimal controls and the optimal state trajectories for a predefined monotonically decreasing channel gain function. When $P = p_{\text{tx}}$ i.e. no circuit power is considered, the energy efficient transmit power $p_{\text{tx},0}$ is constantly zero, and p_{tx}^* decreases in a continuous fashion to zero. When P has the discontinuous affine form given in (3.53), the decreasing p_{tx}^* jumps to zero right after the point at which it is equal to the corresponding energy efficient transmit power.

3.3.4.2 Optimal transmission strategy for the block-fading channel

A relevant and common scenario that necessitates the treatment of partially constant channels is the transmission over block-fading channels. We let T_b denote the duration of each block, and assume $T = N \cdot T_b$ where $N \in \mathbb{N}^+$. The independent channel realizations on the N blocks are assumed perfectly known in advance. We introduce two different ways for obtaining the optimal control in the following.

- PMP based search algorithm

The search procedure described previously can be tailored for the block-fading channel and is summarized in Algorithm 1. We sort and examine the blocks in the descending order of their channel gains. In each iteration, we regard the considered block as the *critical block* on which the transmit power can be either zero or the corresponding energy efficient transmit power. The channel gain and the energy

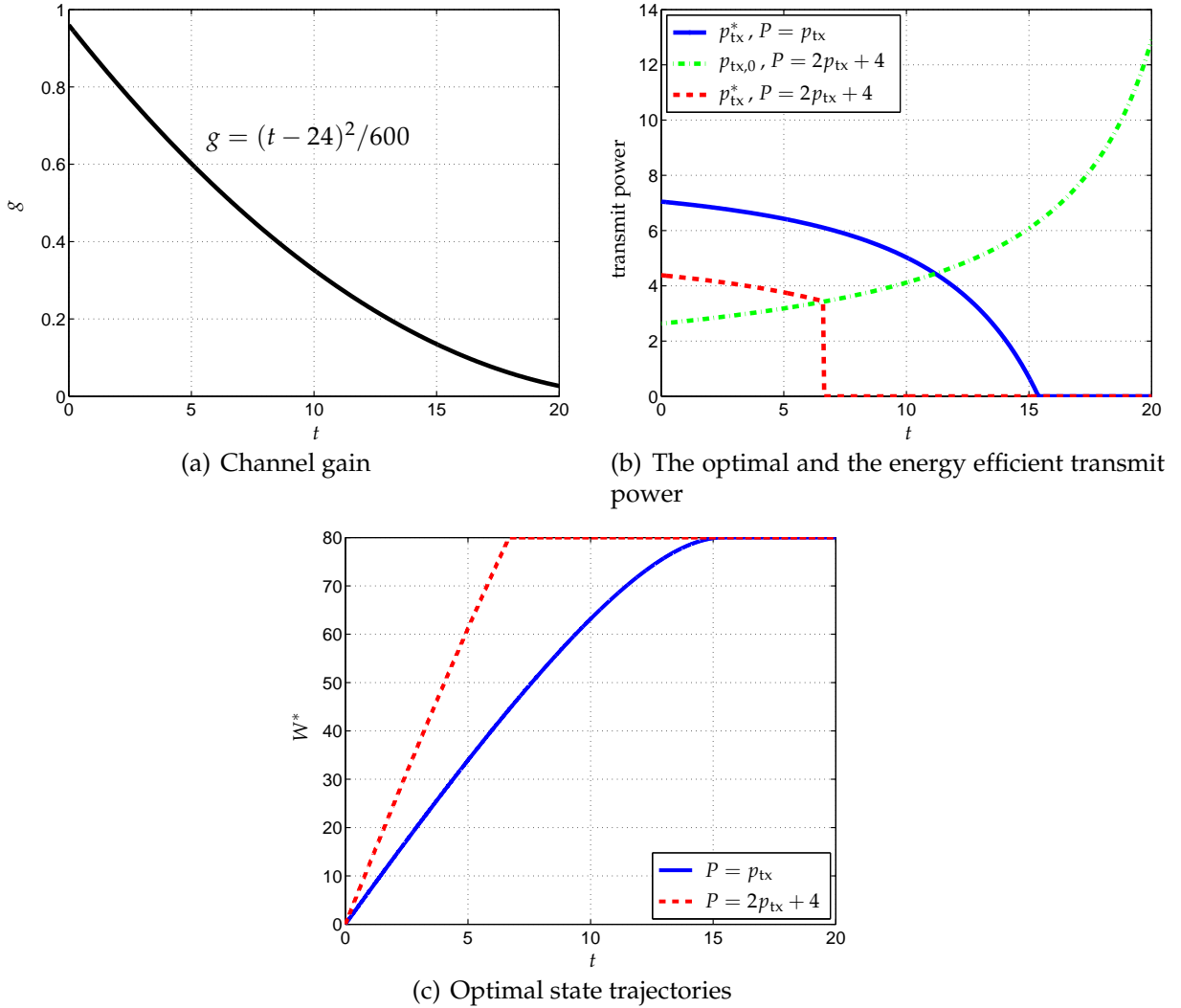


Fig. 3.8: Optimal transmit power and optimal trajectories for a monotonically decreasing channel function, $A_0 = 80$, functions R and P given by (3.53) with $B = 1$, $\sigma = 1$

efficient transmit power determine together the constant marginal gain μ according to (3.55). During the blocks with worse channel conditions, the transmitter is turned into sleep mode, while during the blocks with better channel conditions, the transmitter employs the transmit power given by the difference between μ and the respective noise-to-channel-gain ratio. If the corresponding total energy consumption is larger than A_0 , then the critical block under consideration should not be active, and the transmit power on the active blocks needs to be recomputed with the regular water-filling procedure, *i.e.* via an iterative search for the optimal μ . Otherwise, the time-sharing solution on the critical block that exhausts the remaining energy is computed. In case such a solution does not exist, we move on to the next best block and repeat the procedure.

We exemplify the two possible cases resulting from Line 9 and Line 12 of Algorithm 1 in Fig. 3.9. The time interval of interest contains $N = 5$ blocks, and in both cases there

Algorithm 1 Finding the optimal control for a block-fading channel**Require:** Channel gains of all blocks, and subroutine to compute $p_{\text{tx},0}$ **Ensure:** Optimal transmit power and the corresponding active time for each block

- 1: Sort and index all blocks in descending order of their channel gains: $g(1) > g(2) > \dots > g(N)$
- 2: Compute $p_{\text{tx},0}(n)$ according to (3.47), $n = 1, \dots, N$
- 3: Initialize the transmit power: $p_{\text{tx}}(n) \leftarrow 0, n = 1, \dots, N$
- 4: **for** $n = 1, \dots, N$ **do**
- 5: Block n is assumed critical: $\mu \leftarrow p_{\text{tx},0}(n) + \frac{\sigma^2}{g(n)}$
- 6: Transmit power for previous blocks: $p_{\text{tx}}(i) \leftarrow \mu - \frac{\sigma^2}{g(i)}, i = 1, \dots, n-1$
- 7: Total energy consumption for previous blocks: $W \leftarrow T_b \sum_{i=1}^{n-1} (c_1 p_{\text{tx}}(i) + c_0)$
- 8: **if** $W \geq A_0$ **then**
- 9: Compute $p_{\text{tx}}(i), i = 1, \dots, n-1$ with regular water-filling procedure
- 10: **return**
- 11: **end if**
- 12: Block n can be active: $p_{\text{tx}}(n) \leftarrow p_{\text{tx},0}(n), T_a \leftarrow \frac{A_0 - W}{P(p_{\text{tx}}(n))}$
- 13: **return if** $T_a \leq T_b$
- 14: **end for**

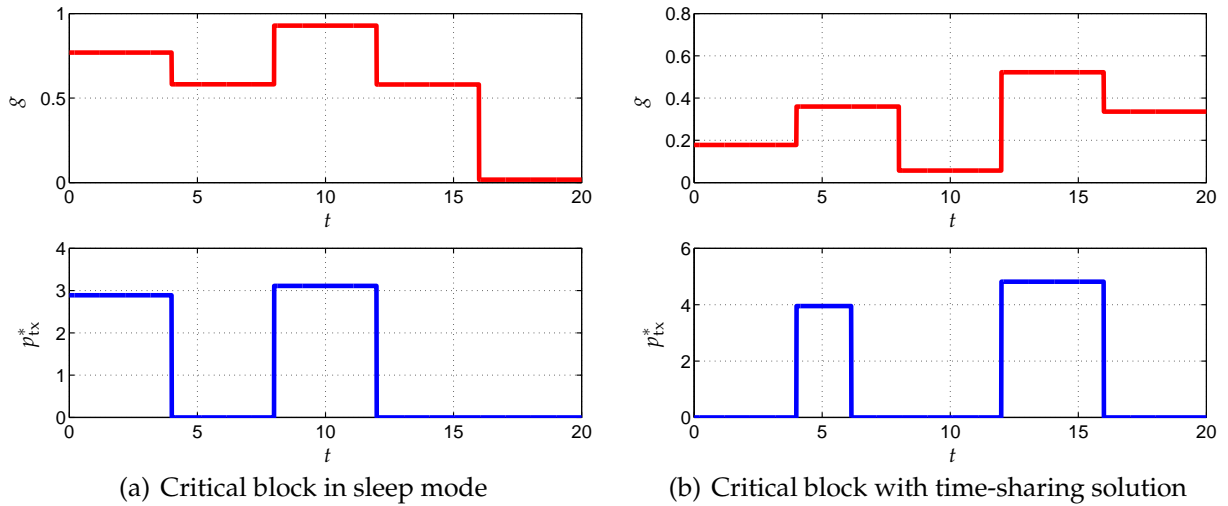


Fig. 3.9: Optimal transmit power for block-fading channels, $A_0 = 80$, $T_b = 4$, functions R and P given by (3.53) with $c_1 = 2$, $c_0 = 4$, $B = 1$, $\sigma = 1$

are 3 blocks over which the transmitter is in sleep mode. As shown in Fig. 3.9(a), the transmitter is completely active over the other 2 blocks in this case, but enabling the next best block *i.e.* the critical block would cost too much energy. For the case shown in Fig. 3.9(b) on the other hand, time-sharing takes place on the critical block, and the transmit power for the best block can be computed directly from the optimal marginal gain without going through the regular water-filling procedure.

- Convex optimization formulation

For the block-fading channel, one can also reformulate the infinite-dimensional optimization (3.3) into a finite-dimensional resource allocation problem. More specifically, we let $w_n \geq 0$, $n = 1, \dots, N$ be the energy allocated to each of the blocks, and let $J(w, g)$ denote the maximal achievable throughput on a block with channel gain g and energy consumption w . The throughput maximization problem is formulated as a constrained optimization on the energy allocation parameters as

$$\begin{aligned} \max_{\{w_1, \dots, w_N\}} \quad & \sum_{n=1}^N J(w_n, g_n) \\ \text{s.t.} \quad & \sum_{n=1}^N w_n \leq A_0, \quad w_n \geq 0, \quad n = 1, \dots, N. \end{aligned} \quad (3.56)$$

As the channel stays constant on each block, the function J can be evaluated by using the optimal control derived for Case II, and it is a concave function of w given fixed g . Consequently, the optimization problem (3.56) is convex and any standard solver of convex optimization can be applied to obtain the optimal energy allocation, from which the optimal transmit power can be computed. This method, although straightforward and easy to implement, is not as insightful as the PMP based method, and can have high complexity when the number of blocks is large.

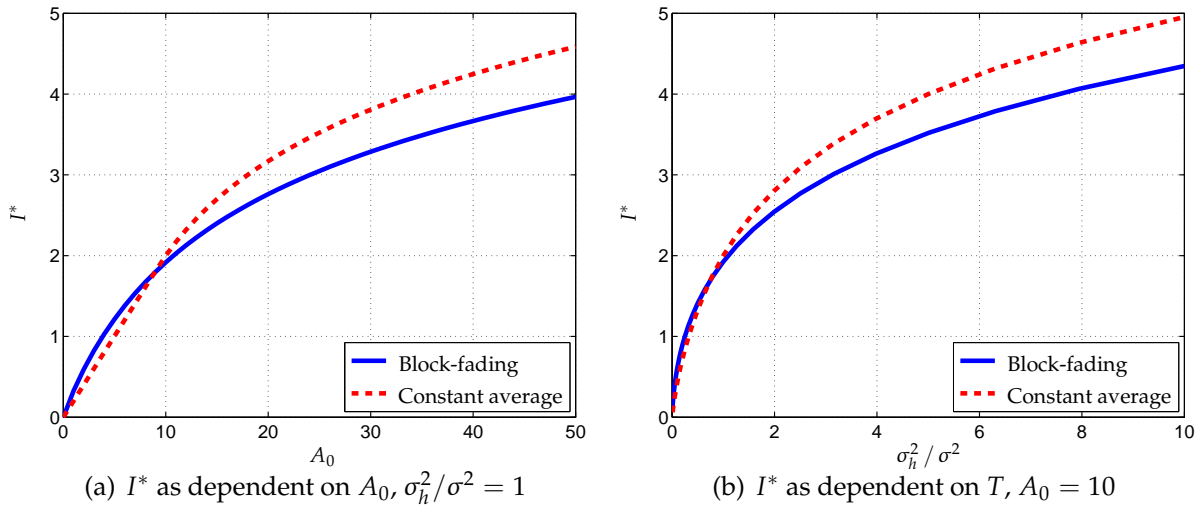


Fig. 3.10: Maximum throughput I^* as dependent on A_0 and σ_h^2/σ^2 , $T = 1$, $N = 10$, functions R and P given by (3.53) with $c_1 = 2$, $c_0 = 4$, $B = 1$

We simulate the scenario with a Rayleigh fading channel where the channel coefficient $h \sim \mathcal{CN}(0, \sigma_h^2)$ is assumed to change independently from block to block, *i.e.* the real and imaginary parts of h are i.i.d. zero-mean Gaussian with variance $\sigma_h^2/2$. The maximal achievable throughput I^* as dependent on the energy budget A_0 and the ratio between the variance of the channel and the noise is illustrated in Fig 3.10. The blue solid curves represent the averaged results over 10^3 realizations of the block-fading channel on the time interval of interest. The red dashed curves, on the other hand, are generated

assuming a constant channel with the channel gain σ_h^2 . The crossing of the curves can be explained as follows: if constant transmit power were employed, the throughput on the time-invariant channel would be larger than that of the block-fading channel due to the strict concavity of the rate function, and the difference becomes smaller if the energy is not adequate or the average channel gain is reduced. The optimal energy allocation enables diversity gain by spending more energy on blocks with good channel conditions. This gain surpasses the said difference in the low energy or low SNR regime, causing the blue curves to come above the red ones as shown in the figures.

3.3.5 Case III + IV

Features of Case III and IV are now combined: we assume a block-fading channel and the transmitter employs uncoded MQAM for data transmission. A random variable Φ characterizing the effect of shadowing is added to the concrete system model introduced in Case III, which is assumed to change independently from block to block. We employ the log-normal shadowing model [66] and modify the receive SNR formula (3.32) as

$$\gamma = \frac{p_{\text{rx}}}{N_0 B} = \frac{1}{M_1 G_1 N_0 B} \cdot \frac{p_{\text{tx}}}{10^{\Phi/10} d^\kappa}, \quad (3.57)$$

where Φ is Gaussian distributed with zero mean and variance σ_Φ^2 . Recall that for a given modulation order and a target BER, the minimum required receive SNR can be computed according to (3.33). The transmit power that is demanded then follows from (3.36), which depends now not only on the modulation order and the constant system parameters, but also on the time-varying parameter Φ . To this end, the Pareto boundary of the discrete (P, R) pairs on the power-rate graph changes from block to block, as dependent on the realization of Φ , which is exemplified in Fig. 3.11. Each marked point in the figure represents one modulation order. We see that not only are the positions of the points changed for different Φ , but also is the set of energy efficient operation modes different.

We assume the transmitter is aware of the realizations of Φ on all blocks before the transmission starts, and denote them with ϕ_1, \dots, ϕ_N where N is the total number of blocks as before. The throughput maximization problem can be formulated in a similar way as (3.56), where J is evaluated by finding the time-shares of the energy efficient operation modes corresponding to the designated energy consumption. Equivalently, one can optimize directly over the time-shares instead of the energy consumption. We let \mathbf{P}_n and \mathbf{R}_n be the vector of power consumptions and achievable rates of the energy efficient modulation orders for block n , respectively, and let the vector $\boldsymbol{\alpha}_n$ contain the time-sharing factor of each mode which is a real number between 0 and 1. The throughput maximization problem is then formulated as a linear program as

$$\begin{aligned} \max_{\{\boldsymbol{\alpha}_1, \dots, \boldsymbol{\alpha}_N\}} \quad & T_b \sum_{n=1}^N \mathbf{R}_n^T \boldsymbol{\alpha}_n \\ \text{s.t.} \quad & T_b \sum_{n=1}^N \mathbf{P}_n^T \boldsymbol{\alpha}_n \leq A_0, \\ & \mathbf{1}^T \boldsymbol{\alpha}_n = 1, \quad \boldsymbol{\alpha}_n \succeq \mathbf{0}, \quad n = 1, \dots, N. \end{aligned} \quad (3.58)$$

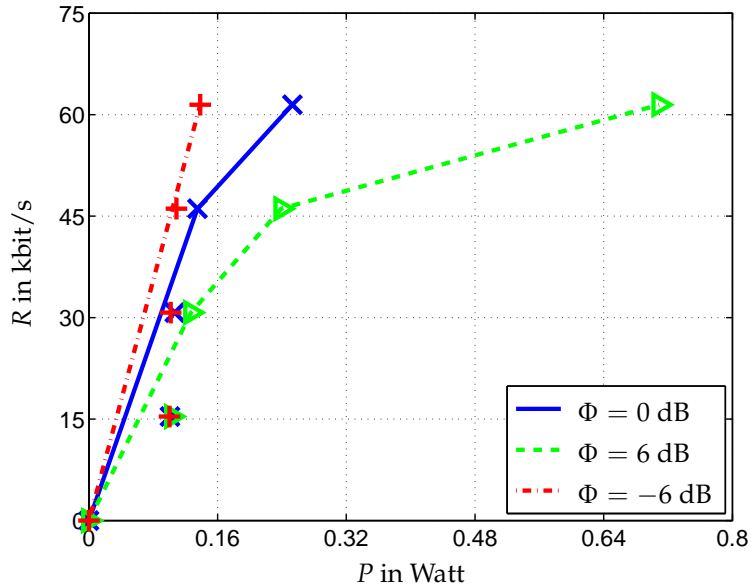


Fig. 3.11: Pareto boundaries of (P, R) pairs for MQAM transmission over a block-fading channel, $d = 15$ meters

When the number of available modulation orders is not very large, the linear programming formulation is less complex to solve than the convex optimization in the form of (3.56). Moreover, the result provides the system directly with the operational actions that should be taken.

Upon observing the obtained optimal control, we find that in most cases, there is only one block with the time-sharing of two modulation orders while all other blocks employ a single operation mode. This motivates us to propose a heuristic algorithm which chooses one modulation order for a number of blocks each, and allows time-sharing on one of the remaining blocks. We propose to select the modulation orders based on their energy efficiency represented by the rate-to-power ratio, until the total energy consumption exceeds the given budget. Then, for each loaded block, we examine the reduction in throughput when the energy consumption on the block is cut to fit the total budget with the time-sharing solution that consumes this required energy. The block that leads to the least throughput reduction is chosen to employ the corresponding time-sharing solution, and all the other blocks are either inactive or use exclusively a single modulation order. This heuristic algorithm, which has much lower complexity than the optimal linear program, is summarized in Algorithm 2.

From the simulation results shown in Fig. 3.12, we see clearly that the heuristic algorithm achieves almost the optimal performance for both test scenarios: in the first one we fix the energy budget and let the transmission distance vary, and in the second we do the contrary. This suggests the applicability of the heuristic algorithm for systems with different levels of energy sufficiency.

3.3.6 Case V

We have discussed with Case IV the optimal control of the transmitter when the channel is time-varying and known in advance, which is an idealized scenario established for

Algorithm 2 Heuristic algorithm for the control of MQAM transmission over a block-fading channel with given energy budget

Require: Energy budget A_0 , fading parameters ϕ_1, \dots, ϕ_N , the achievable rate and power consumption models that enable the computation of the (P, R) pairs for all available modulation orders on each block

Ensure: Time shares of each modulation order on each block

- 1: $W \leftarrow$ total energy consumption when the highest order is chosen for every block
 - 2: **return if** $W \leq A_0$
 - 3: $w_n \leftarrow 0, n = 1, \dots, N$
 - 4: **while** $W = \sum_{n=1}^N w_n < A_0$ **do**
 - 5: Find among the unselected energy efficient modulation orders the one with the maximal energy efficiency and denote its power-rate value as (P, R)
 - 6: $n \leftarrow$ block index of the pair (P, R) , $w_n \leftarrow P \cdot T_b$
 - 7: **end while**
 - 8: **return if** $W = A_0$
 - 9: $\mathcal{B} \leftarrow \{n : W - w_n < A_0\}$
 - 10: **for each** $n \in \mathcal{B}$ **do**
 - 11: Compute the time-sharing solution on block n to consume the energy $A_0 - W + w_n$
 - 12: $\Delta R_n \leftarrow$ reduction in throughput
 - 13: **end for**
 - 14: $i \leftarrow \operatorname{argmin}_n \Delta R_n$
 - 15: Replace the exclusive modulation order usage on block i with the corresponding time-sharing solution
-

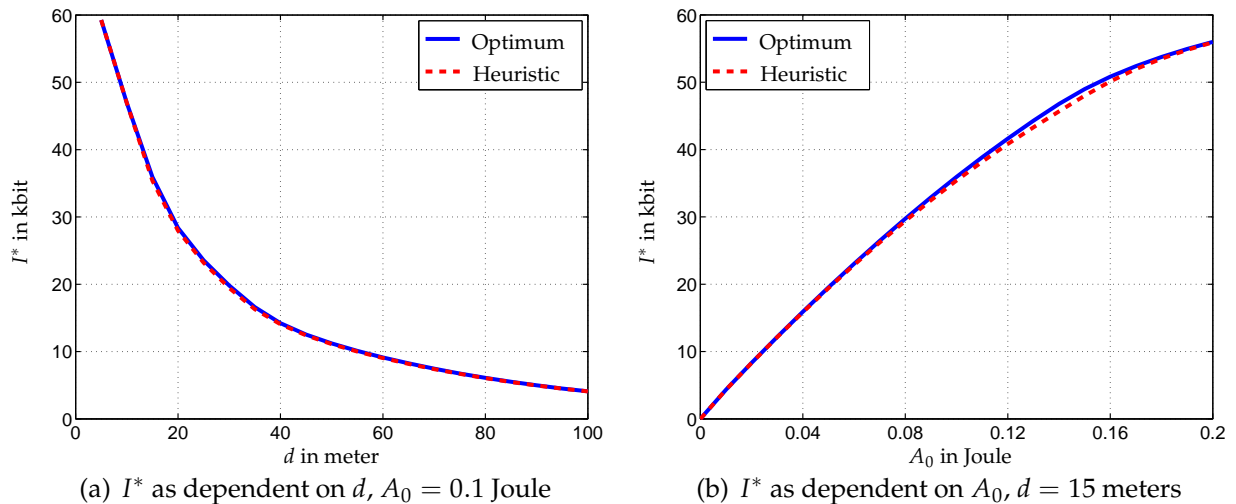


Fig. 3.12: Maximum throughput I^* as functions of d and A_0 for MQAM transmission over a block-fading channel, $\sigma_{\Phi} = 3$ dB, $T = 1$ sec, $N = 100$

theoretical analysis. To move towards the more practical situation, we assume in this case that the transmitter only has instantaneous as well as statistical channel state information (CSI) about the underlying communication channel, which is assumed Rayleigh and block-fading. That is, beside the probability distribution of the random

channel coefficient, the transmitter knows at the beginning of each block its realization for the block, without any delay or error. Naturally, the transmitter could make its operational decision online based on this information.

Suppose at the beginning of the n -th block *i.e.* time instant $t = (n - 1)T_b$, the transmitter has the remaining energy budget of A_{n-1} , $n = 1, \dots, N$, and the knowledge of the channel gain on block n given as g_n . Based on A_{n-1} and g_n , the transmitter makes a decision on how much energy is allocated to block n , denoted with w_n , while the rest amount $A_n = A_{n-1} - w_n$ would be exploited by later blocks. We define the function $V_n(w)$ for $n = 1, \dots, N$ and $w \geq 0$, which stands for the maximal expected sum throughput on blocks $n, n + 1, \dots, N$ given the available energy w , where no instantaneous CSI is available. Intuitively, in order to maximize the total throughput, the decision on the energy allocation for block n should be made according to

$$w_n = \operatorname{argmax}_{0 \leq w \leq A_{n-1}} (J(w, g_n) + V_{n+1}(A_{n-1} - w)), \quad n = 1, \dots, N - 1, \quad (3.59)$$

i.e. the sum throughput of block n and the expected throughput on all subsequent blocks is maximized. As the feasible energy allocation is constrained on the closed interval $[0, A_{n-1}]$ and the objective function is finite, the optimal solution to the maximization always exists. The energy that is still available is updated after each block, before the next decision is to be made. For the last block, we have $w_N = A_{N-1}$.

In computing the sequence of functions V , we apply *backward induction* as

$$\begin{aligned} V_N(w) &= E_g [J(w, g)], \\ V_n(w) &= \max_{0 \leq w' \leq w} \left(V_{n+1}(w - w') + E_g [J(w, g)] \right), \quad n = 1, \dots, N - 1, \end{aligned} \quad (3.60)$$

where $J(w, g)$ represents the maximal achievable throughput by using energy w on a single block with channel gain g . The recurrence relation (3.60) is based on Bellman's *Principle of Optimality* [72] that, for the throughput on blocks n to N to be maximized, the throughput on blocks $n + 1$ to N needs to be maximized with the respective energy input². To this end, the optimization on a horizon of $N - n + 1$ blocks is broken down into subproblems with a single block, and with $N - n$ blocks which can be further reduced to subproblems with fewer blocks. One can therefore start with solving the single-block problem for all possible input, and obtain results for multi-block problems incrementally. Such an approach is called the *dynamic programming* (DP), the essence of which is presented by the dynamic relationship (3.60). The function V is called the *value function* in this context, and the time interval between consecutive decision-making points, in our case a block, is referred to as a *stage*.

Depending on the rate and the power consumption models, the function J can be computed based on the optimal solutions of Case I, II, or III. Recall from our previous discussions that J is concave in w in all three cases. Since g is always positive, the expectation of J with respect to g is also concave in w . As a result, the maximization

² The principle is originally stated as: an optimal policy has the property that whatever the initial state and initial decision are, the remaining decisions must constitute an optimal policy with regard to the state resulting from the first decision.

in the recurrence relation (3.60) is solved by equally splitting the available energy to the $N - n + 1$ blocks with independently changing channel, which means

$$V_n(w) = (N - n + 1) E_g \left[J \left(\frac{w}{N - n + 1}, g \right) \right], \quad n = 1, \dots, N. \quad (3.61)$$

We compute the value function offline for a number of energy levels resulting from discretizing the energy space $[0, A_0]$, and store the results so that less computations are required during the online operation.

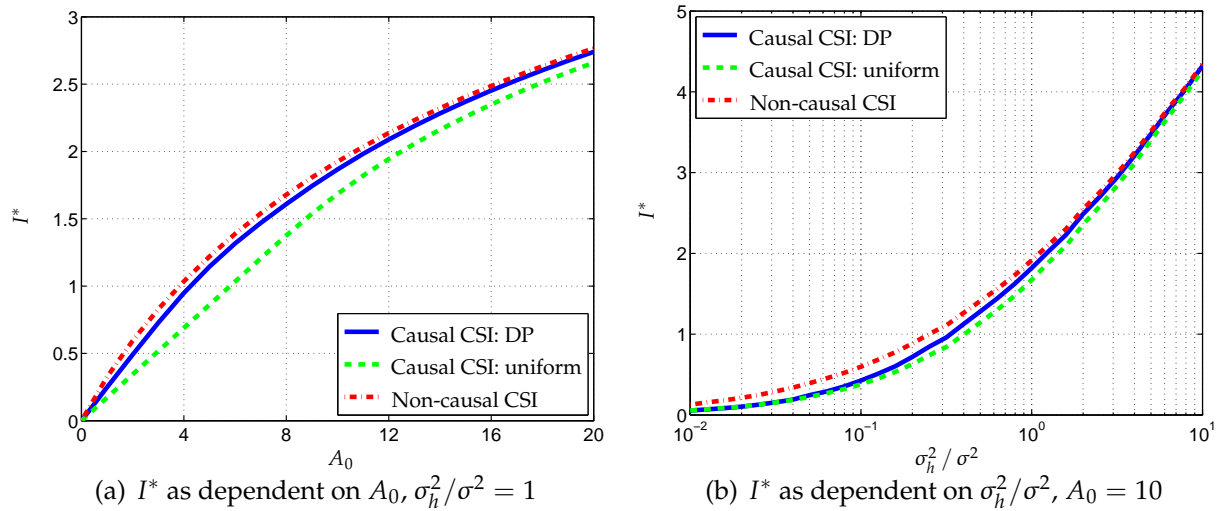


Fig. 3.13: Maximum throughput I^* as dependent on A_0 and σ_h^2/σ^2 , $T = 1$, $N = 10$, functions R and P given by (3.53) with $c_1 = 2$, $c_0 = 4$, $B = 1$

Numerical results are demonstrated in Fig. 3.13, where we compare the maximal throughput achieved by having only causal CSI and employing DP, to that of equally allocating the available energy to each block. The scenario where the transmitter has non-causal CSI, the solution of which has been discussed in Case IV, is also shown which provides an upper limit for the causal CSI case. We first fix the average channel condition and vary the energy budget, and then do the contrary. It can be observed that having causal CSI is almost as good as having non-causal CSI when the energy is abundant *i.e.* approaching the right side in both figures, which degrades the performance of the system by only a few percents. The throughput achieved with uniform energy allocation also comes close to the optimum attained by DP in this case. When the energy is relatively scarce, the absence of non-causal CSI can lead to as much as 50% decrease in throughput, and the gap between employing DP and the uniform energy allocation increases to 10%-20% of the latter as well. Nevertheless, based on these test results, the uniform energy allocation strategy appears a good candidate for the control of the transmitter due to its simplicity and robustness.

3.3.7 Case VI

Lastly, we consider a scenario that is rather different from all the previous ones. In contrast to the fixed, deterministic parameter T , we consider here that the duration of the time

interval on which the available energy A_0 is to be spent is a random variable, denoted with τ . One could think of this scenario as if the transmitter is restrained by a random deadline at which the transmission has to terminate, and it wishes to deliver on average as much data as possible before the deadline. In the context of energy harvesting supported communications, the time interval can be seen as the stage between two consecutive energy arrivals, presuming the arrivals discrete. The scenario happens if the transmitter aims at maximizing the throughput until the next arrival instant, which is unknown but usually conforms to some statistical distribution. To this end, we assume that τ is exponentially distributed, which follows from the common modeling of random arrivals known as the *Poisson process*, and that the channel condition is time-invariant. We come back to the PMP for obtaining the optimal control in this case.

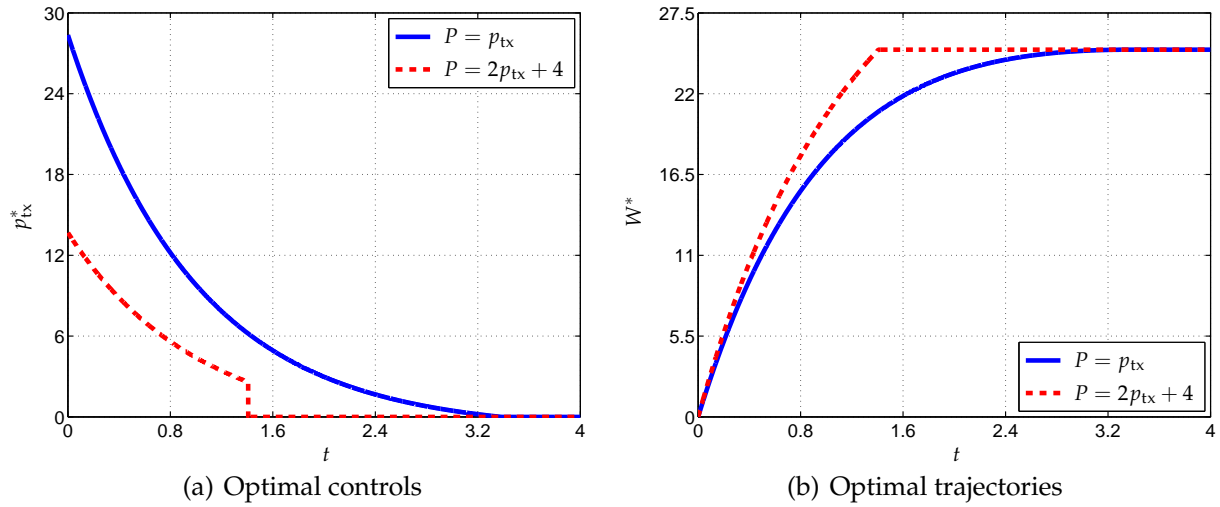


Fig. 3.14: Optimal transmit power and optimal state trajectories for the discounted rate function, $A_0 = 25$, $\nu = 1$, blue curves correspond to model (3.20) and red curves correspond to model (3.27), $B = 1$, $\sigma = 1$

The optimization objective is adjusted to the expected throughput until the deadline, which can be derived as

$$\begin{aligned}
 I(p_{\text{tx}}) &= \mathbb{E} \left[\int_0^{\tau} R(p_{\text{tx}}) dt \right] = \int_0^{+\infty} p_{\tau}(\tau) \int_0^{\tau} R(p_{\text{tx}}) dt d\tau \\
 &= \int_0^{+\infty} R(p_{\text{tx}}) \int_t^{+\infty} p_{\tau}(\tau) d\tau dt = \int_0^{+\infty} R(p_{\text{tx}}) (1 - F_{\tau}(t)) dt \\
 &= \int_0^{+\infty} e^{-\nu t} R(p_{\text{tx}}) dt, \tag{3.62}
 \end{aligned}$$

where p_{τ} and F_{τ} stand for the probability density and the cumulative distribution functions of the exponentially distributed random variable τ , respectively, and ν denotes the rate of the distribution. Note from (3.62) that the Lagrangian depends explicitly on time via the term $e^{-\nu t}$, which can be seen as a discounting factor for the data rate and has no influence on the strict concavity of the Lagrangian in p_{tx} . The Hamiltonian and the

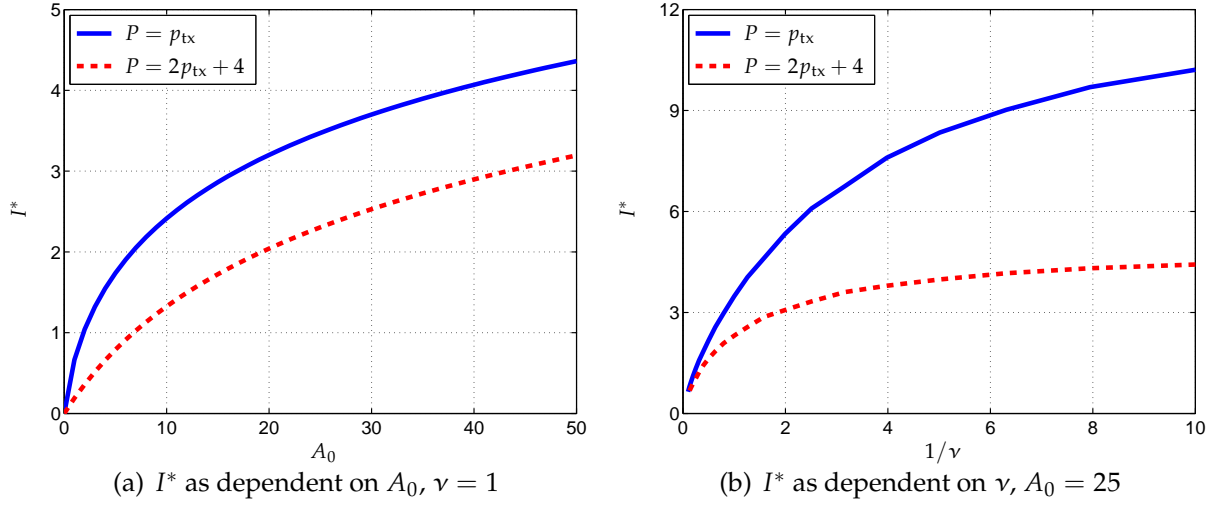


Fig. 3.15: Maximal expected throughput achieved by employing the respective optimal control, blue curves correspond to model (3.20) and red curves correspond to model (3.27), $B = 1$, $\sigma = 1$

first-order condition for the establishment of (3.6) are given in this case by

$$H(t, p_{\text{tx}}, \lambda) = -e^{-\nu t} \cdot R(p_{\text{tx}}) + \lambda \cdot P(p_{\text{tx}}), \quad (3.63)$$

$$H_{p_{\text{tx}}}(t, p_{\text{tx}}^*, \lambda^*) = -e^{-\nu t} \cdot R_{p_{\text{tx}}}(p_{\text{tx}}^*) + \lambda^* \cdot P_{p_{\text{tx}}}(p_{\text{tx}}^*) = 0, \quad (3.64)$$

where λ^* is the constant costate since H does not depend on W explicitly. For a strictly concave function R and a convex function P , $H(t, p_{\text{tx}}^*, \lambda^*)$ is strictly convex in p_{tx} , which is minimized either by p_{tx}^* that solves (3.64), or by $p_{\text{tx}}^* = 0$ if the solution to (3.64) is negative. When the functions R and P are given by the generic model (3.20), we have the following optimal control:

$$p_{\text{tx}}^* = \left(\frac{B e^{-\nu t}}{\lambda^* \ln 2} - \sigma^2 \right)^+, \quad t \geq 0, \quad (3.65)$$

where λ^* is the constant that leads to

$$\int_0^{t_1} P(p_{\text{tx}}^*) dt = A_0 \quad (3.66)$$

with t_1 denoting the endpoint of operation, *i.e.* $p_{\text{tx}}^* > 0$ for $t \in [0, t_1]$ and $p_{\text{tx}}^* = 0$ for $t \in (t_1, +\infty)$. Obviously, the optimal control is a monotonically decreasing function of time. The transversality condition (3.9) requires

$$H(t_1, p_{\text{tx}}^*(t_1), \lambda^*(t_1)) = -e^{-\nu t_1} \cdot R(p_{\text{tx}}^*(t_1)) + \lambda^* \cdot P(p_{\text{tx}}^*(t_1)) = 0 \quad (3.67)$$

to be fulfilled, which further leads to

$$(R_{p_{\text{tx}}} \cdot P - R \cdot P_{p_{\text{tx}}})(p_{\text{tx}}^*(t_1)) = 0, \quad (3.68)$$

showing that the optimal transmit power at t_1 is equal to the energy efficient transmit power $p_{\text{tx},0}$. For the generic model (3.20) where P is continuous at $p_{\text{tx}} = 0$, we have

$p_{\text{tx},0} = 0$ which means the optimal transmit power smoothly fades away at t_1 . On the other hand, in the case that P has the affine discontinuous form (3.27), we have $p_{\text{tx},0} > 0$ and the formula for the optimal transmit power can be modified as

$$p_{\text{tx}}^* = \begin{cases} \frac{B e^{-\nu t}}{\lambda^* c_1 \ln 2} - \sigma^2, & t \leq -\frac{1}{\nu} \left(\ln \left(\frac{\lambda^* c_1 \ln 2}{B} \right) + \ln(\sigma^2 + p_{\text{tx},0}) \right), \\ 0, & \text{otherwise,} \end{cases} \quad (3.69)$$

which suggests a sudden decrease of p_{tx}^* at the endpoint t_1 . The constant λ^* should ensure that the available energy A_0 is fully exploited. We notice that the derivations and results presented above bear a lot of resemblance with those of Case IV. We show an example of the optimal controls and the corresponding optimal state trajectories in Fig. 3.14, and demonstrate the average throughput achieved by employing the optimal control with respect to A_0 and ν in Fig. 3.15, respectively. Note that the mean value of the random variable τ is given by $1/\nu$. Therefore, in Fig. 3.15(b), increasing $1/\nu$ corresponds to the prolongation of the transmission interval on average, and the behavior of the achieved throughput as increasing with decreased rate can be expected.

3.4 Optimal Control of the Receiver

We turn our focus now onto the receive side, and discuss the optimal control of a receiver on the time interval $[0, T]$ given a fixed energy budget. Instead of the transmit power or the modulation format, the control variable we consider at the receive side is the bit resolution employed by the A/D converter. As introduced in Section 2.3.1, the ADC resolution b is a key parameter that governs the trade-off between the spectral and energy efficiency of the receiver. We shall treat the capacity lower bound (2.26) as the rate function R , and the power consumption model (2.29) as the power function P in this section:

$$R = B \log_2 \left(\frac{1 + \gamma}{1 + \gamma \cdot 2^{-2b}} \right), \quad P = \begin{cases} a_1(2^b - 1) + a_0, & b > 0, \\ 0, & b = 0, \end{cases} \quad (3.70)$$

where γ is the receive SNR, a_0 and a_1 are known constant parameters, and B is the signal bandwidth which is also constant. We discuss two control scenarios and derive the respective optimal receive strategies. In the first scenario, the ADC resolution is assumed real-valued, whereas in the second it is restricted to integer numbers. Although having different physical meanings and interpretations, the control problems we formulate here are mathematically very similar or even equivalent to some of the problems at the transmit side. Consequently, the corresponding conclusions obtained previously are directly applied without giving detailed derivation or reasoning.

3.4.1 Case I

We consider that on the time interval $[0, T]$, a transmitter is to send information to a receiver which is powered by a limited amount of energy. The transmitter is able to cooperate with the receiver so that the maximal amount of data can be conveyed, meaning that the transmitter adapts its transmission strategy *e.g.* the transmit power, the modulation and coding scheme, as desired by the receiver. The communication channel

is assumed invariant on the time interval, with the power gain α exactly known, and the transmitter and receiver are assumed perfectly synchronized.

In this case we let our control variable, the ADC resolution b be a non-negative real number. Upon examining the rate and the power function (3.70), we find that R is strictly concave in b since

$$R_b = \frac{2B\gamma}{2^{2b} + \gamma}, \quad R_{bb} = -\frac{4B\gamma \cdot 2^{2b} \cdot \ln 2}{(2^{2b} + \gamma)^2} < 0, \quad (3.71)$$

whereas P is convex in b for $b > 0$. This is to say, we have mathematically the same scenario as Case II of the transmitter. Instead of the energy efficient transmit power, we now have the *energy efficient bit resolution* b_0 as the solution to the equation

$$(R_b \cdot P - R \cdot P_b)(b) = 0, \quad (3.72)$$

and the corresponding power consumption is denoted with $p_0 = P(b_0)$. In complete analogy to the transmit side, the throughput-maximizing receive strategy is stated as: *If $A_0/T > p_0$, then the bit resolution $P^{-1}(A_0/T)$ should be employed constantly on $[0, T]$; otherwise, the energy efficient bit resolution b_0 should be used for a time period of length A_0/p_0 , and the receiver is turned into sleep mode for the rest of the time interval.*

Plugging R , P , and their respective derivatives into (3.72), we obtain the relation

$$\frac{2\gamma}{2^{2b_0} + \gamma} \cdot \left(2^{b_0} - 1 + \frac{a_0}{a_1}\right) = 2^{b_0} \cdot \ln \left(\frac{1 + \gamma}{1 + \gamma \cdot 2^{-2b_0}}\right), \quad (3.73)$$

from which b_0 can be solved numerically. To see how b_0 changes with γ and the ratio $\bar{a} = a_0/a_1$, we define the function

$$F = 2^{b_0} \cdot \ln \left(\frac{1 + \gamma}{1 + \gamma \cdot 2^{-2b_0}}\right) - \frac{2\gamma(2^{b_0} - 1 + \bar{a})}{2^{2b_0} + \gamma} = 0, \quad (3.74)$$

and calculate its partial derivatives

$$F_{b_0} = 2^{b_0} \ln 2 \left[\ln \left(\frac{1 + \gamma}{1 + \gamma \cdot 2^{-2b_0}}\right) + \frac{4\gamma \cdot 2^{b_0} (2^{b_0} - 1 + \bar{a})}{(2^{2b_0} + \gamma)^2} \right] > 0,$$

$$F_{\bar{a}} = -\frac{2\gamma}{2^{2b_0} + \gamma} < 0,$$

$$\begin{aligned} F_{\gamma} &= 2^{b_0} \left[\frac{2^{2b_0} - 1}{(1 + \gamma)(2^{2b_0} + \gamma)} - \frac{2(2^{b_0} - 1 + \bar{a})2^{2b_0}}{(2^{2b_0} + \gamma)^2} \right] \\ &= 2^{b_0} \left[\frac{2^{2b_0} - 1}{(1 + \gamma)(2^{2b_0} + \gamma)} - \frac{2^{3b_0}}{\gamma(2^{2b_0} + \gamma)} \cdot \ln \left(\frac{1 + \gamma}{1 + \gamma \cdot 2^{-2b_0}}\right) \right] \\ &< 2^{b_0} \left[\frac{2^{2b_0} - 1}{(1 + \gamma)(2^{2b_0} + \gamma)} - \frac{2^{3b_0}}{\gamma(2^{2b_0} + \gamma)} \cdot \frac{\gamma(2^{2b_0} - 1)}{2^{2b_0}(1 + \gamma)} \right] \end{aligned} \quad (3.75)$$

$$= \frac{2^{b_0}(2^{2b_0} - 1)(1 - 2^{b_0})}{(1 + \gamma)(2^{2b_0} + \gamma)} < 0, \quad (3.76)$$

where the inequality $\ln(1+x) > \frac{x}{1+x}$ for $x > 0$ is applied in (3.75). Consequently, we have

$$\frac{db_0}{d\bar{a}} = -\frac{F_{\bar{a}}}{F_{b_0}} > 0, \quad \frac{db_0}{d\gamma} = -\frac{F_{\gamma}}{F_{b_0}} > 0, \quad (3.77)$$

meaning that b_0 is monotonically increasing in both \bar{a} and γ . This is to say, from an energy efficiency point of view, higher ADC resolution is in favor when the channel condition is good or when the constant power consumption that is only associated with the active mode is comparatively large. Moreover, for very low and very high γ and a fixed \bar{a} , b_0 fulfills asymptotically the equations:

$$\begin{aligned} \gamma \rightarrow 0: \quad & 2^{b_0}(2^{2b_0} - 3) = 2(\bar{a} - 1), \\ \gamma \rightarrow +\infty: \quad & 2^{b_0}(b_0 \ln 2 - 1) = \bar{a} - 1. \end{aligned} \quad (3.78)$$

On the other hand, for a fixed receive SNR, $b_0 = 0$ if $\bar{a} = 0$, and b_0 increases boundlessly when $\bar{a} \rightarrow +\infty$. We illustrate the dependencies of the energy efficient bit resolution b_0 on the ratio \bar{a} and on the receive SNR γ in Fig. 3.16.

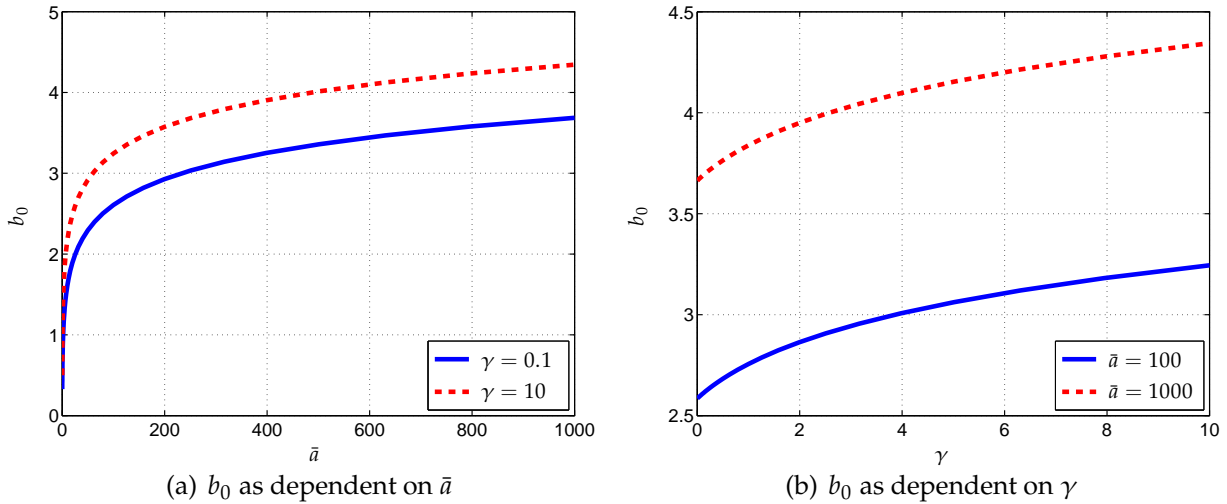


Fig. 3.16: Energy efficient bit resolution as dependent on a_0/a_1 and the receive SNR

Based on the optimal receive strategy, the maximal throughput achieved on $[0, T]$, denoted with I^* , is given by

$$I^* = \begin{cases} \frac{A_0}{p_0} \cdot B \log_2 \left(\frac{1+\gamma}{1+\gamma \cdot 2^{-2b_0}} \right), & \frac{A_0}{T} < p_0, \\ TB \left[\log_2(1+\gamma) - \log_2 \left(1 + \frac{a_1^2 \gamma}{(A_0/T - a_0 + a_1)^2} \right) \right], & \text{otherwise.} \end{cases} \quad (3.79)$$

With fixed γ and T , I^* as a function of A_0 consists of a linear part which corresponds to the first conditional branch in (3.79), and a strictly concave part which corresponds to the second. As A_0 approaches infinity, I^* converges to $TB \log_2(1+\gamma)$, suggesting that the receiver is limited by the receive SNR but not quantization in this case. With A_0 and

γ fixed, I^* as a function of T is monotonically increasing and strictly concave for $T < A_0/p_0$, and stays constantly at its maximal value for $T \geq A_0/p_0$ where the energy efficient bit resolution b_0 is employed to exhaust all energy. These analyses are verified with the numerical examples shown in Fig. 3.17.

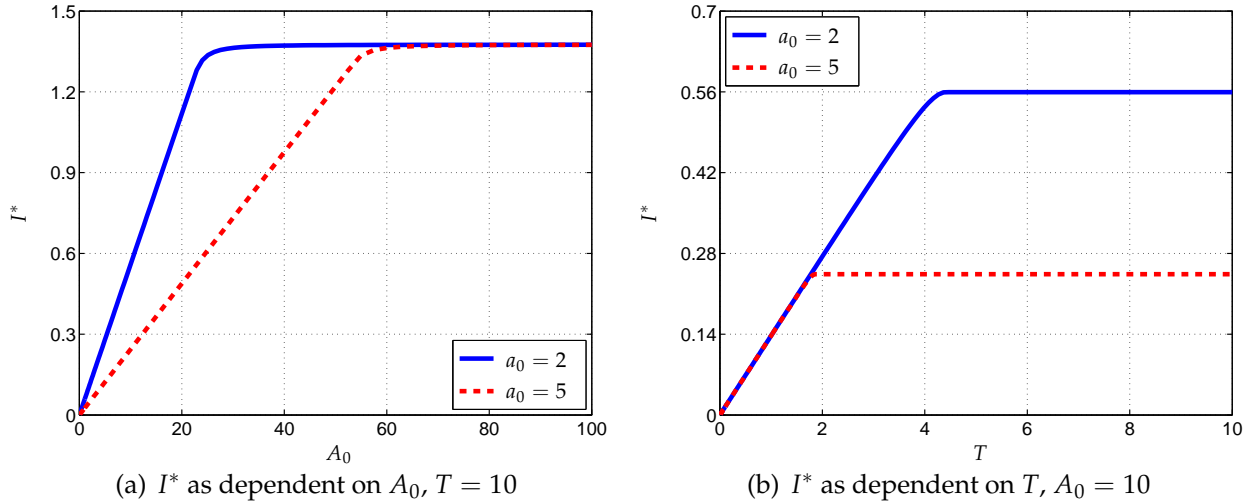


Fig. 3.17: Maximal achievable throughput as dependent on A_0 and T for real-valued b , $a_1 = 0.1$, $\gamma = 0.1$, $B = 1$

3.4.2 Case II

In practice, the bit resolution of the A/D converter assumes an integer value from a finite set $\{0, 1, \dots, b_{\max}\}$. The situation here is mathematically equivalent to Case III of the transmit side, where the modulation order is chosen from a finite discrete set. The conclusion on the optimal control strategy carries over directly: *the desired average power consumption A_0/T is realized by the time-sharing of its bounding bit resolutions on the Pareto boundary of the feasible power-rate pairs.*

As illustrated in Fig. 3.18, each feasible ADC resolution b is marked on the power-rate graph according to its coordinates $(P(b), R(b))$. The Pareto boundary for the set of all feasible resolutions is constructed by connecting the energy efficient bit resolutions with straight lines. Note that the concept of energy efficient bit resolution here is different from that of Case I, where b is assumed a non-negative real number. We have defined b_0 as the solution of (3.72), and call it the energy efficient bit resolution in Case I since it maximizes the bit per Joule metric. For $b > b_0$, higher rate is achieved with more power consumption, and the ratio between the rate and the power consumption decreases. In Case II here, we have a finite number of integer-valued bit resolutions, and call some of these energy efficient if they satisfy: there is no achievable point on the power-rate graph at which a higher rate is obtained with less power consumption. The linear interpolation of the points representing the energy efficient bit resolutions results in the Pareto boundary, which is concave in P . For a given average power A_0/T , one needs to find the neighboring energy efficient bit resolutions and compute the required time-sharing factor, in order to achieve the maximal throughput on the operation interval. The parameters a_0 , a_1 , and γ all have an impact on which bit resolutions are energy efficient, and the role of a_0 is more

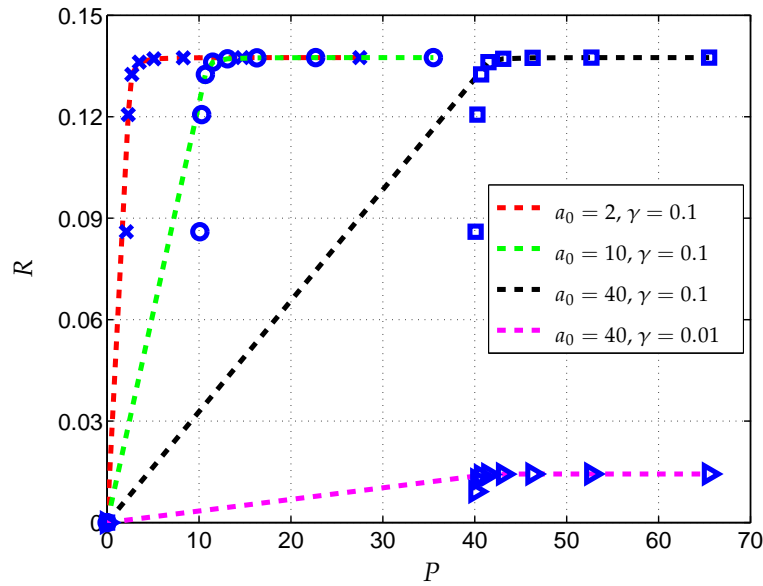


Fig. 3.18: Feasible operation modes (markers) and the Pareto boundary (dashed curves), $a_1 = 0.1, b_{\max} = 8, B = 1$

critical with this respect than the others. Also note from Fig. 3.18, that the achievable rate increases rapidly with small b while the power consumption is not significantly boosted, whereas for large b the rate almost saturates but the power consumption increases drastically. This is to say, from an energy efficiency point of view, lower bit resolutions are more favorable for the design and operation of the receiver.

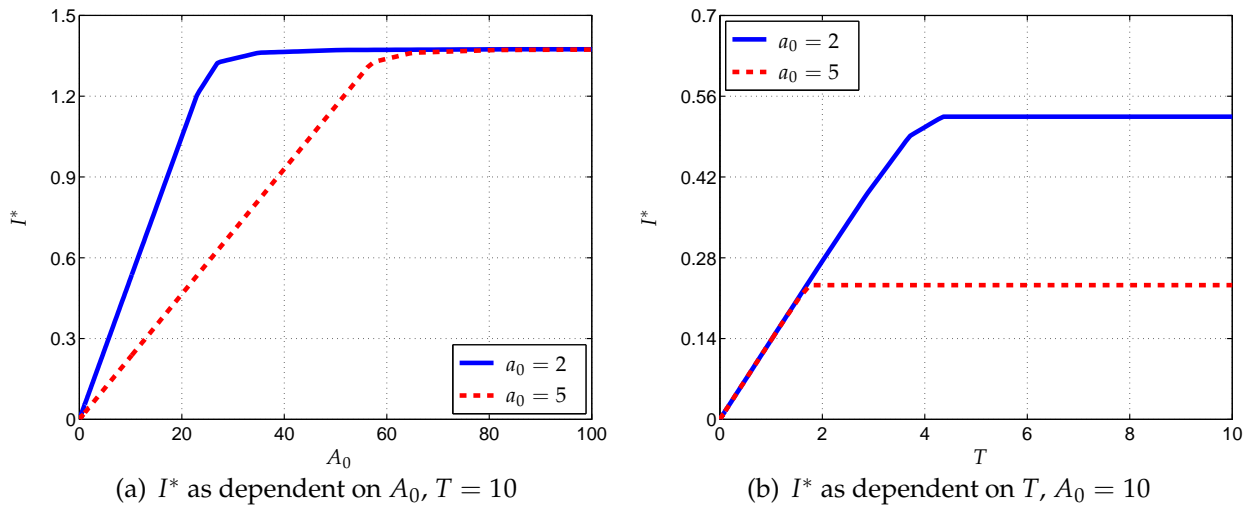


Fig. 3.19: Maximal achievable throughput as dependent on A_0 and T for integer-valued $b, a_1 = 0.1, \gamma = 0.1, B = 1$

The maximal achievable throughput in this case, as shown in Fig. 3.19, is very similar to that of Case I. With fixed T , I^* as a function of A_0 is piecewise linear and hence less smooth than its counterpart in Case I. The upper bound that I^* converges to is unchanged since it depends only on the receive SNR γ . On the contrary, the upper bound of I^* is

reduced compared to Case I when A_0 is fixed and T is varied. This is due to the restriction of b to be an integer, which makes the maximal energy efficiency that can be achieved in Case II smaller than the energy efficiency corresponding to b_0 .

3.5 Optimal Control of a Pair of Transmitter and Receiver

We have discussed in the last two sections respectively, the optimal control of a transmitter and a receiver operating on the finite time interval $[0, T]$ with a given energy budget A_0 . The natural question to arise at this point is: how about jointly optimize a pair of transmitter and receiver? More specifically, we consider the point-to-point communication between a transmitter and a receiver, and take the transmit power at the transmit side and the ADC resolution at the receive side as the two control variables which are to be adapted jointly. With the respective energy budgets A_1 and A_2 , the transmitter and the receiver carry out the communication in a cooperative way with the common goal of achieving the maximal possible throughput on the given time interval $[0, T]$. To this end, we think of the system as having a central control unit which is aware of all the relevant system parameters, performs the offline optimization, and informs the transmitter and the receiver how they should operate before communication starts. We assume perfect synchronization between the transmitter and the receiver, and a constant communication channel on the given time interval which is known exactly.

3.5.1 Case I

We let p_{tx} be the transmit power and b be the ADC resolution, respectively, and assume both of them to be non-negative real numbers in this case. The achievable rate of the system has the form given in (2.26), but is now a function of both p_{tx} and b :

$$R = B \log_2 \left(\frac{1 + \gamma}{1 + \gamma \cdot 2^{-2b}} \right), \quad \text{where } \gamma = \frac{\alpha p_{\text{tx}}}{\sigma^2}. \quad (3.80)$$

The discontinuous affine model (3.27) is adopted for the power consumption of the transmitter, which is denoted with P_1 , and (2.29) is taken to address the power consumption of the receiver which is denoted with P_2 :

$$P_1 = \begin{cases} c_1 \cdot p_{\text{tx}} + c_0, & p_{\text{tx}} > 0, \\ 0, & p_{\text{tx}} = 0, \end{cases} \quad P_2 = \begin{cases} a_1(2^b - 1) + a_0, & b > 0, \\ 0, & b = 0. \end{cases} \quad (3.81)$$

The throughput maximization problem (3.3) can be written in this case as

$$\begin{aligned} \max_{p_{\text{tx}}, b} \quad & \int_0^T R(p_{\text{tx}}, b) dt \\ \text{s.t.} \quad & \dot{W}_1 = P_1(p_{\text{tx}}), \quad W_1(0) = 0, \\ & \dot{W}_2 = P_2(b), \quad W_2(0) = 0, \\ & W_1(T) \leq A_1, \quad W_2(T) \leq A_2, \end{aligned} \quad (3.82)$$

where W_1 and W_2 stand for the state of the transmitter and the receiver *i.e.* their cumulative energy consumption since $t = 0$, respectively. Note that the system states

are decoupled in the control variables. For better tractability of the problem, we perform a variable transform and reformulate (3.82) as an optimization on P_1 and P_2 :

$$\begin{aligned} \max_{P_1, P_2} \quad & \int_0^T R(P_1, P_2) dt \\ \text{s.t.} \quad & \dot{W}_1 = P_1, \quad W_1(0) = 0, \\ & \dot{W}_2 = P_2, \quad W_2(0) = 0, \\ & W_1(T) \leq A_1, \quad W_2(T) \leq A_2, \end{aligned} \quad (3.83)$$

where the rate function R is expressed as

$$R(P_1, P_2) = \begin{cases} 0, & P_1 P_2 = 0, \\ B \log_2 \left(\frac{1 + \gamma}{1 + \gamma \cdot 2^{-2b}} \right), & P_1 > c_0, P_2 > a_0, \end{cases} \quad (3.84)$$

with $\gamma = \alpha(P_1 - c_0)/(c_1 \sigma^2)$, $2^{-2b} = a_1^2/(P_2 - a_0 + a_1)^2$. The isolated point $R(0, 0) = 0$ renders the domain of the problem disjoint and the function R non-concave in the control variables. Moreover, the first- and second-order partial derivatives of R for $P_1 > c_0, P_2 > a_0$ can be calculated as

$$\begin{aligned} R_{P_1} &= \frac{B\alpha}{c_1 \sigma^2 \ln 2} \cdot \frac{2^{2b} - 1}{(1 + \gamma)(2^{2b} + \gamma)}, \\ R_{P_1 P_1} &= -\frac{B\alpha^2}{c_1^2 \sigma^4 \ln 2} \cdot \frac{(2^{2b} - 1)(2^{2b} + 2\gamma + 1)}{(1 + \gamma)^2(2^{2b} + \gamma)^2}, \\ R_{P_2} &= \frac{2B}{\ln 2} \cdot \frac{\gamma}{(2^{2b} + \gamma)(P_2 - a_0 + a_1)}, \\ R_{P_2 P_2} &= -\frac{2B}{\ln 2} \cdot \frac{\gamma(3 \cdot 2^{2b} + \gamma)}{(2^{2b} + \gamma)^2(P_2 - a_0 + a_1)^2}, \\ R_{P_1 P_2} &= \frac{2B\alpha}{c_1 \sigma^2 \ln 2} \cdot \frac{2^{2b}}{(2^{2b} + \gamma)^2(P_2 - a_0 + a_1)}. \end{aligned} \quad (3.85)$$

It is clear that R is concave in both P_1 and P_2 since $R_{P_1 P_1} < 0, R_{P_2 P_2} < 0$ given that $P_1 > c_0, P_2 > a_0$. However, the determinant of the Hessian matrix of R can be evaluated as

$$\begin{aligned} |\mathbf{H}(R)| &= R_{P_1 P_1} R_{P_2 P_2} - (R_{P_1 P_2})^2 \\ &= \frac{2B^2 \alpha^2}{c_1^2 \sigma^4 \ln^2 2} \cdot \frac{\gamma(3 \cdot 2^{2b} + \gamma)(2^{2b} - 1)(2^{2b} + 2\gamma + 1) - 2(1 + \gamma)^2 2^{4b}}{(1 + \gamma)^2(2^{2b} + \gamma)^4(P_2 - a_0 + a_1)^2}, \end{aligned} \quad (3.86)$$

the sign of which is not definite. This is to say, even on the continuous domain $(c_0, +\infty) \times (a_0, +\infty)$, the function R is not always jointly concave in P_1 and P_2 . We propose in the following a reconstruction method to obtain a function \tilde{R} from R that is defined on $[0, +\infty) \times [0, +\infty)$, and is jointly concave in P_1 and P_2 .

3.5.1.1 Reconstruction of the rate surface

For a pair of arbitrary power consumption values (P_1, P_2) with $P_2 > 0$, we let the ratio between P_1 and P_2 be denoted with β , which gives $P_1 = \beta P_2$. In the 3-dimensional space

which describes the achievable rate of the system as a function of P_1 and P_2 , the origin and β uniquely determine a vertical plane which intersects with the surface defined by R . On this vertical plane, we make the tangent line from the origin towards the intersecting curve with R . The situation is similar to what is illustrated as Case II in Fig. 3.2, and we call the interval between the origin and the P_2 -coordinate of the tangent point the *time-sharing region*, which corresponds to the straight line segment that is constructed. If we make the tangent lines for all positive β and enforce the value zero for $P_2 = 0$, a new rate function \tilde{R} is defined on $[0, +\infty) \times [0, +\infty)$, the surface of which consists of a part that corresponds to the time-sharing regions and a curved part that is exactly the same as R . Denoting the P_2 -coordinate of the tangent point in direction β with $\mu(\beta)$, we formally define this new rate function as

$$\tilde{R}(P_1, P_2) = \begin{cases} 0, & P_2 = 0, \\ \frac{P_2}{\mu(\beta)} \cdot R(\beta\mu(\beta), \mu(\beta)), & 0 < P_2 < \mu(\beta), \\ R(P_1, P_2), & P_2 \geq \mu(\beta) \end{cases} \quad \text{with } \beta = \frac{P_1}{P_2}. \quad (3.87)$$

Every point on the surface of \tilde{R} is obviously achievable. The concavity of \tilde{R} with respect to P_1 and P_2 can be verified numerically, and is proven analytically in Appendix A2. The procedure is briefly summarized in the sequel. We consider two arbitrary points $X(\beta_1 v_1, v_1)$ and $Y(\beta_2 v_2, v_2)$ on the P_1 - P_2 plane, where $\beta_1, \beta_2 > 0, v_1, v_2 > 0$. Any point Z resulting from the time-sharing of X and Y can be expressed as

$$Z(\lambda\beta_1 v_1 + (1-\lambda)\beta_2 v_2, \lambda v_1 + (1-\lambda)v_2) \triangleq Z(\beta_Z v, v) \\ \text{with } \beta_Z = \frac{\lambda\beta_1 v_1 + (1-\lambda)\beta_2 v_2}{\lambda v_1 + (1-\lambda)v_2}, \quad v = \lambda v_1 + (1-\lambda)v_2, \quad (3.88)$$

where $0 \leq \lambda \leq 1$ represents the time-sharing factor. We denote the data rate at point Z after the construction by \tilde{R}_Z . When Z is in the corresponding time-sharing region, we shall show the concavity of \tilde{R} by verifying $d^2\tilde{R}_Z/d\lambda^2 < 0$; when Z is beyond the time-sharing region, we resort to the Hessian matrix of R and show it is negative definite for $v \geq \mu(\beta_Z)$. In order to determine whether Z is in or beyond the corresponding time-sharing region, we characterize the tangent point by writing the equation

$$\frac{R(\beta\mu, \mu)}{\mu} = \left. \frac{dR(\beta u, u)}{du} \right|_{u=\mu}, \quad (3.89)$$

which means the slope of the tangent line on the vertical plane specified by β and the origin is equal to the derivative of R at the tangent point. This leads to an implicit function of μ defined by

$$G(\beta, \mu) = R(\beta\mu, \mu) - \mu(R_{P_1}(\beta\mu, \mu) + \beta \cdot R_{P_2}(\beta\mu, \mu)) = 0, \quad (3.90)$$

which can be further calculated as

$$\ln\left(\frac{1+\gamma}{1+\gamma \cdot 2^{-2b}}\right) = \frac{\alpha\beta\mu}{c_1\sigma^2} \cdot \frac{2^{2b}-1}{(1+\gamma)(2^{2b}+\gamma)} + \frac{2\gamma\mu}{(2^{2b}+\gamma)(\mu-a_0+a_1)}, \quad (3.91)$$

where $\gamma = \alpha(\beta\mu - c_0)/(c_1\sigma^2)$, $2^{2b} = (\mu - a_0 + a_1)^2/a_1^2$. The derivative of μ with respect to β can be calculated by means of G as

$$\begin{aligned} \frac{d\mu}{d\beta} &= -\frac{G_\beta(\beta, \mu)}{G_\mu(\beta, \mu)} \\ &= -\frac{-\mu^2(\beta R_{P_1 P_1} + R_{P_1 P_2})}{-\mu(\beta^2 R_{P_1 P_1} + 2\beta R_{P_1 P_2} + R_{P_2 P_2})} = -\frac{\mu(\beta R_{P_1 P_1} + R_{P_1 P_2})}{\beta^2 R_{P_1 P_1} + 2\beta R_{P_1 P_2} + R_{P_2 P_2}} \end{aligned} \quad (3.92)$$

An inequality condition between γ and μ can be obtained from (3.91). This relation is then used to show $d^2\tilde{R}_Z/d\lambda^2 < 0$ and $|\mathbf{H}(R)| > 0$, for the respective cases that point Z is in or beyond the corresponding time-sharing region.

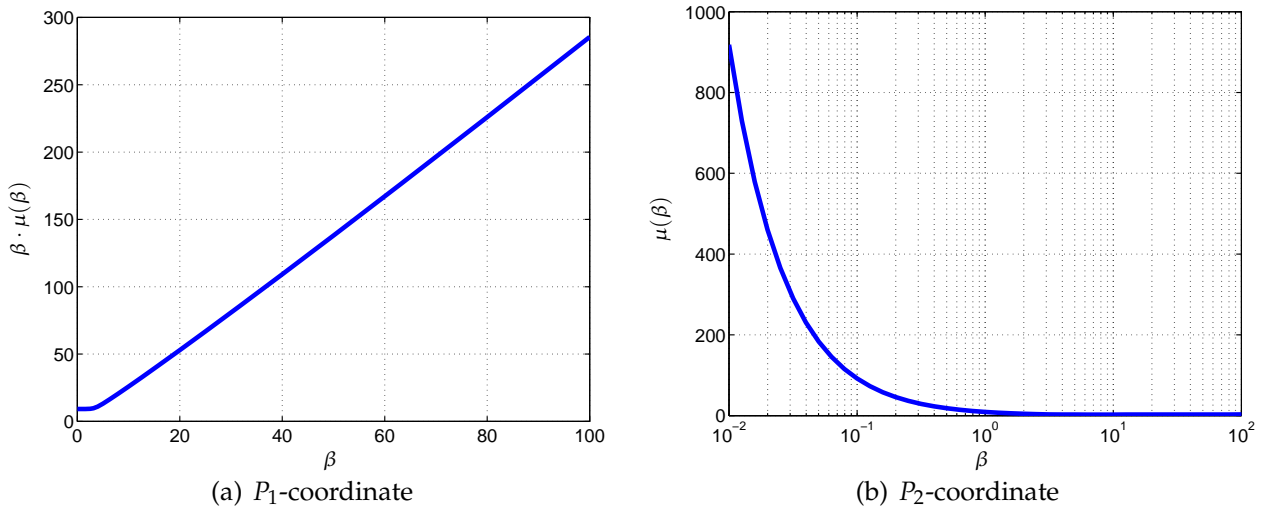


Fig. 3.20: Variations of the tangent point with respect to β , $a_0 = 2$, $a_1 = 0.1$, $c_0 = 4$, $c_1 = 2$, $\alpha/\sigma^2 = 1$

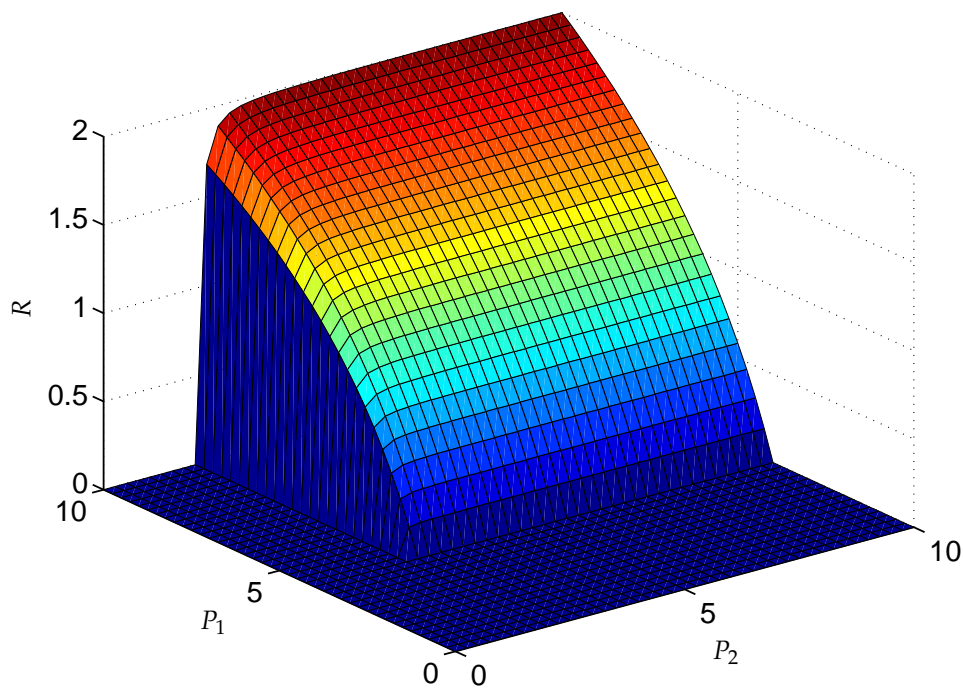
The variations of the P_2 - and P_1 -coordinates of the tangent point with respect to β are illustrated in Fig. 3.20 for a set of chosen parameters. For very small β , μ goes to infinity but $\beta\mu$ converges; for very large β , μ converges but $\beta\mu$ goes to infinity. The asymptotic values satisfy the equations

$$\begin{aligned} \beta \rightarrow 0 : \quad (1 + \gamma) \ln(1 + \gamma) &= \frac{\alpha\beta\mu}{c_1\sigma^2}, \\ \beta \rightarrow +\infty : \quad \ln\left(\frac{\mu - a_0 + a_1}{a_1}\right) &= \frac{\mu}{\mu - a_0 + a_1}, \end{aligned} \quad (3.93)$$

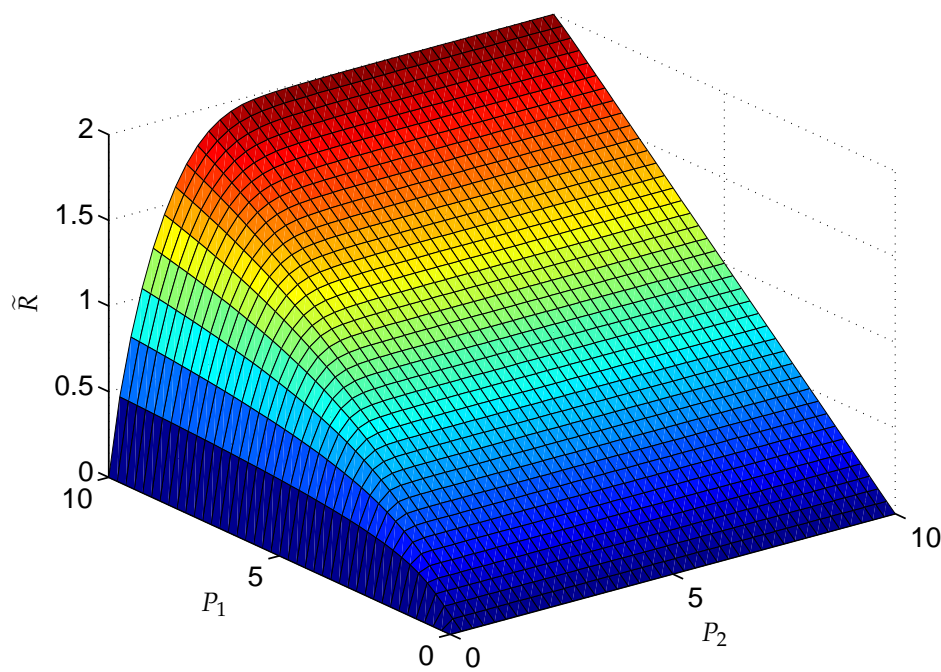
which can be obtained from (3.91). In both cases the tangent points are infinitely far away from the origin, yet the achievable rates at those points are finite.

3.5.1.2 Optimal control strategy

We illustrate an exemplary rate function R and the constructed new rate function \tilde{R} in Fig. 3.21. The non-convex part in the original surface has been replaced with straight lines which represent the time-sharing of the origin and the corresponding tangent points,



(a) Original function



(b) Constructed function

Fig. 3.21: Construction of the concave rate function \tilde{R} , $a_0 = 2$, $a_1 = 0.1$, $c_0 = 4$, $c_1 = 2$, $\alpha/\sigma^2 = 1$, $B = 1$

bringing about a convex shaped surface for the new function \tilde{R} . The most obvious difference by the construction, as can be seen in the figures, lies in the completion of the surface for the undefined region $\{(P_1, P_2) : 0 < P_1 < c_0 \text{ or } 0 < P_2 < a_0\}$. Note that every point on the surface of \tilde{R} is either on the surface of R or is constructed using points on the surface of R .

Algorithm 3 Obtaining the optimal control for Case I of a transmitter and a receiver with individual energy budgets

Require: System parameters T, a_0, a_1, c_0, c_1 , channel gain α , energy budgets A_1 and A_2

Ensure: Optimal power consumption functions P_1^* and P_2^*

- 1: $\beta \leftarrow A_1/A_2$, compute $\mu(\beta)$ by solving (3.91)
 - 2: **if** $A_2/T > \mu(\beta)$ **then**
 - 3: Transmitter and receiver operate actively for the whole time interval $[0, T]$ with $P_1^* = A_1/T, P_2^* = A_2/T$
 - 4: **else**
 - 5: Transmitter and receiver operate actively for a time period of $A_2/\mu(\beta)$ with power $P_1^* = \beta \cdot \mu(\beta), P_2^* = \mu(\beta)$, and then turn into sleep mode
 - 6: **end if**
-

To obtain the optimal control of the two transceivers, we do not need to construct the whole new surface but to explore the important property of \tilde{R} being concave. Clearly, the energy budgets of both sides should be exhausted in order to achieve the maximal throughput, for otherwise we can always increase the transmit power or the ADC resolution and attain a higher data rate. This means, the average power consumption of the transmitter and the receiver are fixed to A_1/T and A_2/T , respectively. Since the constructed rate function \tilde{R} is concave, the data rate at point $(A_1/T, A_2/T)$ gives the maximal average data rate on the considered time interval. If the corresponding point is on the surface of R , then $P_1^* = A_1/T$ and $P_2^* = A_2/T$ should be used during the whole interval, meaning that the transmit power and the ADC resolution are kept constant; otherwise, the power consumption values at the corresponding tangent point should be employed to deplete the given energy, and the two transceivers are turned into sleep modes for the rest of the interval. The key to determining which strategy should be taken lies in the ratio between the average power consumption values given by A_1/A_2 . This is to say, for solving a specific problem (3.82), we only need to compute the coordinates of one single tangent point. The optimal solution to the problem can be found using Algorithm 3. The optimal transmit power and ADC resolution can then be recovered from (3.81).

3.5.2 Case II

We consider now the discrete counterpart of Case I: MQAM transmission is employed for the communication between the transmitter and the receiver, where the transmitter can choose the radiated power from a finite set, and the ADC resolution of the receiver is restricted to integer values. Instead of approximating the achievable rate with the capacity lower bound (2.25) or (2.26), we evaluate numerically the mutual information between the channel input and output for equally probable QAM symbols and distortion-minimizing

A/D converters. The resulting data rate is achievable but not equal to the channel capacity in general. We are motivated to investigate this model for two reasons: first, the obtained achievable rate is a more reasonable approximation of the system behavior than (2.26) in the medium-to-high SNR regime; second, the model takes more practical aspects of the system into account, and can be seen as an extension of Case III of the transmit side to the jointly optimal control problem.

3.5.2.1 Analysis of the mutual information

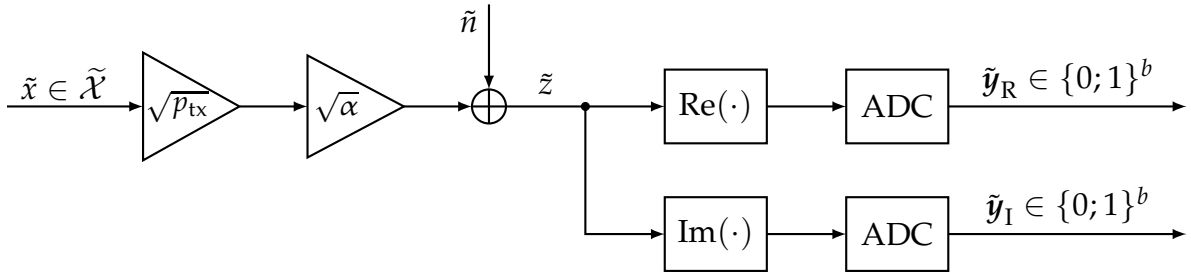


Fig. 3.22: Quantized channel with MQAM input modeled as a DMC

As shown in Fig. 3.22, we model the quantized channel with MQAM input as a *discrete memoryless channel* (DMC). The input symbol \tilde{x} belongs to the set of constellation points $\tilde{\mathcal{X}} = \{\tilde{x}_i | i = 1, \dots, M\}$, which has the cardinality $|\tilde{\mathcal{X}}| = M$ and unit average power, leading to the relation

$$\sum_{i=1}^M \Pr\{\tilde{x} = \tilde{x}_i\} \cdot |\tilde{x}_i|^2 = 1 \quad \Rightarrow \quad \sum_{i=1}^M |\tilde{x}_i|^2 = M. \quad (3.94)$$

The transmit power p_{tx} that can be employed is restricted to a discrete set $\mathcal{P} = \{0, \Delta_p, 2\Delta_p, \dots, N_p\Delta_p\}$, where $\Delta_p \in \mathbb{R}^+$, and $N_p\Delta_p$ gives the maximal transmit power that is allowed. We consider only large-scale fading of the wireless channel, and denote its power gain with α . The received signal is corrupted by the additive noise \tilde{n} , which is assumed i.i.d. zero-mean circularly symmetric complex Gaussian (ZMCCG) with variance σ^2 . The average receive SNR is then given as $\gamma = \alpha p_{\text{tx}}/\sigma^2$. The in-phase and quadrature components of the receive signal are then separated and quantized by the respective ADCs, both of which employ the same bit resolution b , yielding the binary outputs $\tilde{\mathbf{y}}_{\text{R}}, \tilde{\mathbf{y}}_{\text{I}} \in \{0; 1\}^b$. As in Case III of the transmit side, we also assume square constellations here *i.e.* \sqrt{M} is assumed an even number. Since the phase shift of the channel is assumed perfectly compensated, the in-phase and quadrature components have the same statistical property and contribute each to one half of the mutual information between $\tilde{\mathbf{y}} = \tilde{\mathbf{y}}_{\text{R}} + j \cdot \tilde{\mathbf{y}}_{\text{I}}$ and \tilde{x} . To this end, we study either one of the orthogonal subchannels as shown in Fig. 3.23, where all the involved quantities are real-valued.

We let $\mathcal{X} = \{x_i | i = 1, \dots, \sqrt{M}\}$ be the set of real (or imaginary) coordinates of the constellation points, where the cardinality $|\mathcal{X}| = \sqrt{M}$ is an even number. The additive white noise $n \sim \mathcal{N}(0, \sigma^2/2)$, leading to the conditional probability distribution of the

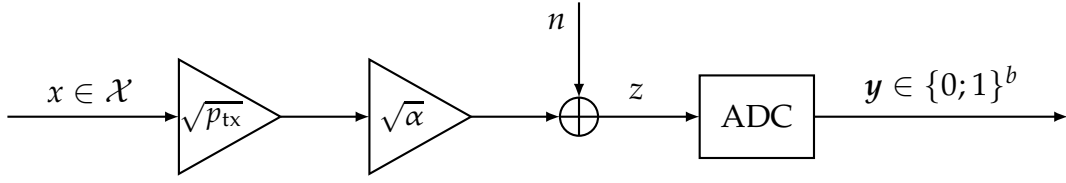


Fig. 3.23: DMC modeling of the in-phase or quadrature branch

quantizer input z given as

$$f_{z|x}(z|x_i) = \frac{1}{\sigma\sqrt{\pi}} \exp\left(-\frac{(z - \sqrt{\alpha p_{\text{tx}}} x_i)^2}{\sigma^2}\right), \quad i = 1, \dots, \sqrt{M}. \quad (3.95)$$

With equally probable input symbols, the probability density function of z can be calculated as

$$f_z(z) = \sum_{i=1}^{\sqrt{M}} \Pr\{x = x_i\} \cdot f_{z|x}(z|x_i) = \frac{1}{\sigma\sqrt{\pi M}} \sum_{i=1}^{\sqrt{M}} \exp\left(-\frac{(z - \sqrt{\alpha p_{\text{tx}}} x_i)^2}{\sigma^2}\right). \quad (3.96)$$

Using b bits to represent each sample of z , the ADC divides the possible range of z *i.e.* $(-\infty, +\infty)$, into $L = 2^b$ intervals with the decision thresholds t_1, \dots, t_{L-1} . To make the notation consistent, we define in addition $t_0 = -\infty$ and $t_L = +\infty$. In a practical system, the output of the quantization operation is usually the representative value q_j of the interval j on which z is found, *i.e.* $y = q_j$ if $t_{j-1} \leq z < t_j$. Since we investigate here the mutual information, what is of concern is the probability distribution of the output of the ADC rather than the specific values it takes. We can, therefore, also assign the quantizer output to the binary index of the interval on which the input finds itself, as is shown by $\mathbf{y} \in \{0;1\}^b$ in Fig. 3.23. A common design criterion of the decision thresholds is to minimize the average distortion which is defined by the mean squared error between the input and the corresponding representative value. We assume the ADC employs the minimum-distortion quantizer, which can be acquired numerically by using the Lloyd-Max algorithm [73].

Let the conditional probability of z falling on interval j given that the symbol x_i is sent be denoted with s_{ji} . From the definition we have

$$\begin{aligned} s_{ji} &\triangleq \Pr\{t_{j-1} \leq z < t_j | x = x_i\} = \int_{t_{j-1}}^{t_j} f_{z|x}(z|x_i) dz \\ &= \frac{1}{2} \left(\operatorname{erf}\left(\frac{t_j - \sqrt{\alpha p_{\text{tx}}} x_i}{\sigma}\right) - \operatorname{erf}\left(\frac{t_{j-1} - \sqrt{\alpha p_{\text{tx}}} x_i}{\sigma}\right) \right), \quad i = 1, \dots, \sqrt{M}, j = 1, \dots, L, \end{aligned} \quad (3.97)$$

where $\operatorname{erf}(\cdot)$ denotes the Gauss error function. The conditional entropy of \mathbf{y} given x is then computed as

$$H(\mathbf{y}|x) = \sum_{i=1}^{\sqrt{M}} \Pr\{x = x_i\} \cdot H(\mathbf{y}|x = x_i) = -\frac{1}{\sqrt{M}} \sum_{i=1}^{\sqrt{M}} \sum_{j=1}^L s_{ji} \log_2 s_{ji}. \quad (3.98)$$

The probabilities of z on interval j , denoted with s_j , $j = 1, \dots, \sqrt{M}$, constitute the probability mass function of the channel output \mathbf{y} and enable the computation of its

entropy:

$$\begin{aligned} s_j &\triangleq \Pr\{t_{j-1} \leq z < t_j\} = \sum_{i=1}^{\sqrt{M}} \Pr\{x = x_i\} \cdot \Pr\{t_{j-1} \leq z < t_j | x = x_i\} \\ &= \frac{1}{\sqrt{M}} \sum_{i=1}^{\sqrt{M}} s_{ji}, \quad j = 1, \dots, \sqrt{M}, \end{aligned} \quad (3.99)$$

$$H(\mathbf{y}) = - \sum_{j=1}^L s_j \log_2 s_j. \quad (3.100)$$

The mutual information between the channel input x and output \mathbf{y} is then calculated as $I(x; \mathbf{y}) = H(\mathbf{y}) - H(\mathbf{y}|x)$ based on (3.97)-(3.100). Note that the evaluation of $I(x; \mathbf{y})$ does not require any Monte-Carlo simulation. Due to the orthogonality between the in-phase and quadrature subchannels, a formula for the achievable rate of the system is given as

$$R = 2I(x; \mathbf{y}) \quad \text{in bit/channel use} \quad \text{or} \quad R = 2I(x; \mathbf{y})/T_s \quad \text{in bit/sec}, \quad (3.101)$$

where T_s is the duration of one MQAM symbol in second.

Because of the symmetry in the constellation and in the distribution of the additive noise, the set of decision thresholds that lead to the minimum mean distortion is also symmetric about the origin. When $b = 1$, the domain of z is divided into two intervals with the threshold $t_1 = 0$. In this case we have

$$s_{1i} = \frac{1}{2} \left(1 - \operatorname{erf} \left(\frac{\sqrt{\alpha p_{\text{tx}}} x_i}{\sigma} \right) \right), \quad s_{2i} = \frac{1}{2} \left(1 + \operatorname{erf} \left(\frac{\sqrt{\alpha p_{\text{tx}}} x_i}{\sigma} \right) \right), \quad i = 1, \dots, \sqrt{M}, \quad (3.102)$$

$$s_1 = \frac{1}{\sqrt{M}} \sum_{i=1}^{\sqrt{M}} s_{1i} = \frac{1}{\sqrt{M}} \cdot \frac{\sqrt{M}}{2} = 0.5 = s_2, \quad (3.103)$$

where the terms with the error function in the summation of (3.103) can be paired up and canceled out. The mutual information can then be expressed in closed-form by virtue of the error function as

$$\begin{aligned} I(x; \mathbf{y}) &= H(\mathbf{y}) - H(\mathbf{y}|x) = 1 + \frac{1}{\sqrt{M}} \sum_{i=1}^{\sqrt{M}} \sum_{j=1}^L s_{ji} \log_2 s_{ji} \\ &= 1 + \frac{1}{\sqrt{M}} \sum_{i=1}^{\sqrt{M}} \left(1 - \operatorname{erf} \left(\frac{\sqrt{\alpha p_{\text{tx}}} x_i}{\sigma} \right) \right) \left(\log_2 \left(1 - \operatorname{erf} \left(\frac{\sqrt{\alpha p_{\text{tx}}} x_i}{\sigma} \right) \right) - 1 \right). \end{aligned} \quad (3.104)$$

In the very low SNR regime *i.e.* $\gamma \rightarrow 0$, we have the following asymptotic result based on the approximations $\operatorname{erf}(x) \approx 2x/\sqrt{\pi}$ and $\ln(1+x) \approx x$ for $x \rightarrow 0$:

$$\begin{aligned} &\left(1 - \operatorname{erf} \left(\frac{\sqrt{\alpha p_{\text{tx}}} x_i}{\sigma} \right) \right) \left(\log_2 \left(1 - \operatorname{erf} \left(\frac{\sqrt{\alpha p_{\text{tx}}} x_i}{\sigma} \right) \right) - 1 \right) \\ &+ \left(1 + \operatorname{erf} \left(\frac{\sqrt{\alpha p_{\text{tx}}} x_i}{\sigma} \right) \right) \left(\log_2 \left(1 + \operatorname{erf} \left(\frac{\sqrt{\alpha p_{\text{tx}}} x_i}{\sigma} \right) \right) - 1 \right) \approx 2 \left(\frac{1}{\ln 2} \cdot \operatorname{erf}^2 \left(\frac{\sqrt{\alpha p_{\text{tx}}} x_i}{\sigma} \right) - 1 \right) \\ &\approx 2 \left(\frac{4\gamma x_i^2}{\pi \ln 2} - 1 \right), \end{aligned} \quad (3.105)$$

$$R \approx 2 + \frac{2}{\sqrt{M}} \sum_{i=1}^{\sqrt{M}/2} 2 \left(\frac{4\gamma x_i^2}{\pi \ln 2} - 1 \right) = \frac{4\gamma}{\pi \sqrt{M} \ln 2} \quad (\text{bit/channel use}), \quad (3.106)$$

where the property of the constellation points as having unit average power is applied in the last equation. Notice that the achievable rate decreases with the square root of the modulation order M as indicated by (3.106), meaning that R is maximized by the lowest modulation scheme available in the very low SNR regime. This result is due to the assumption of equally probable input symbols, which is not capacity-achieving in general. The capacity lower bound (2.25) can be approximated by $\gamma(1 - \rho)/\ln 2$ for $\gamma \rightarrow 0$, which is equal to (3.106) with $M = 4$ and $\rho = 1 - 2/\pi = 0.3634$, which is exactly the value indicated by Table 2.1. In the very high SNR regime on the other hand, we have

$$\gamma \rightarrow +\infty : \begin{cases} s_{1i} = 0, s_{2i} = 1 & \text{for } x_i > 0, \\ s_{1i} = 1, s_{2i} = 0 & \text{for } x_i < 0, \end{cases}$$

$$R = -4 \cdot 0.5 \log_2(0.5) - 0 = 2 \quad (\text{bit/channel use}), \quad (3.107)$$

i.e. the achievable rate reaches its upper limit of 2 bits per channel use as imposed by the two 1-bit quantizers. With $b > 1$, the decision thresholds need to be determined numerically by using the Lloyd-Max algorithm, and closed-form expressions for R do not exist in general.

The achievable rate of the system as dependent on the average receive SNR is illustrated in Fig. 3.24, where the capacity lower bound (2.25) and the Shannon capacity for the AWGN channel are plotted for comparison. With higher modulation orders and higher ADC resolutions, the gap between R and the Shannon capacity closes up, yet R always converges to $\min\{\log_2 M, 2b\}$ for sufficiently large γ . In the low SNR regime, the lower bound (2.25) and the achievable rate (3.101) are very close to each other, whereas in the high SNR regime, (2.25) lies in between the curves representing (3.101) and the Shannon capacity, and converges very slowly to the asymptotic upper limit of $2b$.

In Fig. 3.24 we have illustrated the *matched* cases where $\log_2 M = 2b$, meaning that the upper limits on the achievable rate as imposed by the modulation scheme and the A/D conversion are identical. A few *mismatched* cases are shown in Fig. 3.25. For QPSK as an example, using an ADC resolution higher than 1 bit is beneficial in the low-to-medium SNR regime, yet the SNR above which R saturates is almost the same for different resolutions. This trend stays invariant even if the distribution of the input symbols is optimized by using the Blahut-Arimoto algorithm [74] for instance.

3.5.2.2 Energy efficient operation modes and the optimal control strategy

The power consumption of the transmitter and the receiver, denoted with P_1 and P_2 respectively, can be computed in the same way as introduced in Section 3.3.3 and Section 2.3.1. The additional system parameters are summarized in Table 3.3.

Having introduced the system model, analyzed the achievable rate, and specified how the power consumption can be modeled, we discuss next the determination of the energy efficient operation modes as well as the optimal control strategy of the transmitter and the receiver. In this case, each operation mode of the system corresponds to a triple (p_{tx}, M, b) which specifies the transmit power, the modulation order, and the ADC resolution that are employed. The feasible triples are then translated to a set of discrete points in the 3-dimensional space composed by P_1 , P_2 and R . More specifically, there are in total $N_p \times |\mathcal{M}| \times b_{\text{max}} + 1$ of these points due to the N_p positive transmit power levels, the $|\mathcal{M}|$

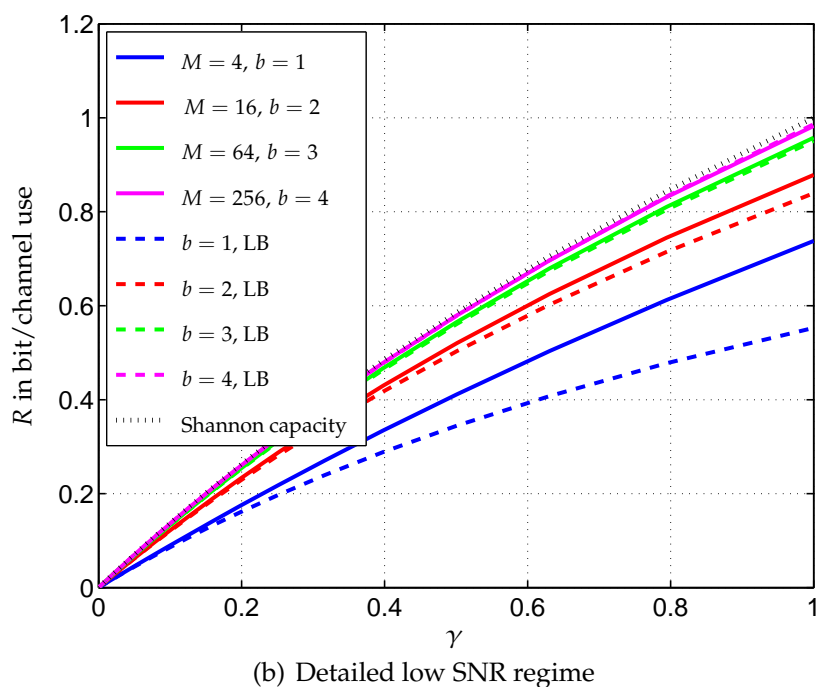
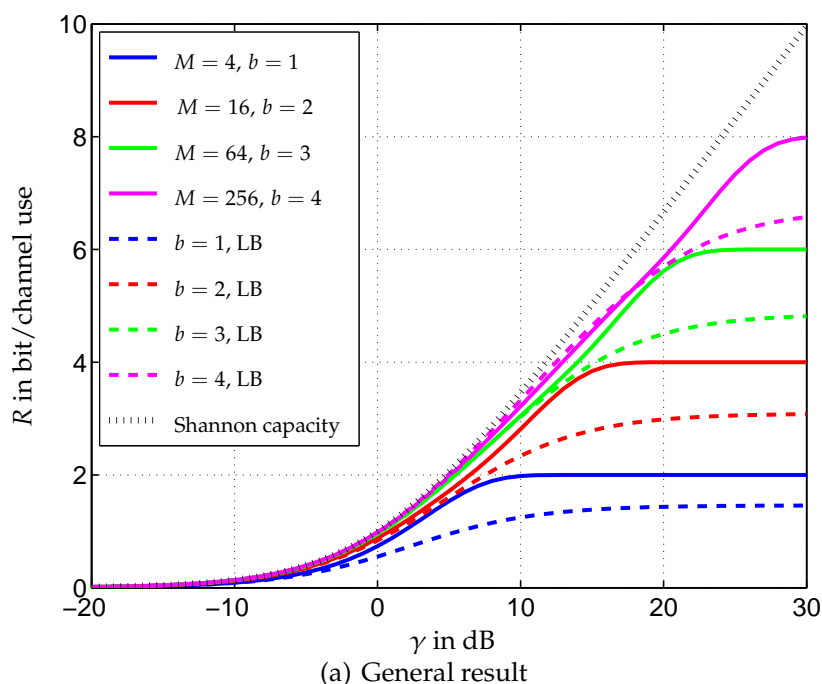


Fig. 3.24: Function R as dependent on the average receive SNR γ , solid curves represent the achievable rate of the system in terms of mutual information between the channel input and output for equiprobable input symbols obtained with (3.101), while dashed curves represent the capacity lower bound of the quantized channel obtained with (2.25). Shannon capacity of the AWGN channel is given by the dotted curve as reference.

available modulation orders, the b_{\max} eligible ADC resolutions, and the all zero point which corresponds to the origin. An operation mode $(p_{\text{tx}}, M, b)_i$, $i \in \{1, \dots, N_p \times |\mathcal{M}| \times$

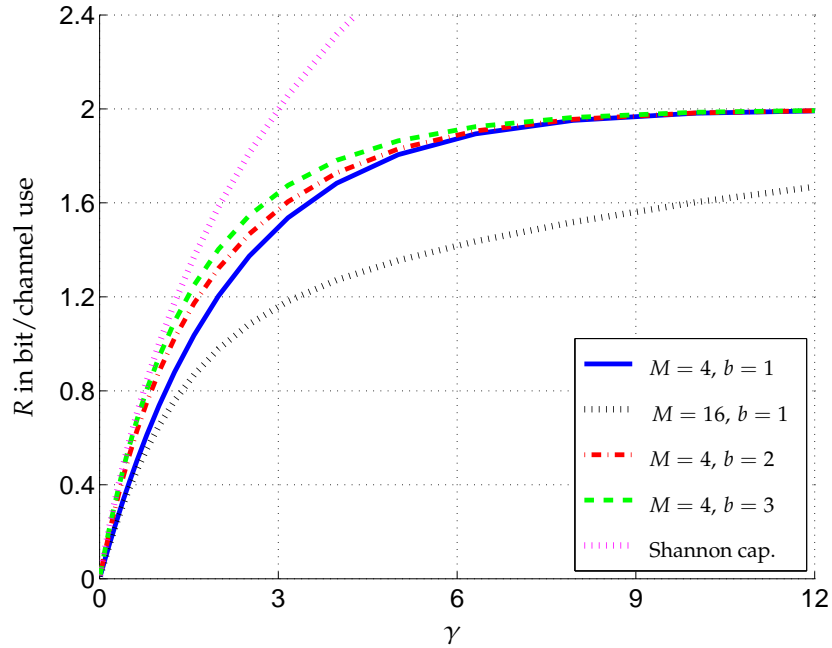


Fig. 3.25: Achievable rate (3.101) as dependent on the average receive SNR, with matched and mismatched modulation orders M and ADC resolutions b

Table 3.3: System parameters for MQAM transmission over quantized channels

Constant circuit power of TX	$c_0 = 100$ mW
Constant circuit power of RX	$a_0 = 100$ mW
Granularity of feasible transmit power levels	$\Delta_p = 5$ mW
Maximal transmit power	$N_p \Delta_p = 100$ mW
Available modulation formats	$M \in \mathcal{M} = \{4, 16, 64, 256\}$
Available ADC resolutions	$b \in \{1, 2, 3, 4\}$
Scaling factor in the ADC power consumption	$a_1 = 5$ mW

$b_{\max} + 1\}$ is called energy efficient, if there does not exist a convex combination of the (P_1, P_2, R) triples of other operation modes which results in no more power consumption than $(P_1, P_2)_i$ but an achievable rate larger than R_i . Mathematically, this means

$$\begin{aligned}
 R_i &\geq \max_{\lambda \succeq \mathbf{0}} \lambda^T \mathbf{R} \\
 \text{s.t. } &\mathbf{1}^T \lambda = 1, \quad \lambda^T \mathbf{P}_1 \leq P_{1,i}, \quad \lambda^T \mathbf{P}_2 \leq P_{2,i}
 \end{aligned} \tag{3.108}$$

needs to be satisfied for $(p_{\text{tx}}, M, b)_i$ to be energy efficient, where $\mathbf{P}_1, \mathbf{P}_2, \mathbf{R} \in \mathbb{R}^{N_p |\mathcal{M}| b_{\max} + 1}$ are the vectors containing the power consumptions and the achievable rates of all feasible operation modes, and $\lambda \in [0, 1]^{N_p |\mathcal{M}| b_{\max} + 1}$ contains their time-sharing factors which sum up to 1. The zero operation mode guarantees the feasibility of the maximization in (3.108), and is energy efficient by definition. The other operation modes need to be examined by solving and checking (3.108), and once an operation mode is determined

as energy inefficient, it can be eliminated from the subsequent optimizations to reduce the computational complexity of the procedure. Note that (3.108) is a straightforward criterion to determine the subset of energy efficient operation modes, which can be applied in an exhaustive way to all feasible modes if the total number of them is not very high. For a more effective and efficient implementation, one may apply convex hull algorithms from computational geometry *e.g.* [75]. We let $\bar{P}_1, \bar{P}_2, \bar{R}$ be the vectors of power consumptions and achievable rates of the energy efficient operation modes, which are subvectors of P_1, P_2, R , and are of the same dimension.

For the throughput maximization problem on the finite time interval $[0, T]$ where the transmitter and the receiver have fixed energy budgets A_1 and A_2 respectively, one needs to find the maximal achievable rate corresponding to the power consumption $(A_1/T, A_2/T)$ by employing the feasible operation modes. The problem is equivalent to

$$\begin{aligned} \max_{\mu \succeq 0} \quad & \mu^T \bar{R} \\ \text{s.t.} \quad & \mathbf{1}^T \mu = 1, \quad \mu^T \bar{P}_1 \leq \frac{A_1}{T}, \quad \mu^T \bar{P}_2 \leq \frac{A_2}{T} \end{aligned} \quad (3.109)$$

where μ contains the time-share of each energy efficient operation mode, since the energy inefficient modes do not contribute to the optimal time-sharing solution that leads to the maximal achievable data rate for a given pair of power consumptions. We let μ^* be the optimal solution of (3.109), and call the energy efficient operation modes that correspond to the positive entries of μ^* the *active modes* with respect to $(A_1/T, A_2/T)$. From a geometric point of view, a concave surface in the 3D space of P_1, P_2 and R is constructed based on all the energy efficient operation modes. The point on the surface corresponding to the power consumption pair $(A_1/T, A_2/T)$ lies in the polygon determined by the said active modes. The polygon is usually a triangle since it is quite unlikely, that more than three energy efficient operation modes are on the same plane in the power-rate space. This means, the optimal control strategy consists in general of the time-sharing of three different operation modes. Moreover, as the projection of the surface of achievable rates does not cover the whole P_1 - P_2 plane, there can be cases where the available energy at the transmitter and/or the receiver is not exhausted at the end of the time interval.

We illustrate in Fig. 3.26 the feasible as well as the energy efficient operation modes and the constructed achievable rate surface in the power-rate space for three different communication distances d . For small d , the operation modes with relatively large M and b tend to be energy efficient. As d increases, more operation modes with lower modulation order and coarser A/D conversion become energy efficient. Note that the achievable rate exhibits the saturation behavior in the receive SNR for given M and b , which means for sufficiently large γ , the increment in R is trivial no matter how large the transmit power becomes. To this end, we can set a small offset $\epsilon > 0$ and regard the operation modes with $R > (1 - \epsilon) \min\{\log_2 M, 2b\}$ as energy inefficient. For the shown simulation results $\epsilon = 10^{-3}$ is chosen.

The optimal state trajectories W_1^* of the transmitter and W_2^* of the receiver are demonstrated in Fig. 3.27 for a pair of chosen energy budgets. For $d = 20, 50$ and 100 meters, the optimal control strategies all involve the time-sharing of three different operation modes, which are obtained by solving (3.109) and are listed in Table (d). Consequently, the resulting optimal state trajectories all consist of three straight line

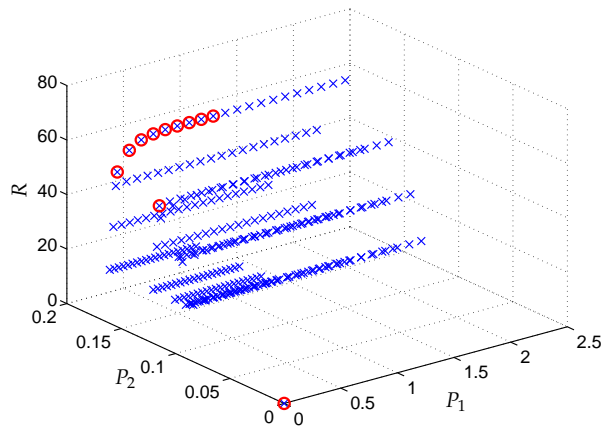
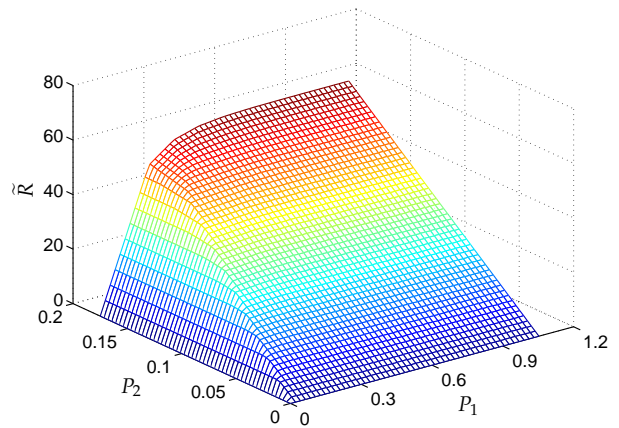
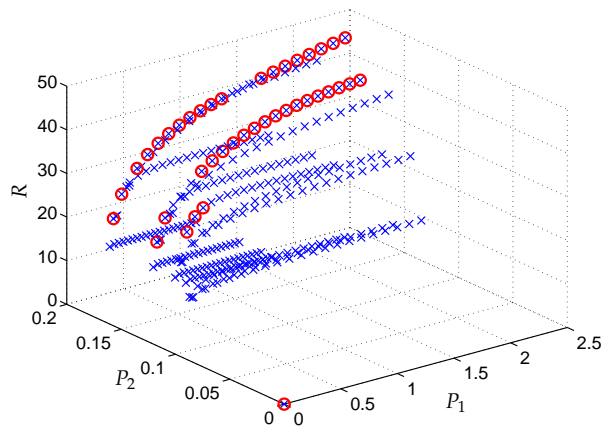
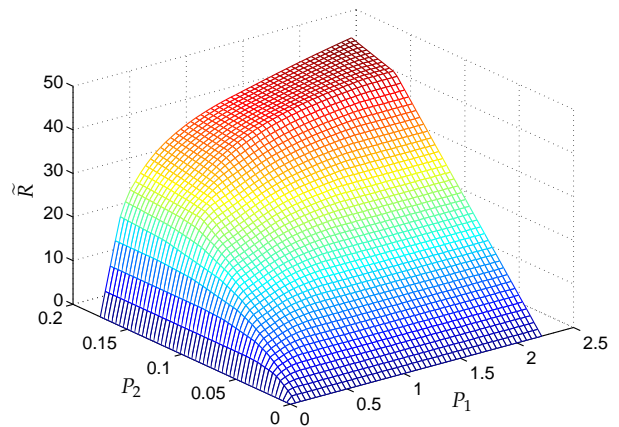
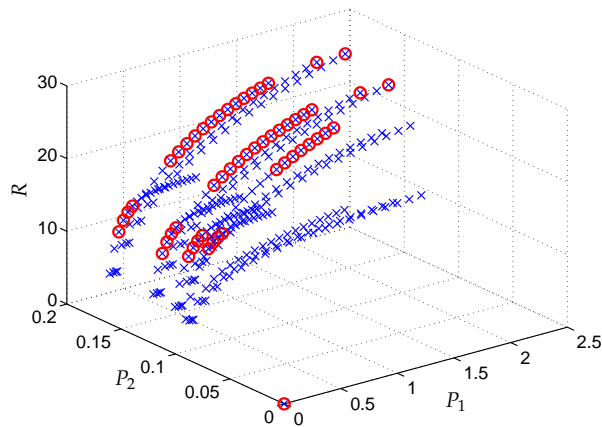
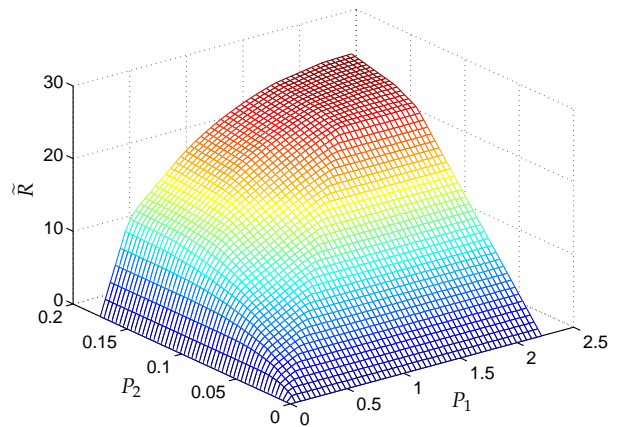
(a) $d = 20$ meters(b) $d = 20$ meters(c) $d = 50$ meters(d) $d = 50$ meters(e) $d = 100$ meters(f) $d = 100$ meters

Fig. 3.26: Operation modes (left) and the constructed achievable rate surface (right) in the power-rate space, blue crosses stand for feasible operation modes while red circles stand for energy efficient operation modes, P_1, P_2 are in Watt, R and \tilde{R} are in kbit/sec

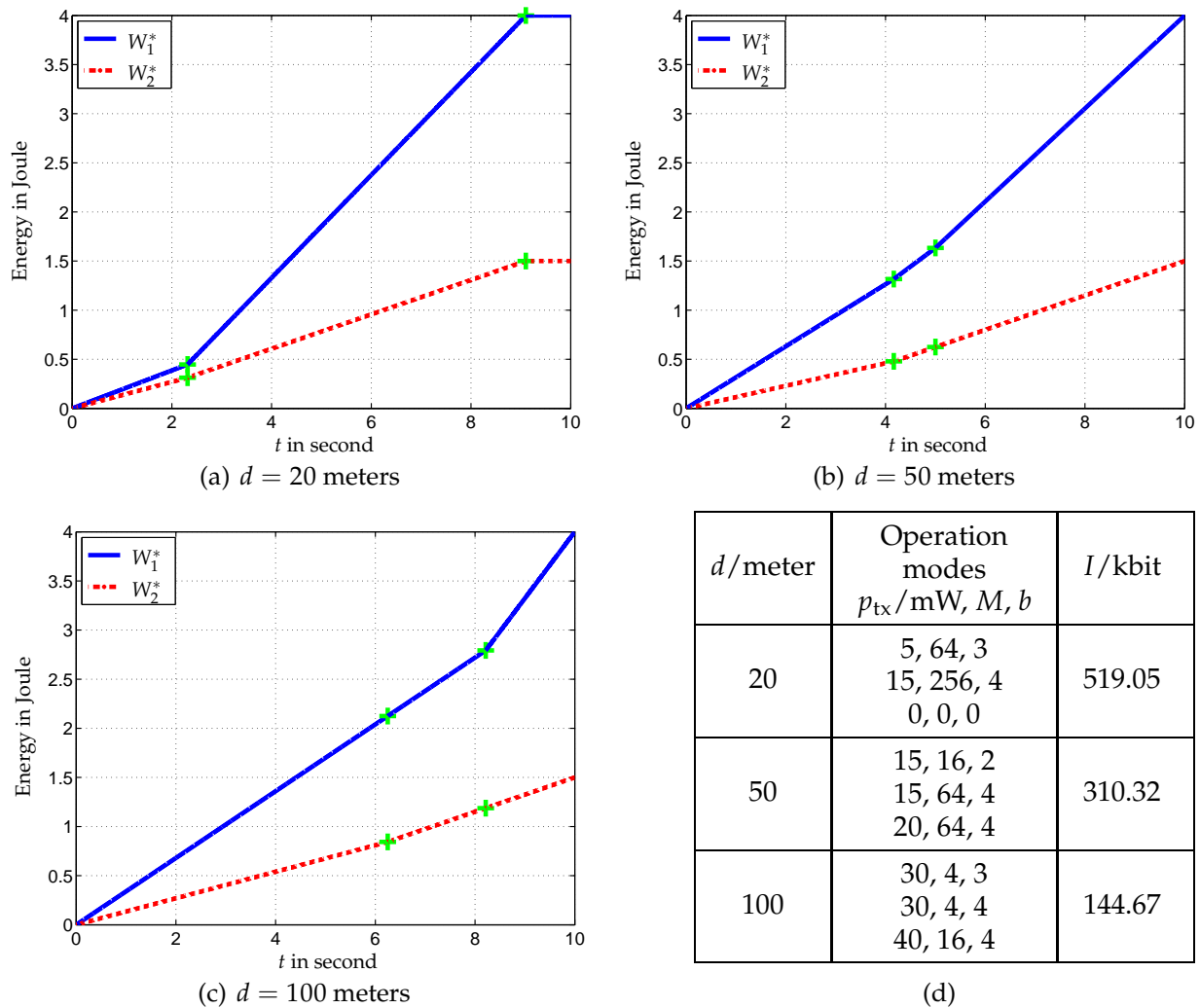


Fig. 3.27: Optimal state trajectories of the transmitter and the receiver as well as the corresponding maximal throughput, $T = 10$ sec, $A_1 = 4$ Joule, $A_2 = 1.5$ Joule, the green crosses indicate the switches between different operation modes

segments with different slopes. It can be noted that the modulation orders and the ADC resolutions of the active modes do not always match.

The jointly optimal control strategy is compared to a distributed solution in terms of the achieved throughput in Fig. 3.28. In the case without central control and the transmitter and the receiver are not aware of the situation of each other, a distributed solution has to be employed where the operation of each transceiver is only based on the local energy information. We propose a fixed modulation scheme *i.e.* a single M is selected and employed throughout the operation interval, while the transmitter and the receiver have the freedom to choose their transmit power and ADC resolution, respectively. We assume that the two transceivers choose the highest operation mode possible to make the most use of the available energy. As shown in the figures, there is always a performance gap between the optimal centralized control and the distributed solution. How large is the gap depends on the selected modulation order and also the energy budgets of both

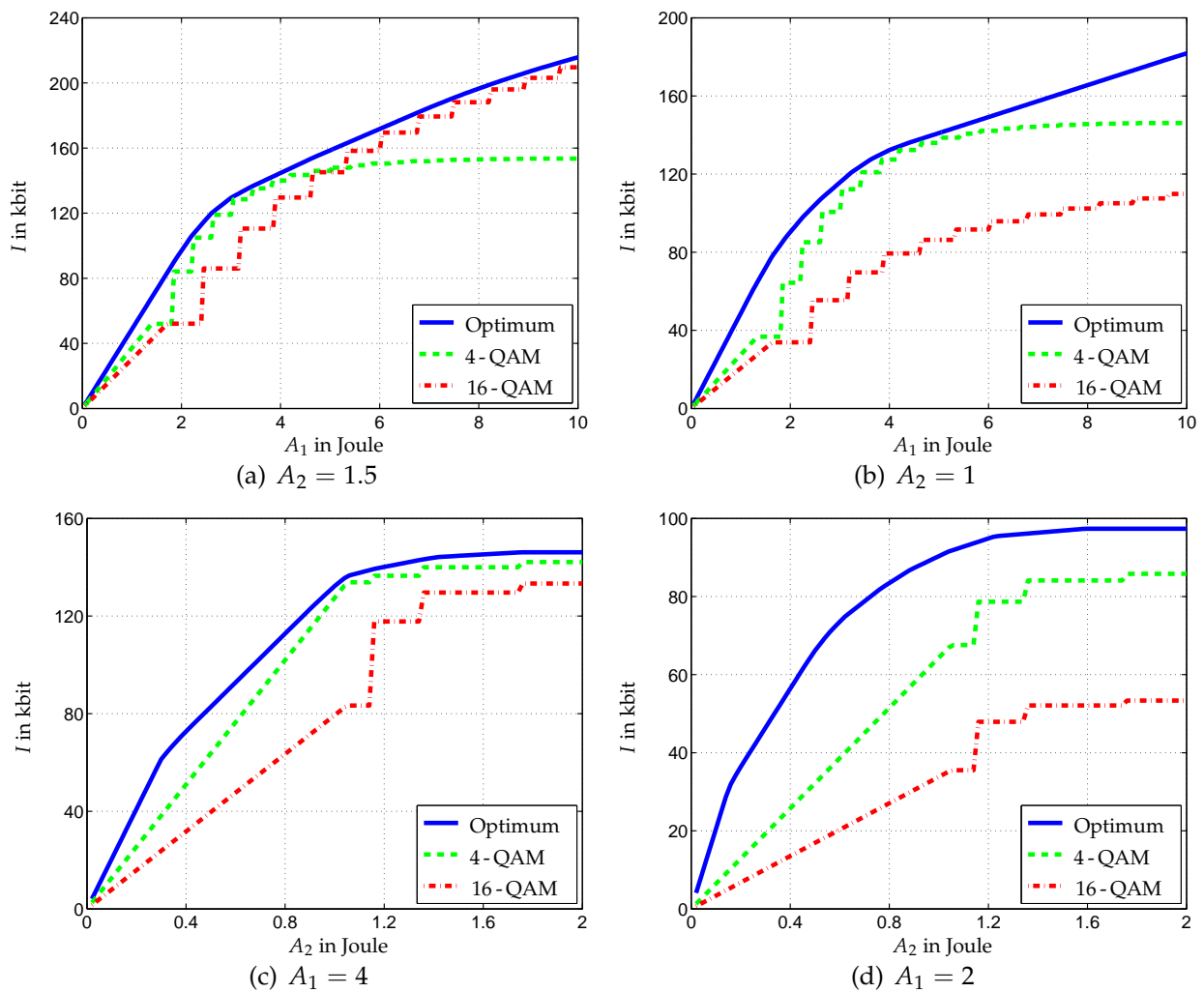


Fig. 3.28: Throughput achieved with the optimal control strategy and a distributed solution which employs a fixed modulation order, $T = 10$ sec, $d = 100$ meters

transceivers. In some situations the performance of the distributed solution comes very close to that of the optimal control, while in some other situations the system suffers considerably from the lack of effective cooperation.

3.6 Summary

We have discussed in this chapter the throughput maximization problem of a communication system that operates on a finite time interval with a given energy budget. The focus is on how the available energy should be spent over the available time, such that the total amount of data conveyed is maximized. To this end, we formulate the problem within the framework of the optimal control theory, and introduce the Pontryagin's maximum principle to aid the derivation of the optimal solution. We consider the problem for the transmitter, the receiver, and a pair of transmitter and receiver, where a number of different cases are investigated for each system. In scenarios where the channel condition stays constant and is known by the system, the key to finding

the throughput-maximizing control strategy lies in the determination of the energy efficient operation modes. This can be accomplished by constructing a concave relation between the achievable data rate and the power consumption of the system. Based on the obtained results, scenarios with time-varying channels can be solved. Depending on the availability of non-causal channel knowledge, convex optimization algorithms or dynamic programming techniques are employed in the derivations. Moreover, the variations of the maximal achievable throughput in the energy budget and in the duration of the operation interval are studied for many of the cases. The conclusions drawn from these fixed-energy problems shall lay the basis of the varying-energy problems we investigate in the next chapter.

4. Optimal Control of Energy Harvesting Transceivers

Centering around the energy efficiency of wireless communication systems, we have reviewed and discussed previously some important performance trade-offs on the component and link levels of these systems. In the last chapter, we focus on the efficient utilization of energy in a system constrained by a fixed energy budget. To support even better sustainability of wireless devices, *energy harvesting* techniques, which have emerged and developed quickly over the past decades, can be employed to provide additional or exclusive power supply for these devices by harnessing energy from their surrounding environment. From an operational point of view, this helps prolong the operation time of the systems before any human intervention is necessary, *e.g.* for a battery change or recharge. Such an advantage is of particular importance to wireless sensor networks deployed in prohibited environment and to wearables for healthcare where maintenance of the system can be inconvenient or difficult. From an environmental point of view, exploiting the ambient energy contributes to the evolution of *Green Communications* [76] as it helps alleviate the increasing demand on fixed power supply utilities and batteries. On the other hand, the power densities that the energy harvesting techniques are able to provide, although dependent on the energy sources, the materials used for the harvesters, and the specific converting techniques, are in general very limited which restricts applications mostly to low-power devices. Nevertheless, the potential of energy harvesting techniques applied to wireless communications are worth exploring, and have indeed attracted significant attention from both academia and industry.

In this chapter, we will focus on wireless communication devices powered purely by harvested environmental energy, and refer to them as *energy harvesting nodes*. The functional module that each of these devices is equipped with, which harnesses and stores the ambient energy, is referred to as the *energy harvester*. One of the essential features of operating with an energy harvester, as opposed to operating with fixed power supply utilities, lies in the time-variant and intermittent nature of the harvested energy. As the external energy source is often unsteady and not part of the control system, the arrival of the harvested energy can be modeled as a stochastic process. This is to say, when and how much energy can be harnessed is random and practically unknown in advance. If there is some time correlation or characteristic pattern in the behavior of the energy source, the energy arrivals can be predictable to a certain extent. Moreover, the energy harvester can be designed to regularize its output, making the energy that becomes available for communication tasks less random and sporadic. We do not consider these issues within the scope of this thesis, *i.e.* the energy harvested over time is assumed completely random

and uncorrelated. As a consequence of the inconstant and intermittent power supply, new resource allocation strategies and design methodologies are required for energy harvesting nodes. More specifically, how the available energy is spent over *time* is the main focus here, which calls for a *dynamic* viewpoint of the system under consideration. To this end, the *optimal control theory* and the theory on *Markov decision processes* are sought for as the appropriate tools for the treatment of related problems. In consistency with the terminology thereof, the parameters of the energy harvesting node that can be adapted are referred to as *control variables*, and the way they are adapted is called the *control*.

As mentioned before, there has been a burst of research activities since a few years ago on the operation and optimization of energy harvesting nodes. In [77], various aspects of energy harvesting sensor systems have been surveyed, including their architecture, energy conversion and storage technologies, and exemplary harvesting based applications. Detailed measurement results of an indoor radiant energy harvesting system are presented in [78], where energy management strategies are also developed for different environments and communication scenarios. In [79], a throughput maximization framework is established for an energy harvesting transmitter with non-causal energy arrival information, from which we see the possibility and necessity of making connections to the optimal control theory and exploiting results of the studies on energy efficient communications. To this end, we take into account the circuit power of the energy harvesting nodes and investigate its impact on the optimal operation strategy. Not only were we among the first to consider this important issue [80], but we also established more general results than the several other works that deal with a similar problem [81,82]. The optimization framework can be elaborated and extended to include more ingredients such as a fading channel [83,84], non-linear behavior and imperfections of the battery [85], *etc.* We investigate in some of these directions also with the consideration on circuit power [86,87]. Another category of problems arise if only causal and statistical energy arrival information is assumed at the transmitting node, which have been studied in research papers such as [84,88–90]. Unlike the case with non-causal energy arrival information in which we usually maximize the short-term throughput, optimization of infinite-horizon is formulated instead to meet the goal of designing an operation policy that works the best on average. Although different methods such as Markov decision process and dynamic programming are found suitable here, some basic conclusions we have drawn previously in the non-causal information case lay the basis for the construction of the optimal operation strategy. Similar investigations can be performed for an energy harvesting receiver, and a pair of communicating energy harvesting nodes, where multiple control variables are involved [91,92]. Based on the studies on these basic scenarios, more complex communication setups and techniques such as relaying [93,94] and multiple access systems [95,96] are explored under energy harvesting constraints. One may refer to [97] for recent developments in energy harvesting wireless communications.

In this chapter, we first present a short overview of energy harvesting techniques that are commonly applied to power wireless devices, and then follow the optimization framework established in the last chapter to discuss the general throughput maximization problem. In Section 4.2, we consider the case with a priorily known energy arrival functions. Properties of the optimal solution are deduced from a geometric perspective, and algorithms for the construction of the optimal state trajectories are proposed and proven. The optimal control of energy harvesting nodes with causal and statistical

Table 4.1: Considered scenarios for communications using energy harvesting nodes

EH node	Arrival knowledge	Control variable	Channel state	Reference
TX	non-causal	transmit power (continuous)	constant	[80,98]
			time-varying	[87]
		modulation order (discrete)	constant	[86]
			time-varying	[87]
	causal	transmit power	constant	[99]
		modulation order	time-varying	[100]
RX	non-causal	ADC resolution and bandwidth (continuous)	constant	[101]
TX and RX	non-causal	transmit power and ADC resolution (continuous)	constant	[102]
	causal	transmit power, modulation order, and ADC resolution	constant	[103]

knowledge of the energy arrival process is treated in Section 4.3, where the objective is changed to maximizing the average throughput over an infinite time horizon, and the mathematical tools used are Markov decision processes and dynamic programming. In particular, we apply the policy-iteration algorithm to obtain the optimal operation policy with respect to a number of single-stage strategies. The joint control of two energy harvesting nodes communicating over a single link is also investigated in the respective sections. In addition, decentralized control strategies are proposed for the two nodes when only local state information is available. Our investigations under various scenario assumptions are listed in Table 4.1, where the previous publications of the respective parts are referenced. Note that some of the scenarios are not discussed or presented in detail due to their similarity in terms of solution methods with others. The chapter is summarized and concluded in Section 4.4.

4.1 Energy Harvesting Techniques

Various forms of energy, such as solar, thermal, and kinetic energy, can be captured and gathered from the environment to power wireless communication devices. The process of harnessing energy from ambient sources and converting it to electrical energy, which is then utilized for powering wireless devices and carrying out communications, is known as *energy harvesting* or *energy scavenging*. In the following, we give a brief introduction to common energy harvesting and storage techniques. For a more thorough and dedicated treatment of the topic, one may refer to [28,77,104].

4.1.1 Photovoltaic

The harnessing and utilization of solar energy is very common in our daily lives, from building-integrated systems with large-scale solar panels on rooftops [105] to low-power portable electronics such as pocket calculators. Using semiconducting materials that exhibit the *photovoltaic effect*, which refers to the production of electric current from the excitation of electrons upon exposure to light, photovoltaic energy harvesters are able to provide power densities that are much higher than other harvesting techniques. Yet the presence and intensity of the light sources greatly affect the output power, which can be intermittent and differ by several orders of magnitude. Another limiting factor of photovoltaic energy harvesting is the area restriction for deployment which confines the output power level, as the latter is proportional to the area of the solar panels. For small sized stand-alone electronics, this can be a major concern which calls for efficient energy management so as to better support the desired quality of service of the system. In addition, the costs of materials, manufacturing, and maintenance are also relevant for large-scale systems.

4.1.2 Piezoelectric, electromagnetic, and electrostatic

Kinetic energy can be converted into electrical energy with piezoelectric, electromagnetic, or electrostatic transduction mechanisms. In response to mechanical strain, piezoelectric materials such as piezoelectric crystals and certain ceramics become polarized and produce electric current or voltage, the value of which is proportional to the applied strain. This effect can be employed to harvest energy from deformations caused by human motions, *e.g.* walking or pressing buttons. Induction based electromagnetic transduction and capacitor based electrostatic transduction on the other hand, exploit the relative displacement that occurs within the system because of external vibrations. The three mechanisms exhibit different characteristics and are suitable for different application scenarios, with their respective constraints and preferences. As alternating current is produced with these transducers, rectifiers are needed to turn the signal into direct current for further use.

4.1.3 Thermoelectric

A temperature difference in metal or semiconductor materials causes the charge carriers to diffuse from the hot end to the cold end, resulting in an electric voltage. By virtue of this property known as the *thermoelectric effect*, thermal energy can be converted and harvested. Thermoelectric energy harvesting is reliable and is of particular interest to power medical devices and consumer electronics, due to the potential utilization of the body heat. An example of application is the thermoelectric wristwatch, which is driven by the electrical power converted from the body heat of the wearer. The conversion efficiency of thermoelectric energy harvesters depends on the materials used, and improves with larger temperature differences. However, it is typically rather low, achieving the value of a few percent.

4.1.4 Radio frequency

Ambient RF energy can be harvested using a high gain antenna and a rectifier which converts the RF signal into direct current. The output power of an RF energy harvester is in the order of $0.1 \mu\text{W}$ in general, which is relatively lower than other harvesting techniques. However, RF energy is omnipresent, and this makes it especially suitable for wireless sensor nodes deployed in places where battery replacement is difficult. Moreover, the rapidly growing wireless services and the ever expanding wireless network coverage help improve the applicability and the strength of RF signals in the background, *e.g.* from analog/digital TV broadcast, cellular networks, and Wi-Fi services. In some cases, RF signals are intentionally sent from a base station to power distributed energy harvesting nodes.

The common energy harvesting techniques are listed in Table 4.2, where their power densities are roughly given by the orders of magnitude.

Table 4.2: Common energy harvesting techniques

Type of energy	Source	Power density
Light	Sun (outdoor)	$10^4 \mu\text{W}/\text{cm}^2$
	Illumination (indoor)	$10 \mu\text{W}/\text{cm}^2$
Kinetic	Human motion, vibration	$1 \text{ mW} \sim 100 \text{ W}$
Thermal	Temperature difference	$100 \mu\text{W}/\text{cm}^2$
RF	RF fields, RF waves	$0.1 \mu\text{W}/\text{cm}^2$

4.1.5 Energy storage

Energy storage is the process of converting the harvested energy to forms that can be stored for longer time, more economically, and with less loss. Batteries and supercapacitors are the traditional and rising energy storage media for wireless sensors. While batteries have higher energy densities and less leakage, supercapacitors have higher power densities which make them more suitable for bursty energy input and output. Moreover, supercapacitors are more durable in terms of charge-discharge cycles. As a result, the choice for the energy storage medium depends on the system specification and application scenario. For a given system, the capacity and other characteristics of the energy storage in turn influence the optimal design of resource allocation algorithms and operation strategies that are to be employed.

4.2 Optimal Control with Non-causal Energy Arrival Information

In the previous chapter, we have investigated the throughput maximization problem for transceivers with a fixed energy budget. The problem is called *basic*, because it can be viewed as a static phase in an energy harvesting process *i.e.* no energy is harvested during the time interval of interest, and also because its solution provides important insight and serves as the building block for the solution of the *general* problem. For an energy harvesting transceiver, the energy that becomes available for communications is

in general a function of time which depends on the environment, the energy harvester, the capacity of the energy storage, *etc.* This means, in view of the formulation of the basic problem (3.3), the distinction of the general problem mainly lies in the constraint on the system state. Depending on the type of information the transceiver has about this constraint function, the control optimization is formulated respectively and solved using different mathematical tools. More specifically, when *non-causal* knowledge about the available energy is assumed for the energy harvesting node, the optimal transmit/receive strategy can be obtained offline with the optimal control theory and convex optimization algorithms. On the other hand, if the node only has causal and statistical information about the potential energy arrivals, stochastic models and control methodologies are employed which produce a set of rules to guide the online operation of the system.

Due to the aforementioned differences, we focus on the optimal control problem with non-causal energy arrival knowledge in this section, and leave the causal knowledge case to the next one. After the formulation of the general throughput maximization problem, we derive and discuss the properties of the optimal transmit and receive strategies, as well as how to obtain them in different cases.

4.2.1 Problem formulation

Our goal is to find, among all *admissible* controls, the one that leads to the maximal throughput on the time interval of interest. For a control to be admissible, it needs to fulfill constraints imposed both by physics and by system design. In the context of energy harvesting nodes, the most critical constraint is that at any time instant, the cumulative energy expenditure of the system can not surpass the cumulative energy that becomes available. Since the harvesting of ambient energy is time-variant and practically unknown in advance, the integration of this condition into the optimal control problem depends on the assumption we make about the system and can be quite a subtle issue. To start with, we analyze first a basic form of the general control problem, the solution of which will be employed later as the most important building block for the general optimal solution.

Recall that we aim at maximizing the throughput of an energy harvesting node on a given time interval $[0, T]$, and that the state of the system W is defined as the cumulative energy consumption of the node. As the node has no fixed power supply but depends solely on the ambient energy, W is upper bounded by the cumulative harvested energy plus the energy that is initially available from the battery, $\forall t \in [0, T]$. This condition may be called the *passivity constraint* as the node only consumes the harvested energy but does not produce any energy on its own. It may also be called the *causality constraint* from the viewpoint that the node can not consume any energy that is to be harvested in the future.

We let $\tilde{A}(t)$ denote the cumulative maximal energy that can be harvested, and $A(t)$ denote the cumulative actual harvested energy, $t \in [0, T]$. It is necessary to distinguish between these two functions, when the storage capacity of the node is limited. In the extreme case, if the node does not consume any power but only harnesses energy, the storage eventually gets full and the node becomes incapable of further obtaining ambient energy even if it is available. We term such occasions as *energy miss* events, which result in a gap between $\tilde{A}(t)$ and $A(t)$. On the other hand, if the node has infinite storage capacity, then whatever energy can be harvested from the environment can be stored and eventually utilized, leading to $\tilde{A}(t) = A(t)$. We denote the storage capacity of the energy

harvesting node with E_{\max} , and assume it a finite constant. The passivity constraint or the causality constraint imposes a pointwise upper bound on the state trajectory as

$$W(t) \leq A(t), \quad \forall t \in [0, T]. \quad (4.1)$$

Taking into account the nature of common external energy sources and potential power control mechanisms of the energy harvester, we assume that the function \tilde{A} of t is piecewise continuous, *i.e.* it is continuous in its domain except for a finite number of discontinuities. Note that \tilde{A} is non-decreasing as a cumulative energy function. A discontinuous point then corresponds to a sudden increment representing the arrival of a certain amount of energy within very short time. We refer to this kind of arrival as *energy packets*. On the other hand, the system state W of t , which is also non-decreasing, should be piecewise smooth *i.e.* having continuous first-order derivative except for a finite number of points. This is due to the assumption that the energy harvesting node is capable of switching between discrete values of the control variable within very short time, but is not able to dissipate infinite power. As for the non-causal information case under consideration, we assume that \tilde{A} is perfectly known by the energy harvesting node before the communication takes place.

It is clear from the above analysis that, while the function $\tilde{A}(t)$ is completely determined by the environment and the equipped energy harvester, the function $A(t)$ can be dependent on $W(t)$ and E_{\max} due to the possible energy miss events. To circumvent this complication, we propose a pre-processing step to construct the maximal function A from \tilde{A} for which it is possible to avoid energy miss events altogether. Given $E_{\max} < \infty$ and the maximal power consumption $P_{\max} < \infty$, we initialize A with \tilde{A} and construct the state trajectory W_{\max} from $t_1 = 0$ on according to Algorithm 4. The trajectory goes with the maximal increasing rate possible, *i.e.* $\dot{W}_{\max} = P_{\max}$ or $\dot{W}_{\max} = \dot{\tilde{A}}$ for the parts where W_{\max} coincides with \tilde{A} but $\dot{\tilde{A}} < P_{\max}$. At each intermediate end point of the trajectory, we examine whether an energy miss event is inevitable indicated by $A(t_1) > W_{\max}(t_1) + E_{\max}$. If so, the right part of the curve $A(t)$ with $t \in [t_1, T]$ should be shifted downward by the amount $A(t_1) - W_{\max}(t_1) - E_{\max}$, suggesting that the node has missed the chance of harnessing the corresponding energy. The final state $W_{\max}(T)$ reveals the maximal energy consumption of the node on $[0, T]$. As no additional energy can be utilized, we set the part of A that is above this level to $W_{\max}(T)$. The constructed $A(t)$ is a genuine and tighter bound on W than $\tilde{A}(t)$, and is called the *effective* cumulative available energy function. We give an exemplary construction result in Fig. 4.1(a), where the harvested energy as represented by the curve \tilde{A} becomes available in the form of energy packets, rendering \tilde{A} and consequently A to be increasing staircase functions.

The data transmission or reception models we investigate possess the property that $R(P_1) > R(P_2)$ if $P_1 > P_2$. As a result, the available energy should be fully used in the sense that no energy miss event happens and that all energy is exhausted at the termination point T . To assure the first condition, we define a lower bound $D(t)$ on the state trajectory which represents the minimal amount of energy that has to be consumed by time t in order to avoid energy misses. On the time-energy graph, this corresponds to shifting A downward by E_{\max} and obtaining

$$D(t) = \max(0, A(t) - E_{\max}), \quad \forall t \in [0, T]. \quad (4.2)$$

Algorithm 4 Construct the effective cumulative available energy function $A(t)$

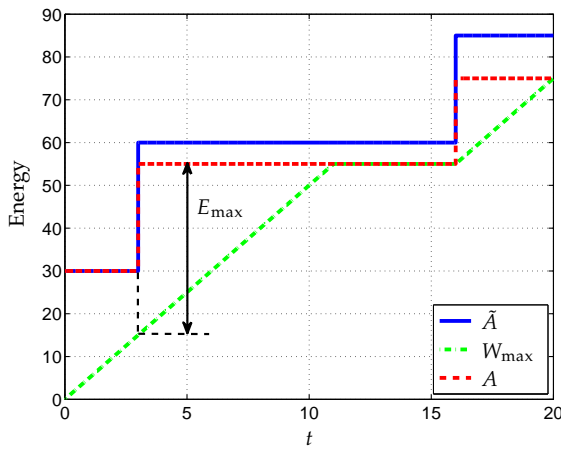
Require: $E_{\max} < \infty, P_{\max} < \infty, \tilde{A}(t), t \in [0, T]$

Ensure: $A(t), t \in [0, T]$

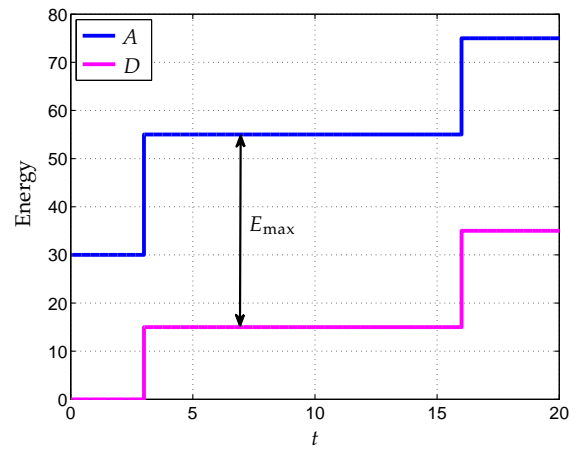
```

1:  $A \leftarrow \tilde{A}, t_1 \leftarrow 0, W_{\max}(t_1) \leftarrow 0, \Delta t$ : infinitesimal step in time
2: while  $t_1 < T$  do
3:   if  $A(t_1) > W_{\max}(t_1)$  then
4:     if  $A(t_1) > W_{\max}(t_1) + E_{\max}$  then
5:        $A(t) \leftarrow A(t) - (A(t_1) - W_{\max}(t_1) - E_{\max}), t \in [t_1, T]$ 
6:     end if
7:      $W_{\max}(t) \leftarrow W_{\max}(t_1) + P_{\max} \cdot \Delta t, t \in (t_1, t_1 + \Delta t]$ 
8:   else
9:      $W_{\max}(t) \leftarrow A(t_1) + \min(\dot{A}(t_1), P_{\max}) \cdot \Delta t, t \in (t_1, t_1 + \Delta t]$ 
10:  end if
11:   $t_1 \leftarrow t_1 + \Delta t$ 
12: end while
13: if  $W_{\max}(T) < A(T)$  then
14:    $A(t) \leftarrow \min(A(t), W_{\max}(T)), t \in [0, T]$ 
15: end if

```



(a) Construction of A with $P_{\max} = 5$



(b) Lower bound D and the admissible region

Fig. 4.1: Geometric view of the general throughput maximization problem: time-varying boundaries for the state trajectory

For the exemplary curve A we constructed in Fig. 4.1(a), the corresponding lower bound D is shown in Fig. 4.1(b). Any state trajectory W satisfying $D \leq W \leq A$ on a pointwise basis is physically feasible as well as free from energy misses. If the final state $W(T) = A(T)$ is also fulfilled, then the trajectory is qualified as one of the candidate optimal trajectories, which we call *admissible*. Correspondingly, an *inadmissible* trajectory violates either or both conditions, and can not lead to the maximal throughput. The region bounded by the curves A and D on the time-energy graph is called the *admissible region*.

Finally, we give the formal expression of the general throughput maximization problem of an energy harvesting node as

$$\begin{aligned}
 \max_u \quad & \int_0^T R(t, u) dt \\
 \text{s.t.} \quad & \dot{W} = P(u), W(0) = 0, \\
 & D \leq W \leq A, \\
 & W(T) = A(T).
 \end{aligned} \tag{4.3}$$

Compared with our objective, *i.e.*, to control the energy harvesting node from time 0 to T by continuously adapting the control variable in such a way, that the maximal throughput can be achieved while the causality constraint is not violated, (4.3) contains in addition the lower bound and final state conditions. These are necessary for optimality, and more importantly, provide us with a causality constraint that is independent of the control we choose, therefore leading to a much more tractable problem structure.

4.2.2 Transmit strategies

When discussing the optimal solution of the basic problem in Chapter 3, we have considered several cases with different system models and obtained quite distinct optimal trajectories. In the following, we solve the general problem for each case based on the respective optimal solutions of the basic problem.

4.2.2.1 Case I

If the transmit power can be adapted continuously in magnitude and the power consumption function P is convex on $[0, +\infty)$, we have that the throughput-maximizing strategy given fixed energy budget is to use constant transmit power, which corresponds to the optimal trajectory W^* as a straight line. Based on this result, the following theorem and the its direct consequence, the *optimality criterion*, can be obtained and proven.

Theorem 1. *Let $W(t)$, $t \in [0, T]$ be an admissible trajectory to the general problem (4.3) and $L(t)$, $t \in [t_1, t_u]$ be the straight line segment that adjoins $(t_1, W(t_1))$ and $(t_u, W(t_u))$ where t_1, t_u satisfy $0 \leq t_1 < t_u \leq T$. If L satisfies $D \leq L \leq A$ and $L \neq W$ on $t \in [t_1, t_u]$, then the new admissible trajectory*

$$W_{\text{new}} = \begin{cases} W, & t \in [0, t_1], \\ L, & t \in (t_1, t_u), \\ W, & t \in [t_u, T]. \end{cases} \tag{4.4}$$

leads to an increase in throughput.

Proof. The constructed trajectory W_{new} is identical to W except on the subinterval (t_1, t_u) . Therefore, we only need to prove that on $[t_1, t_u]$, the straight line segment L gives larger throughput than any other admissible trajectory. Since W is admissible, we have

$$D(t_1) \leq W(t_1) \leq A(t_1), \quad D(t_u) \leq W(t_u) \leq A(t_u). \tag{4.5}$$

Let us define the horizontal lines $A_b(t) \equiv W(t_u)$ and $D_b(t) \equiv W(t_l)$, $t \in [t_l, t_u]$. For any trajectory \tilde{L} adjoining $(t_l, W(t_l))$ and $(t_u, W(t_u))$ to be admissible, it should satisfy the boundary conditions

$$\max(D, D_b) \leq \tilde{L} \leq \min(A, A_b), \quad \forall t \in [t_l, t_u]. \quad (4.6)$$

The resulting admissible region is a subset of the rectangular region bounded by A_b and D_b , which is exactly the admissible region of the basic problem between $(t_l, W(t_l))$ and $(t_u, W(t_u))$ with the energy budget $W(t_u) - W(t_l)$. Therefore, the optimal trajectory to this basic problem, *i.e.* L , leads to the maximal throughput among all admissible trajectories \tilde{L} . Consequently, for $W(t) \not\equiv L(t)$, $t \in [t_l, t_u]$, the replacement with L in W always results in an increase of the throughput. \square

Theorem 1 states that if there exist two points on an admissible trajectory which can be connected with a straight line segment without violating any boundary condition, *i.e.* the resulting trajectory is still admissible, then the replacement with the corresponding straight line segment would increase the throughput. To this end, we claim the *optimality criterion* which is a necessary condition for an admissible trajectory to be optimal: *there do not exist any two points on the optimal trajectory W^* that can be adjoined by a distinct admissible straight line.*

We let W_0 be an admissible trajectory which satisfies the optimality criterion. The following lemma characterizes the slope changes on W_0 , *i.e.* under which conditions should the transmit power be changed, and how should it be changed.

Lemma 1. *The points at which W_0 changes slope are either on A or on D . Moreover, the slope change at a point on D is negative, whereas the slope change at a point on A is positive.*

Proof. We prove the lemma by assuming its contrary and then showing that the optimality criterion is violated. This is conveniently achieved with the schematic drawings shown in Fig. 4.2. The trajectories in red are all admissible, but the existence of the dashed green lines indicates that they violate the optimality criterion. When the slope change happens at a point which is neither on A nor on D , as shown in Subfigure (a), a straight line segment can always be constructed above or under the point, depending on whether the slope change is positive or negative. Similarly, we see in Subfigures (b) and (c) that, when a negative slope change happens at a point on A , or a positive slope change happens at a point on D , the optimality criterion shall not be satisfied. \square

With the enforced properties on R and P for Case I, the basic throughput maximization problem (3.3) is convex, rendering the local optimum found by the PMP the unique global optimal solution. Convexity of the general problem (4.3), however, can be impaired by the lower boundary D on the state trajectory which causes the set of feasible controls non-convex.¹ Yet fortunately, we can validate the existence and uniqueness of the optimal trajectory with the following theorem.

Theorem 2. *The admissible trajectory that satisfies the optimality criterion is unique, and it corresponds indeed to the optimal control of (4.3).*

¹The upper boundary A does not ruin the convexity of the set of feasible controls given convex functions P . Also, if P is affine in p_{tx} , the general problem can be shown convex.

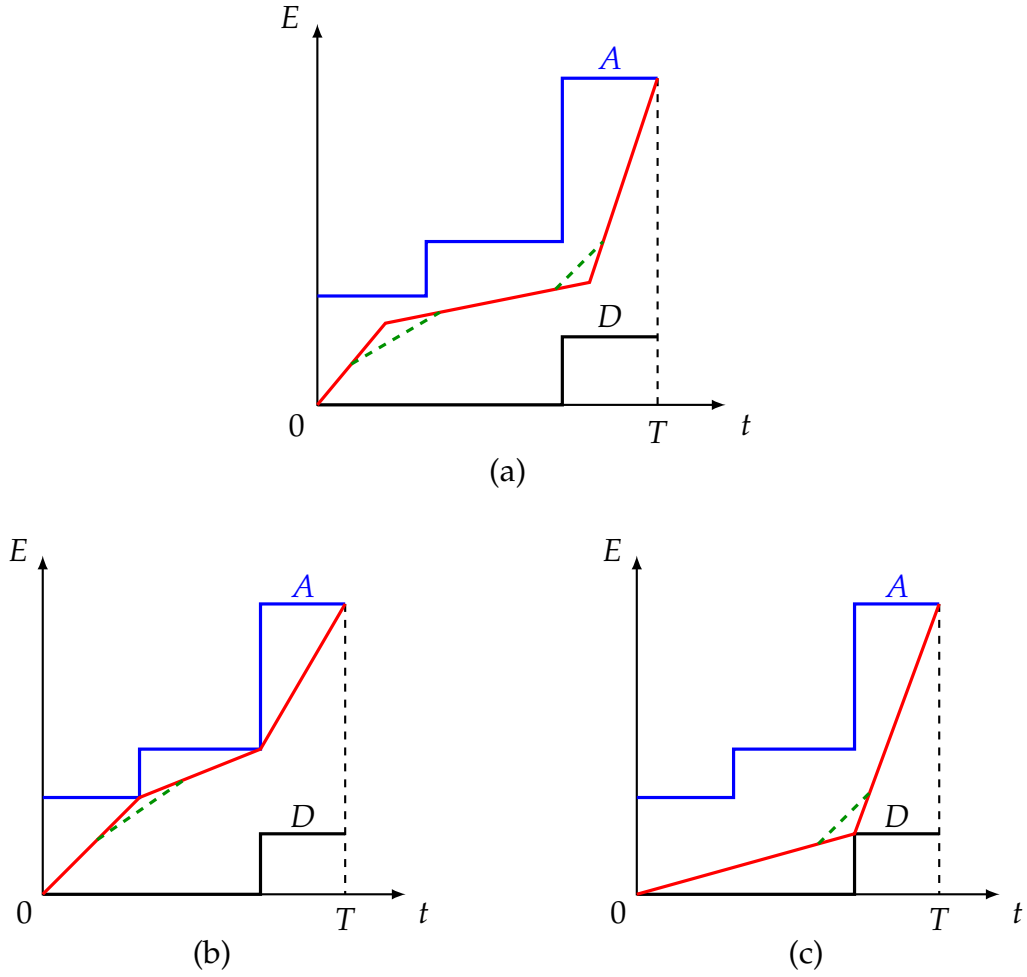


Fig. 4.2: Violations of the optimality criterion for Case I

Proof. Let us start with the uniqueness part. Suppose the admissible trajectory that satisfies the optimality criterion is not unique. Let W_a and W_b be two admissible trajectories satisfying the optimality criterion and $W_a \not\equiv W_b$. They share the same starting point $(0, 0)$ and both terminate at $(T, A(T))$. Since the two trajectories are not identical, they must differ over some subinterval of $[0, T]$. Let $t_l \geq 0$ be the left boundary of the subinterval, *i.e.* the last time instant at which the two trajectories coincide, and $t_u \leq T$ be the right boundary which is the first time instant that the two trajectories intersect again. Without loss of generality, we establish the relation

$$D(t) \leq W_b(t) < W_a(t) \leq A(t), \quad t \in (t_l, t_u). \quad (4.7)$$

From $W_a > D$ and Lemma 1, we know that the slope of W_a does not decrease over (t_l, t_u) . Since W_a is a nondecreasing function, it can be seen that W_a is convex over (t_l, t_u) . Similarly, W_b can be found concave on (t_l, t_u) . Starting from the same point $(t_l, W_a(t_l)) = (t_l, W_b(t_l))$, the convex function W_a which is strictly larger than the concave function W_b can not intersect with W_b again at point $(t_u, W_a(t_u))$, leading to a contradiction. As a result, the admissible trajectory that satisfies the optimality criterion has to be unique.

Next we show that the unique admissible trajectory that satisfies the optimality criterion, denoted with W_0 , leads to larger throughput than any other admissible trajectory, denoted with W_1 . Since $W_0 \not\equiv W_1$, with the same argument before, there exists some subinterval $[t_1, t_u]$ over the interior of which the two trajectories differ, but at the boundary points $W_0(t_1) = W_1(t_1)$, $W_0(t_u) = W_1(t_u)$. Again we assume $D(t) \leq W_1(t) < W_0(t) \leq A(t)$ for $t \in (t_1, t_u)$, which means the slope of W_0 does not decrease on the subinterval. The gap between the two trajectories is characterized by

$$\Delta W(t) \triangleq W_0(t) - W_1(t) = \int_{t_1}^{t_u} P_0 \, dt - \int_{t_1}^{t_u} P_1 \, dt \triangleq \int_{t_1}^{t_u} \Delta P \, dt \quad (4.8)$$

$$\Delta W(t) \begin{cases} > 0, & t \in (t_1, t_u), \\ = 0, & t = t_1 \text{ or } t = t_u, \end{cases} \quad (4.9)$$

where P_0 and P_1 are the respective power consumption over time corresponding to the two trajectories. With a little abuse of notation, we directly write $R(P)$ in the following to indicate the achievable rate R as dependent on the power consumption P . The difference in throughput, $\Delta I = I_0 - I_1$, is bound to be positive since

$$\begin{aligned} \Delta I &= \int_{t_1}^{t_u} R(P_0) \, dt - \int_{t_1}^{t_u} R(P_1) \, dt = \int_{t_1}^{t_u} (R(P_0) - R(P_0 + \Delta P)) \, dt \\ &> - \int_{t_1}^{t_u} R_P(P_0) \cdot \Delta P \, dt \end{aligned} \quad (4.10)$$

$$= \int_{t_1}^{t_u} \Delta W \cdot \frac{d}{dt}(R_P(P_0)) \, dt - (R_P(P_0) \cdot \Delta W)|_{t_1}^{t_u} > 0, \quad (4.11)$$

where the inequality in (4.9) is due to the strict concavity of R in P (see Case I in Section 3.3.1), and integration by parts is applied from (4.9) to (4.10) noting that $\Delta \dot{W} = \Delta P$. Since the first-order derivative R_P is positive and strictly decreasing in P , the non-decreasing P_0 renders $R_P(P_0)$ to be non-increasing in time. Therefore, the first term in (4.10) is positive. As the second term is obviously trivial, we have $\Delta I > 0$, which means on the subinterval $[t_1, t_u]$, the trajectory W_0 gives better throughput than W_1 . The same conclusion can be drawn for the case that $W_0 < W_1$ on the subinterval of interest. Consequently, we are able to claim that the unique admissible trajectory satisfying the optimality criterion is the global optimal trajectory for (4.3). \square

In [106], the essentially same theorem for the case $P = p_{tx}$ is proven by the verification of the convexity of the problem, as well as the compactness of the admissible region which guarantees the existence of the optimal solution. Some of the conditions used therein are in fact unnecessarily strong. In our case, the extension to convex functions P damages the convexity of the problem, yet with the approach shown above, the global optimality of the unique admissible trajectory that satisfies the optimality criterion can still be proven. The key feature to the establishment of the conclusion is the strict concavity of the achievable rate as a function of the power consumption, which is also the essential reason why using constant transmit power is the optimal solution to the basic problem.

Our remaining task now is to find a way to construct the admissible trajectory W_0 that satisfies the optimality criterion. Due to the similarity in mathematics, the algorithm

proposed in [106], though for a different problem setup, can be tailored and applied. We summarize the procedure and its validation in the following.

Consider a time instant $t_0 \in [0, T)$. It can be observed that as soon as the total energy consumption during $[0, t_0)$ is determined, the throughput maximization problem over the time slot $[t_0, T]$ is independent of the specific transmission strategy employed during $[0, t_0)$. To this end, the construction of W_0 can proceed in a recursive fashion. Let the point (t_0, E_0) be in the admissible region, *i.e.* $D(t_0) \leq E_0 \leq A(t_0)$. Straight lines of nonnegative slopes starting from this point, denoted by $L_{(t_0, E_0)}(t)$, can be distinguished by whether they intersect with the upper boundary A or the lower boundary D first. Note that *intersection* here means, take D and the time instant $t_1 > t_0$ as an example, that $L_{(t_0, E_0)}(t_1) = D(t_1)$ if D is continuous at point t_1 , or $L_{(t_0, E_0)}(t) - D(t)$ changes sign at t_1 if D is discontinuous at that point. Let $\mathcal{S}_A(t_0, E_0)$ and $\mathcal{S}_D(t_0, E_0)$ denote the sets of slopes which lead $L_{(t_0, E_0)}$ to intersect with A and D first, respectively. To ensure that $\mathcal{S}_D(t_0, E_0)$ is non-empty, we define the discontinuity $D(T^+) = A(T)$ at the termination. Since $A(t) > D(t)$ for all $t \in [0, T)$, one can see that

$$k_A > k_D, \quad \forall k_A \in \mathcal{S}_A(t_0, E_0), k_D \in \mathcal{S}_D(t_0, E_0), \quad (4.12)$$

which further leads to

$$\inf \mathcal{S}_A(t_0, E_0) = \sup \mathcal{S}_D(t_0, E_0) \triangleq k(t_0, E_0). \quad (4.13)$$

Note that the critical slope $k(t_0, \alpha_0)$ belongs either to $\mathcal{S}_A(t_0, E_0)$ or to $\mathcal{S}_D(t_0, E_0)$. Using these notations and definitions, we describe the construction procedure of the optimal trajectory in Algorithm 5.

Algorithm 5 Construction of the optimal trajectory for Case I

Require: Boundary curves $A(t)$ and $D(t)$, $t \in [0, T]$

Ensure: Optimal trajectory W_0

- 1: $(t_1, E_1) \leftarrow (0, 0)$, $W_0(0) \leftarrow 0$
 - 2: **repeat**
 - 3: $(t_0, E_0) \leftarrow (t_1, E_1)$
 - 4: Determine the critical slope $k(t_0, E_0)$
 - 5: $W_0(t) \leftarrow L_{(t_0, E_0)}(t)$ with slope $k(t_0, E_0)$ until the intersection point (t_1, E_1)
 - 6: **until** $t_1 = T$
-

Starting with $(0, 0)$, the algorithm constructs the trajectory W_0 segment by segment from a series of feasible points. In each of the iterations, the critical slope at (t_0, E_0) , which is the current end point of W_0 , is determined and used as the direction in which the trajectory evolves. In principle, W_0 takes the straight line with slope $k(t_0, E_0)$ until it intersects with A or D . The intersection point then becomes the starting point for the next iteration. If (t_0, E_0) is on the upper boundary A and $k(t_0, E_0)$ is equal to $\dot{A}(t_0^+)$, we assume that W_0 shall intersect with A after an infinitesimal step. The same goes for (t_0, E_0) on D with $k(t_0, E_0) = \dot{D}(t_0^+)$. To this end, W_0 would follow the corresponding boundary curve until the point at which the equal tangent condition is no longer fulfilled. During the time that W_0 coincides with either of the boundary curves, the power consumption of the

node is equal to the energy arrival rate. If it happens with the upper boundary A , then the corresponding part of A is convex; if it happens with the lower boundary D , then the corresponding part of D is concave.

Theorem 3. *The trajectory W_0 constructed with Algorithm 5 does not violate the optimality criterion, and is therefore the optimal trajectory to the throughput maximization problem (4.3), i.e. $W_0 = W^*$.*

Proof. From the construction procedure, it is clear that the trajectory W_0 adjoins $(0, 0)$ and $(T, A(T))$, and lies completely within the admissible region. Therefore, W_0 is admissible. Moreover, it can be seen that the changes of slopes can only happen at points which are either on A or on D . Consider that in some iteration, the trajectory is constructed from (t_0, E_0) until (t_1, E_1) , where the end point is on D . This implies $W_0(t) < A(t)$ for $t \in (t_0, t_1]$, since otherwise the construction would stop at the intersection point with A . According to the definition of the critical slope (4.13), there exists some small number $\epsilon > 0$, such that any straight line $L_{(t_0, E_0)}(t)$ with slope in the range $(k(t_0, E_0), k(t_0, E_0) + \epsilon)$ intersects $A(t)$ at a point $t'_0 > t_1$. Consider in the next iteration, a straight line $L_{(t_1, E_1)}(t)$ with the slope $\kappa \in (k(t_0, E_0), k(t_0, E_0) + \epsilon)$ is constructed, which intersects with one of the boundary curves at (t'_1, E'_1) . The slope of the straight line connecting (t_0, E_0) and (t'_1, E'_1) is also within the range of $(k(t_0, E_0), k(t_0, E_0) + \epsilon)$, which means the intersection point (t'_1, E'_1) has to be on A . As a result, we have $k(t_1, E_1) \leq k(t_0, E_0)$, suggesting that the slope changes on the lower boundary D is negative. Similarly, it can be shown that the slope changes on the upper boundary A is positive. Therefore, we conclude that, around every point on W_0 where the slope of the trajectory changes, it is infeasible to construct an admissible line segment as described by Theorem 1. Hence, W_0 does not violate the optimality criterion. Based on Theorem 2, W_0 is the unique optimal trajectory of (4.3), for which we have previously given the notation W^* . \square

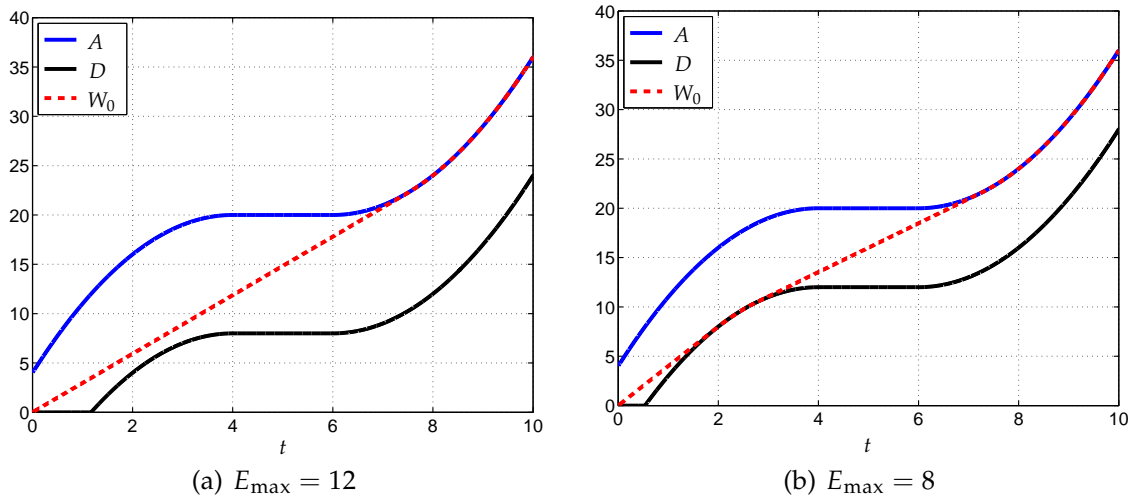


Fig. 4.3: Construction of the optimal trajectory: a continuous energy input example

We design some examples to illustrate the construction of the optimal trajectory. In the example shown by Fig. 4.3, the effective cumulative energy arrival is defined by the

piecewise continuous function

$$A(t) = \begin{cases} 20 - (t - 4)^2, & t \in [0, 4), \\ 20, & t \in [4, 6), \\ 20 + (t - 6)^2, & t \in [6, 10]. \end{cases} \quad (4.14)$$

With $E_{\max} = 12$, as depicted in Fig. 4.3(a), the critical slope at the origin is determined by the tangent line to A , as this line does not intersect with D before the tangent point at $t_1 \approx 7.48$. The optimal trajectory follows the straight tangent line until t_1 and then coincides with A , since A is convex in its last piece. When the storage capacity is reduced to 8, as shown in Fig. 4.3(b), the admissible region in the shape of a tunnel becomes narrower and is therefore more restrictive. The optimal control changes as the critical slope at the origin belongs now to \mathcal{S}_D , meaning that W_0 should take the tangent line to D until the tangent point $t_1 \approx 2.76$. After that, W_0 coincides with D for a short time before the derivative of D becomes smaller than the slope of the tangent line to A , at which point W_0 takes the straight tangent line again. The tangent point is at $t_2 \approx 7.24$, after which W_0 coincides with A . Taking the rate function $R = \log_2(1 + p_{\text{tx}})$ and the power function $P = p_{\text{tx}}$, we achieve a throughput of 14.95 for the first case, and 14.84 for the second. As can be expected, when the energy arrival rate changes frequently which leads to a less regular cumulative energy arrival curve, finding the critical slope in each iteration can be rather complicated.

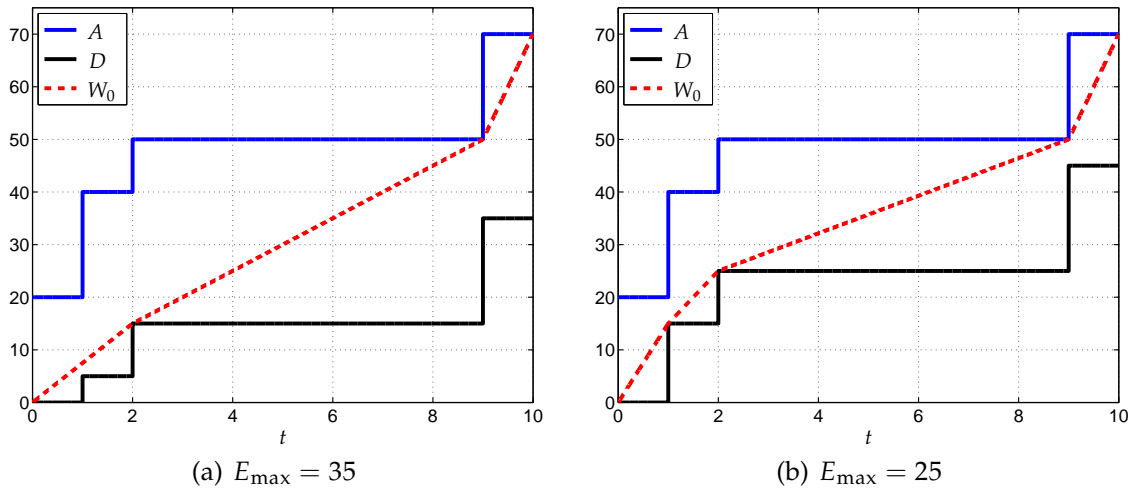


Fig. 4.4: Construction of the optimal trajectory: a discrete energy input example

When the energy arrives in the form of packets, the cumulative energy arrival curve is a staircase function. Constructing the optimal trajectory in this case is more straightforward, since the change of the slope can only happen at the discrete time instants that new packets arrive, rendering the computation of the critical slope much simpler. The optimal trajectories, with two examples shown in Fig. 4.4, are piecewise linear. We again observe the difference in the optimal controls caused by the variation in E_{\max} . The throughput achieved with $E_{\max} = 35$ is larger than that with $E_{\max} = 25$, as can be expected.

4.2.2.2 Case II

The power consumption P in this case has an isolated point at $p_{\text{tx}} = 0$, due to the constant circuit power c_0 that is only incurred during the active mode. For $p_{\text{tx}} > 0$ the function is assumed convex. Recall that the optimal trajectory for the basic problem, depending on the relation of the energy efficient transmit power $p_{\text{tx},0}$ and $P^{-1}(A_0/T)$, is either a straight line segment, or consists of a horizontal part and a straight line of slope $p_0 = P(p_{\text{tx},0})$. Based on this result, we propose a construction algorithm for the optimal trajectory of the general problem following a similar procedure as in Case I: we first declare the optimality criterion that the optimal trajectory must fulfill, then propose an algorithm to construct a trajectory which does not violate this criterion. In the end, we prove that the constructed trajectory is indeed the optimum.

We have mentioned the concept of *equivalent* trajectories when discussing the optimal solution of the basic problem. Here we give a formal definition which is also suitable for the general problem.

Definition 1. Let W_1 and W_2 be two admissible trajectories of (4.3) which differ only on a finite number of subintervals $(t_{1,i}, t_{u,i})$, $i = 1, 2, \dots, K$, $0 \leq t_{1,1} < t_{u,1} \leq \dots \leq t_{1,K} < t_{u,K} \leq T$. If on these subintervals, W_1 and W_2 both consist only of horizontal lines and straight lines with slope p_0 , then W_1 and W_2 are called equivalent, denoted by $W_1 \sim W_2$.

One can see that equivalent trajectories following this definition yield the same throughput. We also write $W_1(t) \sim W_2(t)$ for $t \in [t_1, t_u]$, if $W_1(t_1) = W_2(t_1)$, $W_1(t_u) = W_2(t_u)$, and the two trajectories consist only of horizontal lines and straight lines with slope p_0 on $t \in [t_1, t_u]$. This defines the partial equivalence, as opposed to the complete equivalence given by Definition 1. On the equivalent subinterval $[t_1, t_u]$, W_1 and W_2 also produces the same throughput.

Theorem 4. Let W be an admissible trajectory of (4.3) and $L(t)$, $t \in [t_1, t_u]$ be a curve that adjoins $(t_1, W(t_1))$ and $(t_u, W(t_u))$ where t_1, t_u satisfy $0 \leq t_1 < t_u \leq T$. Denote the slope of the straight line that connects $(t_1, W(t_1))$ and $(t_u, W(t_u))$ with k .

- 1) If $k < p_0$ and $L(t)$ satisfies
 - $L(t)$ consists only of horizontal lines and straight lines with slope p_0 ,
 - $L(t) \not\sim W(t)$, $t \in [t_1, t_u]$,
 - $D(t) \leq L(t) \leq A(t)$, $\forall t \in [t_1, t_u]$,
- 2) If $k \geq p_0$ and $L(t)$ satisfies
 - $L(t)$ is a straight line segment,
 - $L(t) \not\sim W(t)$, $t \in [t_1, t_u]$,
 - $D(t) \leq L(t) \leq A(t)$, $\forall t \in [t_1, t_u]$,

then replacing the part of W between $[t_1, t_u]$ with L increases the throughput.

Theorem 4 suggests that reconstructing part of a given admissible trajectory with the optimal trajectory of the corresponding basic problem, if feasible, leads to an improvement in the achieved throughput. The proof is similar to that of Theorem 1 and we do not restate it here. The *optimality criterion* for an admissible trajectory of Case II follows as: *along an optimal trajectory W^* there do not exist any two points between which the part of W^* can be reconstructed as indicated by Theorem 4.*

A few properties of the optimal trajectory can be deduced.

Lemma 2. *The slope at any point on W^* is greater than or equal to p_0 except for the horizontal parts.*

Since the upper boundary A is strictly above the lower boundary D and we are considering a continuous-time model, the reconstruction around a point t for which $\dot{W}(t) < p_0$ is always possible. We illustrate the violation of the optimality criterion in Fig. 4.5 (a) when Lemma 2 is not fulfilled.

Lemma 3. Any horizontal part of W^* is arrived at and/or followed by a straight line segment of slope p_0 . More specifically, let $W^*(t)$, $t \in [t_1, t_2]$ be a horizontal line. If $(t_1, W^*(t_1))$ is not on D , then W^* must arrive at $(t_1, W^*(t_1))$ with a straight line segment of slope p_0 ; if $(t_2, W^*(t_2))$ is not on A , then W^* must be followed by a straight line segment of slope p_0 after $(t_2, W^*(t_2))$; otherwise, the horizontal line is connected at both ends with straight lines of slope p_0 .

Horizontal lines appear in the optimal trajectory because of the time-sharing between the sleep mode and using the energy efficient transmit power $p_{tx,0}$, and are therefore connected with straight lines of slope p_0 . The only two possible scenarios that a horizontal line is not connected to a straight line of slope p_0 are: the starting point of the line is on D , and, the end point of the line is on A . Any other case is suboptimal as we can reconstruct the connecting part by using straight lines of slope p_0 , as shown in Fig. 4.5 (b) and Fig. 4.5 (c).

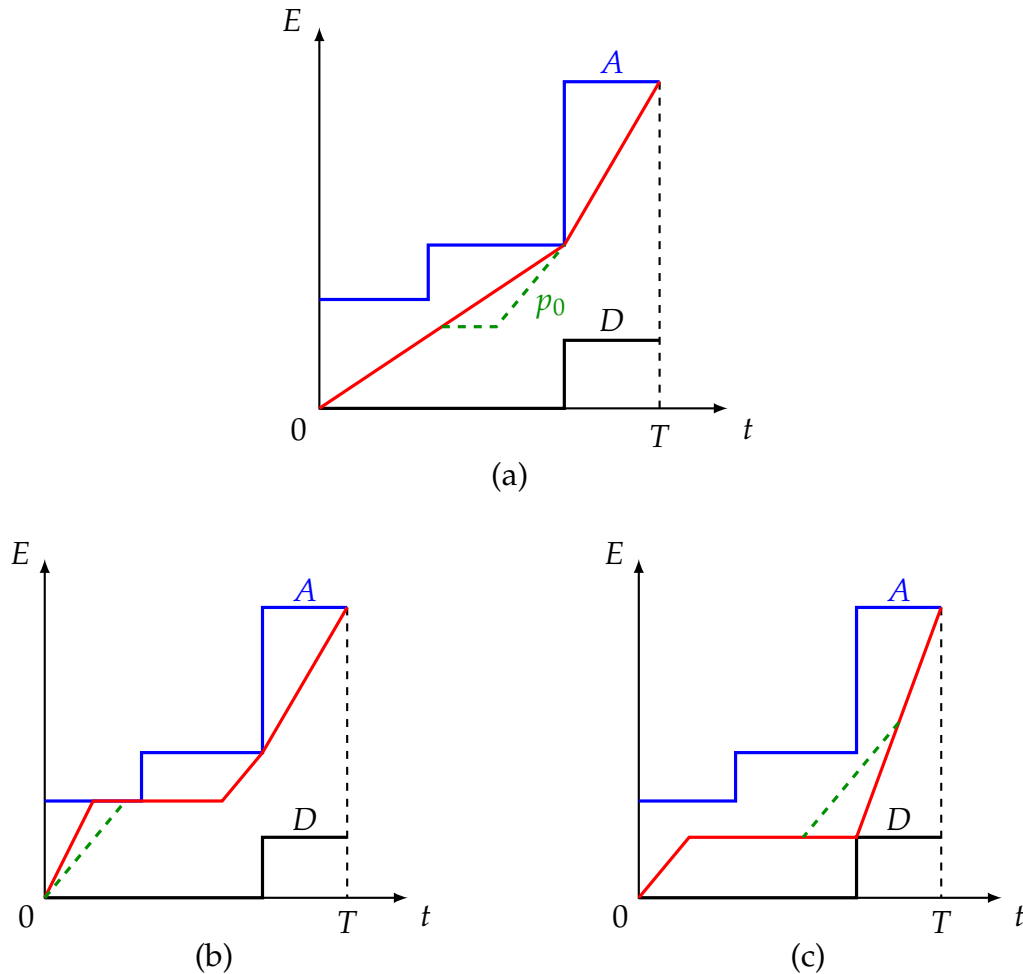


Fig. 4.5: Violations of the optimality criterion for Case II

Besides these two properties, the optimal trajectory should also satisfy Lemma 1 for the part where its derivative is larger than p_0 .

Now we suppose an admissible trajectory W^* has been found optimal and it contains at least one horizontal part. Then there exist infinitely many admissible trajectories that are equivalent to W^* , and they all lead to the same maximal throughput. The theorem below guarantees the uniqueness of the optimal admissible trajectory in the sense of equivalence.

Theorem 5. *The admissible trajectories that satisfy the optimality criterion are either equivalent or identical. The controls they correspond to are all optimal for (4.3).*

Proof. Suppose there exist two distinct admissible trajectories W_a and W_b which do not violate the optimality criterion. As before, we let (t_l, t_u) be a subinterval over which $W_a \neq W_b$ and $W_a(t_l) = W_b(t_l)$, $W_a(t_u) = W_b(t_u)$, and assume without loss of generality, that $D(t) \leq W_b(t) < W_a(t) \leq A(t)$, $t \in (t_l, t_u)$.

If both trajectories do not contain horizontal lines on (t_l, t_u) , then according to the proof of Theorem 2, they can not intersect at $(t_u, W_a(t_u))$. Due to the same reason, W_a must arrive at $(t_u, W_a(t_u))$ with a horizontal line. Let $t_0 \in (t_l, t_u)$ be the starting point of this horizontal line. Since $W_a(t_0) > D(t_0)$, the point $(t_0, W_a(t_0))$ is reached with a straight line of slope p_0 according to Lemma 3. As the slope of W_a does not decrease except for the horizontal lines, it can be inferred that W_a consists only of straight lines with slope p_0 and horizontal lines on $t \in [t_l, t_u]$. Moreover, the first segment of W_a after t_l must be a straight line of slope p_0 , as $W_a > W_b$. The condition $\dot{W}_a(t_l) > \dot{W}_b(t_l)$ and Lemma 2 then require that W_b follows a horizontal line after t_l . Based on Lemma 3, W_b also consists only of straight lines with slope p_0 and horizontal lines, which is to say, $W_a(t) \sim W_b(t)$, $t \in [t_l, t_u]$. The argument holds for all subintervals on which the two trajectories differ, which is to say, if W_a is not identical to W_b , then it must be equivalent with W_b .

Let W_0 be an admissible trajectory which does not violate the optimality criterion. We have learned from the proof of Theorem 2, that the strict concavity of the achievable rate as a function of the power consumption plays the key role in showing the global optimality of such a trajectory for Case I. For Case II, the R - P curve is made concave by the time sharing between the sleep mode and using the energy efficient transmit power, as illustrated in the middle in Fig. 3.2. To this end, if we assume an admissible trajectory W_1 which differs from W_0 on (t_l, t_u) but shares the same boundary points, then the same throughput is achieved on this interval if both trajectories consist only of horizontal lines and straight lines of slope p_0 . Otherwise, W_0 yields larger throughput which is shown using the same steps (4.8)-(4.11). Note that the strict inequalities in (4.10) and (4.11) still hold since $P_0 \geq p_0$, $\forall t \in [t_l, t_u]$. Consequently, the equivalent trajectories that fulfill the optimality criterion correspond all to the global optimal controls of (4.3). \square

We can construct one of the optimal trajectories using Algorithm 6. Note that Step 2 is always possible since $A > D$ and a continuous-time model is considered. It should be taken care of, when implementing Step 2, that the number of mode switches is well controlled. To this end, multiple subintervals with $\dot{W}_0 < p_0$ can be treated together to reduce the number of mode switches.

Theorem 6. *The trajectory W_0 constructed with Algorithm 6 does not violate the optimality criterion, and is therefore one of the optimal admissible trajectories of (4.3).*

Algorithm 6 Construction of the optimal trajectory for Case II**Require:** Boundary curves A and D , energy efficient power consumption p_0 **Ensure:** Optimal trajectory W_0

- 1: $W_0 \leftarrow$ construction result of Algorithm 5
- 2: On each subinterval where $\dot{W}_0 < p_0$, replace the part of W_0 with horizontal lines and straight lines of the slope p_0 while keeping the admissibility of the trajectory

Proof. Theorem 3 guarantees that the trajectory W_0 , as after Step 1, is admissible and can not be reconstructed with the second option described in Theorem 4. Step 2 is in itself the construction procedure indicated by the first option in Theorem 4. It is also clear, that after Step 2 there is no more subinterval that can be reconstructed. Therefore, the trajectory W_0 resulting from Algorithm 6 fulfills the optimality criterion, which qualifies it as one of the optimal trajectories of (4.3). \square

We illustrate the constructed trajectories and the maximal throughput in Fig. 4.6 where a discrete energy arrival profile is assumed. The affine power consumption model (3.27) is employed, and we vary the parameters c_0 and c_1 to observe the difference in the optimal trajectories. With no circuit power taken into account, the trajectory W_0 consists of 4 straight line segments with different slopes, as shown in Fig. 4.6(a). As the circuit power increases, the energy efficient transmit power becomes larger. The segment with the smallest slope needs to be replaced with a horizontal line and a straight line of slope p_0 , which is the case depicted in Fig. 4.6(b). As p_0 further increases, more segments are reconstructed as shown in Fig. 4.6(c), suggesting that the node stays for longer time in sleep mode. The maximal throughput achieved as dependent on the circuit power parameters is shown in Fig. 4.6(d).

4.2.2.3 Case III

Diverging from the information theoretic model, we assume for this case that the transmitter is restricted to a discrete set of modulation schemes. The key step in finding the optimal control of the basic problem, as discussed in Section 3.3.3, is to determine the energy efficient modulation schemes which contribute to the Pareto-boundary of the available power-rate pairs. The required average power consumption is then achieved by the time-sharing between the so-called bounding operation modes. Applying this result to the general problem and considering the similarity with Case II, we propose the following construction algorithm for the optimal trajectory.

It can be proven, with a similar procedure for Case II, that the state trajectory constructed using Algorithm 7 is the global optimal trajectory. We do not repeat the validation here and directly show some simulation results. The system parameters have been summarized in Table 3.2. For each simulation, we generate randomly a discrete energy arrival profile and compute the throughput achieved with the constructed optimal trajectory. The arrival of the energy packets is assumed a Poisson process, *i.e.* the interarrival time follows the exponential distribution and is independent of each other. The length of the packets, denoted with E_0 , is assumed fixed or uniformly distributed. In either case, we take care that $E_0 \leq E_{\max}$. Notice that the generated energy arrival profiles

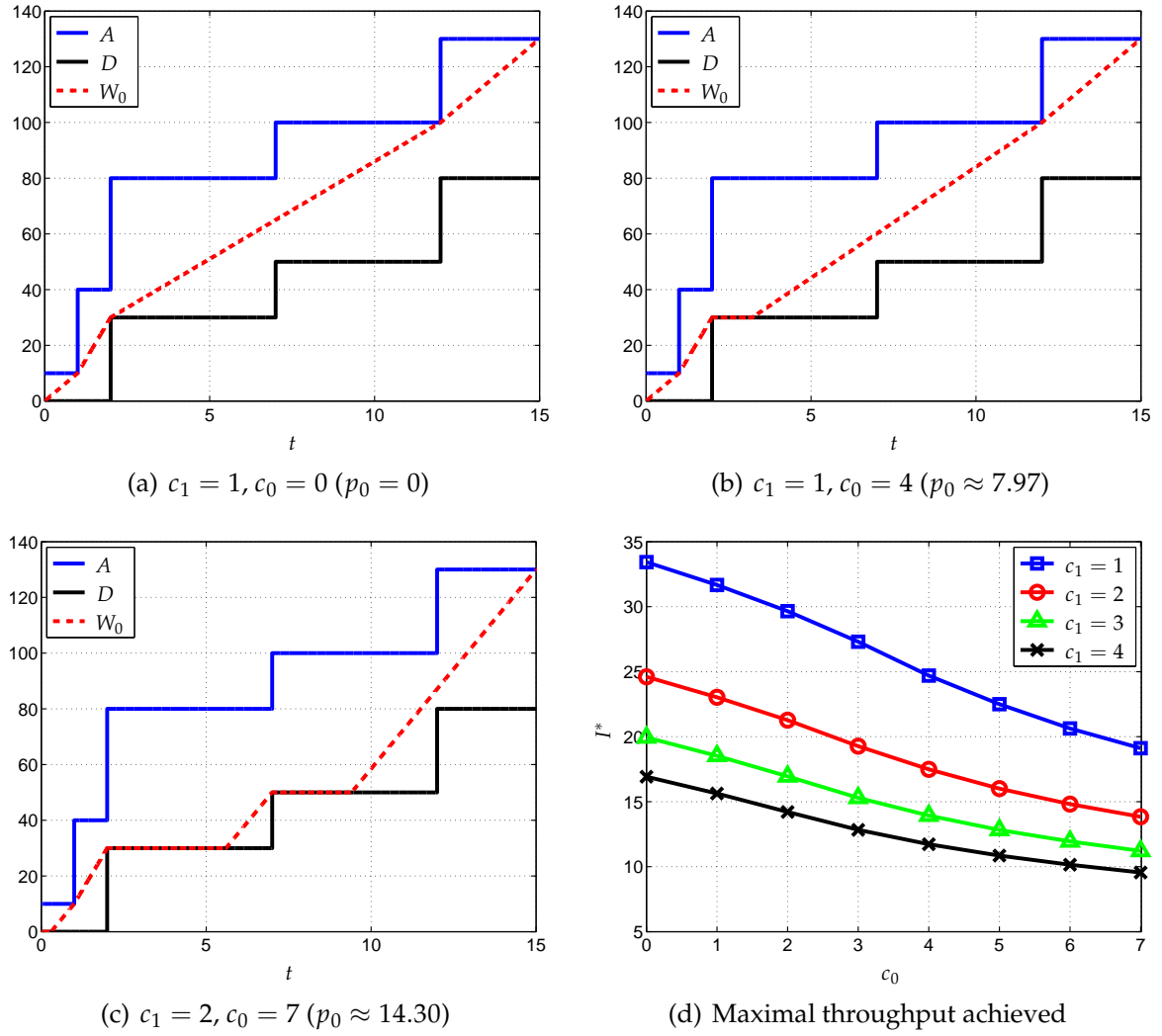


Fig. 4.6: Optimal state trajectories and the maximal throughput with a given discrete energy profile, functions R and P are given by (3.27) with $B = 1, \sigma = 1$

Algorithm 7 Construction of the optimal trajectory for Case III

Require: Boundary curves A and D , power-rate pairs of energy efficient operation modes $\{(P_0, R_0), \dots, (P_K, R_K)\}$

Ensure: Optimal trajectory W_0

- 1: $W_0 \leftarrow$ construction result of Algorithm 5
 - 2: **for** $i = 1, \dots, K$ **do**
 - 3: On each subinterval where $P_{i-1} \leq \dot{W}_0 < P_i$, replace the part of W_0 with straight lines of the slopes P_{i-1} and P_i while keeping the admissibility of the trajectory
 - 4: **end for**
-

correspond to the cumulative harvested energy functions \tilde{A} . The effective cumulative energy arrival functions A are obtained taking into account the storage capacity E_{\max} and the maximal power consumption of node. Since we assume a fixed set of modulation formats and a common BER requirement, the maximal power consumption increases with

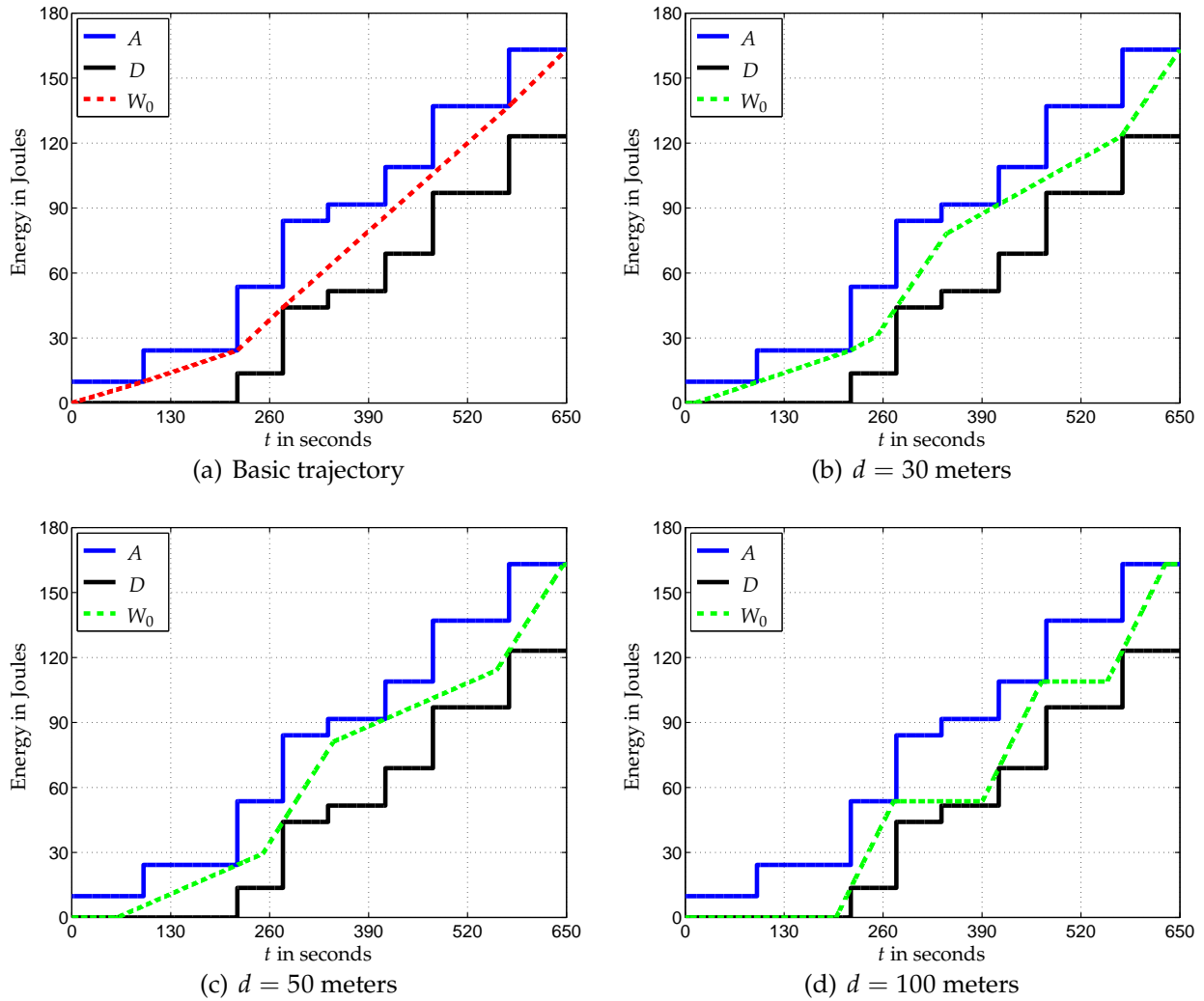


Fig. 4.7: Optimal state trajectories for MQAM transmission with a randomly generated energy profile, $E_{\max} = 40$ Joule, $E_0 \sim \mathcal{U}(0, 0.8E_{\max})$

the transmission distance, meaning that the energy miss events are more likely to happen for short-range communications.

We first show the construction results for one randomly generated energy profile in Fig. 4.7. The trajectory produced by Algorithm 5, termed as the basic trajectory, is depicted in Fig. 4.7(a). The optimal trajectories for different transmission distances are obtained by appropriately applying the time-sharing solutions of the corresponding energy efficient operation modes to the basic trajectory. In the remaining three figures, we see that depending on the involved operation modes, the limiting points on the boundary curves appear at different positions. When implementing the replacement step of Algorithm 7, it should be taken care that switching between different modulation formats occurs as seldom as possible. Note that the outcome trajectory can be further smoothed by considering multiple subintervals that share a common operation mode jointly. The maximal achievable throughput for the transmission distances ranging from 10 to 100 meters is shown in Fig. 4.8.

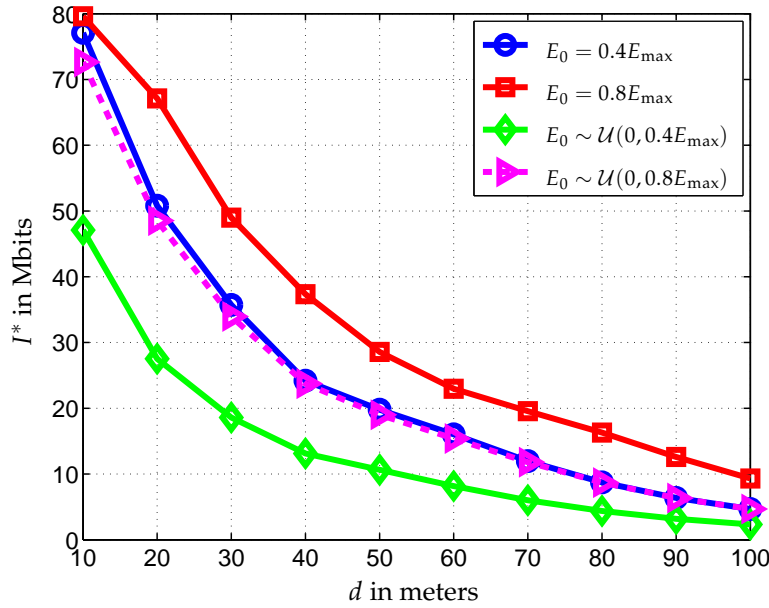


Fig. 4.8: Averaged maximal throughput for MQAM transmission with random energy profiles, $E_{\max} = 40$ Joule, number of symbols = 10^7 , mean interarrival time = 100 seconds, number of repetitions = 10^3

4.2.2.4 Case IV

With a time-varying channel, the optimal control is no longer constant. Yet the optimal transmit power plus the inverse of the channel gain should stay time-invariant, according to (3.46) and (3.54). Therefore, naming the constant μ the *marginal gain*, we translate the constant slope condition for Case I and Case II to the *constant marginal gain* condition. For example, when the optimal control of the basic problem is given by (3.46), the optimality criterion for the state trajectory of the general problem can be stated as: *there do not exist any two points on the optimal trajectory W^* that can be adjoined by a distinct curve with a constant marginal gain*. Although lack of geometric intuition, the optimal trajectory can be obtained by exploiting the analogy with the previous cases and basing the construction algorithm on the *critical marginal gains*, as summarized in Algorithm 8. Note that what is presented is a generic and theoretical algorithm which suits any channel gain function. The determination of the critical marginal gain requires a searching process and may be rather difficult depending on the shape of the boundary curves.

We focus in the following on block-fading channels and discuss the cases that the transmitter has non-causal CSI, instantaneous CSI, or only statistical CSI. The arrival of energy is assumed discrete, and the affine power consumption model (3.27) is employed. In this scenario, the optimal transmit power is piecewise constant as it might only change when the channel varies or when an energy packet arrives, except for the switches between active and sleep modes. As a result, we decide for the transmit power to be employed on a per *stage* basis, where a stage is a subinterval of $[0, T]$ over which there is no energy arrival and the channel gain stays constant. The starting point of each stage, at which the operation during the stage is determined, is called the *decision epoch*. Approaches different from before are to be exploited when we view the system as

Algorithm 8 Construction of the optimal trajectory for Case IV

Require: Boundary curves A and D , channel gain function g , $P = c_1 p_{\text{tx}} + c_0$ with $c_1 \geq 1$, $c_0 > 0$

Ensure: Optimal trajectory W_0

1: $(t_1, E_1) \leftarrow (0, 0)$, $W_0(0) \leftarrow 0$

2: **repeat**

3: $(t_0, E_0) \leftarrow (t_1, E_1)$

4: Determine the critical marginal gain $\mu(t_0, E_0)$

5: $W_0(t) \leftarrow$ the curve with the constant marginal gain $\mu(t_0, E_0)$ until the intersection point (t_1, E_1)

6: **until** $t_1 = T$

evolving through the stages based on the decisions we have made and the changes of external parameters.

When the transmitter has non-causal knowledge about the channel states, the optimal transmit power can be computed offline. One straightforward way to do this is to reformulate the infinite-dimensional optimization (4.3) into a finite-dimensional resource allocation problem. To this end, let us assume that the time interval $[0, T]$ consists of S stages, the divisions of which are due to channel changes and the arrival of energy packets. The energy allocated to each stage, denoted with w_s , $s = 1, \dots, S$, are taken as optimization variables. We let $I(w, g, \tau)$ denote the throughput achieved on a stage of length τ and channel gain g , when the energy w is allocated. This function is evaluated according to the solution of the basic problem discussed in Section 3.3.2, and has been proven concave in w for fixed g and τ . At each arrival instant, the total energy allocated to the previous stages should be bounded within the admissible range. Consequently, the throughput maximization problem (4.3) is reformulated as the constrained optimization on the energy allocation parameters as

$$\begin{aligned}
 & \max_{\{w_1, \dots, w_S\}} \sum_{s=1}^S I(w_s, g_s, \tau_s) \\
 & \text{s.t.} \quad \sum_{s=1}^{L_i-1} D(t_i^+) \leq w_s \leq A(t_i^-), \quad i = 1, \dots, L, \\
 & \quad \quad \sum_{s=1}^S w_s = A(T), \quad w_s \geq 0, \quad s = 1, \dots, S,
 \end{aligned} \tag{4.15}$$

where t_i and L_i stand for the arrival instant and the corresponding stage index of energy packet i , respectively, and L is the total number of energy arrivals on $[0, T]$. Since problem (4.15) is convex, any standard solver of convex optimization can be applied for obtaining the optimal energy allocation, from which the optimal transmit power can be computed.

When the transmitter does not have any knowledge about the channel realization, we can employ the *value-iteration* (VI) algorithm [107] to attain the optimal operation *policy*, which guides the energy harvesting node to adapt its transmit power optimally. As a first step to apply the algorithm, we need to specify some essential elements *e.g.* the *state* of the system and the *action* that can be taken, with the corresponding physical

quantities. Since the transmitting node has no instantaneous CSI, it can not determine the energy-efficient transmit power $p_{\text{tx},0}$ for each stage, and is therefore not able to employ the optimal time-sharing solution. To this end, we take the energy-efficient transmit power for the average channel gain, denoted with $\bar{p}_{\text{tx},0}$, as the lower limit of the transmit power that the node actively employs. As before, the node varies its transmit power only at the decision epochs, except for switching between active and sleep modes. The state of the system is defined as the amount of stored energy, and the action as a choice of energy allocation. Let X_s be the system state at decision epoch s . Depending on whether there is an energy arrival just before that instant, X_s can have a zero or positive lower limit, yet the upper limit $X_s \leq E_{\max}$ must be satisfied for all stages. Note that the action, *i.e.* the energy consumption w_s of stage s , is restricted to the range $[0, X_s]$.

The key procedure of the VI algorithm is the so-called *backward induction*, where the expected throughput given any system state is optimized inductively from the last decision epoch backwards. To this end, the energy space needs to be discretized so that there is a finite number of system states and also a finite number of feasible actions. The quantization step size, denoted with δ , affects both the computational complexity of the algorithm as well as the precision of the obtained optimal solution, and therefore should be chosen carefully. We assume $E_{\max} = \delta N$ where N is an integer number, rendering $N + 1$ system states in total. The underlying theory of the backward induction is the Bellman's principle of optimality which we have encountered in Section 3.3.6.

Let the function $G_s(X)$ indicate the maximal expected throughput that can be achieved on stages s until S given state X , and $\pi(s, X)$ be the corresponding optimal action to take for stage s . The task of the backward induction is to determine the policy π via computing G_S, G_{S-1}, \dots, G_1 for all system states. For the last stage, the *throughput to expect* function G_S and the corresponding optimal action are given by

$$G_S(X) = \mathbb{E} [J(X, g_S, \tau_S)], \quad \pi(S, X) = X, \quad X = 0, \delta, \dots, \delta N, \quad (4.16)$$

where the expectation is on the channel gain g_s , and the function J is computed as

$$J(X, g, \tau) = \begin{cases} \frac{X}{\bar{p}_0} \cdot B \log_2 (1 + g\bar{p}_{\text{tx},0}), & \bar{p}_0\tau > X, \\ \tau \cdot B \log_2 (1 + gP^{-1}(\frac{X}{\tau})), & \text{otherwise.} \end{cases} \quad (4.17)$$

For previous stages, we have

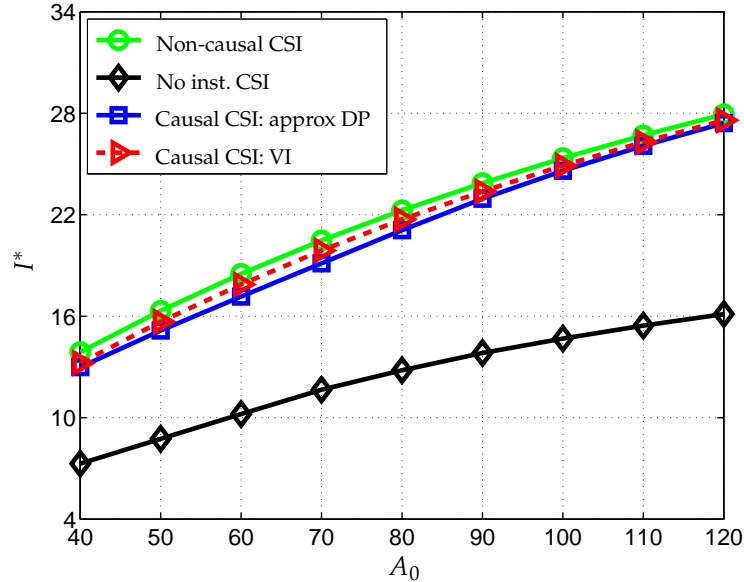
$$G_s(X) = \max_{w \in \{0, \delta, \dots, X\}} \left\{ \mathbb{E} [J(w, g_s, \tau_s)] + G_{s+1}(\delta \cdot \min(\lfloor \frac{X-w+U_s}{\delta} \rfloor + 1, N)) \right\}, \quad (4.18)$$

$$\pi(s, X) = \operatorname{argmax}_{w \in \{0, \delta, \dots, X\}} \left\{ \mathbb{E} [J(w, g_s, \tau_s)] + G_{s+1}(\delta \cdot \min(\lfloor \frac{X-w+U_s}{\delta} \rfloor + 1, N)) \right\}, \quad (4.19)$$

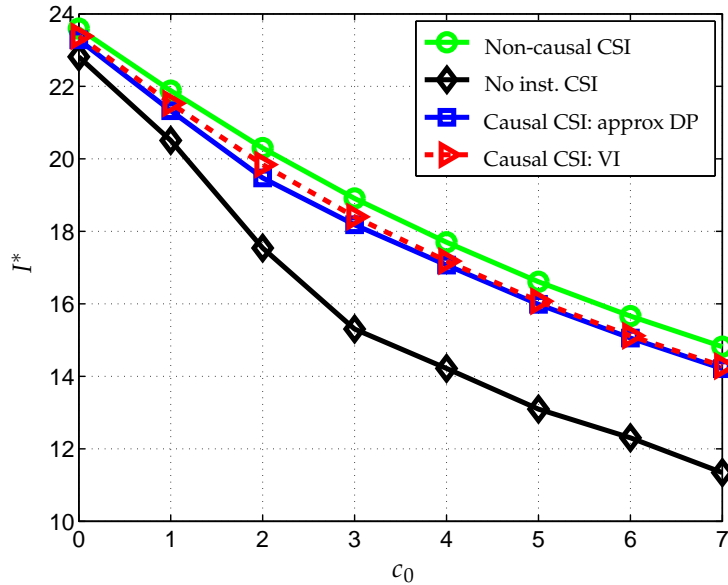
$$\text{where } U_s = \begin{cases} A(t_i^+) - A(t_i^-), & s = L_i, \\ 0, & \text{otherwise,} \end{cases} \quad s = S - 1, \dots, 1, \quad X = 0, \delta, \dots, \delta N.$$

When the actual transmission takes place, the transmitter, knowing the available energy at each decision epoch but not knowing the channel condition, simply chooses its action according to the function π . Note that the algorithm essentially breaks the multi-stage

decision-making problem down to single-stage problems as suggested by (4.18) and (4.19), but the enumeration of system states for each stage can be computationally extremely expensive.



(a) Basic problem, $c_1 = 2, c_0 = 4$



(b) General problem, $c_1 = 2, E_{\max} = 25$

Fig. 4.9: Averaged maximal throughput achieved over known, partially-known, and unknown block-fading channels, $T = 10, T_b = 1$, functions R and P are given by (3.27) with $B = 1, \sigma = 1$, number of repetitions = 10^3

In the scenario that the transmitter has statistical as well as instantaneous CSI, we can include the channel gain as another component of the system state and apply basically the same algorithm. Representative values and quantization thresholds for the channel gain are obtained from applying the Lloyd-Max quantizer to the Rayleigh distribution. The

function J in (4.16), (4.18) and (4.19) are replaced with the function I since the optimal time-sharing solution for each stage is applicable because of the instantaneous CSI.

Due to the intensive computational requirement caused by the large number of system states, we propose a dynamic programming based approximation algorithm for the causal CSI case. Instead of obtaining the optimal policy via the backward induction, we determine the sequence of actions online by sequentially solving the optimization

$$w_s^* = \operatorname{argmax}_{0 \leq w \leq X_s} \left\{ \mathbb{E} [I(w, g_s, \tau_s)] + \bar{G}_{s+1} (\delta \cdot \min(\lfloor \frac{X_s - w + U_s}{\delta} \rfloor + 1, N)) \right\}, \quad s = 1, \dots, S - 1, \quad (4.20)$$

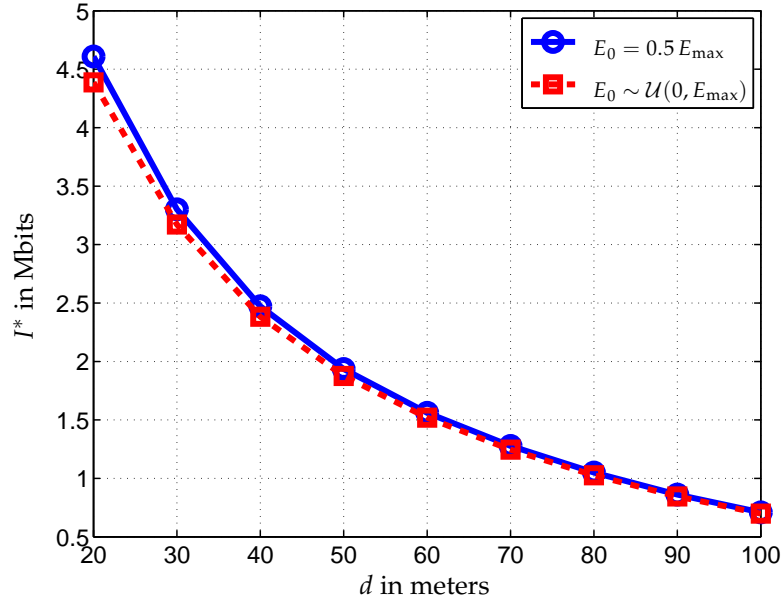
where $\bar{G}_s(X)$ represents the maximal throughput that can be achieved on stages s until S given state X and the constant average channel gain. For the last stage, we have $w_S^* = X_S$ to exhaust the available energy. The function $\bar{G}_s, s = 2, \dots, S$ can be computed offline for all system states, but not necessarily with backward induction. As the average channel gain is assumed for all stages, the evaluation of \bar{G}_s can be realized using Algorithm 6 and is much simpler than the evaluation of G_s .

The results of some numerical simulations are depicted in Fig. 4.9, where the energy arrival profile is taken from Fig. 4.4. We immediately see, that having causal CSI yields a performance that comes very close to that of having non-causal CSI. The lack of instantaneous CSI results in a performance degradation which is more severe when the circuit power is large. This can be understood as the energy efficient transmit power and subsequently the optimal time-sharing solution on a single stage can not be determined without the CSI. On the other hand, the approximation algorithm proposed for the causal CSI case exhibits almost the optimal performance as given by the VI algorithm, while the latter suffers from much higher computational complexity.

4.2.2.5 Case III + IV

For the uncoded MQAM transmission over a block-fading channel, we find in Section 3.3.5 that the energy efficient operation modes depend on the channel conditions. We also propose a heuristic algorithm to determine the modulation order on each block based on the ordering of energy efficiencies of all operation modes. Let us shortly review the algorithms before coming to the simulation results. In the case that the transmitter has perfect non-causal CSI, *i.e.* it knows all realizations of Φ on $[0, T]$ before the operation takes place, the optimal energy allocation for each stage can be found by solving (4.15), where the function I is evaluated according to the optimal single-stage solution. As the number of candidate modulation schemes is quite small, we can also formulate the problem as an optimization of the time shares of each candidate modulation scheme on all stages. Such a formulation leads to a constrained linear program, which can be solved more efficiently than the original non-linear program. Note that energy miss events are possible since we have an upper limit of transmit power given by the highest modulation order allowed. As a result, a pre-processing step is required where the inevitable energy miss events are detected and the boundary curves are adjusted accordingly.

The heuristic Algorithm 1 can be extended and further developed to solve the general problem in the non-causal CSI case as well. To cope with the time-varying energy constraints, the algorithm is repeatedly applied to make sure that the obtained state trajectory is admissible. More specifically, we start with the global domain and use



(a) Maximal throughput achieved given non-causal CSI

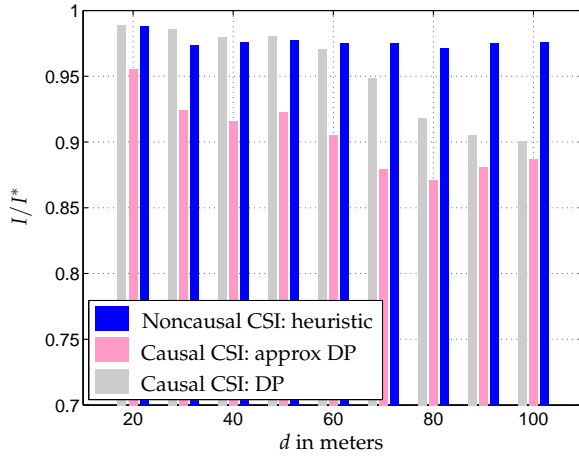
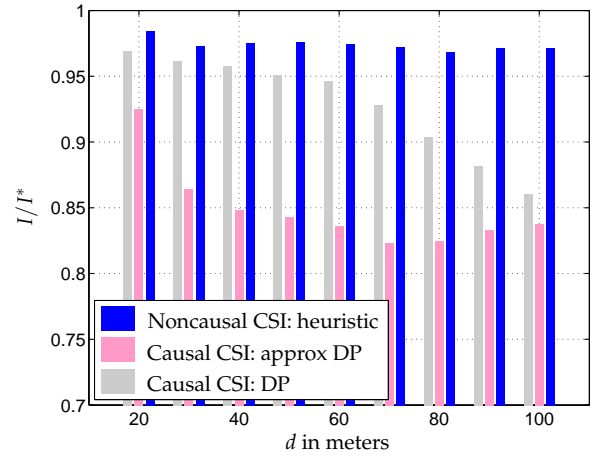
(b) $E_0 = 0.5 E_{\max}$ (c) $E_0 \sim \mathcal{U}(0, E_{\max})$

Fig. 4.10: Averaged maximal throughput with MQAM transmission over non-causally or causally-known block-fading channels, number of blocks = 20, number of symbols in each block = 4×10^4 , $\sigma_{\Phi} = 3$ dB, mean interarrival time = 20 seconds, number of repetitions = 10^3 , $E_{\max} = 8$ Joule

the basic algorithm to find a modulation adaptation scheme without considering the restrictions imposed by the boundary curves, *i.e.* as if we have a basic problem with $A_0 = A(T)$. If the corresponding state trajectory happens to be admissible, the algorithm terminates; otherwise, we formulate a subproblem from $t = 0$ to the time instant that the first constraint violation happens. This subproblem is again treated like a basic problem, and its energy budget is given by the value of the boundary curve A or D at the point that the violation takes place. In this way, we break the general problem into a sequence of subproblems which could eventually be solved with the basic heuristic algorithm.

In the case that the transmitting node has causal CSI, the channel gain is included as another element of the system state and the VI algorithm is applicable as well. The approximated DP algorithm on the other hand, optimizes the action for each stage online where the average channel gain is assumed constantly for all future stages. Based on the test results from Case IV, this approximation algorithm achieves near-optimal performance with much lower complexity, due to which reason we implement it here for the comparative study instead of the optimal VI algorithm. Since with the uncoded MQAM model we assume reliable transmission subject to a predefined BER, the no CSI case is not explored here.

For the numerical simulations, we employ the framework from Case III to generate random energy arrivals. The averaged maximal throughput achieved in the non-causal CSI case is shown in Fig. 4.10(a), where the size of the energy packets is either deterministic and equal to half of the energy storage, or is a uniformly distributed random variable on the range $[0, E_{\max}]$. The results are rather similar, with the deterministic case having a slight advantage. In Fig. 4.10(b) and Fig. 4.10(c), the throughput achieved with the heuristic algorithm in the non-causal CSI case, the DP and approximate DP algorithms in the causal CSI case are compared to the optimum shown in 4.10(a) in the form of their ratio. The heuristic algorithm we propose for the general problem clearly achieves near-optimal performance with losses less than 5%. The lack of non-causal CSI is also not largely harmful, as the approximate DP algorithm reaches more than 80% of the optimal performance for both arrival profiles and all transmission distances.

4.2.3 Receive strategies

The control of an energy harvesting receiver, as we have discussed in Section 3.4, involves the adaptation of the bit resolution of the A/D converter as a real number or an integer. The solutions to the basic problem have been derived and connected to their counterparts at the transmit side: due to the constant power consumption a_0 which is only associated with the active mode, the optimal controls in the two cases involve time-sharing of the energy efficient bit resolutions and are equivalent to Case II and III of the transmitter. Since the construction of the optimal state trajectory of the general problem is based on that of the basic problem, the corresponding algorithms we have proposed for the transmit side can be directly applied: Algorithm 6 to the former case and 7 to the latter. Additional considerations of a time-varying channel and different degrees of channel state knowledge at the receiver can be treated using the same approaches for the transmitter as well.

4.2.4 Transmit and receive Strategies

For a pair of transceivers that can be jointly controlled, we have discussed in Section 3.5 the optimal solution to the basic throughput maximization problem where the transmitter and the receiver each have a fixed energy budget to exploit. In the general case, the amount of available energy is a function of time which depends on the uncontrolled environment. Assuming non-causal information about this function, we can formulate an optimal control problem which aims at maximizing the short-term throughput with an upper boundary on the state trajectory. The problem has a similar form as (4.3), except that there would be two state equations and two sets of constraints on the state

trajectories, one for the transmitter and one for the receiver. As we have explained in Section 4.2.2, when the channel is assumed unchanged during the time interval of interest, the optimal control of an energy harvesting transmitter can be found via construction of the optimal state trajectory W^* . Based on the solution of the basic problem, W^* is either uniquely determined by the boundary curves in a geometric sense, such as described by Algorithm 5, or is further tailored to accommodate the required time-sharing modes as described by *e.g.* Algorithm 6. Unfortunately, there is no equivalent solution here for the communicating pair of energy harvesting nodes, and complex iterative algorithms would be needed to find the optimal state trajectories. If the energy arrivals are discrete *i.e.* in the form of energy packets, we can formulate the throughput maximization problem as a non-linear optimization on the allocated energy for each stage as defined by the intervals between consecutive arrivals. This optimization is convex due to the concavity of the rate function \tilde{R} (see Section 3.5) and the linear constraints on the optimization variables. Standard convex optimization tools can therefore be applied to obtain its optimal solution. Moreover, we are able to derive some necessary conditions for the optimal state trajectories, which shall be explained in the following.

We first consider the less general scenario that one of the two nodes has a time-varying energy arrival curve while the other has a fixed energy budget. Without loss of generality, let us take the transmitter as the one with a fixed energy budget. In essence, the optimal strategy for the basic problem is to use constant power; the energy consumption ratio only determines whether time-sharing with the sleep mode is necessary. To this end, a preliminary state trajectory of the receiver can be constructed using Algorithm 5, which would be optimum if no time-sharing is required. As the power consumption and respectively the ADC resolution of the receiver is determined, the control of the transmitter is equivalent to one that sends data over a time-varying channel, which has been discussed as Case IV in Section 3.3.4. Since \tilde{R} is concave in P_1 for fixed P_2 , the optimal control which minimizes the Hamiltonian as suggested by (3.6) satisfies

$$-\tilde{R}_{P_1}(P_1^*, P_2^*) + \lambda_1^* = 0, \quad \forall t \in [0, T], \quad (4.21)$$

where λ_1^* is the optimal costate of the transmitter which is a constant. This is to say, the derivative of \tilde{R} with respect to P_1 stays constant when evaluated by the optimal transmit and receive controls. As a result, the optimal state trajectory of the transmitter is not a straight line but varies its slope according to the power consumption of the receiver, which is similar to the constant marginal gain condition discussed in Section 3.3.4. We say in this case, that the change of slope in the state trajectory of the transmitter is initiated by the receiver. The energy allocation for each stage on which the receiver has a constant power consumption is determined for the transmitter by using iterative algorithms or convex optimization tools. Once this is accomplished, the energy consumption ratio between the two nodes on each stage can be computed and used to decide whether time-sharing with the sleep mode is necessary. With these steps, the throughput-maximizing transmission and reception strategies can be found.

We design and demonstrate a simple example in Fig. 4.11, where the transmitter has a fixed energy budget of 10, and the receiver is supported by two energy packets which arrive at $t = 0$ and $t = 12$, respectively. The storage capacities of the two nodes are assumed very large so that they do not play any role here. It can be seen that the

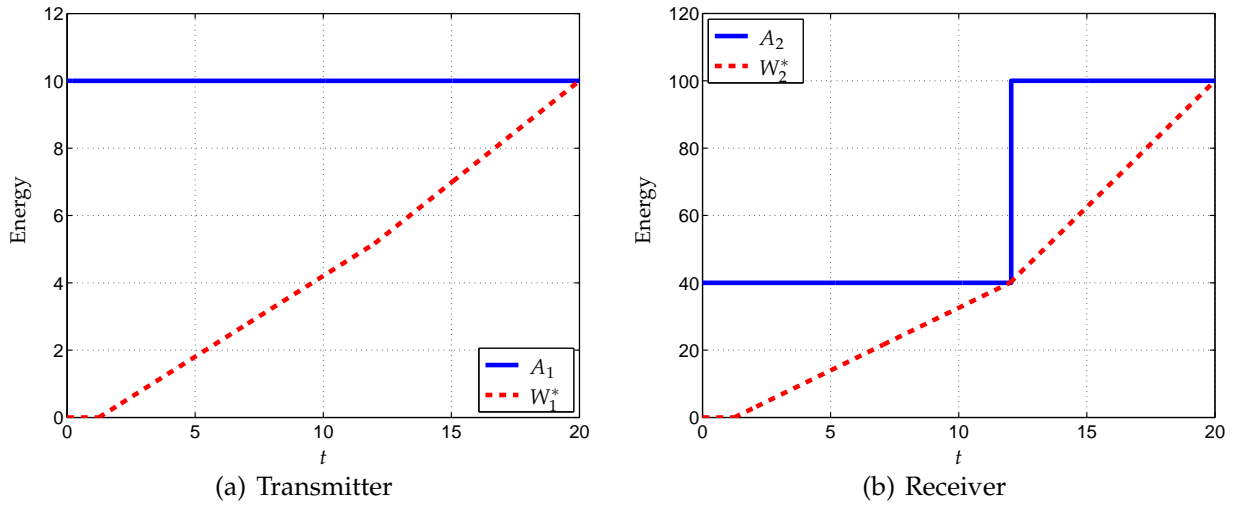


Fig. 4.11: Optimal state trajectories for a pair of energy harvesting nodes, where the transmitter has a fixed energy budget and the receiver is supported by two energy packets on the time interval $[0, 20]$, $c_0 = 0$, $c_1 = a_0 = a_1 = 1$, α , B , and σ are all normalized

point $(12, 40)$ on the time-energy graph of the receiver is a turning point for its optimal state trajectory. A preliminary trajectory which consists of two straight line segments and passes through the points $(0, 0)$, $(12, 40)$, and $(20, 100)$ can be constructed. The change of slope at the turning point is inevitable due to the imposed upper boundary in available energy. In order to fulfill (4.21), the optimal state trajectory of the transmitter also has a positive slope change at $t = 12$. The energy consumption of the transmitter before and after this point can be computed with searching algorithms or convex optimization tools. After the energy allocation is determined, we calculate the energy consumption ratios between the two nodes on the two stages, and find that time-sharing with the sleep mode is necessary for the first stage. The resulting state trajectories are shown in the figures.

For the general problem, we state the optimality criterion that a pair of optimal state trajectories W_1^* and W_2^* should satisfy as follows: there does not exist a subinterval $[t_a, t_b]$ of $[0, T]$ such that the parts of W_1^* and W_2^* on the subinterval can be replaced by the optimal state trajectories of the corresponding basic problem without violating the given energy constraints. Based on this necessary condition, we infer that the change of slope in the optimal state trajectory can happen either on the boundary or in the interior of the admissible region. In the former case, the change of slope has to be positive if the intersection point is on the upper boundary, and negative if the intersection point is on the lower boundary. The latter case on the other hand, only happens due to the change of slope in the state trajectory of the other node at the same time instant. Around these points where the slope change is initiated by the other node, the derivative of the rate function with respect to the power consumption of the node should give a constant. Notice that the change of slope we mention here does not include the change of operation mode due to the potential employment of a sleeping period with a certain time-share.

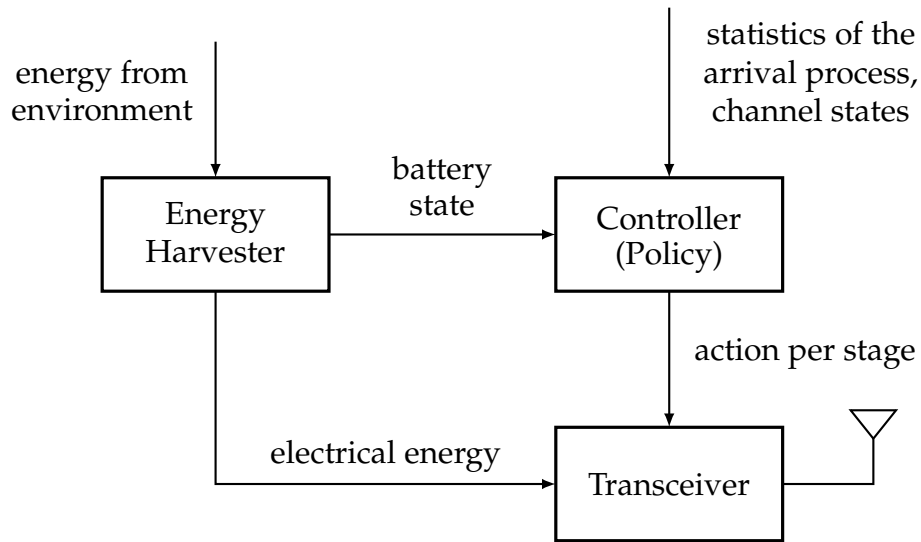
4.3 Optimal Control with Causal Energy Arrival Knowledge

It has been assumed in the last section, that the energy harvesting node has non-causal knowledge about the energy that is to be harvested on the time interval of interest. Since we do not consider the energy sources as part of the control system and presume that the harvesting of environmental energy is a random process, this assumption is idealized for the purpose of theoretical evaluation of the performance limit of the system. In this section, we investigate the case that the energy harvesting node only has causal knowledge about the energy arrivals. This scenario is of more practical relevance, although a number of assumptions would still be needed regarding the statistical properties of the arrival process to make the problem more tractable.

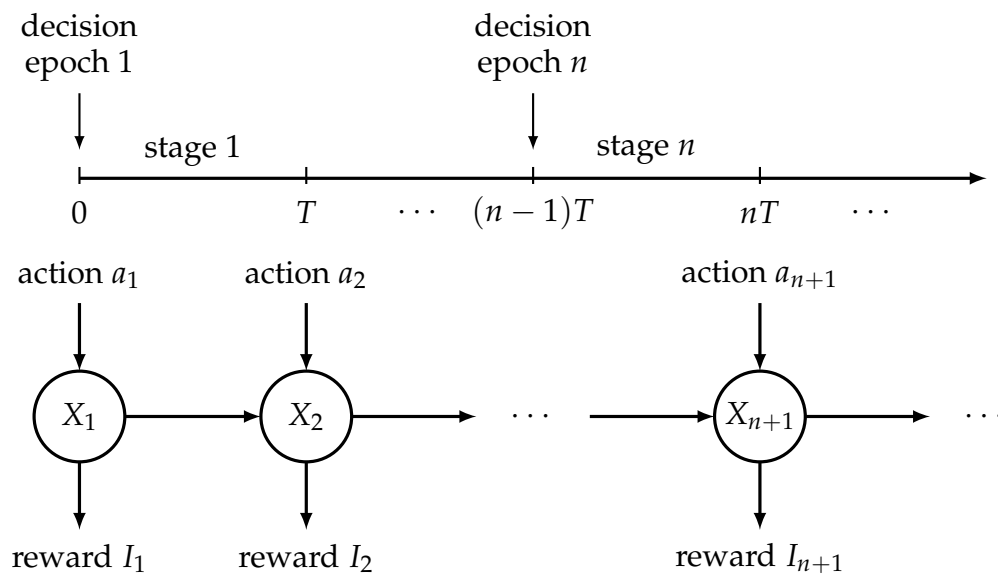
In Chapter 3, we have employed a continuous-time model and formulated the throughput maximization problem on the given time interval $[0, T]$ with a given energy budget. The Pontryagin's maximal principle has been applied to obtain the optimal control for this so-called basic problem under different circumstances. These results serve as the corner stones for the construction of the optimal state trajectory of the general problem, as discussed in the first part of last section. In the scenario of a block-fading channel and the node obtains the channel state information causally, we take a different approach and view the system as a *Markov decision process* (MDP) to deal with the randomness present in the system. To this end, the time interval of interest is divided into stages, and the system decides for an operational action at the beginning of each stage, depending on the state of the system at that moment. Instead of the maximal principle which plays a central role in the optimal control theory, the mathematical tools for this framework are those of dynamic programming, value-iteration, *etc.* In this section, we further employ this framework to model the control optimization of one or a pair of energy harvesting nodes, the block diagram and working mechanism of which are illustrated with Fig. 4.12, due to the stochastic nature of the energy arrival process. We set the optimization goal to maximizing the long-term average throughput, which falls into the category of *infinite-horizon* problems. The *policy-iteration* algorithm, which would be more suitable for this kind of problem than the value-iteration algorithm, is introduced and applied to find the optimal control strategy. Similar to the situation presented in the last section, the receiver does not need special treatment as it shares in common the optimal single-stage operation with the transmitter. For the control of a pair of energy harvesting transmitter/receiver, centralized as well as distributed solutions shall both be proposed. The modeling of an energy harvesting node as MDP, the formulation of the average throughput maximization problem, the application of the policy-iteration algorithm, and finally the simulation results for an energy harvesting transmitter are explained and demonstrated through Subsections 4.3.1 to 4.3.5, respectively. Following these, presentations on the control optimization of a transmit-receive pair can be found in Subsection 4.3.6.

4.3.1 MDP modeling and the average throughput maximization

We first focus on the transmit side scenario where the channel is assumed time-invariant. As the two essential elements of a Markov process, the *state* of the system is defined in this case as the amount of energy in the storage medium, and the *state transitions* correspond to the shift from one state to another according to certain probability distributions. In order



(a) Block diagram of the system



(b) Sequential decision process and terminology

Fig. 4.12: Control and operation of an energy harvesting node

to have a finite-state system, the state space $[0, E_{\max}]$ is discretized with quantization step δ , leading to the set of feasible states $\mathcal{S} = \{0, \delta, \dots, \delta L\}$, where $L = E_{\max}/\delta$ is assumed an integer. The state of the node changes due to the energy consumption caused by the data transmission, as well as to the arrivals of energy from the harvesting process. We consider that the system is operated on a per *stage* basis, meaning that the state transition is only tracked at the beginning of a stage, based on which an operational action for the undergoing stage is determined. Since the harvested energy is assumed to arrive at discrete time instants, it is natural to think of defining the stages by the arrival moments of the energy packets, as we have done before. However, this leads to stages of unequal lengths which can be less robust and undesirable when new aspects such as a block-fading channel, or an energy harvesting receiver are added into the picture. As a result, we design the stages to be of equal length T , where notice should be taken that the T here has a different meaning than the one used in the last chapter and the last section.

We illustrate the underlying sequential decision process of the energy harvesting node in Fig. 4.12(b). The arrival of the energy packets is assumed a stationary Poisson process with known intensity λ_0 . Let U_i and t_i denote the size of packet i and the time instant at which it arrives, respectively. Due to the Poisson process assumption, the interarrival time between two consecutive packets, $\lambda_i = t_{i+1} - t_i$, is exponentially distributed with λ_0 as its mean value. From the viewpoint of every decision epoch, the time it takes until the next energy packet arrives is identically distributed because of the memoryless property of the exponential distribution. The amounts of energy that are contained in each packet *i.e.* $U_i, n = 1, 2, \dots$, are assumed i.i.d. random variables taking positive values with a stationary probability density function. The random energy arrival process as described above is known as *compound Poisson* [108].

During each stage, there can be one or more energy arrivals, or no arrival at all. Let \mathcal{I}_n be the set of packet indices i such that $(n-1)T \leq t_i < nT, n = 1, 2, \dots$. The state of the node at decision epoch $n+1$, denoted with X_{n+1} , is evolved from the state X_n at decision epoch n according to

$$X_{n+1} = Q_E\left(X_n - W_n + \sum_{i \in \mathcal{I}_n} U_i\right), \quad (4.22)$$

where W_n stands for the energy consumption on stage n , and the function $Q_E(X)$ rounds the energy value X down to the closest element from the set \mathcal{S} . In the optimization process described below we will impose the restriction $W_n \leq X_n, \forall n$, which guarantees that (4.22) gives a valid system state. The occupation of the new state follows a probability distribution which depends on the previous state, the action taken, the length of the stage, and the property of the energy arrival process. We let $\Phi(S_{i'}|S_i, a)$ denote the transition probability from state S_i to state $S_{i'}$ given that the action a is taken. The relation $\sum_{i' \in \mathcal{S}} \Phi(S_{i'}|S_i, a) = 1$ holds due to consistency, $\forall S_i \in \mathcal{S}$.

Notice, that (4.22) is an approximation in that the update of the system state is assumed to take place at the next decision epoch instead of at the very instants that the packets arrive. As a result, the node is not able to respond immediately to the increment in the available energy. Besides, we could be optimistic about the amount of missed energy during the stage. Yet the principle here is that we do not look into the details of energy variation during a stage, since that would lead to unnecessarily tedious computations of the transition probabilities of the system states, which are not accurate anyway as the energy levels are discretized. In the mean time, we take care that a reasonable value is

chosen for T , such that the induced deviation from the true situation is well limited. Also notice that the value of δ should match the choice of T , such that a balance between granularity and complexity can be accomplished.

Based on the state X_n , an action a_n is chosen from a finite set for the stage n which can be the energy allocated to the stage, the modulation order to employ, *etc.* Some action could be infeasible for a certain state, *e.g.* when the system is in state X , allocating the energy $a > X$ to the stage would not be possible. This requires the definition of a finite set of feasible actions for each state, which we denote with $\mathcal{A}(X)$. The energy consumption W_n can be obtained, directly or through some calculations, given the action a_n and a predetermined operation strategy on a single stage. Furthermore, associated with the action is a reward of stage n in terms of throughput, denoted with I_n . We optimize the system for the maximal *average throughput per stage*, which falls into the infinite-horizon problem category of MDP. This performance metric is suited for the case that the system is to operate for a long time, or that there is no specified endpoint of operation. The optimization variable is the *policy* which provides the node with a prescription of which action to take from each state. Note that the policy we consider is Markovian as it depends only on the current state but not on any previous ones. We formulate the maximization of the average throughput per stage as

$$\begin{aligned} \max_{\pi} \quad & \rho \triangleq \lim_{N \rightarrow \infty} \frac{1}{N} \sum_{n=1}^N I_n \\ \text{s.t.} \quad & X_1 = X^0, \\ & \pi(X) = a \in \mathcal{A}(X), \quad \forall X \in \mathcal{S}, \end{aligned} \quad (4.23)$$

where X^0 is the initial state of the node, and the policy π must be feasible as the constraint indicates. We denote the optimal solution of (4.23) with π^* , and the corresponding maximal average throughput with ρ^* . The existence and uniqueness of ρ^* with respect to different X^0 shall be discussed when we explain the policy-iteration algorithm.

4.3.2 Single-stage solutions

The optimization of the policy π is based on the transmission strategy chosen for every stage. For example, we may choose to employ constant transmit power on every stage, and the policy gives the particular values of the transmit power depending on the system states. The policy and the single-stage strategy together determine the throughput and the energy consumption of each stage. It is important to note that the optimality of π^* is with respect to the underlying single-stage transmission strategy, and is not necessarily global.

How to operate on a single stage is related to the basic problem discussed in Chapter 3, as we assume that the energy arrivals during the stage affect the system state only at the next decision epoch. A single stage can therefore be considered as a time interval without any energy arrivals, for which the policy directly or indirectly gives the energy budget. Candidate transmission strategies can be proposed based on the optimal solutions of the respective basic problems, as listed below.

- For the information-theoretic model with no circuit power or a convex circuit power function (Case I in Section 3.3.1): let the policy indicate the energy consumption on

the stage, and employ constant transmit power on each single stage. One can allow for distinct energy consumptions given different system states, or only one energy consumption for all states. In the former case, which is abbreviated as *CON* in the following, we have $\mathcal{A}(X) = \{0, \delta, \dots, X\}$, whereas for the latter which is termed as *ONE*, the chosen energy consumption a serves as a decision threshold:

$$\pi(X) = \begin{cases} 0, & X < a, \\ a, & X \geq a, \end{cases} \quad \forall X \in \mathcal{S}. \quad (4.24)$$

- For the information-theoretic model with a discontinuous circuit power function (Case II in Section 3.3.2): let the policy indicate the energy consumption on the stage, and employ the optimal control *i.e.* constant transmit power or time-sharing between the sleep mode and the energy efficient transmit power on each single stage. As before, we propose the strategy *CON* which allows for different energy consumptions for different states, and the strategy *ONE* which gives one energy consumption that is used for all states.
- For the MQAM model (Case III in Section 3.3.3): the strategy *CON* now stands for the usage of a single modulation order on an entire stage, while an additional strategy *TS*, similar to the *CON* strategy for the previous two cases, employs the time-sharing between two neighboring energy efficient modulation orders to achieve an indicated energy consumption on the stage. The strategy *ONE* in this case refers to the exclusive usage of one selected modulation order whenever there is enough energy for a whole stage. Obviously, this modulation order should be selected from the energy efficient ones, which form usually a very small set.

From the description one can expect, that the policy optimization of the *CON* and *TS* strategies is more complicated than the *ONE* strategy, and should also achieve better performance due to the more degrees of freedom that are allowed. We introduce in the sequel the policy-iteration algorithm to tackle this problem and show how it can be applied, also in the case of a block-fading channel, and then demonstrate simulation results.

4.3.3 Policy-iteration algorithm

The value-iteration and policy-iteration algorithms are the two common methods for optimizing dynamic systems with sequential decision making. The policy-iteration algorithm is oriented towards problems of infinite horizon, and is therefore suited for our average throughput maximization problem. The mechanism of the algorithm is introduced in Appendix A4. With the goal of maximizing the average throughput per stage, a reasonable transmitter would try to use the available energy steadily, and yet reduce the occurrence of energy miss events. Based on the statistical properties of the energy arrival process, it can be observed that the Markov process underlying such a transmitter has only one recurrent chain. This means the optimal limit as defined in (4.23) does exist, and it is independent of the initial state of the system.

For our specific application, we start the algorithm from the value-determination operation with the *myopic* policy, meaning that for each state, the action that maximizes the immediate throughput on the following stage is chosen. For the *CON* strategy, this

would suggest $\pi(X) = X, \forall X \in \mathcal{S}$. The transition matrix P and the vector of immediate rewards q under this policy can be evaluated, and we solve the set of linear equations

$$\rho \cdot \mathbf{1} + (\mathbf{I} - P)v = q \quad (4.25)$$

to obtain ρ and the vector of relative values v . Then, during the policy-improvement routine that follows, the policy is updated according to

$$\pi(i) = \operatorname{argmax}_{a \in \mathcal{A}_i} \left(q_i(a) + \sum_{j=1}^S p_{ij}(a)v_j \right), \quad i = 1, \dots, S, \quad (4.26)$$

with which the algorithm goes for the value-determination operation again. The iterations terminate when there is no increment in the obtained average throughput or when the increment falls below a predefined threshold. In our numerical simulations, the algorithm converges already with a very small number of iterations.

4.3.4 Transmission over a block-fading channel

When the communication channel undergoes block fading, we assume causal CSI at the transmitter and include the quantized channel gain as another element of the system state. We let the channel gain on each stage be constant for convenience, which requires that the duration of a stage is no longer than that of a block. If the block length is relatively large in the sense that the probability of multiple energy arrivals during one block is non-trivial, we need to divide the block into several stages. Noticing that the position of a stage in the block is also relevant to the state transition probabilities because of the channel gain which does or does not change in the next stage, we include it as the third element of the system state. To this end, the system state becomes a triple denoted by (X, g, ι) , where g is one of the representative channel gains resulting from quantizing the probability density function of the random channel gain with the Lloyd-Max quantizer, and $\iota \in \{1, \dots, N_i\}$ stands for the position of the stage in a block with $N_i = T_b/T_s$. We assume that N_i is an integer and the number of representative values for the channel gain is N_c . The total number of system states is therefore given by $S \times N_i \times N_c$. The policy-iteration algorithm works in the same way as described above, only with an expanded state space. The single-stage strategies we consider are similar as before, namely:

- Strategy CON: a single modulation order is chosen for each system state which is to be employed for a whole stage, and the energy level indicated by the state should be able to support it;
- Strategy TS: the action determines the energy consumption and in turn the average power dissipation on the stage, which is to be realized by using the two neighboring energy efficient modulation orders in the appropriate time-sharing manner;
- Strategy ONE: a single modulation order is chosen for all system states, which is employed whenever there is enough energy for it to be used on a whole stage, otherwise the transmitter is turned into sleep mode.

In the value-determination operation, we need to solve a set of linear equations with the number of unknowns equal to the number of system states. This renders the complexity of the policy-iteration algorithm rather high when the state space is large.

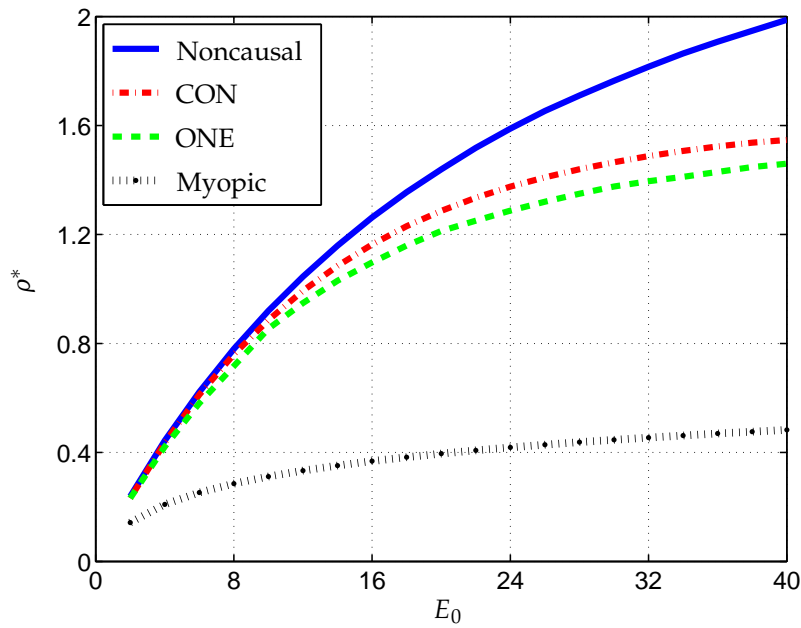
We propose as a remedy an averaged version of the algorithm, where we ignore the instantaneous CSI and employ the expected immediate throughput for the vector \mathbf{q} in (4.25) and (4.26). To this end, the state space involves only the discretized energy levels and is of dimension S . Degradation in the maximal average throughput can be expected when this simplification is made, which, according to our simulation results, is favorably insignificant.

4.3.5 Simulation results and analysis

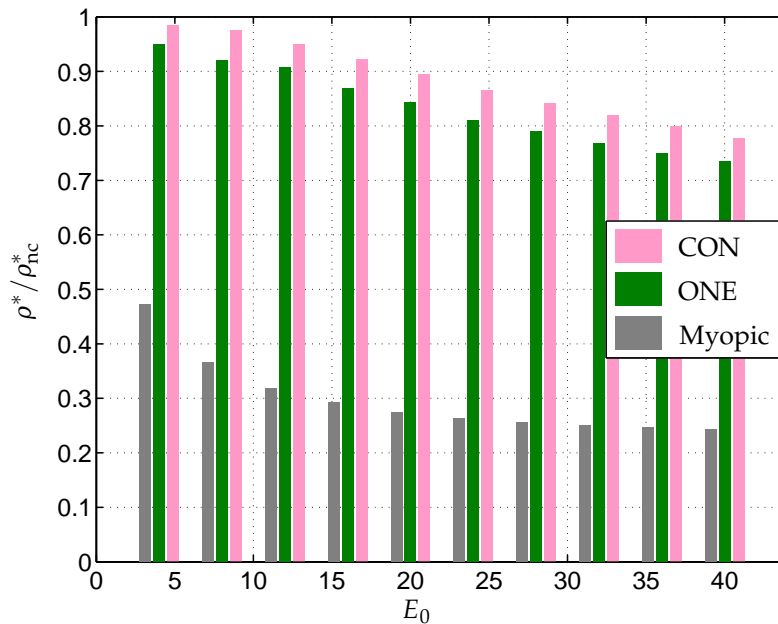
We have discussed the optimization of an energy harvesting transmitter which has causal information about the harvested energy, and present now the simulation results. As before, the energy arrival process is assumed Poisson with i. i. d. energy packet size. For all simulations we fix the mean interarrival time to 10 and the stage length to $T = 1$, which lead to dominant probabilities of no energy arrival or only one energy arrival on each stage. The optimization algorithms are tested for different scenarios and provide the optimal policies with respect to the given single-stage strategies. Monte-Carlo simulations are then performed for 2×10^4 stages to verify whether the maximal average throughput indicated by the algorithm coincides with the simulated value. As the two are indeed extremely close to each other, in the figures shown below we only depict the average throughput obtained with the simulations.

We first examine the most basic scenario with a time-invariant channel, the information-theoretic data rate model, and no circuit power consideration *i.e.* as abstracted by (3.20). The maximal average throughput obtained with the policy-iteration algorithm for strategies CON, ONE, and myopic is shown in Fig. 4.13. The result for the case of non-causal energy arrival information is also included for comparison. In Fig. 4.13(a), we plot the maximal average throughput as a function of the deterministic and equal size of the energy packets E_0 . Both CON and ONE strategies outperform the myopic strategy significantly, and the CON strategy has an advantage over the ONE strategy which becomes more obvious with intensive energy input. The performance gap between the optimized system without non-causal energy arrival information and the one with this information is illustrated in Fig. 4.13(b). The trend is clear that the more intensive the energy input is, the more important the non-causal energy arrival information becomes. When the energy packet fills the entire storage *i.e.* $E_0 = E_{\max}$, more than 20% of the throughput gap can be inspected. These observations can be understood intuitively as the management of energy plays a more important role when there is abundance in the available energy, requiring more dynamics in the control variable to avoid energy miss events. On the other hand, if the environment is relatively poor in supporting the energy harvester, which results in a low intensity of the energy arrival process with respect to the storage capacity, using an appropriately chosen low transmit power constantly is good enough in the long run. Exemplary optimal policies are illustrated in Fig. 4.14, where the monotonicities of π^* in terms of the energy consumption for the subsequent stage with respect to the system state X as well as to the packet size E_0 can be seen.

When the size of the incoming energy packets is uniformly distributed on the interval $[u_1, u_2]$, the case of which is shown in Fig. 4.15, the maximal average throughput



(a) Maximal average throughput



(b) Comparison to the non-causal arrival information case

Fig. 4.13: Maximal average throughput for input energy packets of the same size E_0 , functions R and P given by (3.20) with $B = 1$ and $\sigma = 1$, $\delta = 0.25$, $E_{\max} = 40$

decreases slightly with growing $u_2 - u_1$. The comparison between the CON, ONE, and myopic strategies is similar to that of the identical energy packet size case.

In Fig. 4.16, we demonstrate the variation in the maximal average throughput with respect to the storage capacity E_{\max} . We fix the statistics of the energy input, so that increasing E_{\max} implies more room for the harvested energy and less chance of energy miss events. For both CON and ONE strategies, the maximal average throughput grows

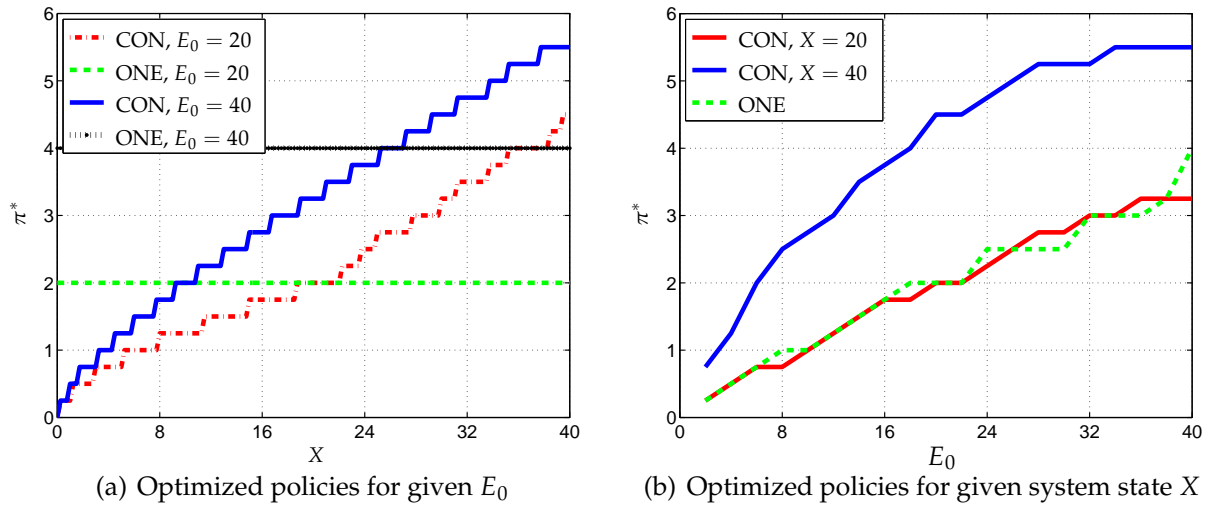


Fig. 4.14: Throughput-maximizing transmission policies for input energy packets of the same size E_0 , functions R and P given by (3.20) with $B = 1$ and $\sigma = 1$, $\delta = 0.25$, $E_{\max} = 40$

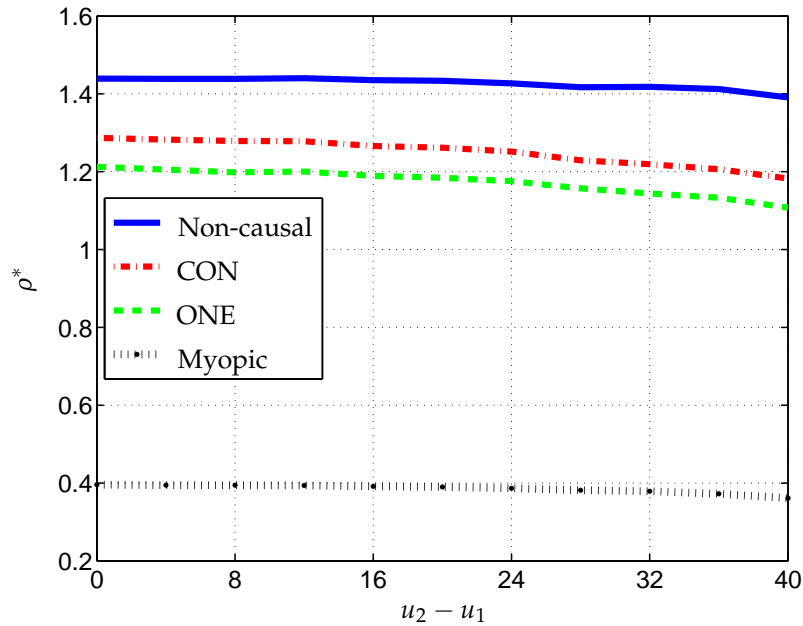


Fig. 4.15: Maximal average throughput for input energy packets of uniformly distributed sizes on $[u_1, u_2]$, functions R and P given by (3.20) with $B = 1$ and $\sigma = 1$, $\delta = 0.25$, $E_{\max} = 40$, $(u_1 + u_2)/2 = 20$

rapidly before E_{\max} reaches 8 to 10 times of E_0 . After E_{\max} amounts to 15 times of E_0 , the maximal average throughput almost saturates and further increment is very limited. The advantage of the CON strategy over the ONE strategy also becomes trivial in this regime. Besides the finite, although large, energy storage, the gap between the CON and ONE strategies to the non-causal energy arrival information case is also due to the quantization of the energy space with step size δ . Note that large storage capacities usually require more space or cost in practice. If the statistics of the harvested energy can be learned, a reasonable storage capacity can be chosen based on the curves shown in Fig. 4.16

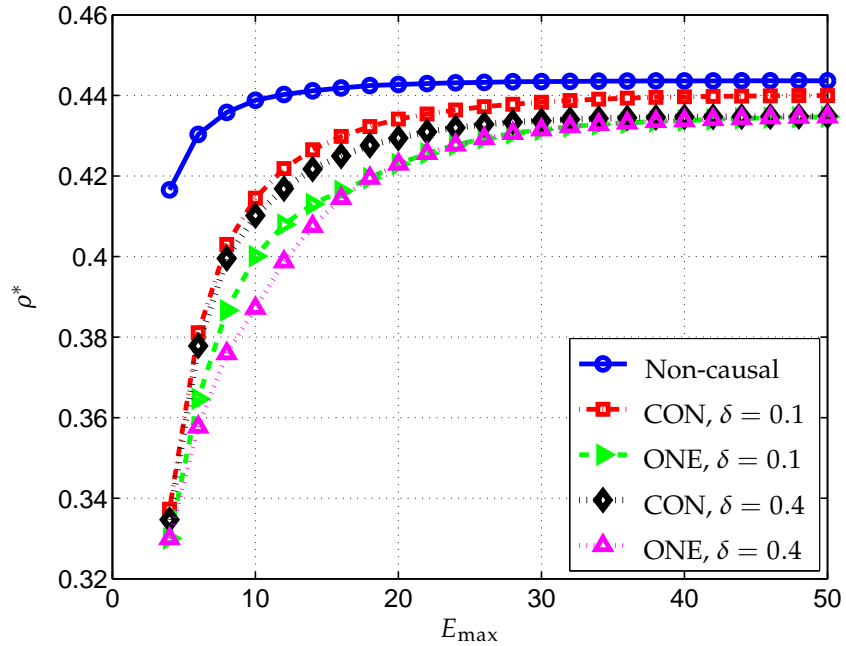
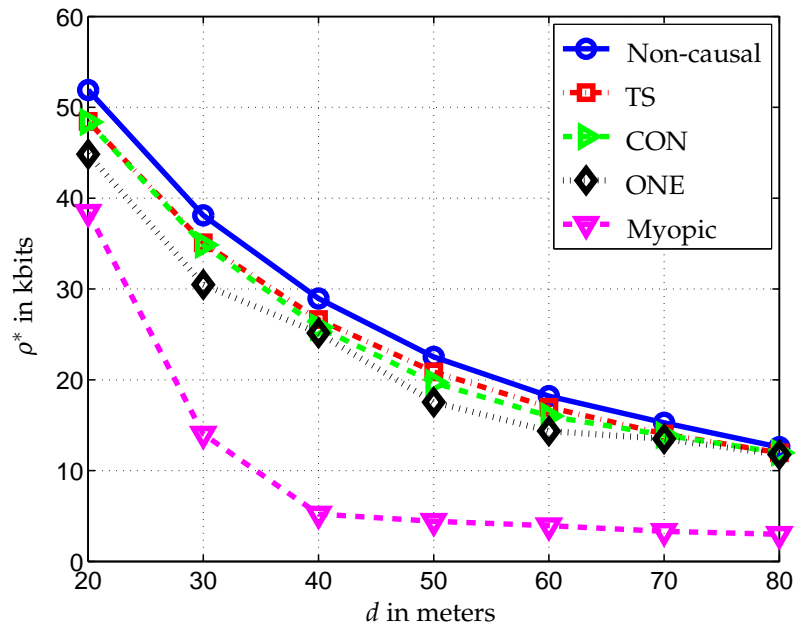


Fig. 4.16: Maximal average throughput with different energy storage capacities, functions R and P given by (3.20) with $B = 1$ and $\sigma = 1$ (information-theoretic model without circuit power consideration), input energy packets of the same size $E_0 = 2$

and other specifications of the system, which helps the system achieve a good balance between performance and cost.

Including affine circuit power into the energy consumption model does not influence the main conclusions we have drawn about the several transmission strategies and their comparison against the non-causal energy arrival information case, as indicated by simulations which are not shown here due to similarity. Moreover, similar observations can also be made when the energy harvesting node employs MQAM transmission, for which case we depict the maximal average throughput for increasing transmission distances in Fig. 4.17. The performance gap between the CON strategy and the non-causal information case is noted to be even smaller compared to previous results. The TS strategy which allows for the time-sharing between two modulation orders on a single-stage performs slightly better than the CON strategy, while the simple ONE strategy is almost as good for large d as the other two. The monotonic behaviors of the optimized policies with respect to the system state are also illustrated.

Next we investigate the MQAM transmission over block-fading channels of block length 4. The statistical information about the energy arrival process is kept unchanged as before, leading to $N_i = 4$ stages per block. Even if we choose a small number of representative values for the quantized channel gain, the total number of system states would be dozens of times as in the constant channel case. The remedy we propose for this is to exclude channel gain from the system state and use the expected throughput as the performance metric in the policy-iteration algorithm. The performance degradation of the system when such a simplification is employed is demonstrated in Fig. 4.18, for the TS and CON strategies respectively. Apparently, the gap is not remarkable over a range of intensities of the energy arrival process, especially for the TS strategy.



(a) Maximal average throughput

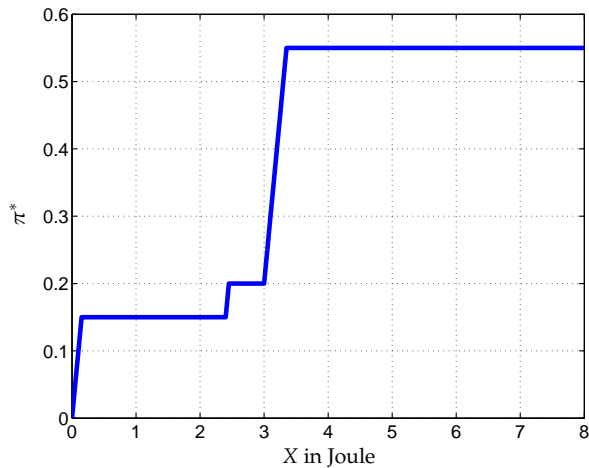
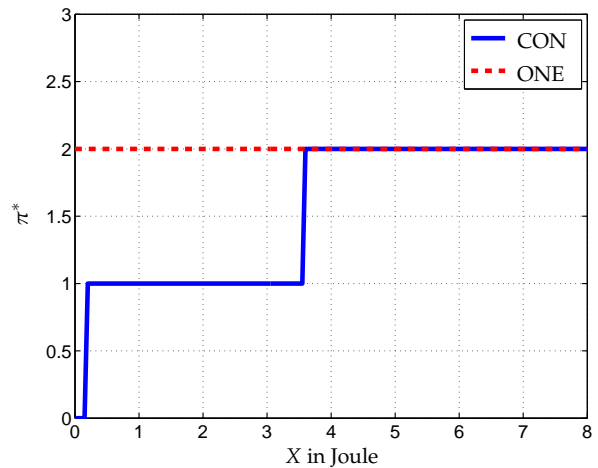
(b) Optimal policy in terms of energy allocation for the TS strategy, $d = 50$ meters(c) Optimal policies in terms of modulation indices for the CON and ONE strategies, $d = 50$ meters

Fig. 4.17: Maximal average throughput for MQAM transmission and the corresponding optimized policies, $\delta = 0.1$ Joule, $E_{\max} = 8$ Joule, input energy packets of the same size $E_0 = 4$ Joule

Finally, we illustrate the maximal average throughput over increasing transmission distances for different single-stage strategies in Fig. 4.19. The curves for the TS, CON and ONE strategies as plotted in the figures are attained using the full policy-iteration algorithm, *i.e.* without the averaging simplification. The result of the non-causal information case is obtained with the heuristic algorithm for MQAM transmission over known block-fading channels, which has been tested to yield near-optimal performance (see Case III +IV in the last section, and also Fig. 4.10). We use this result as a comparison reference since the system is simulated for a huge number of blocks, rendering the

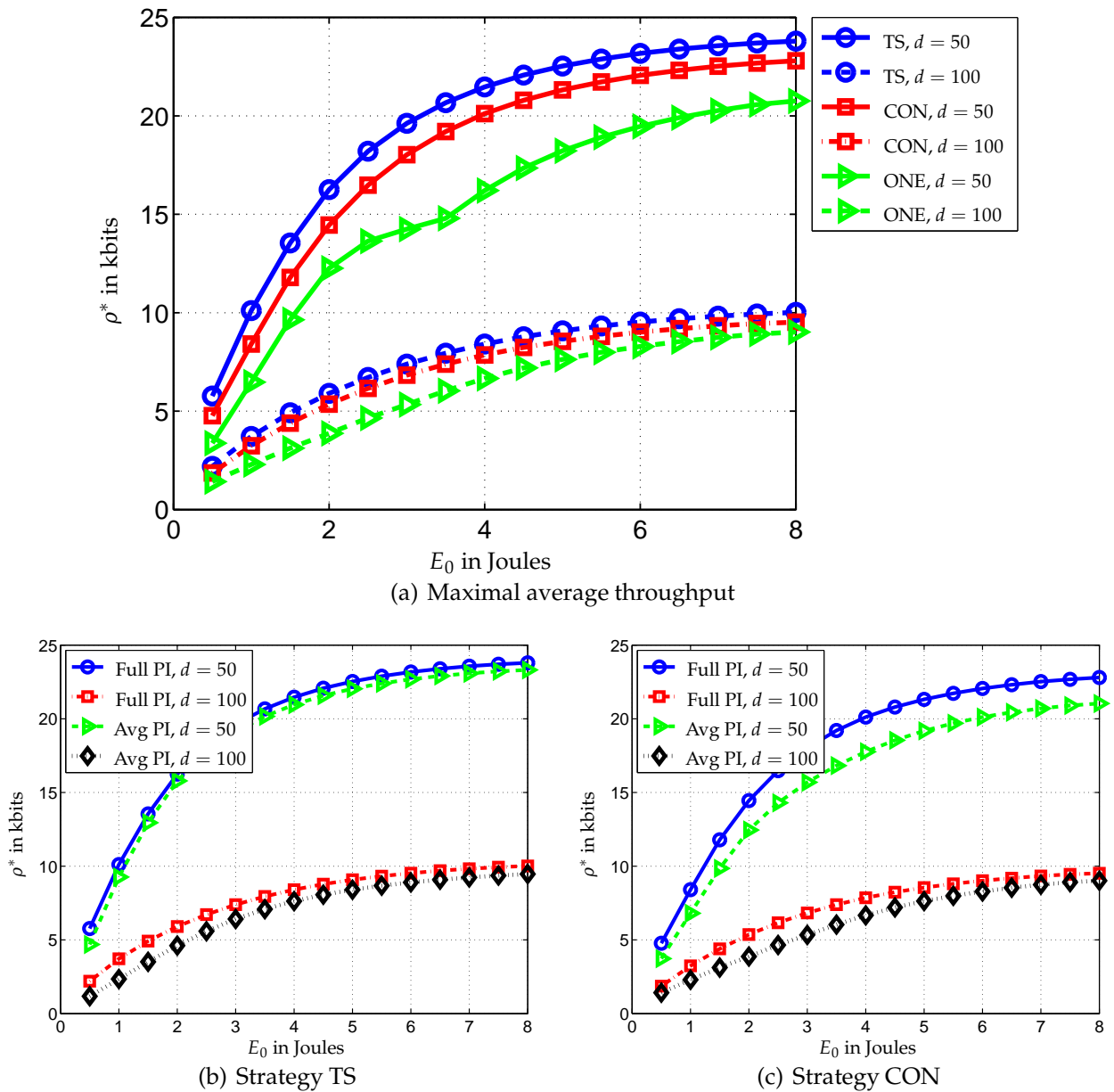


Fig. 4.18: Maximal average throughput for MQAM transmission over a block-fading channel, $\delta = 0.1$, $E_{\max} = 8$, $\sigma_{\Phi} = 3$ dB

evaluation of the optimal performance tedious and unnecessarily expensive. With less energy input, the lack of non-causal energy arrival information does not lead to considerable performance degradation. When more energy is delivered to the system, this gap becomes more obvious, but still not significant indeed. For both input parameters, the TS and CON strategies demonstrate almost the same performance. The simplest ONE strategy, although not giving a very smooth curve, also does not fall far behind.

In summary, the various simulation results presented above indicate that when the random process of energy arrivals is well structured with known statistics, the lack of non-causal energy arrival information does not cause severe performance degradation. The policy-iteration algorithm is effective in optimizing the long-term performance of

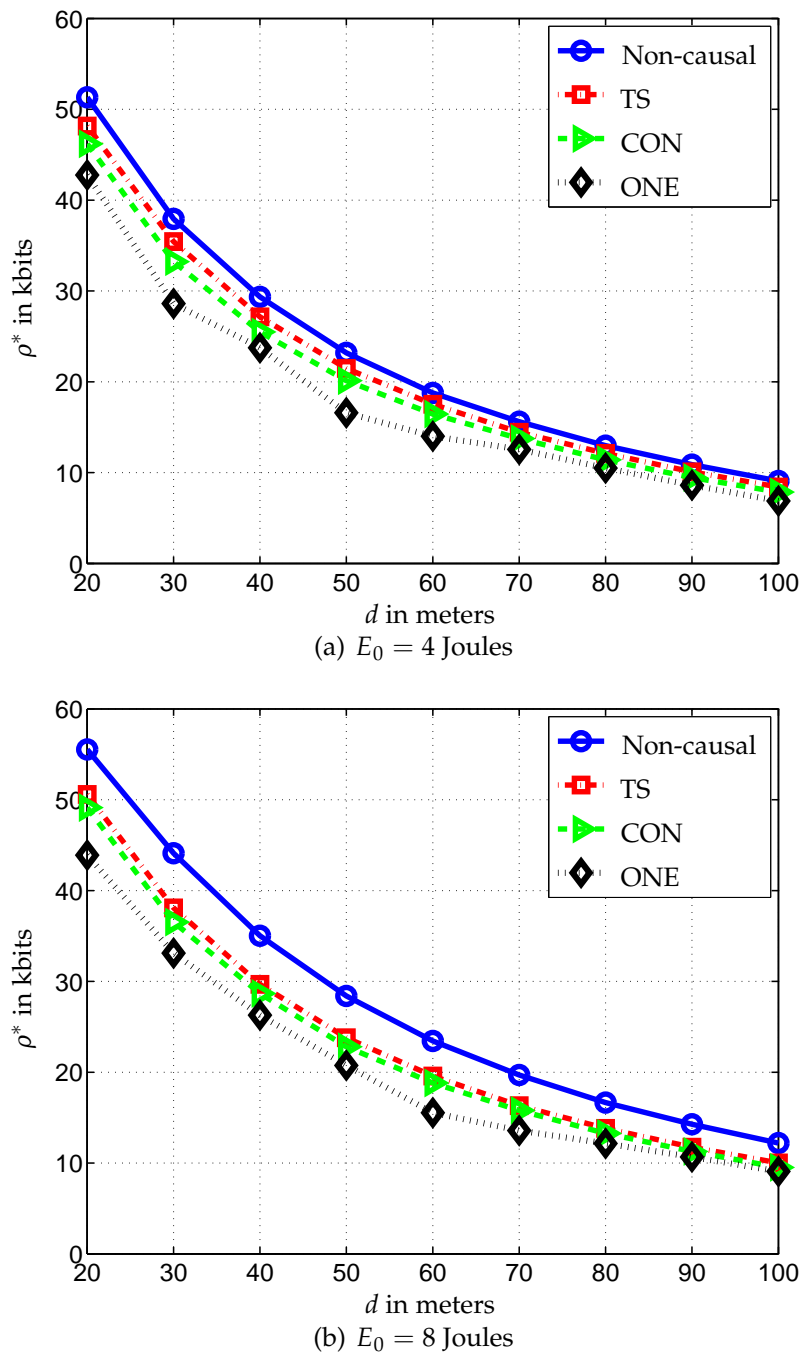


Fig. 4.19: Maximal average throughput for MQAM transmission over a block-fading channel, $\delta = 0.1$ Joule, $E_{\max} = 8$ Joule, $\sigma_{\Phi} = 3$ dB, energy packets are of the same size E_0

the system given a good single-stage strategy. On the other hand, using an optimized constant, state-independent policy in the stationary scenario we consider yields also good performance, which can be obtained with very low complexity without even provoking the policy-iteration algorithm.

4.3.6 Joint control of a pair of energy harvesting transceivers

We consider in this section the joint control of a pair of energy harvesting transceivers with only causal energy arrival information. It is assumed that the channel is time-invariant, and the two nodes learn about the energy arrivals causally and locally, but do not necessarily exchange this information. Same as for the single transceiver case, the time axis is again divided into stages, and the two nodes decide their actions at the beginning of each stage *i.e.* at the decision epochs in a centralized or distributed manner, with the goal of maximizing the long-term global average throughput.

We assume in addition, that the energy arrival processes of the two transceivers are not only compound Poisson, but also independent of each other. This may correspond to the case that the two nodes are located in different environments, or that they employ different techniques for energy harvesting. We first derive the optimal centralized control using the policy-iteration algorithm, and then investigate the distributed case that the transmitter and the receiver only have local state information and are not aware of the instantaneous situation of the other. From a design point of view, communication between the two nodes to exchange state information is possible, yet the overhead takes up resources in terms of energy and time as well. As the simulation results indicate, the decentralized optimization performs quite close to the centralized case, which undermines the necessity to exchange the local state information.

We employ the quantized MQAM framework introduced in Section 3.5.2 and model the system as one or two Markov decision processes, depending on whether the control is centralized or distributed, and aim at maximizing the average throughput in the long-term. As the channel is assumed constant, the states of the nodes are given exclusively by the amount of energy in the respective storage. The state spaces of the transmitter and the receiver, denoted with \mathcal{S}_1 and \mathcal{S}_2 , are confined to discrete sets of energy values obtained from uniformly sampling the feasible ranges $[0, E_{\max,1}]$ and $[0, E_{\max,2}]$, where $E_{\max,1}$, $E_{\max,2}$ are the respective storage capacities of the two nodes. Given a particular state, the transmitter chooses an action for the subsequent stage from a set of feasible actions. More specifically, an action refers to a certain amount of energy that is allocated to the subsequent stage, which is to be realized by a particular transmit power level and a modulation order. Suppose $i\delta_1$ is the energy value at state $S_i \in \mathcal{S}_1$, where δ_1 stands for the quantization step size, $i = 0, 1, \dots, \lceil E_{\max,1}/\delta_1 \rceil + 1$. The set of feasible actions $A_1(S_i)$ is then taken as $\{0, \delta_1, \dots, i\delta_1\}$. A similar setup can be done for the receive side. On the other hand, as the receiver can only choose its ADC resolution from the set $\mathcal{B} = \{0, 1, \dots, b_{\max}\}$, we can also let the action simply be the adaptation to a certain ADC resolution. The set of feasible actions of any state $S_j \in \mathcal{S}_2$, denoted with $A_2(S_j) = \{0, 1, \dots, \bar{b}_j\}$, is then a subset of \mathcal{B} where \bar{b}_j stands for the highest bit resolution the state S_j can support for the whole duration of one stage. The value of \bar{b}_j can be computed based on the power consumption model (2.29) and the quantization step size δ_2 .

As before, we optimize the system for the maximal average throughput with respect to the so-called policies, which provide the two nodes with a prescription of which action to take from each state. Let π_1 and π_2 be a pair of transmit and receive policies. They can be seen as functions that map each state in the respective state spaces to a deterministic,

feasible action:

$$\pi_1(S_i) = a_k \in A_1(S_i), \quad \pi_2(S_j) = a_l \in A_2(S_j), \quad \forall S_i \in \mathcal{S}_1, S_j \in \mathcal{S}_2. \quad (4.27)$$

Notice that the policies we consider are Markovian, *i.e.* they depend only on the current state but not on any previous ones. For a given decision epoch and a chosen action, the system state at the next decision epoch follows a probability distribution which can be computed based on the parameters of the energy arrival process. Let $\Phi_1(S_{i'}|S_i, a_k)$ denote the transition probability from state S_i to state $S_{i'}$ given that the action a_k is taken at the transmitter. The following relation must be fulfilled due to consistency

$$\sum_{i' \in \mathcal{S}_1} \Phi_1(S_{i'}|S_i, a_k) = 1, \quad \forall S_i \in \mathcal{S}_1. \quad (4.28)$$

Similar constraints are imposed on the transition probability function Φ_2 for the receiver. Given policies π_1 and π_2 as well as the states of the two nodes, the reward on the subsequent stage is given as

$$\Xi_{\pi_1, \pi_2}(S_i, S_j) = T \cdot R(P_1(\pi_1(S_i)), P_2(\pi_2(S_j))), \quad S_i \in \mathcal{S}_1, S_j \in \mathcal{S}_2, \quad (4.29)$$

where T is the duration of the stage. The average throughput maximization problem is then formulated as

$$\begin{aligned} \max_{\pi_1, \pi_2} \quad & \rho \triangleq \lim_{N \rightarrow +\infty} \frac{1}{N} \sum_{n=0}^{N-1} \Xi_{\pi_1, \pi_2}(X_1(n), X_2(n)) \\ \text{s.t.} \quad & X_1(0) = S_1^0, X_2(0) = S_2^0, \end{aligned} \quad (4.30)$$

where $X_1(n)$, $X_2(n)$, S_1^0 and S_2^0 are the states at stage n and the initial states of the transmitter and the receiver, respectively.

With finite storage capacity, the average throughput ρ of the system is clearly bounded. Since the energy arrival processes are assumed Poisson, *i.e.* inter-arrival times between consecutive packets are exponentially distributed, there is always the possibility of reaching the full state of the energy storage from any state. This is to say, the decision processes of both the transmitter and the receiver have only one recurrent chain, rendering the influence of the initial states to fade away after a large number of stages, and the optimal gain, denoted with g^* , to exist as a constant [109].

Recall we have emphasized the important assumption that the state transitions of the transmitter and the receiver are independent of each other due to the independent energy arrival processes, which causes the two nodes to couple only through the reward function R . Several works have concentrated on this type of problems and proposed a number of algorithms for finding optimal or suboptimal solutions *e.g.* [110, 111]. In the following, we first treat the system as a centralized multi-agent system and obtain the optimal joint policy using the policy-iteration algorithm. The result serves as a performance upper bound for the decentralized system, to which searching methods as well as a bilinear programming approach are applied which attain near-optimal solutions.

4.3.6.1 Centralized control via policy-iteration

Here we assume that there is a central control unit in the system which has the knowledge of the *global* state, *i.e.* the local states of both nodes. At each decision epoch, it determines a global action, and informs the two nodes with their respective local actions. To this end, the system can be treated as one MDP with the state space $\mathcal{S} = \mathcal{S}_1 \times \mathcal{S}_2$, for which a joint policy $\pi = (\pi_1, \pi_2)$ is in pursuit. Due to the independence of the two nodes in terms of state transitions, the joint transition probability function Φ satisfies the condition

$$\begin{aligned} \Phi(S_{i'}, S_{j'} | S_i, S_j, a_k, a_l) &= \Phi_1(S_{i'} | S_i, a_k) \cdot \Phi_2(S_{j'} | S_j, a_l), \\ \forall S_i, S_{i'} \in \mathcal{S}_1, S_j, S_{j'} \in \mathcal{S}_2, a_k \in A_1(S_i), a_l \in A_2(S_j). \end{aligned} \quad (4.31)$$

The policy-iteration algorithm, as we have introduced in Appendix A4 and applied previously to optimal control problems of an energy harvesting transmitter, can also be exploited for solving this compound system. For a given policy π , we compute in the value-determination phase the transition probabilities from each state, and solve the following set of linear equations for all $i \in \{1, \dots, |\mathcal{S}_1|\}$, $j \in \{1, \dots, |\mathcal{S}_2|\}$:

$$\rho + v_{ij} = q_{ij} + \sum_{i', j'} \Phi(S_{i'}, S_{j'} | S_i, S_j, \pi(S_i, S_j)) v_{i'j'}, \quad (4.32)$$

where q_{ij} stands for the immediate reward *i.e.* the expected achievable throughput on the subsequent stage starting with state (S_i, S_j) . The resulting solutions $\{v_{ij}\}$, also known as the relative values, serve as inputs to the policy-improvement routine that follows. By solving the optimization problem

$$\begin{aligned} \max_{\pi(S_i, S_j)} \quad & q_{ij} + \sum_{i', j'} \Phi(S_{i'}, S_{j'} | S_i, S_j, \pi(S_i, S_j)) v_{i'j'} \\ \text{s. t.} \quad & \pi(S_i, S_j) \in (A_1(S_i), A_2(S_j)) \end{aligned} \quad (4.33)$$

for each global state (S_i, S_j) , we attain an improved policy which is then fed back to the value-determination operation. The algorithm can be started with the policy-improvement routine with all relative values initialized to 0, and be terminated if the increment in the average throughput falls below a predefined threshold. We find via numerical experiments that the algorithm converges already with very few iterations, usually less than 10. However, as the scale of the problem goes with $|\mathcal{S}_1| \cdot |\mathcal{S}_2|$, the required computations can be still prohibited.

4.3.6.2 Brute-force and joint equilibrium-based search

Let us now return to the decentralized scenario where the transmitter and the receiver only have respective local state information. A straightforward way of operating the system is to allow one single modulation order at the transmitter, one single ADC resolution at the receiver, and a pair of *threshold states* indicating whether the nodes should be active. This operational strategy can be described formally by the policy $\pi(S_i, S_j) = (\pi_1(S_i), \pi_2(S_j))$ as

$$\pi_1(S_i) = \begin{cases} M_c, & i \geq i_c, \\ 0, & \text{otherwise,} \end{cases} \quad \pi_2(S_j) = \begin{cases} b_c, & \gamma > 0, j \geq j_c, \\ 0, & \text{otherwise,} \end{cases} \quad (4.34)$$

where i_c and j_c denote the threshold states of the transmitter and the receiver, respectively, and M_c and b_c indicate the per-stage modulation order and the ADC resolution to be employed once the system states are above the respective thresholds. Note that the receiver is assumed to be able to detect and respond to the case when there is no receive signal, *i.e.* it turns into sleep mode irrespective to how much energy it has in the storage. The transmitter, on the other hand, sends data even if the receiver is asleep due to the lack of feedback information. One can consider the receive SNR as another component of the receiver state, which strengthens the asymmetry between the transmitter and receiver and could potentially improve the system performance. We do not take this step here as it can be treated with the same optimization procedure but only expands the state space.

One can simply choose the threshold as the lowest energy state that includes the specified action in its feasible action set. To this end, exhaustive search can be performed to find the best pair of constant actions and the corresponding thresholds, where for each action pair, the local policies are evaluated using Monte-Carlo simulations. We refer to this method as the *brute-force search* in the sequel.

A more sophisticated treatment is to optimize both the pair of constant actions and the pair of threshold states. With exhaustive search this would require $O(|\mathcal{S}_1| \cdot |\mathcal{M}| \cdot |\mathcal{S}_2| \cdot b_{\max})$ policy evaluations. To avoid the high complexity, we apply an iterative method proposed by [112] which suggests alternatively fixing the policy of one node while optimizing the policy of the other. In our case, we first choose an action and a feasible threshold state for the transmitter. With the corresponding transmit policy fixed, we enumerate all feasible combinations of actions and thresholds of the receiver. Then, with the best receive policy fixed, we perform the enumeration for the transmitter. The iteration cycles are terminated when there is no more improvement in the achieved average throughput. The method is called *joint equilibrium-based* in [112], suggesting that the solution found can be a local optimum which is often the case in our numerical simulations. In general, this method does not provide better performance than the brute-force search; in cases where the algorithm is stuck at a bad local optimum, the performance could be even worse.

4.3.6.3 Bilinear programming approach

The decentralized and transition-independent structure of our problem resembles much similarity with a bilinear program (BP), where the cost function is bilinear and the feasible regions of the two sets of variables are disjoint [113]. As efficient algorithms exist for tackling BP, we try to formulate our problem as a BP where the key step is to *randomize* the local policies and introduce the limiting state-action probabilities as optimization variables. To this end, we let $p_1(S_i, a_k)$ and $p_2(S_j, a_l)$ denote the limiting probability that the transmitter is in state S_i and the action $a_k \in A_1(S_i)$ is chosen, and the limiting probability that the receiver is in state S_j and the action $a_l \in A_2(S_j)$ is chosen, respectively. We then optimize for a probabilistic distribution of actions for each state, instead of for

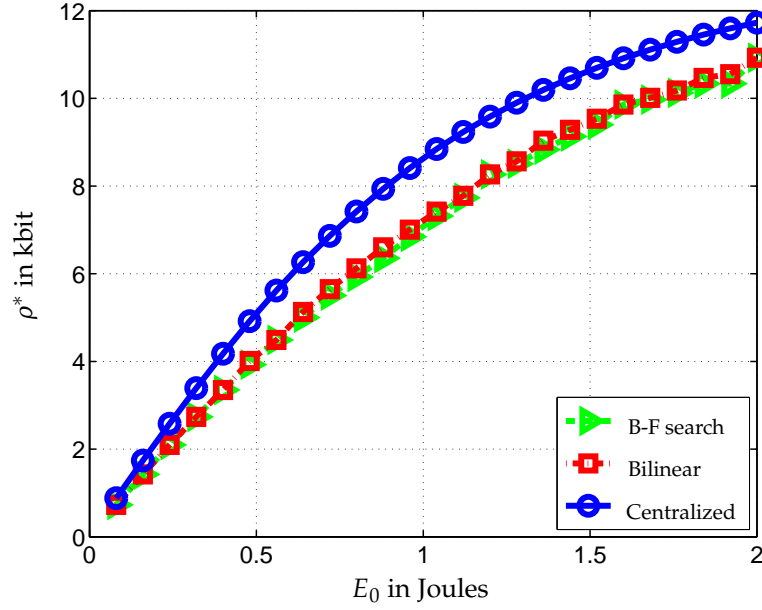


Fig. 4.20: Average throughput achieved with the proposed methods, $E_{\max} = 2$ Joule, $\delta_1 = \delta_2 = 0.08$ Joule, $d = 50$ meters, $T = 1$, $\lambda_0 = 0.1$, results averaged over 10^6 stages

one deterministic action. The BP reformulation of problem (4.30) is given by

$$\begin{aligned} \max_{p_1, p_2} \quad & \sum_{S_i \in \mathcal{S}_1} \sum_{a_k(S_i)} \sum_{S_j \in \mathcal{S}_2} \sum_{a_l(S_j)} p_1(S_i, a_k) R(a_k, a_l) p_2(S_j, a_l) \\ \text{s. t.} \quad & 0 \leq p_1(S_i, a_k) \leq 1, \quad \forall S_i \in \mathcal{S}_1, a_k \in A_1(S_i), \\ & 0 \leq p_2(S_j, a_l) \leq 1, \quad \forall S_j \in \mathcal{S}_2, a_l \in A_2(S_j), \\ & \sum_{S_{i'} \in \mathcal{S}_1} \sum_{a_k(S_{i'})} \Phi_1(S_i | S_{i'}, a_k) p_1(S_{i'}, a_k) - \sum_{a_k(S_i)} p_1(S_i, a_k) = 0, \quad \forall S_i \in \mathcal{S}_1, \quad (4.35) \\ & \sum_{S_{j'} \in \mathcal{S}_2} \sum_{a_l(S_{j'})} \Phi_2(S_j | S_{j'}, a_l) p_2(S_{j'}, a_l) - \sum_{a_l(S_j)} p_2(S_j, a_l) = 0, \quad \forall S_j \in \mathcal{S}_2, \quad (4.36) \end{aligned}$$

where we abusively use notations such as $a_k(S_i)$ for $a_k \in A_1(S_i)$ to keep the expressions more concise, and $R(a_k, a_l)$ represents the throughput on one stage if actions a_k and a_l are chosen for the transmitter and the receiver, respectively. The constraints (4.35) and (4.36) correspond to the stationary distribution conditions, *i.e.* the sum probability flowing into a state equals the sum probability flowing out. We apply the common iterative procedure to solve the obtained BP [111,113]: the algorithm starts with any feasible solution p_2 , treats it as constant and solves the resulting linear program of p_1 , and then treats p_1 as constant and solves the resulting linear program of p_2 . The procedure terminates when there is no more increment in the objective function over consecutive iterations. Deterministic local policies can be obtained from p_1^* and p_2^* simply by picking the most probable action for each state. Although suboptimal, the complexity of the method is extremely low, and the algorithm often converges very fast to a satisfactory solution, as we shall observe in the following simulation results.

We implement all proposed algorithms: the centralized policy-iteration based method, the brute-force search, the joint equilibrium-based search, and the bilinear programming

approach, and test them in a homogeneous scenario: the two nodes have the same energy arrival intensity and the same energy storage capacity. The storage capacities and the mean inter-arrival times of the two nodes are chosen to be identical. Energy packets arriving as a Poisson process to each node are assumed to have the same size, the value of which is varied from 4% to 100% of the full storage. The average throughput achieved with the aforementioned methods are demonstrated in Fig. 4.20, where their variations with respect to the sizes of the energy packets can be observed. Note that the results of the joint equilibrium-based search are almost identical to those of the brute-force search, and are therefore not shown in the figure. Apparently, the bilinear programming approach also performs similarly as the brute-force search, with only a slight advantage observed when the arrival intensity is increased. Taken into account its low complexity, we regard the bilinear programming approach as the most suitable for our problem in the medium to rich energy environment, while the brute-force search is also a good choice when the number of feasible modulation orders and ADC resolutions is not high. The centralized control exhibits naturally a larger average throughput, which is not very significant for most arrival intensities due to the independence of the energy arrival processes.

4.4 Summary

The optimal control of energy harvesting transceivers are investigated in this chapter, where the energy arrival process is assumed random and not part of the control system. We discuss the cases that the transceiver has non-causal and causal knowledge about the energy arrivals respectively. The optimal solutions in both cases rely very much on the conclusions we have drawn for the basic problem in Chapter 3. Numerical simulations demonstrate the effectiveness of the algorithms we propose, and also provide theoretical guidance to system design issues such as choosing the appropriate energy storage, whether it is necessary for the system to attain channel state information, to predict energy arrival information, or to acquire state information of communication partners.

5. Conclusions and Outlook

5.1 Summary and Conclusions

The control of communication devices powered by a fixed energy budget or by harvested environmental energy is investigated in this thesis. The topic addresses the energy efficiency of the studied systems, connects communication theory to the classic optimal control theory, and is of high practical relevance as an optimized system can achieve significantly better performance than a simple one without careful design. We focus mainly on basic communication scenarios where a wireless transceiver or a pair of wireless transceivers communicate over a single link, and establish the transmission/reception principles under different assumptions by virtue of the theoretical frameworks of optimal control and dynamic programming. For systems with a given energy budget, we find that the control strategy leading to the maximal throughput on the finite operation interval can be determined based on the property of the achievable rate R as a function of the total power consumption P of the system. If the function is independent of time and strictly concave, then the optimal strategy is to keep the control variable constant on the interval. If, due to considerations on circuit and processing power or restrictions on the control variable, the function has an isolated zero point and is not continuously defined, then time-sharing of the so-called energy efficient operation modes which constitutes a concave Pareto boundary of the function is necessary for the optimal control. When the communication channel is time-varying, a constant marginal gain condition needs to be satisfied and the optimal solution can be obtained using a water-filling procedure. The explorations and the conclusions drawn for the constant energy constrained systems serve as the basis of optimization of energy harvesting transceivers. For these devices, the available energy is a function of time which can be deterministic or random depending on the assumptions made. An energy storage with limited capacity introduces another factor into the design and optimization. With non-causal knowledge about the energy arrival profile, the optimal control strategy can be found using an effective construction method of the state trajectory that meets all optimality criteria. If only causal and statistical knowledge of the arrival profile is available, we model the system as a Markov decision process and find the operation policy that yields the maximal average throughput in an iterative manner. Performance degradation due to the lack of non-causal arrival information is more severe in an energy intensive situation, as revealed by numerical simulations. Below we list a number of potential directions in which our work can be extended in the future.

5.2 Future Perspectives

- Network of energy harvesting nodes

As one of the most important applications of energy harvesting nodes, wireless sensor networks are expected to operate more autonomously and even perpetually thanks to the energy harnessed from the environment. Based on the control principles we have derived for point-to-point communications, energy management and operation policy of sensor networks powered by energy harvesting are to be investigated. Existing literature of energy efficient operation studies on wireless sensor networks should be explored thoroughly to understand the design challenges of these systems, and to distinguish the imperative problems that need to be treated when energy harvesting comes into play. Despite some preliminary works on relaying, broadcast and multiple access channels [114, 115], there are still much to be done regarding the scheduling, routing, and cooperation in the network. Moreover, distributed design solutions are of particular interest as exchanging the energy status is rather unlikely within the network. On the other hand, correlations between the energy arrival processes at adjacent nodes can help reduce the uncertainty thus improve the overall performance, and should therefore be modeled and taken into account carefully.

- Energy harvesting transceivers with compact antenna arrays

The energy harvesting technology is applied to many low-power devices such as autonomous sensors and wearables, which are often limited in their dimensions and unsuitable for deployment of a large antenna array. Compact arrays with a small number of antennas can be a promising candidate for enhancing the performance of these devices. As demonstrated in [116, 117], compact antenna arrays with the antenna spacing much smaller than half of the carrier wavelength have the potential to provide even higher capacity and better energy efficiency than the conventional half-wavelength arrays. To fully realize its potential, the configuration of the array needs to be optimized based on performance considerations and/or physical dimension limitations. Signal processing techniques for energy harvesting multi-antenna systems need to be developed to realize their potential, yet it is important to note, that highly complex schemes are not suited due to the associated high processing cost. The application of 1-bit A/D conversion can be an interesting solution here because of the great reduction in hardware complexity and power consumption it is able to offer, and the loss in information can be partially compensated by using more antennas.

- Cross-layer design of energy harvesting nodes

Energy harvesting nodes can be deployed in different application scenarios where the performance objectives also differ. In many of the cases, the appropriate performance metric is related to higher layer parameters, instead of only to those of the physical layer. For example, in video streaming over wireless networks, the video source rate from the application layer, the time slot allocation from the data link layer, and the modulation scheme chosen at the physical layer have a joint impact on the quality of the received video, and can therefore be optimized at the same time [118]. As a more systematic treatment, the generalized *network utility maximization* problem has been formulated to address the potential of optimizing different layering schemes in

a communication network [119]. It provides a decomposition framework where the decomposed subproblems, each corresponding to a layer, are connected by the dual variables representing the interfaces between layers. These methodologies are known as the *cross-layer design*, which is a useful approach for efficient resource allocation in wireless networks [120,121].

For traditional communication devices powered by batteries or fixed utilities, cross-layer design helps to match the upper layer parameters that directly influence the utility function or the quality of service with the channel conditions. For energy harvesting nodes, the energy state and arrival statistics are additional important characteristics of the physical layer, which can be taken into account in the cross-layer framework. To this end, application-oriented parameters, such as frequency of measurements and coding rate of the information data, should be adapted to both channel and energy statuses. In a networking scenario, the adaptation of these parameters of each node should depend on the channel and energy conditions of all nodes, as well as on each other which determines the overall traffic in the system. Such a problem would involve a large number of variables and may have a complicated structure. As a result, the challenge here is not only to find an optimal solution, but also to develop effective, low-complexity algorithms with satisfactory performance.

Appendix

A1 Properties of the Capacity Lower Bound (2.49)

The capacity lower bound (2.49) of a training based SISO system can be evaluated by using Monte-Carlo simulations, or by exploiting the exponential integral function. We let

$$\varphi \triangleq \frac{(1 + \gamma)(1 + \rho\gamma) + L(1 - \rho)\gamma}{L\gamma^2(1 - \rho)} \quad (\text{A1})$$

and rewrite (2.49) in bit/sec/Hz as

$$C_{L,d} = \text{E} \left[\log_2 \left(1 + \frac{(1 - \rho)\theta}{\varphi + \rho\theta} \right) \right], \quad (\text{A2})$$

where $\theta = |w|^2$ is exponentially distributed with rate 1. Plugging in the corresponding probability density function, we have

$$\begin{aligned} C_{L,d} &= \int_0^{+\infty} e^{-\theta} \log_2 \left(\frac{\varphi + \theta}{\varphi + \rho\theta} \right) d\theta \\ &= \frac{1}{\ln 2} \left(\int_0^{+\infty} e^{-\theta} \ln(\varphi + \theta) d\theta - \int_0^{+\infty} e^{-\theta} \ln(\varphi + \rho\theta) d\theta \right) \\ &= \frac{1}{\ln 2} \left(e^\varphi \int_\varphi^{+\infty} e^{-u} \ln u du - e^{\frac{\varphi}{\rho}} \int_{\frac{\varphi}{\rho}}^{+\infty} e^{-u} \ln u du - \ln \rho \right) \\ &= \frac{1}{\ln 2} \left(e^{\varphi/\rho} \text{Ei}(-\varphi/\rho) - e^\varphi \text{Ei}(-\varphi) \right), \end{aligned} \quad (\text{A3})$$

where Ei denotes the exponential integral defined in the following, and integration by parts is applied in order to obtain (A3).

A1.1 The exponential integral and its expansions

The exponential integral function Ei is defined by the indefinite integral

$$\text{Ei}(x) = \int_{-\infty}^x \frac{e^t}{t} dt \quad (\text{A4})$$

for any non-zero real number x . As shown in Fig. A1, the function increases rapidly and unboundedly for $x > 0$, approaches 0 from below for $x \rightarrow -\infty$, and is discontinuous at

$x = 0$. Although unable to be expressed in terms of elementary functions, the exponential integral has the following series expansions [122]:

$$\text{Ei}(x) = \gamma_E + \ln|x| + \sum_{k=1}^{\infty} \frac{x^k}{k k!} = \gamma_E + \ln|x| + x + \frac{x^2}{4} + \frac{x^3}{18} + \dots, \quad (\text{A5})$$

$$\text{Ei}(x) = e^x \sum_{k=1}^{\infty} \frac{(k-1)!}{x^k} = e^x \left(\frac{1}{x} + \frac{1}{x^2} + \frac{2}{x^3} + \dots \right), \quad x \rightarrow \infty, \quad (\text{A6})$$

where $\gamma_E \approx 0.5772156649$ denotes the Euler-Mascheroni constant.

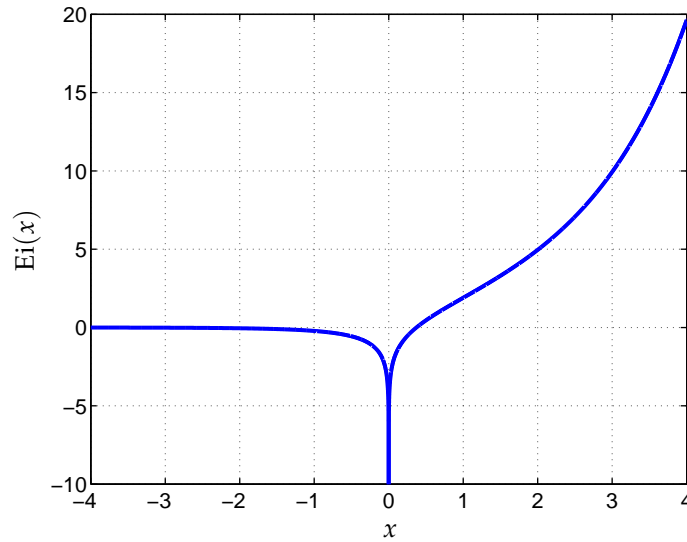


Fig. A1: The exponential integral

A1.2 Monotonicity and asymptotic properties

We show that $C_{L,d}$ as given by (A3) is positive and monotonically decreasing in φ for $\varphi > 0$. Based on the fundamental theorem of calculus, the derivative of Ei is given as

$$\frac{d}{dx} \text{Ei}(x) = \frac{e^x}{x}, \quad (\text{A7})$$

which further leads to

$$\frac{d}{dx} \left(e^x \text{Ei}(-x) \right) = e^x \text{Ei}(-x) + \frac{1}{x}. \quad (\text{A8})$$

For $x > 0$, the function $e^x \text{Ei}(-x)$ satisfies the following inequality [123]

$$-\ln \left(1 + \frac{1}{x} \right) < e^x \text{Ei}(-x) < -\frac{1}{2} \ln \left(1 + \frac{2}{x} \right). \quad (\text{A9})$$

Consequently, we have

$$\frac{d}{dx} \left(e^x \text{Ei}(-x) \right) > \frac{1}{x} - \ln \left(1 + \frac{1}{x} \right) > \frac{1}{x} - \frac{1}{x} = 0, \quad (\text{A10})$$

implying that the function $e^x \text{Ei}(-x)$ is monotonically increasing. Since the distortion factor $\rho < 1$, it follows that $e^{\varphi/\rho} \text{Ei}(-\varphi/\rho) > e^\varphi \text{Ei}(-\varphi)$, and therefore $C_{L,d}$ is indeed positive.

By using (A8) and (A9), we compute and bound the first-order derivative of $C_{L,d}$ with respect to φ as

$$\frac{dC_{L,d}}{d\varphi} = \frac{1}{\ln 2} \left(\frac{1}{\rho} e^{\varphi/\rho} \text{Ei}(-\varphi/\rho) - e^\varphi \text{Ei}(-\varphi) \right) \quad (\text{A11})$$

$$< \frac{1}{\ln 2} \left(-\frac{1}{2\rho} \ln \left(1 + \frac{2\rho}{\varphi} \right) + \ln \left(1 + \frac{1}{\varphi} \right) \right). \quad (\text{A12})$$

Consider the function $f(x)$ defined below and its derivative:

$$f(x) = \frac{(1+ax)^{\frac{1}{a}}}{1+x}, \quad x \geq 0, a > 0, \quad \frac{df}{dx} = \frac{x(1-a)(1+ax)^{\frac{1}{a}-1}}{(1+x)^2}. \quad (\text{A13})$$

For $a < 1$, the function increases monotonically as $\frac{df}{dx}$ is positive. Since $f(0) = 1$, we see that $f(x) > 1$ i.e. $(1+ax)^{\frac{1}{a}} > 1+x$ for $x > 0$. Taking the logarithm on both sides and replacing x with $1/\varphi$, a with 2ρ , we have

$$\frac{1}{2\rho} \ln \left(1 + \frac{2\rho}{\varphi} \right) > \ln \left(1 + \frac{1}{\varphi} \right), \quad (\text{A14})$$

which proves that the right-hand side of (A12) is negative. Note that when the ADC resolution is restricted to integer values, the distortion factor ρ satisfies $2\rho < 1$ according to Table 2.1. As a result, the derivative of $C_{L,d}$ with respect to φ is negative and hence the function decreases monotonically in φ .

In the very low SNR regime, φ and $C_{L,d}$ can be approximated by

$$\gamma \rightarrow 0: \quad \varphi \approx \frac{1}{L\gamma^2(1-\rho)}, \quad C_{L,d} \approx \frac{1-\rho}{\varphi \ln 2} \approx \frac{(1-\rho)^2 L \gamma^2}{\ln 2}, \quad (\text{A15})$$

where the asymptotic series expansion (A6) is applied. The reason why $C_{L,d}$ decreases with $(1-\rho)^2$ and γ^2 is that the variance of the channel estimate decreases linearly with $(1-\rho)$ and γ . Moreover, the spectral efficiency η_B as defined by $(S-L)C_{L,d}/S$ is clearly maximized with $L = S/2$ in this case.

By using (A5), it can be computed that

$$\lim_{\varphi \rightarrow 0} C_{L,d} = \frac{1}{\ln 2} (\ln(\varphi/\rho) - \ln(\varphi)) = -\log_2 \rho, \quad (\text{A16})$$

which is the capacity limit of a quantized channel in the very high SNR regime. However, even when $\gamma \rightarrow +\infty$, $\varphi \rightarrow \frac{\rho}{L(1-\rho)} > 0$, implying that (A16) is not achievable for systems without perfect channel state information.

A2 Concavity of the Constructed Rate Function \tilde{R}

We show in the following that the rate function \tilde{R} defined by (3.87)

$$\tilde{R}(P_1, P_2) = \begin{cases} 0, & P_2 = 0, \\ \frac{P_2}{\mu(\beta)} \cdot R(\beta\mu(\beta), \mu(\beta)), & 0 < P_2 < \mu(\beta), \\ R(P_1, P_2), & P_2 \geq \mu(\beta) \end{cases} \quad \text{with } \beta = \frac{P_1}{P_2} \quad (\text{A17})$$

is jointly concave in $(P_1, P_2) \in [0, +\infty) \times [0, +\infty)$, where the original rate function R is given by (3.80) and the tangent point $\mu(\beta)$ satisfies (3.91).

For any given direction specified by $\beta > 0$, the univariate function $R(\beta u, u)$ is defined on $\{0\} \cup (a_0, +\infty)$ and is monotonically increasing on its continuous domain. Since $R(0, 0) = R(\beta a_0^+, a_0^+) = 0$, it can be inferred that the tangent line from the origin towards $R(\beta u, u)$ is above the function at least until the tangent point is reached. We prove next that $R(\beta u, u)$ is strictly concave in u for $u \geq \mu(\beta)$, by showing its second-order derivative to be negative. To this end, we have

$$\begin{aligned} R_u(\beta u, u) &= \beta R_{P_1}(\beta u, u) + R_{P_2}(\beta u, u), \\ R_{uu}(\beta u, u) &= \beta^2 R_{P_1 P_1}(\beta u, u) + 2\beta R_{P_1 P_2}(\beta u, u) + R_{P_2 P_2}(\beta u, u) \\ &= -\left(\beta \sqrt{-R_{P_1 P_1}} - \sqrt{-R_{P_2 P_2}}\right)^2 - 2\beta \left(\sqrt{R_{P_1 P_1} R_{P_2 P_2}} - R_{P_1 P_2}\right), \end{aligned} \quad (\text{A18})$$

where we omit the arguments of the derivatives in (A18) for a more concise expression, and the negativeness of $R_{P_1 P_1}$ and $R_{P_2 P_2}$ as obtained in (3.85) are taken into account. According to (A18), the relation $R_{P_1 P_1} R_{P_2 P_2} > R_{P_1 P_2}^2$ would immediately lead to $R_{uu} < 0$. From (3.86) we can further calculate that

$$\begin{aligned} R_{P_1 P_1} R_{P_2 P_2} - R_{P_1 P_2}^2 &= \frac{2B^2 \alpha^2}{c_1^2 \sigma^4 \ln^2 2} \cdot \frac{\gamma(3 \cdot 2^{2b} + \gamma)(2^{2b} - 1)(2^{2b} + 2\gamma + 1) - 2(1 + \gamma)^2 2^{4b}}{(1 + \gamma)^2 (2^{2b} + \gamma)^4 (u - a_0 + a_1)^2} \\ &= \frac{2B^2 \alpha^2}{c_1^2 \sigma^4 \ln^2 2} \cdot \frac{3\gamma \cdot 2^{4b} + 2\gamma^2 \cdot 2^{2b} - 4\gamma \cdot 2^{2b} - 2 \cdot 2^{2b} - 2\gamma^2 - \gamma}{(1 + \gamma)^2 (2^{2b} + \gamma)^3 (u - a_0 + a_1)^2} \\ &= \frac{2B^2 \alpha^2}{c_1^2 \sigma^4 \ln^2 2} \cdot \frac{\gamma(2^{2b} - 1)^2 + 2(2^{2b} + \gamma)(\gamma \cdot 2^{2b} - \gamma - 1)}{(1 + \gamma)^2 (2^{2b} + \gamma)^3 (u - a_0 + a_1)^2}. \end{aligned} \quad (\text{A19})$$

Now we try to extract a relation between γ and u based on the tangent equation. Applying the inequality $\ln(1 + x) < x$ for $x > 0$, we have

$$\begin{aligned} \ln\left(\frac{1 + \gamma(\mu)}{1 + \gamma(\mu) \cdot 2^{-2b(\mu)}}\right) &= \frac{\alpha \beta \mu}{c_1 \sigma^2} \cdot \frac{2^{2b(\mu)} - 1}{(1 + \gamma(\mu))(2^{2b(\mu)} + \gamma(\mu))} + \frac{2\gamma(\mu)\mu}{(2^{2b(\mu)} + \gamma(\mu))(\mu - a_0 + a_1)} \\ &< \frac{\gamma(\mu)(2^{2b(\mu)} - 1)}{2^{2b(\mu)} + \gamma(\mu)}, \end{aligned} \quad (\text{A20})$$

where $\gamma(\mu) = \alpha(\beta\mu - c_0)/(c_1\sigma^2)$, $2^{2b(\mu)} = (\mu - a_0 + a_1)^2/a_1^2$. The left hand side can be relaxed by replacing $\alpha\beta\mu/(c_1\sigma^2)$ with $\gamma(\mu)$, which allows for simplification of the inequality and leads to

$$\frac{2\mu}{\mu - a_0 + a_1} < \frac{(2^{2b(\mu)} - 1)\gamma(\mu)}{1 + \gamma(\mu)}. \quad (\text{A21})$$

It then follows

$$\frac{(2^{2b(\mu)} - 1)(\mu - a_0 + a_1) - 2\mu}{2\mu} > \frac{1}{\gamma(\mu)} > 0, \quad (\text{A22})$$

which ensures that

$$\gamma(\mu) > \frac{2\mu}{(2^{2b(\mu)} - 1)(\mu - a_0 + a_1) - 2\mu} > 0. \quad (\text{A23})$$

The right hand side of (A23), when viewed as a function ζ of μ , can be shown monotonically decreasing in μ via the following steps:

$$\begin{aligned} \zeta(\mu) &= \frac{2\mu}{(2^{2b(\mu)} - 1)(\mu - a_0 + a_1) - 2\mu} = \frac{2a_1^2\mu}{(\mu - a_0 + 2a_1)(\mu - a_0)(\mu - a_0 + a_1) - 2a_1^2\mu} \\ &= \frac{2a_1^2\mu}{(\mu - a_0)^3 + 3a_1(\mu - a_0)^2 - 2a_1^2a_0} \end{aligned} \quad (\text{A24})$$

$$\begin{aligned} \zeta_\mu(\mu) &= 2a_1^2 \cdot \frac{(\mu - a_0)^3 + 3a_1(\mu - a_0)^2 - 2a_1^2a_0 - \mu[3(\mu - a_0)^2 + 6a_1(\mu - a_0)]}{[(\mu - a_0)^3 + 3a_1(\mu - a_0)^2 - 2a_1^2a_0]^2} \\ &= -2a_1^2 \cdot \frac{(\mu - a_0)^2(2\mu + a_0) + 3a_1(\mu - a_0)(\mu + a_0) + 2a_1^2a_0}{[(\mu - a_0)^3 + 3a_1(\mu - a_0)^2 - 2a_1^2a_0]^2} < 0. \end{aligned} \quad (\text{A25})$$

Consequently, for $u \geq \mu$, we have

$$\gamma \geq \gamma(\mu) > \zeta(\mu) \geq \zeta(u), \quad (\text{A26})$$

which leads to

$$\begin{aligned} \gamma \cdot 2^{2b} - \gamma - 1 &> \frac{2u(1 + \gamma)}{u - a_0 + a_1} - 1 > \frac{2u(2^{2b} - 1)}{(2^{2b} - 1)(u - a_0 + a_1) - 2u} - 1 \\ &= \frac{2(a_1 \cdot 2^b - a_1 + a_0)2^{2b} - (2^{2b} - 1)a_1 \cdot 2^b}{(2^{2b} - 1)(u - a_0 + a_1) - 2u} \\ &= \frac{2^b(a_1(2^b - 1)^2 + 2a_0 \cdot 2^b)}{(2^{2b} - 1)(u - a_0 + a_1) - 2u} > 0. \end{aligned} \quad (\text{A27})$$

The strict concavity of $R(\beta u, u)$ for $u \geq \mu(\beta)$ then follows from (A18) and (A19). The importance of this result is that it ensures the existence and uniqueness of the tangent point for all $\beta > 0$, and consequently guarantees that our construction method is feasible.

We now consider the point $Z(\beta_Z v, v)$ resulting from the time-sharing of $X(\beta_1 v_1, v_1)$ and $Y(\beta_2 v_2, v_2)$ with the time-sharing factor $\lambda \in [0, 1]$, as formulated in (3.88). If $v \geq \mu(\beta_Z)$ *i.e.* Z is beyond the corresponding time-sharing region, the determinant of the Hessian matrix $\mathbf{H}(R)$ evaluated at Z can be shown positive using the derivations presented above, since (A19) is exactly the formula for the determinant of $\mathbf{H}(R)$. Together with the proven conditions $R_{P_1 P_1} < 0$ and $R_{P_2 P_2} < 0$, the negative definiteness of $\mathbf{H}(R)$ at point Z is confirmed. If, on the other hand, Z is inside the time-sharing region with respect to β_Z , we write the achievable rate at Z as

$$\tilde{R}_Z = \frac{v}{\mu(\beta_Z)} R(\beta_Z \mu(\beta_Z), \mu(\beta_Z)) = v(\beta_Z R_{P_1}|_{\mu_Z} + R_{P_2}|_{\mu_Z}) \quad (\text{A28})$$

where the tangent equation (3.89) is applied and $R_{P_1}|_{\mu_Z}$ represents R_{P_1} evaluated at $(\beta_Z \mu(\beta_Z), \mu(\beta_Z))$. By using the chain rule and also (3.92), we obtain

$$\begin{aligned}\frac{dR_{P_1}}{d\lambda} &= \left(\mu R_{P_1 P_1} + (\beta R_{P_1 P_1} + R_{P_1 P_2}) \frac{d\mu}{d\beta} \right) \frac{d\beta}{d\lambda}, \\ \frac{dR_{P_2}}{d\lambda} &= \left(\mu R_{P_1 P_2} + (\beta R_{P_1 P_2} + R_{P_2 P_2}) \frac{d\mu}{d\beta} \right) \frac{d\beta}{d\lambda}, \\ \frac{d}{d\lambda}(\beta R_{P_1} + R_{P_2}) &= R_{P_1} \frac{d\beta}{d\lambda} + \beta \frac{dR_{P_1}}{d\lambda} + \frac{dR_{P_2}}{d\lambda} = R_{P_1} \frac{d\beta}{d\lambda}, \\ \frac{d\tilde{R}_Z}{d\lambda} &= (\beta_Z R_{P_1}|_{\mu_Z} + R_{P_2}|_{\mu_Z}) \frac{dv}{d\lambda} + v R_{P_1}|_{\mu_Z} \cdot \frac{d\beta_Z}{d\lambda}.\end{aligned}\quad (\text{A29})$$

From $v = \lambda v_1 + (1 - \lambda)v_2$ and $\beta_Z = \frac{\lambda \beta_1 v_1 + (1 - \lambda)\beta_2 v_2}{\lambda v_1 + (1 - \lambda)v_2}$, it can be calculated that

$$\frac{dv}{d\lambda} = v_1 - v_2, \quad \frac{d^2 v}{d\lambda^2} = 0, \quad \frac{d\beta_Z}{d\lambda} = \frac{(\beta_1 - \beta_2)v_1 v_2}{v^2}, \quad \frac{d^2 \beta_Z}{d\lambda^2} = -\frac{2}{v} \frac{dv}{d\lambda} \frac{d\beta_Z}{d\lambda}.\quad (\text{A30})$$

These results help us attain the following from (A29)

$$\begin{aligned}\frac{d^2 \tilde{R}_Z}{d\lambda^2} &= 2R_{P_1}|_{\mu_Z} \frac{d\beta_Z}{d\lambda} \frac{dv}{d\lambda} + v \frac{dR_{P_1}|_{\mu_Z}}{d\lambda} \frac{d\beta_Z}{d\lambda} + v R_{P_1}|_{\mu_Z} \frac{d^2 \beta_Z}{d\lambda^2} = v \frac{dR_{P_1}|_{\mu_Z}}{d\lambda} \frac{d\beta_Z}{d\lambda} \\ &= \frac{(\beta_1 - \beta_2)^2 (v_1 v_2)^2}{v^3} \left(\mu R_{P_1 P_1} - \frac{\mu(\beta R_{P_1 P_1} + R_{P_1 P_2})^2}{\beta^2 R_{P_1 P_1} + 2\beta R_{P_1 P_2} + R_{P_2 P_2}} \right) \Big|_{\mu_Z} \\ &= \frac{(\beta_1 - \beta_2)^2 (v_1 v_2)^2}{v^3} \cdot \frac{\mu(R_{P_1 P_1} R_{P_2 P_2} - R_{P_1 P_2}^2)}{\beta^2 R_{P_1 P_1} + 2\beta R_{P_1 P_2} + R_{P_2 P_2}} \Big|_{\mu_Z} \leq 0,\end{aligned}\quad (\text{A31})$$

where the equality holds if and only if $\beta_1 = \beta_2$. The determination of the sign in (A31) is based on (A18) and the derivations thereafter.

We have heretofore completed the proof that the straight line connecting any two points on the surface of \tilde{R} lies below that surface, hence demonstrating the concavity of \tilde{R} . Notice that the relation $R_{P_1 P_1} R_{P_2 P_2} - R_{P_1 P_2}^2 > 0$ which is fulfilled by the tangent points and the points beyond the tangent region plays a critical role in the whole proof.

A3 Markov Chain and Markov Decision Process

Markov chains and Markov decision processes have found wide and enormous applications in different scientific and engineering disciplines such as finance, manufacturing, automated control, and communications. In this section, we give a brief introduction to both models, with the focus on those concepts that are important to the derivation of the policy-iteration algorithm. Details of the subjects can be found in [107].

A3.1 Markov chain

The evolution of a system involving some random variables can be represented by a stochastic process. In the discrete time case, we can treat a stochastic process as a sequence of random variables denoted with $\{X_n | n = 0, 1, 2, \dots\}$, which assume values in a state space \mathcal{S} of cardinality S . To this end, the system can be seen as occupying state X_n at time

instant n , and making transition to state X_{n+1} for the next time instant according to a certain probability distribution, where the duration between two consecutive transitions is assumed constant. A *Markov chain* or equivalently a *discrete-time Markov process*, named after the Russian mathematician A. Markov, is a stochastic process with the following *memoryless* property:

$$\Pr\{X_{n+1} = x_{n+1} | X_n = x_n, \dots, X_0 = x_0\} = \Pr\{X_{n+1} = x_{n+1} | X_n = x_n\} \quad (\text{A32})$$

for all $n \geq 0$ and $x_k \in S$, $0 \leq k \leq n + 1$, which suggests that conditioned on the current state, the probability distribution of the next state is independent of all the past states. Note that for Markov chains, it is usually assumed that the state space is finite or countable. If the probability $\Pr\{X_{n+1} = x_{n+1} | X_n = x_n\}$, which is referred to as a *transition probability*, is independent of the time index n , we call the corresponding Markov process *stationary* or *time-homogeneous*. For such a process, we index the system states with integer numbers and denote the transition probability from state i to state j with p_{ij} . The matrix $\mathbf{P} \in \mathbb{R}^{S \times S}$ having p_{ij} on its i -th row and j -th column is called the *transition matrix*.

Two states i and j in a Markov process are said to *communicate* if and only if one state can be reached from the other with non-zero probability and vice versa. The Markov process is *irreducible* if every of its states communicates with every other state. Moreover, a state i is called *aperiodic* if the returning probability after N steps is positive for all sufficiently large N . It can be inferred that for an aperiodic state, every state it communicates with is also aperiodic. Irreducible and aperiodic Markov processes constitute an important class of Markov processes as they possess useful asymptotic properties, which we introduce in the sequel.

A3.2 Stochastic matrices

The transition matrix \mathbf{P} in the way we define it has the property that each of its rows sums up to 1, which can be represented by

$$\mathbf{P} \mathbf{1} = \left[\sum_{j=1}^S p_{1j}, \dots, \sum_{j=1}^S p_{Sj} \right]^T = \mathbf{1}, \quad (\text{A33})$$

where $\mathbf{1}$ is the all-one column vector of dimension S . This kind of matrices is called *stochastic matrices* or *Markov matrices*. It can be verified that \mathbf{P}^k , representing the transition probabilities of the Markov chain in k steps, is also a stochastic matrix. Moreover, from (A33) it is clear that $\mathbf{1}$ is a right-eigenvector of \mathbf{P} associated with the eigenvalue 1.

Let $\mathbf{p}(n) \in \mathbb{R}^S$ be the vector of probabilities that the system occupies each state at time instant n . The state-occupancy probability for the next time instant can be written as

$$\mathbf{p}^T(n+1) = \mathbf{p}^T(n) \mathbf{P}, \quad (\text{A34})$$

from which it can be induced that $\mathbf{p}(n)$ depends on the initial state probability $\mathbf{p}(0)$ and the n -th power of \mathbf{P} as

$$\mathbf{p}^T(n) = \mathbf{p}^T(0) \mathbf{P}^n. \quad (\text{A35})$$

For many Markov processes, the initial state probabilities fade away after a very large number of transitions, and the the sequence of vectors \mathbf{p} converges to a vector of *stationary*

state probabilities, which we denote with $\boldsymbol{\rho}$. As the limit of $\boldsymbol{p}(n)$ when n approaches infinity, the vector $\boldsymbol{\rho}$ is unchanged under the application of the transition matrix \boldsymbol{P} , *i.e.*

$$\boldsymbol{\rho}^T = \boldsymbol{\rho}^T \boldsymbol{P}, \quad (\text{A36})$$

suggesting that $\boldsymbol{\rho}$ is a left-eigenvector of \boldsymbol{P} associated with the eigenvalue 1. For the stationary state probabilities to exist and be unique, the Markov process needs to be irreducible and aperiodic. When this is the case, the Perron-Frobenius theorem guarantees that \boldsymbol{P}^k has strictly positive entries for sufficiently large k , and it converges asymptotically to the Perron projection defined by the outer product of the left- and right-eigenvectors of \boldsymbol{P} associated to the unique eigenvalue of the largest magnitude:

$$\lim_{k \rightarrow +\infty} \boldsymbol{P}^k = \mathbf{1}\boldsymbol{\rho}^T. \quad (\text{A37})$$

This is to say, matrix \boldsymbol{P}^k has identical rows in the limiting case, with each row equal to the transpose of the vector of stationary state probabilities.

A3.3 Markov decision process

As introduced above, we consider discrete-time Markov processes for which state transitions happen at equally spaced instants in time. These intervals of equal length are termed as *stages*. Suppose a control unit in the system is able to observe the system states at the beginning of each stage. One of the feasible control actions is then chosen and taken based on the observed state and the incurred profit / cost, which would influence the state transition at the next stage. In this context, the control unit is referred to as the *decision maker* or the *agent*, and the profit or cost associated with an *action* and the subsequent state transition is called the *reward*. Such a control process can be seen as an extension to a stochastic process with the additional ingredients of actions and rewards. If the transition probability from state x_i to state x_j , $\forall x_i, x_j \in \mathcal{S}$, depends only on x_i and the action taken in x_i but not on any previous state or action, then the process has the memoryless property and is called a *Markov decision process* (MDP). The set of decision rules that the decision maker follows, *i.e.* the mapping from system states to actions, is termed as a *policy*. Within the framework of MDP, different policies can be evaluated and compared given a specified performance criterion, which is usually a function of the sequence of rewards the system receives. Common methods to compute the optimal policy, when it exists, include dynamic programming, value-iteration, and policy-iteration algorithms.

A4 Policy-Iteration Algorithm for Average Reward Maximization

Assuming that the transition from state i to j is associated with a stationary reward $r_{ij} \in \mathbb{R}$ and that the reward for stage n is denoted with $R(n)$, we set the optimization goal for the MDP as maximizing the average reward, or the *gain* of the process, which is defined as

$$g \triangleq \lim_{N \rightarrow +\infty} \frac{1}{N} \sum_{n=1}^N R(n). \quad (\text{A38})$$

Given state i , the expected immediate reward for the following stage is computed as

$$q_i = \sum_{j=1}^S p_{ij} r_{ij}, \quad i = 1, \dots, S. \quad (\text{A39})$$

In the steady state *i.e.* the state-occupancy probabilities have converged to ρ , the gain of the process can be written as

$$g = \rho^T \mathbf{q} \quad \text{with} \quad \mathbf{q} = [q_1, \dots, q_S]^T. \quad (\text{A40})$$

On the other hand, we let $u_i(n)$ denote the expected total reward on the next n stages when the system is started in state i , and compute it with

$$u_i(n) = \sum_{j=1}^S p_{ij} (r_{ij} + u_j(n-1)) = q_i + \sum_{j=1}^S p_{ij} u_j(n-1), \quad i = 1, \dots, S, \quad (\text{A41})$$

$$\mathbf{u}(n) = \mathbf{q} + \mathbf{P}\mathbf{u}(n-1), \quad (\text{A42})$$

where (A42) incorporates all the S equations from (A41) into a matrix form. Noting that $\mathbf{u}(1) = \mathbf{q}$, we have for $n \geq 1$

$$\begin{aligned} \mathbf{u}(n) &= \mathbf{q} + \mathbf{P}(\mathbf{q} + \mathbf{P}\mathbf{u}(n-2)) \\ &= (\mathbf{I} + \mathbf{P})\mathbf{q} + \mathbf{P}^2(\mathbf{q} + \mathbf{P}\mathbf{u}(n-3)) = \dots \\ &= (\mathbf{I} + \mathbf{P} + \dots + \mathbf{P}^{n-1})\mathbf{q}, \end{aligned} \quad (\text{A43})$$

which further leads to

$$\lim_{n \rightarrow +\infty} (\mathbf{u}(n) - \mathbf{u}(n-1)) = \lim_{n \rightarrow +\infty} \mathbf{P}^{n-1} \mathbf{q} = \mathbf{1} \rho^T \mathbf{q} = g \cdot \mathbf{1}. \quad (\text{A44})$$

This result suggests that the expected total reward grows asymptotically with the rate g irrespective of from which state the system is started. We therefore write for large n the relation

$$\mathbf{u}(n) = n g \cdot \mathbf{1} + \mathbf{v}, \quad (\text{A45})$$

where the constant vector \mathbf{v} is composed of the asymptotic intercepts of $\mathbf{u}(n)$. Plugging (A45) into (A42), we have

$$\begin{aligned} n g \cdot \mathbf{1} + \mathbf{v} &= \mathbf{q} + \mathbf{P}((n-1)g \cdot \mathbf{1} + \mathbf{v}) \\ g \cdot \mathbf{1} + (\mathbf{I} - \mathbf{P})\mathbf{v} &= \mathbf{q}, \end{aligned} \quad (\text{A46})$$

which, with given transition matrix \mathbf{P} , reveals a set of S linear equations with $S + 1$ unknowns: g, v_1, \dots, v_S . Notice that adding a constant offset o to all components of \mathbf{v} does not influence the fulfillment of (A46). This means, we can not determine the absolute values of \mathbf{v} , but would be able to obtain a set of relative values if we set one of the components to 0. For example, after setting v_S to 0, we attain S linear equations with S unknowns, and can solve for g and the relative values v_1, \dots, v_{S-1} .

The policy-iteration algorithm works in an iterative manner where each iteration cycle consists of two parts: the *value-determination* operation and the *policy-improvement* routine.

Given fixed policy, the value-determination operation computes g and the relative values by solving (A46). The policy is then improved based on the obtained relative values during the policy-improvement phase: for each state i , the maximizer of the optimization

$$\max_{a \in \mathcal{A}_i} q_i(a) + \sum_{j=1}^S p_{ij}(a)v_j \quad (\text{A47})$$

is chosen as the action to take, where \mathcal{A}_i denotes the set of feasible actions at state i . According to (A41) and (A45), the expected total reward for $n + 1$ stages starting with state i can be written, for large n , as follows

$$u_i(n + 1) = q_i + \sum_{j=1}^S p_{ij}(ng + v_j) = q_i + ng + \sum_{j=1}^S p_{ij}v_j. \quad (\text{A48})$$

Since the action affects only q_i and p_{ij} but not g , one needs only to solve (A47) to maximize u_i asymptotically. The updated policy is fed back to the value-determination operation and a new set of relative values can be computed. The algorithm terminates when the difference in the gains of the MDP in two iteration cycles falls below a predefined threshold.

The policy-iteration algorithm yields a sequence of g which increase monotonically, *i.e.* the policy-improvement routine leads indeed to a better policy and a higher gain of the MDP. To show this, we consider two consecutive iterations of the algorithm and label the quantities that evolve through the iterations with the superscripts A and B , respectively. During the policy-improvement routine in the former iteration, we solve the optimization problems (A47) for each state i and obtain a new policy which is used as the input to the value-determination operation in the latter iteration. The set of inequalities

$$\mathbf{q}^B + \mathbf{P}^B \mathbf{v}^A \geq \mathbf{q}^A + \mathbf{P}^A \mathbf{v}^A \quad (\text{A49})$$

can be inferred as a result of the policy-improvement. The sets of linear equations for the two iterations are given respectively by

$$g^A \cdot \mathbf{1} + (\mathbf{I} - \mathbf{P}^A) \mathbf{v}^A = \mathbf{q}^A, \quad g^B \cdot \mathbf{1} + (\mathbf{I} - \mathbf{P}^B) \mathbf{v}^B = \mathbf{q}^B, \quad (\text{A50})$$

and their difference can be computed as

$$(g^A - g^B) \mathbf{1} + \mathbf{v}^A - \mathbf{v}^B - \mathbf{P}^A \mathbf{v}^A + \mathbf{P}^B \mathbf{v}^B = \mathbf{q}^A - \mathbf{q}^B. \quad (\text{A51})$$

Taking (A49) into consideration, we have

$$(g^A - g^B) \mathbf{1} + (\mathbf{I} - \mathbf{P}^B) (\mathbf{v}^A - \mathbf{v}^B) \leq \mathbf{0}. \quad (\text{A52})$$

Let $\Delta g = g^A - g^B$, $\Delta \mathbf{v} = \mathbf{v}^A - \mathbf{v}^B$, and define

$$\Delta g \cdot \mathbf{1} + (\mathbf{I} - \mathbf{P}^B) \Delta \mathbf{v} = \Delta \mathbf{q}. \quad (\text{A53})$$

We notice that (A53) has the same form as (A46), implying that Δg can be written as $\Delta g = \Delta \boldsymbol{\rho}^T \Delta \mathbf{q}$, where $\Delta \boldsymbol{\rho}$ is the stationary state probability under the policy input to iteration B . Consequently, the entries of $\Delta \boldsymbol{\rho}$ and $\Delta \mathbf{q}$ are non-negative and non-positive, respectively, rendering $\Delta g = g^A - g^B \leq 0$. This concludes the proof that the policies produced successively during the policy-iteration algorithm lead to non-decreasing gains.

Bibliography

- [1] Fehske, A.; Fettweis, G.; Malmudin, J.; Biczok, G.: The global footprint of mobile communications: The ecological and economic perspective. – In: *IEEE Communications Magazine*, **49** (8), pp. 55–62, August 2011.
- [2] Recupero, D. R.: Toward a green Internet. – In: *Science*, **339** (6127), pp. 1533–1534, March 2013.
- [3] Heddeghem, W. V.; Lambert, S.; Lannoo, B.; Colle, D.; Pickavet, M.; Demeester, P.: Trends in worldwide ICT electricity consumption from 2007 to 2012. – In: *Computer Communications*, **50** pp. 64–76, September 2014.
- [4] Huawei: 5G: A Technology Vision (white paper). 2013, <http://www.huawei.com/5gwhitepaper/>.
- [5] Andrews, J. G.; Buzzi, S.; Choi, W.; Hanly, S. V.; Lozano, A.; Soong, A. C.; Zhang, J. C.: What will 5G be? – In: *IEEE Journal on Selected Areas in Communications*, **32** (6), pp. 1065–1082, March 2014.
- [6] Prasad, R. V.: Reincarnation in the ambiance: Devices and networks with energy harvesting. – In: *IEEE Communications Surveys & Tutorials*, **16** (1), pp. 195–213, February 2014.
- [7] Gunduz, D.; Stamatiou, K.; Michelusi, N.; Zorzi, M.: Designing intelligent energy harvesting communication systems. – In: *IEEE Communications Magazine*, **52** (1), pp. 210–216, January 2014.
- [8] Research project TREND. <http://www.fp7-trend.eu/>.
- [9] Research project EARTH. <https://www.ict-earth.eu/>.
- [10] Correia, L. M.; Zeller, D.; Blume, O.; Ferling, D.; Jading, Y.; Gódor, I.; Perre, L. V. D.: Challenges and enabling technologies for energy aware mobile radio networks. – In: *IEEE Communications Magazine*, **48** (11), pp. 66–72, November 2010.
- [11] Chen, J.; Niknejad, A. M.: A compact 1V 18.6 dBm 60 GHz power amplifier in 65nm CMOS. – In: *IEEE International Solid-State Circuits Conference Digest of Technical Papers*, pp. 432–433, February 2011.
- [12] Ali, A. M. A.; Morgan, A.; Dillon, C.; Patterson, G.; Puckett, S.; Hensley, M.; Stop, R.; Bhoraskar, P.; Bardsley, S.; Lattimore, D.; Bray, J.; Speir, C.; Sneed, R.: A 16b 250 MS/s IF-sampling pipelined A/D converter with background calibration. – In: *IEEE International Solid-State Circuits Conference Digest of Technical Papers*, pp. 292–293, February 2010.

- [13] Mezghani, A.; Nossek, J. A.: Modeling and minimization of transceiver power consumption in wireless networks. – In: Proc. 2011 International ITG Workshop on Smart Antennas, February 2011.
- [14] Bai, Q.; Nossek, J. A.: Energy efficiency maximization for 5G multi-antenna receivers. – In: Trans. on Emerging Telecommunications Technologies, **26** (1), pp. 3–14, January 2015.
- [15] Björnson, E.; Hoydis, J.; Kountouris, M.; Debbah, M.: Massive MIMO systems with non-ideal hardware: Energy efficiency, estimation, and capacity limits. – In: IEEE Trans. on Information Theory, **60** (11), pp. 7112–7139, November 2014.
- [16] Sankarasubramaniam, Y.; Akyildiz, I. F.; McLaughlin, S. W.: Energy efficiency based packet size optimization in wireless sensor networks. – In: Proc. First IEEE International Workshop on Sensor Network Protocols and Applications, pp. 1–8, 2003.
- [17] Bai, Q.; Nossek, J. A.: On energy efficient cross-layer assisted resource allocation in multiuser multicarrier systems. – In: Proc. IEEE 20th International Symposium on Personal, Indoor and Mobile Radio Communications, September 2009.
- [18] Qiao, D.; Gursoy, M.; Velipasalar, S.: Energy efficiency in the low-SNR regime under queueing constraints and channel uncertainty. – In: IEEE Trans. on Communications, **59** (7), pp. 2006–2017, July 2011.
- [19] Helmy, A.; Musavian, L.; Le-Ngoc, T.: Energy-efficient power adaptation over a frequency-selective fading channel with delay and power constraints. – In: IEEE Trans. on Wireless Communications, **12** (9), pp. 4529–4541, September 2013.
- [20] Muruganathan, S. D.; Ma, D. C.; Bhasin, R. I.; Fapojuwo, A. O.: A centralized energy-efficient routing protocol for wireless sensor networks. – In: IEEE Communications Magazine, **43** (3), pp. 8–13, March 2005.
- [21] Meshkati, F.; Poor, H. V.; Schwartz, S. C.; Mandayam, N. B.: An energy-efficient approach to power control and receiver design in wireless data networks. – In: IEEE Trans. on Communications, **53** (11), pp. 1885–1894, November 2005.
- [22] Chen, Y.; Zhang, S.; Xu, S.; Li, G. Y.: Fundamental tradeoffs on green wireless networks. – In: IEEE Communications Magazine, **49** (6), pp. 30–37, June 2011.
- [23] Rao, J. B.; Fapojuwo, A. O.: A survey of energy efficient resource management techniques for multicell cellular networks. – In: IEEE Communications Surveys & Tutorials, **16** (1), pp. 154–180, February 2014.
- [24] Kwon, H.; Birdsall, T. G.: Channel capacity in bits per joule. – In: IEEE Journal of Oceanic Engineering, **11** (1), pp. 97–99, January 1986.
- [25] Verdú, S.: On channel capacity per unit cost. – In: IEEE Trans. on Information Theory, **36** (5), pp. 1019–1030, September 1990.
- [26] Björnson, E.; Sanguinetti, L.; Hoydis, J.; Debbah, M.: Designing multi-user MIMO for energy efficiency: when is massive MIMO the answer? – In: Proc. IEEE Wireless Communications and Networking Conference, April 2014.
- [27] Shannon, C. E.: A mathematical theory of communication. – In: Bell System Technical Journal, **27** (4), pp. 623–656, October 1948.
- [28] Beeby, S.; White, N.: Energy Harvesting for Autonomous Systems. Artech House, 2014.

-
- [29] G. Auer *et al.*: D2.3: energy efficiency analysis of the reference systems, areas of improvements and target breakdown. 2nd Edition. INFSO-ICT-247733 EARTH, 2012.
- [30] Arnold, O.; Richter, F.; Fettweis, G.; Blume, O.: Power consumption modeling of different base station types in heterogeneous cellular networks. – In: IEEE Future Network and Mobile Summit, June 2010.
- [31] Jensen, A. R.; Lauridsen, M.; Mogensen, P.; Sørensen, T. B.; Jensen, P.: LTE UE power consumption model: For system level energy and performance optimization. – In: Proc. IEEE Vehicular Technology Conference, September 2012.
- [32] Wang, Q.; Hempstead, M.; Yang, W.: A realistic power consumption model for wireless sensor network devices. – In: Proc. 3rd Annual IEEE Communications Society on Sensor and Ad Hoc Communications and Networks, pp. 286–295, September 2006.
- [33] Bachmann, C.; Ashouei, M.; Pop, V.; Vidojkovic, M.; Groot, H. D.; Gyselinckx, B.: Low-power wireless sensor nodes for ubiquitous long-term biomedical signal monitoring. – In: IEEE Communications Magazine, **50** (1), pp. 20–27, January 2012.
- [34] Torfs, T.; Sterken, T.; Brebels, S.; Santana, J.; van den Hoven, R.; Spiering, V.; Zonta, D.: Low power wireless sensor network for building monitoring. – In: IEEE Sensors Journal, **13** (3), pp. 909–915, March 2013.
- [35] The Natural Resources Defense Council (NRDC): Data center efficiency assessment (Issue paper 14-08-A). <https://www.nrdc.org/sites/default/files/data-center-efficiency-assessment-IP.pdf>, August 2014.
- [36] Cui, S.; Goldsmith, A. J.: Energy-constrained modulation optimization. – In: IEEE Trans. on Wireless Communications, **6** (1), pp. 7–12, March 1960.
- [37] Li, Y.; Bakkaloglu, B.; Chakrabarti, C.: A system level energy model and energy-quality evaluation for integrated transceiver front-ends. – In: IEEE Trans. on Very Large Scale Integration (VLSI) Systems, **15** (1), pp. 90–103, January 2007.
- [38] Boccardi, F.; Heath, R. W.; Lozano, A.; Marzetta, T. L.; Popovski, P.: Five disruptive technology directions for 5G. – In: IEEE Communications Magazine, **52** (2), pp. 74–80, February 2014.
- [39] Chandrakasan, A.; Brodersen, R.: Minimizing power consumption in digital CMOS circuits. – In: Proceedings of the IEEE, **83** (4), pp. 498–523, April 1995.
- [40] Kim, N. S.; Austin, T.; Baauw, D.; Mudge, T.; Flautner, K.; Hu, J. S.; Narayanan, V.: Leakage current: Moore’s law meets static power. – In: Computer, **36** (12), pp. 68–75, December 2003.
- [41] Xiong, C.; Li, G. Y.; Zhang, S.; Chen, Y.; Xu, S.: Energy-and spectral-efficiency tradeoff in downlink OFDMA networks. – In: IEEE Trans. on Wireless Communications, **10** (11), pp. 3874–3886, November 2011.
- [42] Larsson, E.; Edfors, O.; Tufvesson, F.; Marzetta, T.: Massive MIMO for next generation wireless systems. – In: IEEE Communications Magazine, **52** (2), pp. 186–195, February 2014.
- [43] Murmann, B.: A/D converter trends: power dissipation, scaling and digitally assisted architectures. – In: Proc. IEEE Custom Integrated Circuits Conference, pp. 105–112, September 2008.

- [44] Mezghani, A.; Nossek, J. A.: Analysis of Rayleigh-fading channels with 1-bit quantized output. – In: Proc. IEEE International Symposium on Information Theory, pp. 260–264, July 2008.
- [45] Singh, J.; Dabeer, O.; Madhow, U.: On the limits of communication with low-precision analog-to-digital conversion at the receiver. – In: IEEE Trans. on Communications, **57** (12), pp. 3629–3639, December 2009.
- [46] Mezghani, A.; Nossek, J. A.: Capacity lower bound of MIMO channels with output quantization and correlated noise. – In: Proc. IEEE International Symposium on Information Theory, July 2012.
- [47] Lee, H. S.; Sodini, C. G.: Analog-to-digital converters: digitizing the analog world. – In: Proceedings of the IEEE, **96** (2), pp. 323–334, February 2008.
- [48] Bussgang, J. J.: Crosscorrelation functions of amplitude-distorted Gaussian signals. – In: Technical Report No. 216, MIT, Cambridge, MA March 1952.
- [49] Cover, T. M.; Thomas, J. A.: Elements of Information Theory. 2nd Edition. New York: John Wiley & Sons, 2012.
- [50] Max, J.: Quantizing for minimum distortion. – In: IEEE Trans. on Information Theory, **6** (1), pp. 7–12, March 1960.
- [51] Gersho, A.; Gary, R. M.: Vector Quantization and Signal Compression. Springer, 1992.
- [52] Tong, L.; Sadler, B. M.; Dong, M.: Pilot-assisted wireless transmissions: general model, design criteria, and signal processing. – In: IEEE Signal Processing Magazine, **21** (6), pp. 12–25, November 2004.
- [53] Hassibi, B.; Hochwald, B. M.: How much training is needed in multiple-antenna wireless links? – In: IEEE Trans. on Information Theory, **49** (4), pp. 951–963, April 2003.
- [54] Gursoy, M. C.: On the capacity and energy efficiency of training-based transmissions over fading channels. – In: IEEE Trans. on Information Theory, **55** (10), pp. 4543–4567, October 2005.
- [55] Bai, Q.; Mittmann, U.; Mezghani, A.; Nossek, J. A.: Minimizing the energy per bit for pilot-assisted data transmission over quantized channels. – In: Proc. IEEE 25th International Symposium on Personal, Indoor and Mobile Radio Communications, September 2014.
- [56] Hager, W. W.: Updating the inverse of a matrix. – In: SIAM Review, **31** (2), pp. 221–239, June 1989.
- [57] Hardy, G. H.; Littlewood, J. E.; Pólya, G.: Inequalities. Cambridge university press, 1952.
- [58] Verdú, S.: Spectral efficiency in the wideband regime. – In: IEEE Trans. on Information Theory, **48** (6), pp. 1319–1343, June 2002.
- [59] Tulino, A. M.; Lozano, A.; Verdú, S.: Bandwidth-power tradeoff of multi-antenna systems in the low-power regime. – In: DIMACS Series in Discrete Mathematics and Theoretical Computer Sciences. American Mathematical Society Press, 2003, pp. 15–42.
- [60] Zerlin, B.; Ivrláč, M. T.; Utschick, W.; Nossek, J. A.; Viering, I.; Klein, A.: Joint optimization of radio parameters in HSDPA. – In: Proc. IEEE 61st Vehicular Technology Conference, pp. 295–299, May 2005.

-
- [61] Gallager, R. G.: Information Theory and Reliable Communication. John Wiley & Son, 1968.
- [62] Pontryagin, L. S.; Boltyanskii, V. G.; Gamkrelidze, R. V.; Mishechenko, E. F.: The Mathematical Theory of Optimal Processes. New York/London: John Wiley & Sons, 1962.
- [63] Liberzon, D.: Calculus of Variations and Optimal Control Theory: a Concise Introduction. Princeton University Press, 2012.
- [64] Pinch, E. R.: Optimal Control and the Calculus of Variations. Oxford University Press, 1993.
- [65] Boyd, S.; Vandenberghe, L.: Convex Optimization. New York, NY, USA: Cambridge University Press, 2004.
- [66] Goldsmith, A.: Wireless Communications. Cambridge University Press, 2005.
- [67] Proakis, J. G.: Digital Communications. 4th Edition. McGrawHill, 2000.
- [68] Wozencraft, J. M.; Jacobs, I. M.: Principles of Communication Engineering. 1st Edition. New York: Wiley, 1965.
- [69] Chiani, M.; Dardari, D.; Simon, M. K.: New exponential bounds and approximations for the computation of error probability in fading channels. – In: IEEE Trans. on Wireless Communications, **2** (4), pp. 840–845, July 2003.
- [70] Lee, T. H.: The Design of CMOS Radio-Frequency Integrated Circuits. Cambridge university press, 2004.
- [71] Gomes, M.; Silva, V.; Cercas, F.; Tomlinson, M.: Analytical analysis of polyphase magnitude modulation method's performance. – In: Proc. IEEE International Conference on Communications, May 2010.
- [72] Bellman, R. E.; Dreyfus, S. E.: Applied Dynamic Programming. Princeton University Press, 2015.
- [73] Gallager, R. G.: Principles of Digital Communication. Cambridge University Press, 2008.
- [74] Dupuis, F.; Yu, W.; Willems, F.: Blahut-Arimoto algorithms for computing channel capacity and rate-distortion with side information. – In: Proc. IEEE International Symposium on Information Theory, pp. 179, June 2004.
- [75] Barber, C. B.; Dobkin, D. P.; Huhdanpaa, H.: The quickhull algorithm for convex hulls. – In: ACM Trans. on Mathematical Software, **22** (4), pp. 469–483, December 1996.
- [76] Murugesan, S.: Harnessing green IT: Principles and practices. – In: IT professional, **10** (1), pp. 24–33, January 2008.
- [77] Sudevalayam, S.; Kulkarni, P.: Energy harvesting sensor nodes: Survey and implications. – In: IEEE Communications Surveys & Tutorials, **13** (3), pp. 443–461, September 2011.
- [78] Gorlatova, M.; Wallwater, A.; Zussman, G.: Networking low-power energy harvesting devices: Measurements and algorithms. – In: IEEE Trans. on Mobile Computing, **12** (9), pp. 1853–1865, September 2013.
- [79] Tutuncuoglu, K.; Yener, A.: Optimum transmission policies for battery limited energy harvesting nodes. – In: IEEE Trans. on Wireless Communications, **11** (3), pp. 1180–1189, March 2012.

- [80] Bai, Q.; Li, J.; Nossek, J. A.: Throughput maximizing transmission strategy of energy harvesting nodes. – In: Proc. 3rd International Workshop on Cross-Layer Design, November 2011.
- [81] Xu, J.; Zhang, R.: Throughput optimal policies for energy harvesting wireless transmitters with non-ideal circuit power. – In: IEEE Journal on Selected Areas in Communications, **32** (2), pp. 322–332, February 2014.
- [82] Orhan, O.; Gunduz, D.; Erkip, E.: Throughput maximization for an energy harvesting communication system with processing cost. – In: Proc. IEEE Information Theory Workshop, pp. 84–88, September 2012.
- [83] Ozel, O.; Tutuncuoglu, K.; Yang, J.; Ulukus, S.; Yener, A.: Transmission with energy harvesting nodes in fading wireless channels: Optimal policies. – In: IEEE Journal on Selected Areas in Communications, **29** (8), pp. 1732–1743, September 2011.
- [84] Ho, C. K.; Zhang, R.: Optimal energy allocation for wireless communications with energy harvesting constraints. – In: IEEE Trans. on Signal Processing, **60** (9), pp. 4808–4818, September 2012.
- [85] Devillers, B.; Gunduz, D.: A general framework for the optimization of energy harvesting communication systems with battery imperfections. – In: Journal of Communications and Networks, **14** (2), pp. 130–139, April 2012.
- [86] Bai, Q.; Nossek, J. A.: Modulation and coding optimization for energy harvesting transmitters. – In: Proc. 9th International Conference on Systems, Communication and Coding, January 2013.
- [87] Bai, Q.; Nossek, J. A.: Throughput maximization for energy harvesting nodes transmitting over time-varying channels. – In: Proc. IEEE International Conference on Communications, June 2013.
- [88] Mitran, P.: On optimal online policies in energy harvesting systems for compound poisson energy arrivals. – In: Proc. IEEE International Symposium on Information Theory, pp. 960–964, July 2012.
- [89] Sharma, V.; Mukherji, U.; Joseph, V.: Efficient energy management policies for networks with energy harvesting sensor nodes. – In: Proc. 46th Annual Allerton Conference on Communication, Control, and Computing, pp. 375–383, September 2008.
- [90] Michelusi, N.; Stamatiou, K.; Zorzi, M.: On optimal transmission policies for energy harvesting devices. – In: Proc. Information Theory and Applications Workshop, pp. 249–254, February 2012.
- [91] Yates, R. D.; Mahdavi-Doost, H.: Energy harvesting receivers: Packet sampling and decoding policies. – In: IEEE Journal on Selected Areas in Communications, **33** (3), pp. 558–570, March 2015.
- [92] Zhou, S.; Chen, T.; Chen, W.; Niu, Z.: Outage minimization for a fading wireless link with energy harvesting transmitter and receiver. – In: IEEE Journal on Selected Areas in Communications, **33** (3), pp. 496–511, March 2015.
- [93] Tutuncuoglu, K.; Varan, B.; Yener, A.: Optimum transmission policies for energy harvesting two-way relay channels. – In: Proc. 2013 IEEE International Conference on Communications Workshops, pp. 586–590, June 2013.
- [94] Luo, Y.; Zhang, J.; Letaief, K.: Optimal scheduling and power allocation for two-hop energy harvesting communication systems. – In: IEEE Trans. on Communications, **12** (9), pp. 4729–4741, September 2013.

-
- [95] Khuzani, M. B.; Mitran, P.: On online energy harvesting in multiple access communication systems. – In: *IEEE Trans. on Information Theory*, **60** (3), pp. 1883–1898, March 2014.
- [96] Jeon, J.; Ephremides, A.: On the stability of random multiple access with stochastic energy harvesting. – In: *IEEE Journal on Selected Areas in Communications*, **33** (3), pp. 571–584, March 2015.
- [97] Ulukus, S.; Yener, A.; Erkip, E.; Simeone, O.; Zorzi, M.; Grover, P.; Huang, K.: Energy harvesting wireless communications: A review of recent advances. – In: *IEEE Journal on Selected Areas in Communications*, **33** (3), pp. 360–381, March 2015.
- [98] Bai, Q.; Nосsek, J. A.: Throughput maximization for energy harvesting nodes with generalized circuit power modeling. – In: *Proc. 13th IEEE International Workshop on Signal Processing Advances in Wireless Communications*, June 2012.
- [99] Bai, Q.; Amjad, R. A.; Nосsek, J. A.: Average throughput maximization for energy harvesting transmitters with causal energy arrival information. – In: *Proc. IEEE Wireless Communications and Networking Conference*, April 2013.
- [100] Bai, Q.; Nосsek, J. A.: Modulation optimization for energy harvesting transmitters with compound poisson energy arrivals. – In: *Proc. 14th IEEE International Workshop on Signal Processing Advances in Wireless Communications*, June 2013.
- [101] Bai, Q.; Mezghani, A.; Nосsek, J. A.: Throughput maximization for energy harvesting receivers. – In: *Proc. 17th International ITG Workshop on Smart Antennas*, March 2013.
- [102] Bai, Q.; Li, J.; Nосsek, J. A.: Energy-constrained throughput maximization for point-to-point communications. – In: *Proc. IEEE International Conference on Acoustics, Speech, and Signal Processing*, May 2014.
- [103] Bai, Q.; Nосsek, J. A.: Joint optimization of transmission and reception policies for energy harvesting nodes. – In: *Proc. 12th International Symposium on Wireless Communication Systems*, August 2015.
- [104] Priya, S.; Inman, D. J.: *Energy Harvesting Technologies*. New York: Springer, 2009.
- [105] Strong, S. J.: World overview of building-integrated photovoltaics. – In: *Conference Record of the 25th IEEE Photovoltaic Specialists Conference*, pp. 1197–1202, May 1996.
- [106] Zafer, M.; Modiano, E.: A calculus approach to energy efficient data transmission with quality-of-service constraints. – In: *IEEE/ACM Trans. on Networking*, **17** (3), pp. 898–911, March 2010.
- [107] Puterman, M. L.: *Markov Decision Processes: Discrete Stochastic Dynamic Programming*. New York: John Wiley & Sons, Inc., 1994.
- [108] Ross, S. M.: *Stochastic Processes*. 2nd Edition. Wiley, 1996.
- [109] Howard, R. A.: *Dynamic Programming and Markov Processes*. New York · London: Technology Press of the Massachusetts Institute of Technology and John Wiley & Sons, Inc., 1962.
- [110] Petrik, M.; Zilberstein, S.: Average-reward decentralized Markov decision processes. – In: *Proc. IJCAI*, pp. 1997–2002, January 2007.
- [111] Petrik, M.; Zilberstein, S.: A bilinear programming approach for multiagent planning. – In: *Journal of Artificial Intelligence Research*, **35** (1), pp. 235–274, June 2009.

- [112] Nair, R.; Tambe, M.; Yokoo, M.; Pynadath, D.; Marsella, S.: Taming decentralized pomdps: Towards efficient policy computation for multiagent settings. – In: Proc. IJCAI, pp. 705–711, August 2003.
- [113] Nahapetyan, A. G.: Bilinear programming. – In: Encyclopedia of Optimization, pp. 279–282, Springer US, September 2009.
- [114] Yang, J.; Ozel, O.; Ulukus, S.: Broadcasting with an energy harvesting rechargeable transmitter. – In: IEEE Trans. on Wireless Communications, **11** (2), pp. 571–583, February 2011.
- [115] Gurakan, B.; Ozel, O.; Yang, J.; Ulukus, S.: Two-way and multiple-access energy harvesting systems with energy cooperation. – In: Conference Record of the Forty Sixth Asilomar Conference on Signals, Systems and Computers, pp. 58–62, November 2012.
- [116] Ivrlač, M. T.; Nossek, J. A.: Toward a circuit theory of communication. – In: IEEE Trans. on Circuits and Systems, **57** (7), pp. 1663–1683, July 2010.
- [117] Bai, Q.; Nossek, J. A.: Design optimization of SIMO receivers with compact uniform linear arrays and limited precision A/D conversion. – In: Proc. 19th International ITG Workshop on Smart Antennas, March 2015.
- [118] Khan, S.; Peng, Y.; Steinbach, E.; Sgroi, M.; Kellerer, W.: Application-driven cross-layer optimization for video streaming over wireless networks. – In: IEEE Communications Magazine, **44** (1), pp. 122–130, January 2006.
- [119] Chiang, M.; Low, S. H.; Doyle, J. C.: Layering as optimization decomposition: A mathematical theory of network architectures. – In: Proceedings of the IEEE, **95** (1), pp. 255–312, January 2007.
- [120] Shakkottai, S.; Rappaport, T. S.; Karlsson, P. C.: Cross-layer design for wireless networks. – In: IEEE Communications Magazine, **41** (10), pp. 74–80, October 2003.
- [121] Georgiadis, L.; Neely, M. J.; Tassiulas, L.: Resource Allocation and Cross-layer Control in Wireless Networks. Now Publishers Inc., 2006.
- [122] Oldham, K. B.; Myland, J.; Spanier, J.: An Atlas of Functions. 2nd Edition. New York: Springer US, 2009.
- [123] Abramowitz, M.; Stegun, I. A.: Handbook of Mathematical Functions: with Formulas, Graphs, and Mathematical Tables. Courier Corporation, 1964.